ADA042688

AFFDL-TR-76-150

INVESTIGATION OF STRESS-STRAIN HISTORY MODELING AT STRESS RISERS

PHASE I

LOCKHEED-GEORGIA COMPANY
MARIETTA, GEORGIA 30063

June 1977

FINAL PHASE I TECHNICAL REPORT

Approved for public release; distribution unlimited

DDC
RECEIVED
AUG 10 1977

AIR FORCE FLIGHT DYNAMICS LABORATORY
AIR FORCE WRIGHT AERONAUTICAL LABORATORIES
AIR FORCE SYSTEMS COMMAND
WRIGHT-PATTERSON AIR FORCE BASE, OHIO 45433

AU NO.
DDC FILE COPY

NOTICE

When Government drawings, specifications, or other data are used for any purpose other than in connection with a definitely related Government procurement operation, the United States Government thereby incurs no responsibility nor any obligation whatsoever; and the fact that the government may have formulated, furnished, or in any way supplied the said drawings, specifications, or other data, is not to be regarded by implication or otherwise as in any manner licensing the holder or any other person or corporation, or conveying any rights or permission to manufacture, use, or sell any patented invention that may in any way be related thereto.

This report has been reviewed by the Information Office (OI) and is releasable to the National Technical Information Service (NTIS). At NTIS, it will be available to the general public, including foreign nations.

This technical report has been reviewed and is approved for publication.

Robert L Neulieb

ROBERT L. NEULIEB
Project Engineer

R. M. Bader

ROBERT M. BADER, Chief
Structural Integrity Branch

FOR THE COMMANDER

Howard L Farmer

HOWARD L. FARMER, Colonel, USAF
Chief, Structural Mechanics Division

Copies of this report should not be returned unless return is required by security considerations, contractual obligations, or notice on a specific document.

AFFDL-TR-[illegible]

UNCLASSIFIED

SECURITY CLASSIFICATION OF THIS PAGE (When Data Entered)

REPORT DOCUMENTATION PAGE

READ INSTRUCTIONS BEFORE COMPLETING FORM

1. REPORT NUMBER: AFFDL-TR-76-150	2. GOVT ACCESSION NO.
3. RECIPIENT'S CATALOG NUMBER	
4. TITLE (and Subtitle): INVESTIGATION OF STRESS STRAIN HISTORY MODELING AT STRESS RISERS,	5. TYPE OF REPORT & PERIOD COVERED: FINAL REPORT. PHASE I 1 May 1975 – 30 Sept 1976
	6. PERFORMING ORG. REPORT #: LG77ER0033 – Phase 1
7. AUTHOR(s): James R. Carroll, G. J. Gilbert, R. F. Wilkinson	8. CONTRACT OR GRANT NUMBER(s): F33615-75-C-3078
9. PERFORMING ORGANIZATION NAME AND ADDRESS: Lockheed-Georgia Company, A Division of Lockheed Aircraft Corporation, Marietta, Georgia 30063	10. PROGRAM ELEMENT, PROJECT, TASK AREA & WORK UNIT NUMBERS: Project 136Z, Task Number 03, Work Unit Number 11
11. CONTROLLING OFFICE NAME AND ADDRESS: Air Force Flight Dynamics Laboratory (AFFDL/FBE), Wright-Patterson AFB, Ohio 45433	12. REPORT DATE: June 1977
	13. NUMBER OF PAGES: 162
14. MONITORING AGENCY NAME & ADDRESS (if different from Controlling Office)	15. SECURITY CLASS. (of this report): UNCLASSIFIED
	15a. DECLASSIFICATION/DOWNGRADING SCHEDULE

16. DISTRIBUTION STATEMENT (of this Report)

Approved for public release; distribution unlimited.

17. DISTRIBUTION STATEMENT (of the abstract entered in Block 20, if different from Report)

18. SUPPLEMENTARY NOTES

19. KEY WORDS (Continue on reverse side if necessary and identify by block number)

Stress-strain history, fatigue life, residual stress, creep and stress relaxation

20. ABSTRACT (Continue on reverse side if necessary and identify by block number)

An experimental and analytical study of the stress and strain history at stress risers was conducted to assess the effects on cracking in aluminum alloy structures. This report covers Phase I of a two-phase program. The program includes cyclic characterization of the 7075-T651 material used, initial residual stress studies, complex sequence testing of super-scale and notched coupons, and analytical modeling of experimental results.

DD FORM 1 JAN 73 1473 EDITION OF 1 NOV 65 IS OBSOLETE

UNCLASSIFIED

SECURITY CLASSIFICATION OF THIS PAGE (When Data Entered)

20. (Continued)

Cyclic and time-dependent creep and/or relaxation were evaluated by measuring strain at the stress riser. Thirty different test sequences were run and strain data recorded for analytical modeling. These test sequences included combinations of overloads, underloads, periods between overloads, and hold periods at sustained load.

Creep and/or stress relaxation occurs at the stress riser during periods of sustained compression loading. This creep and relaxation is very complex and is a function of both notch stress and notch strain. The elastic-plastic stress and strain field definition is important to both the crack initiation and crack propagation phases of the damage process. Test sequences with sustained load periods reduced specimen life by eighty percent for some loading sequences.

FOREWORD

This research and development work reported herein was conducted under Air Force Contract F33615-75-C-3078 by the Lockheed-Georgia Company, a Division of Lockheed Aircraft Corporation. The work was sponsored by the Air Force Flight Dynamics Laboratory, Air Force Systems Command, Wright-Patterson Air Force Base, Ohio. Dr. Robert L. Neulieb of the Fatigue, Fracture, and Reliability Group, Structural Integrity Branch, (FBE), Structural Mechanics Division was the Project Engineer. This report covers the period from 1 May 1975 to 30 September 1976. This work was performed under Project 1367, Task 03, Work Unit 11.

Mr. James R. Carroll was the Lockheed-Georgia Company Program Manager. Other key Lockheed-Georgia technical personnel participating in the program included

- Testing - Mr. G. J. Gilbert
- Analytical Studies - Mr. R. F. Wilkinson
- Computer Programming - Mr. J. F. Holliday

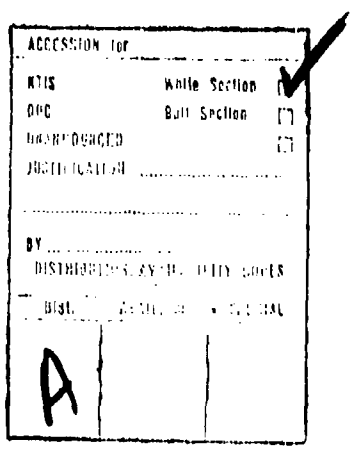

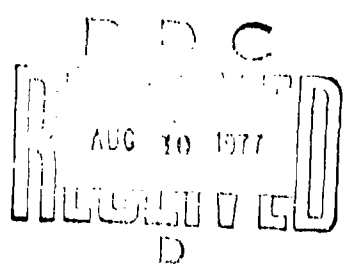

TABLE OF CONTENTS

PRECEDING PAGE NOT FILMED
BLANK

TABLE OF CONTENTS (Continued)

LIST OF FIGURES

LIST OF FIGURES (Continued)

LIST OF FIGURES (Continued)

LIST OF FIGURES (Continued)

LIST OF TABLES

SECTION I
INTRODUCTION

Structural cracking continues to be a major factor in air vehicle design and operation and an accurate assessment of the life of the structures is an essential part of design criteria. In order to accurately assess the life or time to cracking of aircraft structures, it is necessary to describe the detailed stress-strain state at the probable crack initiation site, usually at a stress concentration. A hysteresis type of analysis which describes notch stresses and strains and includes residual stress accountability is becoming a widely used tool for looking at the stress-strain history. This analysis accounts for sequence effects in complex load time histories. Recent published results in References 1 through 3 indicate that there may be time and cyclic dependent changes in the stress-strain state which significantly affect fatigue life but are not currently included in any analytical models.

It has been shown in Reference 1 and 3 that there is a shortening of life when a sustained compression load follows a tension overload in the loading sequence. This is attributed to a relaxation of the induced residual stresses during the period of sustained compressive loading. The program reported here is Phase I of a two-phase program to evaluate the stress-strain history at stress risers, including this relaxation or creep phenomena. An analytical and experimental study has been performed as a first step in formulation of an empirical stress-strain analysis model.

The studies included effects of (1) load and mechanically induced plasticity at the stress riser, (2) cyclic characterization of the material, (3) cyclic dependent variations in the stress-strain field, and (4) time dependent changes (creep) in the stress-strain state during sustained loading periods.

PRECEDING PAGE NOT FILMED
BLANK

SECTION II
SUMMARY

This program was directed to an experimental and analytical study of the stress and strain history at a stress riser to determine effects on cracking in aluminum alloy structures. The program reported here is Phase I of a two-phase program. An experimental approach was devised to determine if meaningful and measurable strain data could be recorded at the stress riser in a centrally notched plate when loaded under complex load-time-temperature test sequences. Program tasks included; monotonic and cyclic characterization of the 7075 material used, initial residual stress studies, complex sequence testing of super-scale and notched coupon specimens, and analytical modeling of experimental results. The existence of cyclic-and time-dependent creep and/or relaxation at the stress riser was evaluated by measuring strain at the hole during loadings. The combinations of loads included overloads, underloads, periods between overloads, and hold periods at sustained load. Thirty different test sequences were run and strain data recorded for analytical modeling.

A large amount of experimental data was obtained during this program and it was shown that meaningful strain history data at a stress riser can be obtained and analytical modeling of the stress-strain history is a vital part in predicting cracking of aluminum alloy structures. The super-scale test specimen is a good tool for evaluating effects of complex loading on time to cracking. This specimen, together with a Lockheed developed strain transducer, have provided a data base for stress-strain history modeling.

A summary of some of the observations made during this program is as follows:

- Overloads introduce beneficial residual stresses which increase fatigue life. An overload immediately followed by an underload results in a shorter life than with the overload only. Increasing the magnitude of the underload decreases life.

- Including hold periods at a sustained compression load reduces the specimen life considerably over that with the underload and no hold period.

- Duration of the sustained load hold period affects life.

- Cyclic periods between overloads and underloads also affect life.

- Creep and/or relaxation occurs during these hold periods at compressive loadings. Time to cracking or life is a function of both a stress and strain change (creep and/or relaxation) which occurs during periods of sustained loading.

SECTION III
EXPERIMENTAL

An experimental program was designed to demonstrate techniques and procedures for determining measurable variations in the plastically induced strain field at a stress riser. Data have been recorded under complex load-time-temperature test conditions. Test conditions have included overloads and underloads, variable length blocks of constant amplitude cycling, periods of sustained loading, and elevated temperatures. These data have been used to empirically model the stress-strain time history around a stress riser - in this case a circular hole in a finite width plate. Significant data which have been recorded include the following;

- Continuous recording of notch strain, load, time and cyclic test conditions
- Material cyclic characterization
- Initial residual stress
- Cycles to crack initiation
- Cycles to rupture
- Creep Data

Thirty complex load-time-temperature test sequences were developed and applied to notched super-scale and coupon test specimens to evaluate the variations in the plastic strain field at the stress riser. These test sequences are representative of the environmental load-time-temperature profiles of a typical fighter or transport wing structure. The sequences include initial tension and/or compression loadings followed by blocks of constant amplitude cycling at a positive 1-g mean stress. In some sequences the compression loadings are followed by periods of sustained load (either at the compression minimum or at the 1-g condition) prior to constant amplitude cycling. Test variables include time at sustained load, length of the constant amplitude block of cycles, compression load magnitude, and test temperature. All specimens were tested to failure.

Continuous recording of strain and load at the stress riser was achieved with a strain transducer and data logger system developed earlier by Lockheed on an in-house program. The transducer/data logger system makes it possible to continuously monitor notch strain and record changes in strain and load under various loading profiles. This system is discussed in more detail in 3.4.1.

In addition to the complex sequence tests, material properties and material cyclic characterization studies have been run. Standard ASTM tests were run to develop static tension and compression data for the 7075-T651 plate used in this program. Monotonic and cyclic stress-strain curves were also developed. The companion specimen test technique was used in these cyclic characterization studies. Data from these tests have been used in formulating an algorithm for simulating the material cyclic response both during strain hardening/softening and in the stable condition.

Additional studies have included; (1) an evaluation of the initial residual stress at the stress riser, (2) a limited crack growth study, and (3) generation of unnotched S-N data for the 7075-T651 plate.

Details of all phases of the experimental program are discussed in paragraphs 3.1 through 3.5. Application of the data in an analytical model formulation is discussed in Section IV and the data analysis and correlation studies are in Section V.

3.1 TEST SEQUENCES

The test sequences developed for this program were selected to be representative of fighter and transport wing load-time-temperature profiles. In selecting the sequences, consideration was given to the plasticity of the strain field around the stress riser and subsequent changes (creep) in the strain state during sustained loadings and constant amplitude cycling. Data in References 1 , 2 , and 3 were also used in selecting the sequences.

Each sequence is illustrated in Figure 1. The test conditions shown are considered to be typical of in-service events for transport and fighter aircraft and the sequence development follows a logical building block format for analytically modeling a wing loading profile. The following paragraphs discuss in more detail the rationale for selecting these test sequences. All stress levels shown in Figure 1 are net section stresses.

SEQUENCE NUMBER	TEST CONDITIONS	REMARKS
1. 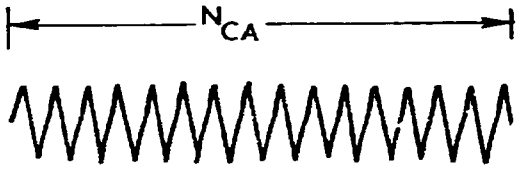	Constant Amplitude (CA) F_{mean} = 15.8 ksi F_{var} = 10.6 ksi (Typical for all sequences)	Develop baseline data – stress selected to be typical of 1G flight and alternating stress
2. 	Tensile Load (F_T) = + 47.3 ksi – Hold (H) = 1.0 hr – CA	Evaluate periods of sustained loading combined with CA tests
3. 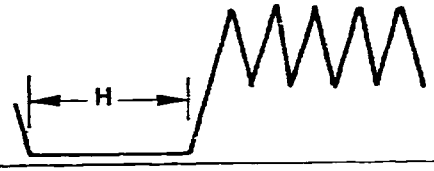	Compression (C) = –7.9 ksi – H = 24 hr – CA	Same as (2)
4. Repeat (3)	C = –15.8 ksi – H = 24 hr – CA	Evaluate periods of sustained loading at high negative mean stresses, on ground
5. Repeat (3)	C = –7.9 ksi – H = 1.0 hr. – CA	Same as (2)
6. 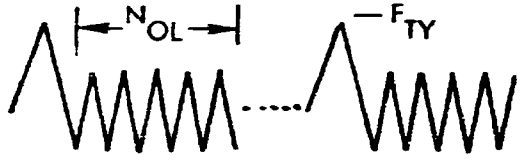	F_T = + 47.3 – CA – N_{OL} = 15,000 cycles – Repeat *	Determine effect of tension overloads on strain time to failure, etc.

Figure 1. Phase I Test Sequences (Sheet 1 of 7)

SEQUENCE NUMBER	TEST CONDITIONS	REMARKS
7. Repeat (6)	F_T - CA - N_{OL} = 1,000 cycles Repeat	Evaluate period (N_{OL}) between overloads
8. 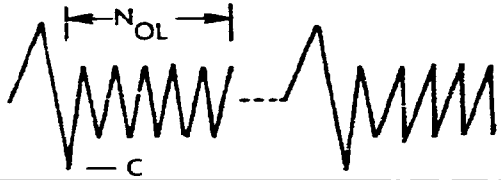	F_T - Compression (C) = -7.9 ksi CA - N_{OL} = 15,000 cycles Repeat	To include load reversals or ground loads combined with overloads and CA
9. Repeat (8)	F_T - C = -15.8 ksi - CA - N_{OL} = 15,000 cycles Repeat	Same as (8) plus evaluate higher on ground compressive stresses
10. Repeat (8)	F_T - C = -7.9 ksi - CA - N_{OL} = 1,000 cycles Repeat	Same as (8)
11. Repeat (8)	F_T - C = -15.8 ksi - CA - N_{OL} = 1,000 Repeat	Same as (9) plus evaluate period between overloads
12. Repeat (8)	F_T - C = -25 ksi - CA - N_{OL} = 15,000 cycles Repeat	Include fighter negative ΔNz in compression loading

Figure 1. Phase I Test Sequences (Sheet 2 of 7)

SEQUENCE NUMBER	TEST CONDITIONS	REMARKS
13 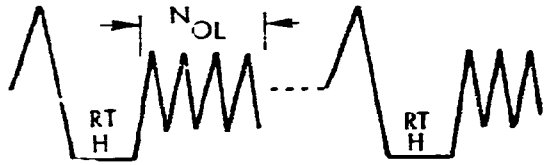	F_T - C = -7.9 ksi - Hold (H) = 24 hr - CA - N_{OL} = 15,000 cycles Repeat	Evaluate periods of sustained loading on ground between flights
14. Repeat (13)	F_T - C = -7.9 ksi - H = 1.0 hr - CA - N_{OL} = 15,000 cycles Repeat	Same as (13) Maximum of 5-24 hr. Hold times for this and all other sequences with H = 24 hr.
15. Repeat (13)	F_T - C = -15.8 ksi - H = 24 hr - CA - N_{OL} = 15,000 cycles Repeat	Same as (13) plus evaluate periods between overload
16. Repeat (13)	F_T - C = -7.9 ksi - H = 24 hr - CA - N_{OL} = 1,000 cycles Repeat	Same as (15)
17. Repeat (13)	F_T - C = -7.9 ksi - H = 1.0 hr - CA - N_{OL} = 1,000 cycles Repeat	Same as (15)

Figure 1. Phase I Test Sequences (Sheet 3 of 7)

SEQUENCE NUMBER	TEST CONDITIONS	REMARKS
18. Repeat (13)	F_T - C = -15.8 ksi - H = 24 hr - CA - N_{OL} = 1,000 cycles Repeat	Same as (15)
19. Repeat (13)	F_T - C = -15.8 ksi H = 1.0 - CA - N_{OL} = 1,000 cycles Repeat	Same as (15)
20. 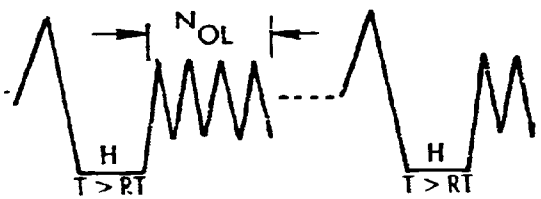	F_T - C = -7.9 ksi - H = 24 hr - CA - N_{OL} = 15,000 cycles Temp = +160°F Repeat	Entire sequence to be run at +160°F typ
21. Repeat (20)	F_T - C = -7.9 ksi - H = 1.0 hr CA - N_{OL} = 15,000 cycles Temp = +160°F Repeat	Evaluate hold time

Figure 1. Phase I Test Sequences (Sheet 4 of 7)

SEQUENCE NUMBER	TEST CONDITIONS	REMARKS
22 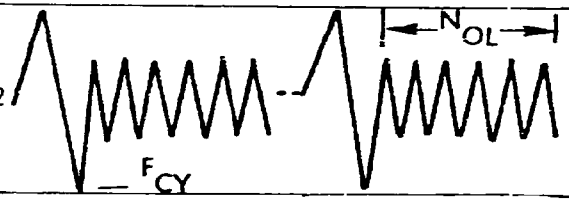	$F_T - C = -32.5$ ksi CA - N_{OL} = 15,000 cycles Repeat	Evaluate high compression load effects on strain relaxation
23. Repeat (22)	$F_T - C = -32.5$ ksi N_{OL} = 1,000 cycles Repeat	Same as (22)
24 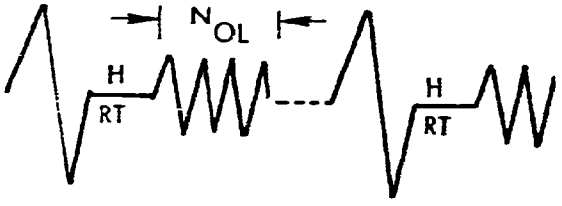	$F_T - C = -32.5$ ksi - F_M=15.8 ksi H = 1.0 hr - CA - N_{OL} = 15,000 cycles Repeat	Combined high tension and compression with sustained flight loading - Fighter
25. Repeat (24)	$F_T - C = -32.5$ ksi - F_M=15.8 ksi H = 1.0 hr - CA - N_{OL} = 1,000 cycles Repeat	Same as (24) plus evaluate N_{OL}

Figure 1. Phase I Test Sequences (Sheet 5 of 7)

SEQUENCE NUMBER	TEST CONDITIONS	REMARKS
26. 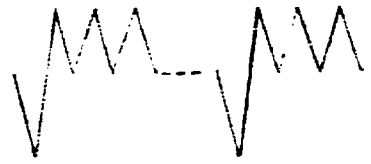	C = -50 ksi - F_M = +15.8 - CA, N_{OL} = 15,000 - Repeat	Initial compression loading
27. 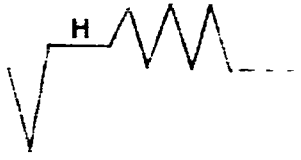	C = -50 Ksi - F_M = +15.8, H = 1.0 Hr. - CA, N_{OL} = 15,000 Repeat	
28. 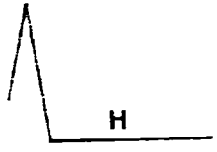	F_T = 47.3 - C = - 7.9 - H = 24.0 Hrs.	
29. 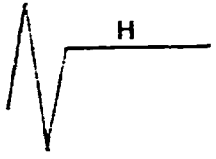	F_T = 47.3 - C = -32.5 - F_M = 15.8, H = 1.0 Hr	

Figure 1. Phase I Test Sequences (Sheet 6 of 7)

SEQUENCE NUMBER	TEST CONDITIONS		REMARKS
30. 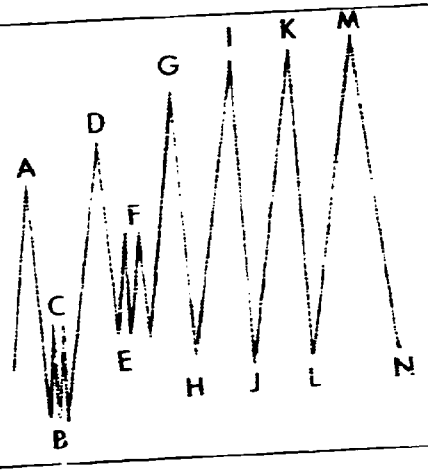	A = 39.6 B = 6.7 C = 6.7 D = 44.2 E = 6.7 F = 33.3 G = 52.1 H, J, L, N=0 I, K, M =55.3	N = 10,000 cycles N = 10,000 cycles	Evaluate cyclic creep

Figure 1. Phase I Test Sequences (Sheet 7 of 7)

Sequence 1. This is a constant amplitude test to establish baseline data free from the effects of overloads, underloads, etc. The stresses selected are considered to be an adequate simulation of 1-g flight mean and alternating stresses for a cargo and a fighter aircraft. These constant amplitude test conditions are the same for all subsequent sequences.

Sequence 2-5. Each of these sequences has an initial hold period with either a sustained tension or compression loading followed by constant amplitude cycling to failure. Two hold times are included, 1.0 and 24 hours. These sequences are considered typical of upper and lower surfaces on a wing of an aircraft on ground followed by flight cycling. The data are considered essential as simple building blocks for any analytical model.

Sequence 6-7. Tension overloads are included which represent periodic high inflight loads that introduce beneficial residual stresses. Variation in the cyclic period between overloads (N_{OL}) is included in these sequences. The Reference 2 data indicate that N_{OL} is a significant parameter in the evaluation of the residual stress-strain field and these sequences are included to develop data necessary for the analytical model development.

Sequence 8-12. These tests combine compressive loading (underloads) with the tension overloads and constant amplitude cycling from preceding sequences. These compressive loads are included to represent ground operation and/or negative loadings as in the case of a fighter. Again, two N_{OL} periods are included to develop basic data for analysis. Variations in the underloads are included to represent negative maneuvers and high on-ground mean stresses.

Sequence 13-19. Periods of sustained loading were introduced in Sequence 13 to evaluate the effect of on-ground conditions under constant loads. Previous data (References 1 and 3) had shown these hold times to significantly affect time to failure. It was anticipated that strain relaxation or creep would be evident and measurable from these sequences and then used in formulation of a strain relaxation module for the analytical model. The one-hour hold periods were repeated through-out the test as indicated; however a maximum of five 24-hour hold periods were run in any given sequence.

Sequence 20-21. This was a repeat of Sequences 13 and 14 except the entire sequences were run at + 160°F.

Sequence 22-23. These sequences include high compressive loadings following the tension overload. Considerable plasticity occurs at the stress riser from those loading sequences and these data are intended to evaluate the effect of this strain state and subsequent detrimental residual strains.

Sequence 24-25. Hold times are introduced following the compression yield in Sequences 23 and 23. Again, primary concern is on the changes in the plastic state at the stress riser during sustained loading. Two N_{OL} periods are included.

Sequence 26-27. In these two tests, the initial tension overload is deleted and the specimens are loaded to 50 Ksi in compression. These sequences are again included to evaluate time and cycle dependent changes in the plastic stress-strain field at the stress riser.

Sequence 28-29. These two test sequences are included to determine if meaningful data can be obtained from a combination of notch strain and strain gradient measured data. These sequences were substituted late in the program to evaluate the trends shown in the Reference 2 data. A detailed discussion of the tests and results are included in paragraph 3.5.2.

Sequence 30. This sequence was included to evaluate cyclic creep. The test includes variable peak overloads combined with blocks of constant amplitude cycling. Results from this have been used in the analytical modeling and are discussed in detail in paragraph 4.1.3.

All tests were run continuously, on a 24-hour basis, such that only the scheduled loadings have an effect on the recorded data. Testing included a minimum of one super-scale specimen for each sequence and three notched coupon specimens for selected sequences. Test specimen geometry is discussed in paragraph 3.3.1. Notched coupons were tested for Sequences 1, 6, 8, 14, 22, and 24 only. Continuous strain-load-time recordings were made for each super-scale test. The notched coupons were tested for fatigue data only.

3.2 MATERIAL PROPERTY TESTS

3.2.1 Static Tests

Static tests were conducted on coupon specimens cut from 7075-T651 aluminum alloy sheet material, 0.25-inch thick. Three tensile and three compressive coupons were removed from each of three 4 feet x 12 feet sheets and tested to determine basic material properties. The tensile and compressive specimen configurations are shown in Figure 2 (a) and 2 (b).

All the tests were performed at room temperature (77°F $\pm$ 5°F) in a universal testing machine, calibrated to ASTM standards. Load was applied at an approximate rate of 2500 pounds per minute and strain was measured with an SR-4 frame/strain-gaged leaf type 2.0-inch gage length extensometer. Load versus strain curves were plotted on an autographic recorder. Tensile and compressive property data are given in Table I.

One tensile coupon was cut from a super scale specimen after the cyclic creep study (Sequence 30) to establish an accurate value for modulus of elasticity of that piece of material. The coupon was removed from an area as remote from the specimen net section as possible. This specimen was machined to the configuration shown in Figure 2 (a), and tested in a universal testing machine as before. Load was applied in increments and a 1.0-inch gage length Tuckerman optical extensometer was used to measure strain at each load increment. Prior to reaching the proportional limit load the specimen was unloaded in order to remove the Tuckerman extensometer and replace it with an SR-4 frame/strain-gaged leaf type extensometer. Load was reapplied but at a constant load rate until failure occurred. A load versus strain curve was plotted on an autographic recorder. The accurate strain data obtained from the Tuckerman extensometer was then used to plot the initial part of a stress-strain curve. After correcting the strain data generated by the SR-4 frame extensometer to match that obtained in the elastic zone with the Tuckerman extensometer, the stress-strain curve was extended to a strain level of 0.025-inch/inch and is presented as Figure 3.

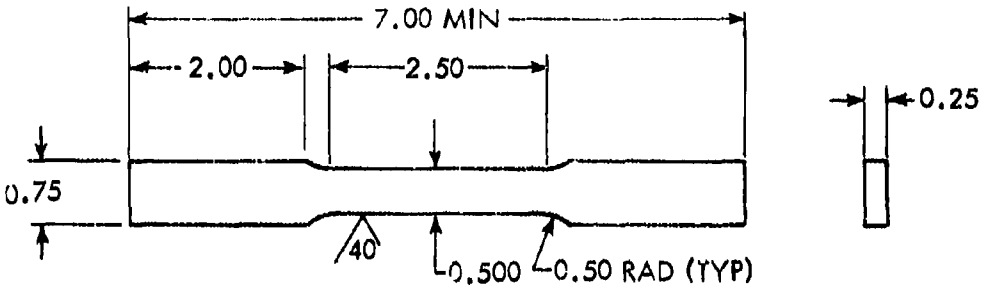

(a) TENSILE COUPON (2.0 INCH GAGE LENGTH)

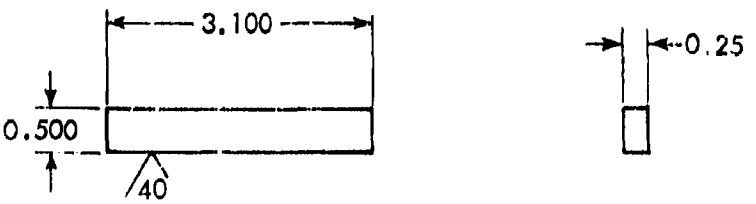

(b) COMPRESSION COUPON

Figure 2. Tensile and Compressive Coupon Specimen Configurations

TABLE I - MATERIAL PROPERTIES DATA

Sheet	F_{C_Y} (KSI)	F_{T_Y} (1) (KSI)	F_{T_U} (KSI)	Elong (%)
1	72.7	77.3	82.8	12.5
	75.0	78.5	83.4	12.5
	73.3	- (2)	83.7	13.0
2	73.1	76.3	82.1	13.0
	74.4	77.1	82.6	12.5
	70.9	73.4	80.3	12.5
3	72.3	76.5	82.7	13.5
	75.2	77.6	83.1	13.5
	70.9	75.2	81.5	13.0
Average	73.1	76.5	82.5	12.9

(1) 0.2 percent offset

(2) Stress-strain curve not adequate for measuring F_{T_Y}.

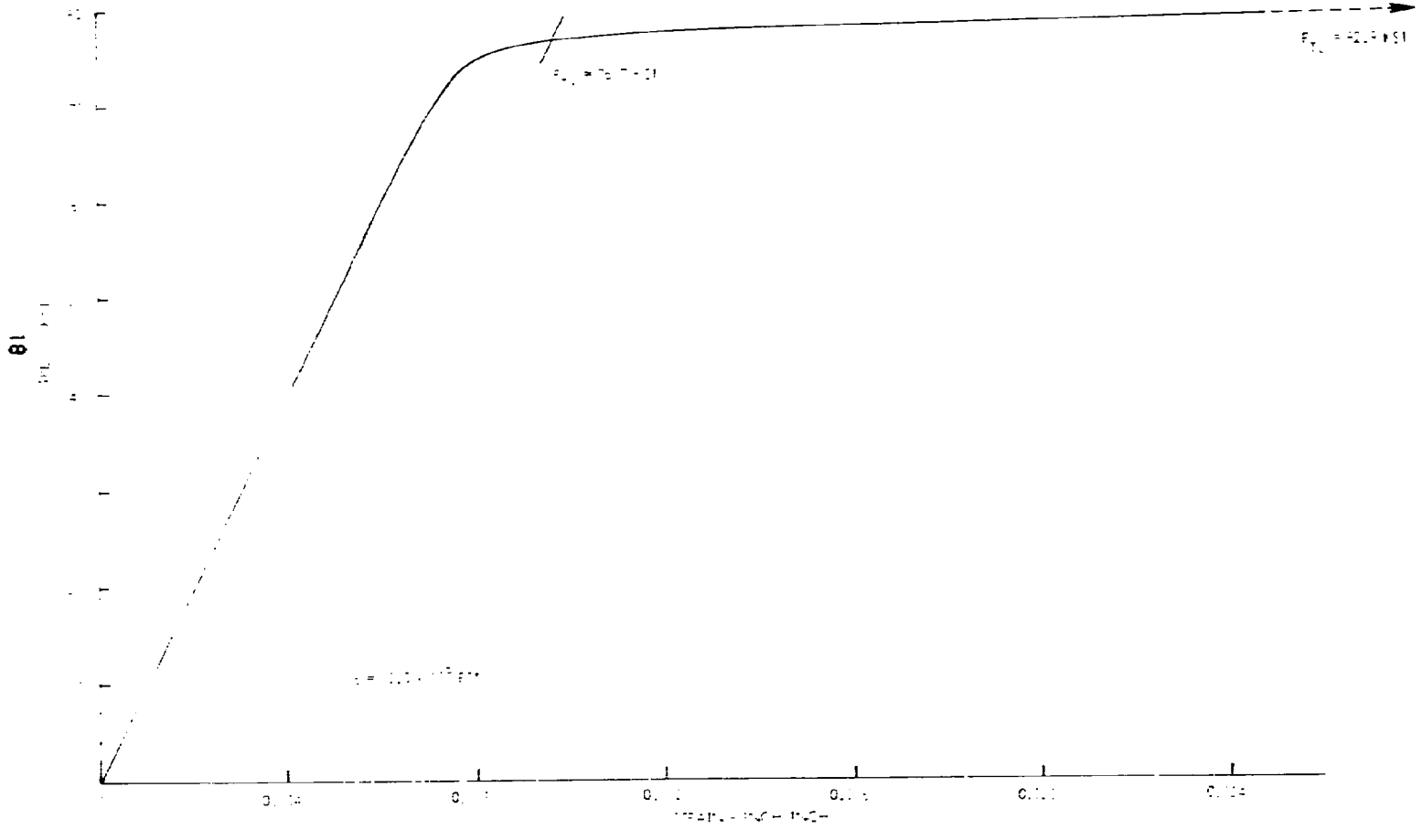

Figure 3. Monotonic Stress-Strain Curve 7075-T651

3.2.2 Material Cyclic Characterization

In order to characterize the stable and transient cycle dependent response of the 7075-T651 plate used, strain controlled tests were run on thirty-seven specimens machined from 1.0-inch thick plate. The specimen geometry is illustrated in Figure 4. Testing was done using the companion specimen test technique and range of fully reversed strain varied from 0.0029 in/in up to 0.049 in/in. Typical hysteresis loops for four test levels are illustrated in Figures 5 through 8. For clarity, only the initial loop and the stable hysteresis loop is shown along with the monotonic locus curve. These data are used in formulating the analytical model for the stable response and for cyclic hardening and softening which is discussed in detail in 4.1.1.

The monotonic stress-strain curve is shown as a solid curve in Figure 9 and the cyclic data points are superimposed on the plot. All testing here was run at a constant strain rate of 0.06 in/in/min. Some interesting and unexpected phenomena were observed during these tests. In the plastic region the data generally behave in the classical manner for the 7075 alloy; that is, the data exhibit strain hardening tendencies. At the knee of the curve there is a slight strain softening, however. In general, at strains above 0.008 in/in the data trends are as expected and the results were considered sufficient and accurate for the program. However, at lower strains, in the elastic region, the cyclic data points exhibit unexpected trends. The first data run exhibited a significant amount of strain softening at strains of 0.00625 and 0.0060 in/in. Two additional data points were run at lower strains to determine the deviation from the monotonic curve. Softening also occurred at 0.0030 in/in; however, at $\Delta \epsilon/2 = 0.0044$ in/in the cyclic data at stabilization was totally unexpected. The specimen strain hardened and, at stabilization, the maximum stress was 85 ksi. The strain hardening is so drastic that the minimum stress at stabilization is positive (1.2 ksi). The path to stabilization for this and other points is illustrated in Figure 10.

Additional specimens were fabricated and tested at strains between 0.0020 and 0.0045 to check the original data developed in this strain range. Some of these data points agree with the monotonic curve; however, there are additional data which show the main strain hardening that occurred previously at 0.0040 in/in. For the delta strain of 0.0029, for example, the maximum and minimum stresses at stabilization are +65 and +11 ksi, respectively. The path to stabilization for two of these data points is also illustrated in Figure 10.

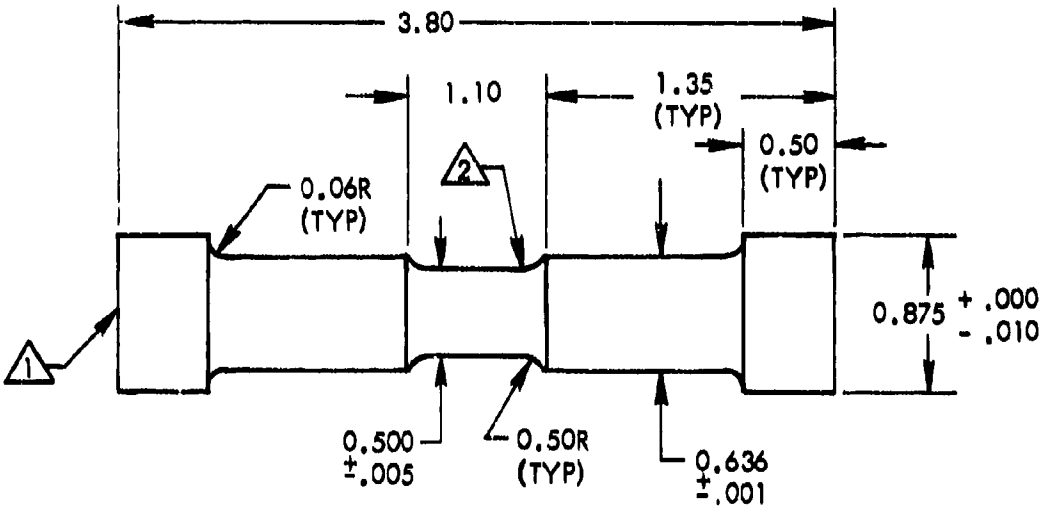

1. MACHINE SPECIMEN ENDS FLAT AND PARALLEL
2. POLISH RADII AND TEST SECTION

Figure 4. Button End Test Specimen

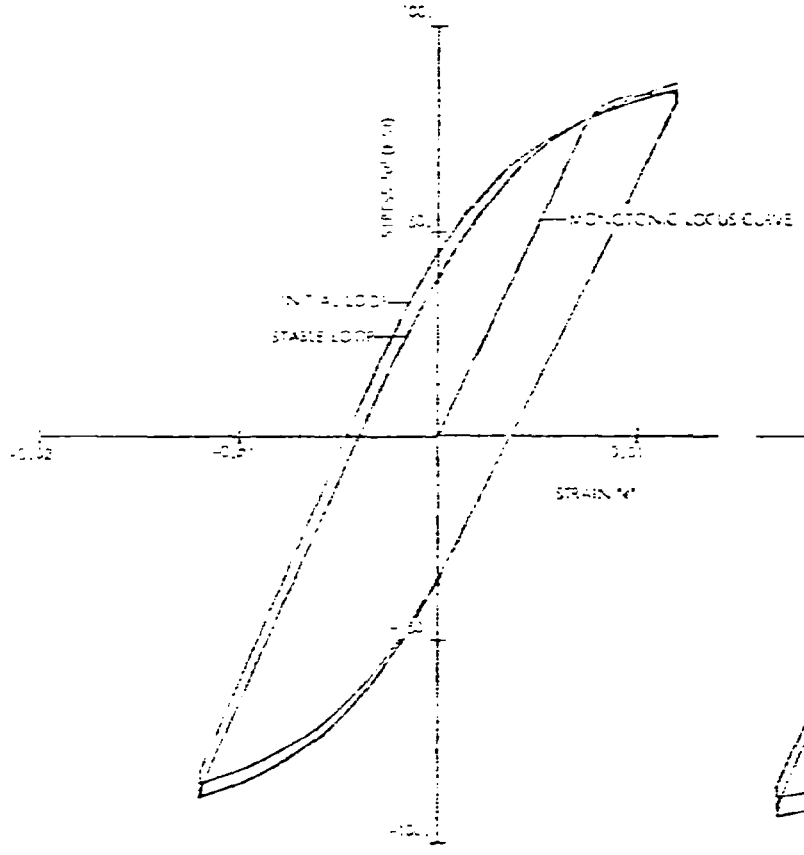

Figure 5. Hysteresis Loops for Test GJ3 ($\Delta\epsilon/2 = 0.0119$)

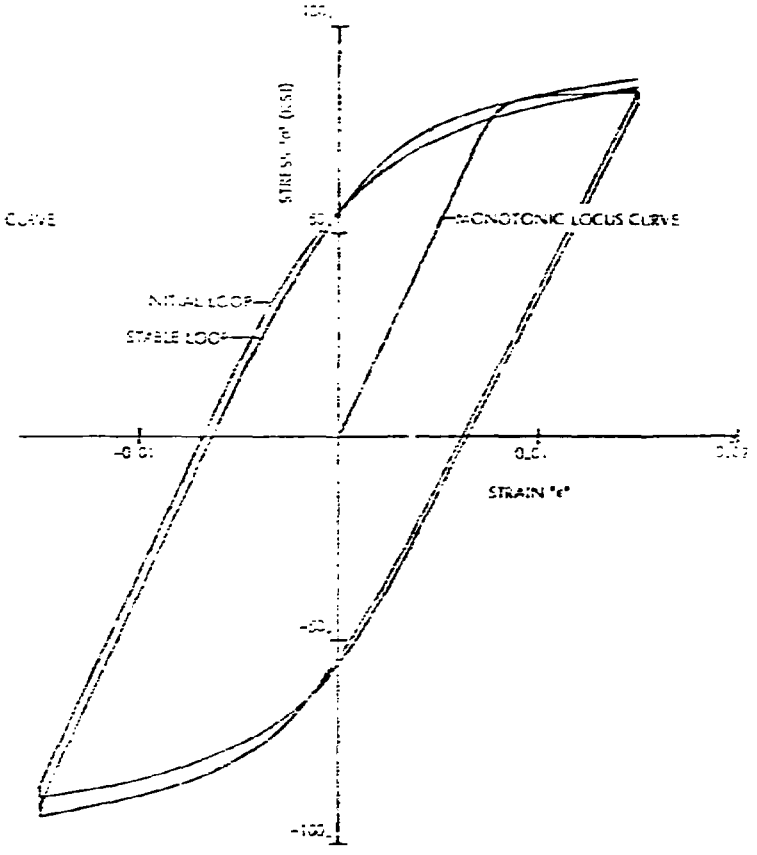

Figure 6. Hysteresis Loops for Test GJ6 ($\Delta\epsilon/2 = 0.0149$)

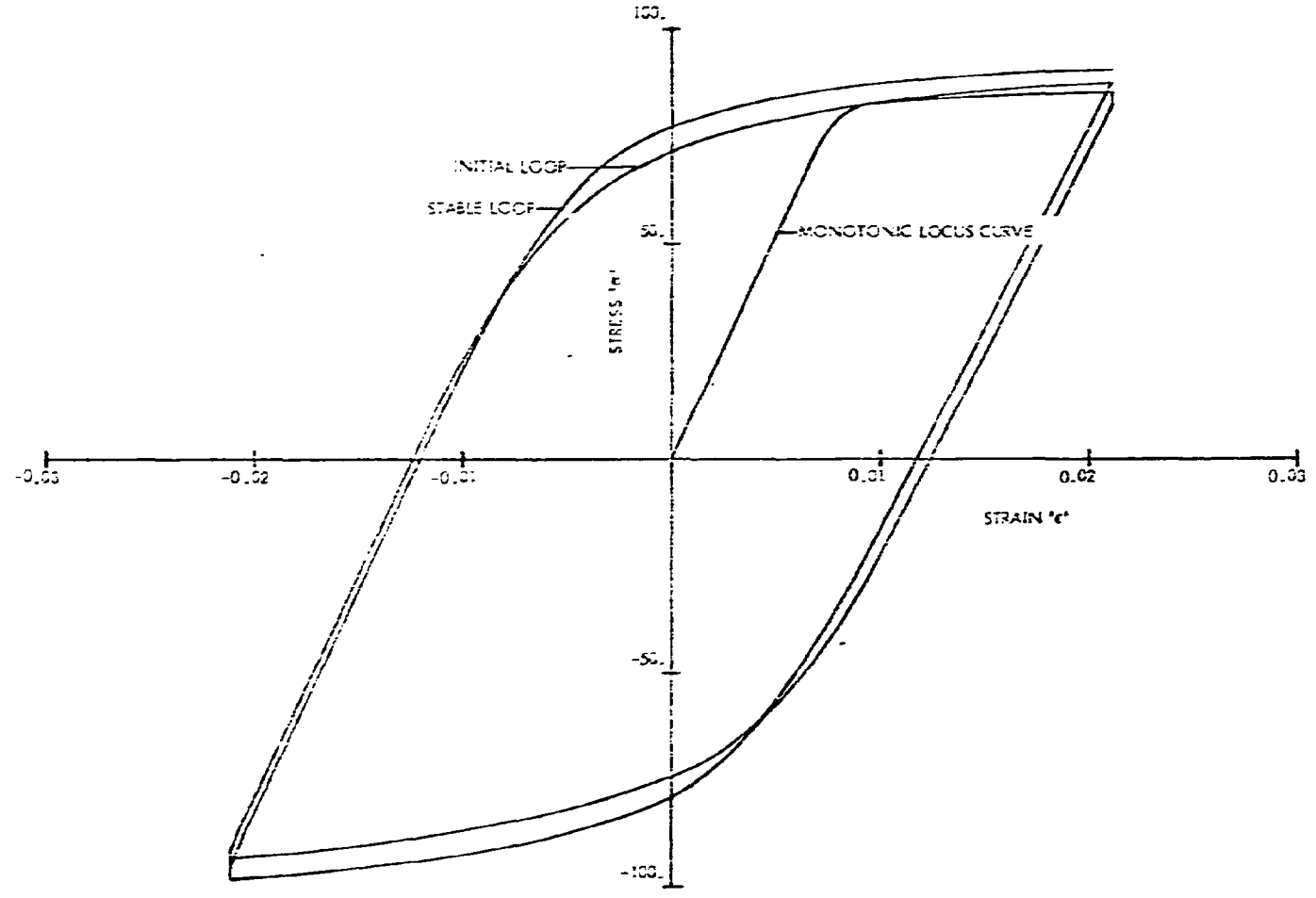

Figure 7. Hysteresis Loops for Test GJ9 ($\Delta\epsilon/2 = 0.0211$)

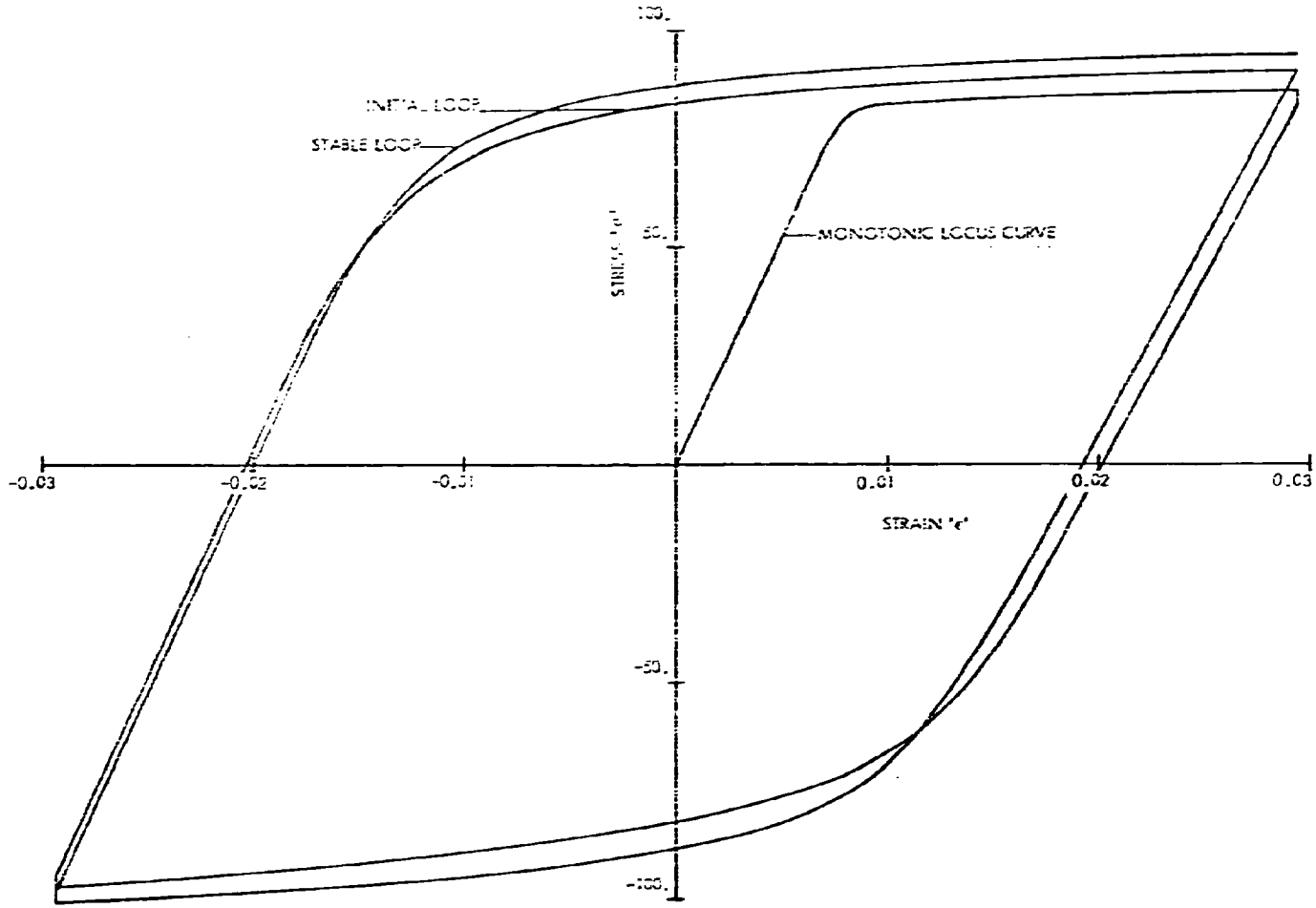

Figure 8. Hysteresis Loops for Test GJ1 ($\Delta\epsilon/2 = 0.0294$)

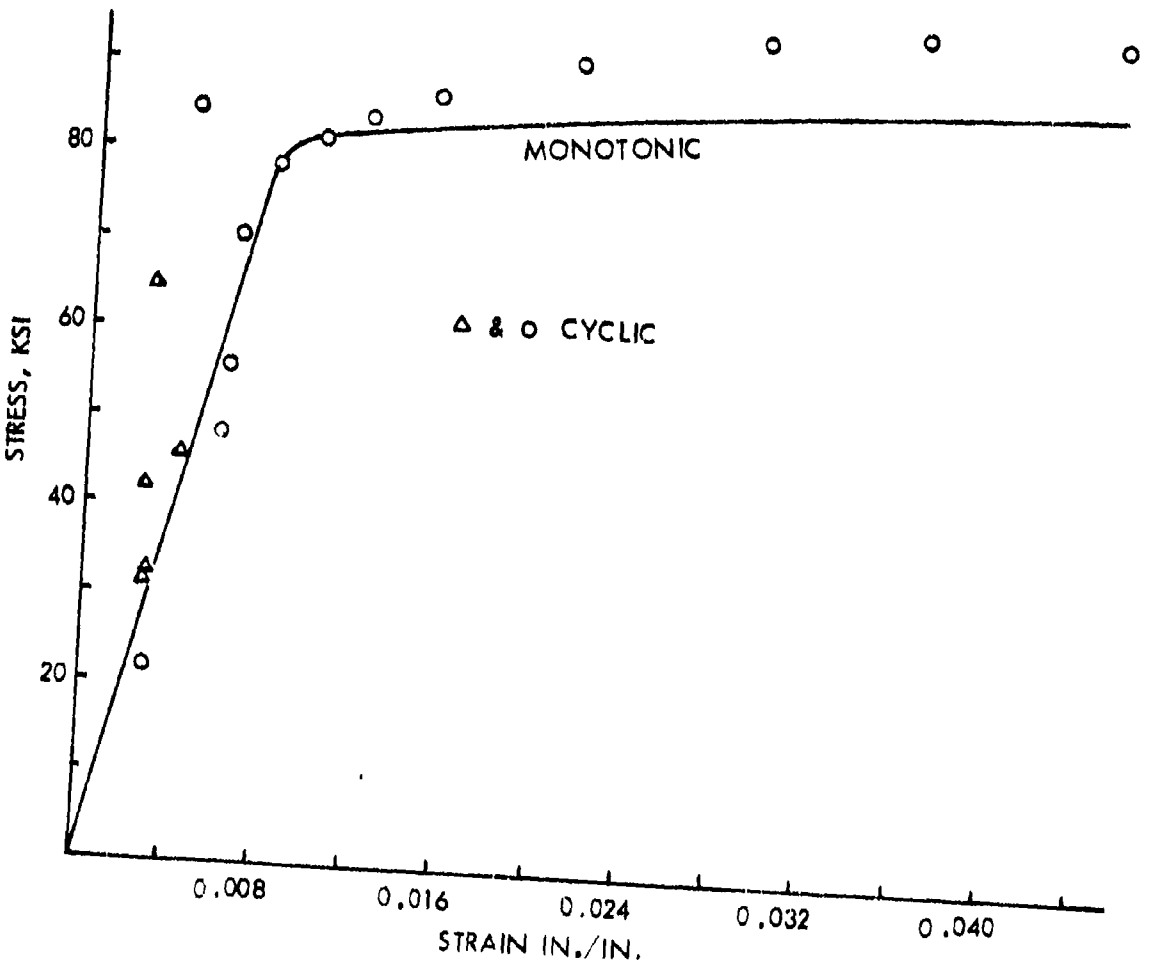

Figure 9. Cyclic and Monotonic Stress-Strain Data (7075-T651)

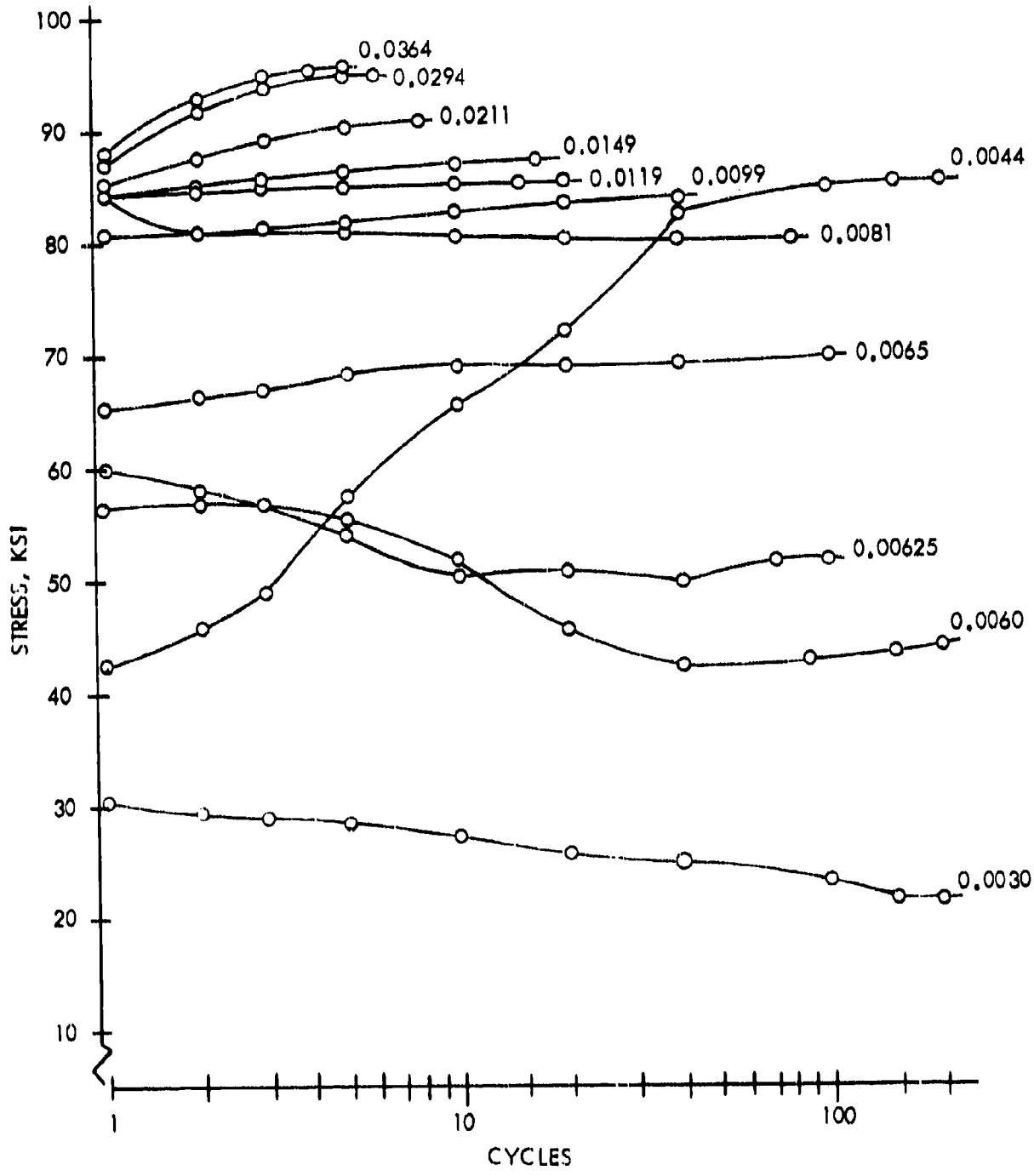

Figure 10. Stress History for 7075-T651 (1.0 Plate)

A search of published data showed no similar results from other sources; however, cyclic tests are not generally run at $\Delta\epsilon$'s in the elastic region of the curve. One possible explanation for this ratcheting effect may be related to the inhomogeneity of the plate material where these specimens were taken. Inclusions, large particle sizes, etc. will cause local stress concentrations which are washed out when a specimen is loaded plastically at large strains. The stress concentrations may dominate the material response at lower strains in the elastic region, however. This may have been the predominate force in the specimens here which demonstrated the stress ratcheting during cycling. Additional research is needed in this area to determine cause and subsequent effect on full-scale structures in service. This research was beyond the scope of the current program and the elastic portion of the monotonic curve has been used in analysis together with the cyclic hardening data in the plastic region.

3.2.3 Unnotched Fatigue Tests

The hysteresis analysis program to be used to predict time to failure or life uses as a basis for damage calculations either unnotched ($K_t = 1.0$) S-N data or ϵ - N data. In order to verify the existing data base and to evaluate the plate material used in this program, a limited fatigue test was run to develop $K_t = 1.0$ S-N data. Thirty 0.25-inch thick, flat dogbone specimens were fabricated from the 7075-T651 plate used for the super-scale and notched coupon specimens and fatigue tested. The resulting data are listed in Table II for six different mean stress levels. One specimen was tested at each alternating stress level shown. These data are plotted as variable stress versus cycles to failure in Figure 11.

3.3 TEST SPECIMEN DESIGN AND FABRICATION

3.3.1 Specimen Configurations

Two specimen configurations were used in the load-time-temperature sequence testing. The specimens are illustrated in Figures 12 and 13 and were fabricated from 0.25-inch thick, 7075-T651 plate. Super-scale specimens are necessary to facilitate installation of the strain transducer, inside the centrally located hole (stress riser), for continuously monitoring strain changes. The smaller notched coupons are included for fatigue testing only for six of the sequences. This is to compare the times to failure between the two configurations and ascertain that there are no size effects in the super-scale data. Based on the data collected, there are no size effects seen which might bias the data.

TABLE II. UNNOTCHED FATIGUE DATA

$F_M = 0$		$F_M = 60$	
F_v = 41.5 Ksi	N = 32,540	F_v = 20.0	N = 26,670
30.0	90,180	15.5	83,320
27.0	161,310	13.0	214,160
22.0	329,220	12.0	>1,600,000 (1)
20.0	556,450	12.0	155,550

(1) Failed in Grips

$F_M = 20$		$F_M = -20$	
F_v = 39.0 KSI	N = 10,300	F_v = 53.0	N = 14,500
33.0	21,500	42.5	61,900
25.0	71,950	38.0	109,000
18.0	306,860	33.0	445,470
15.0	1,612,000	30.0	1,760,000

$F_M = 40$		$F_M = -40$	
F_v = 30.0 KSI	N = 14,930	F_v = 47.0	N = 350,000
24.0	30,800	45.0	610,000
19.0	178,820	37.0	1,790,000 (NF)
17.0	261,000		
14.0	2,000,000 (NF)		

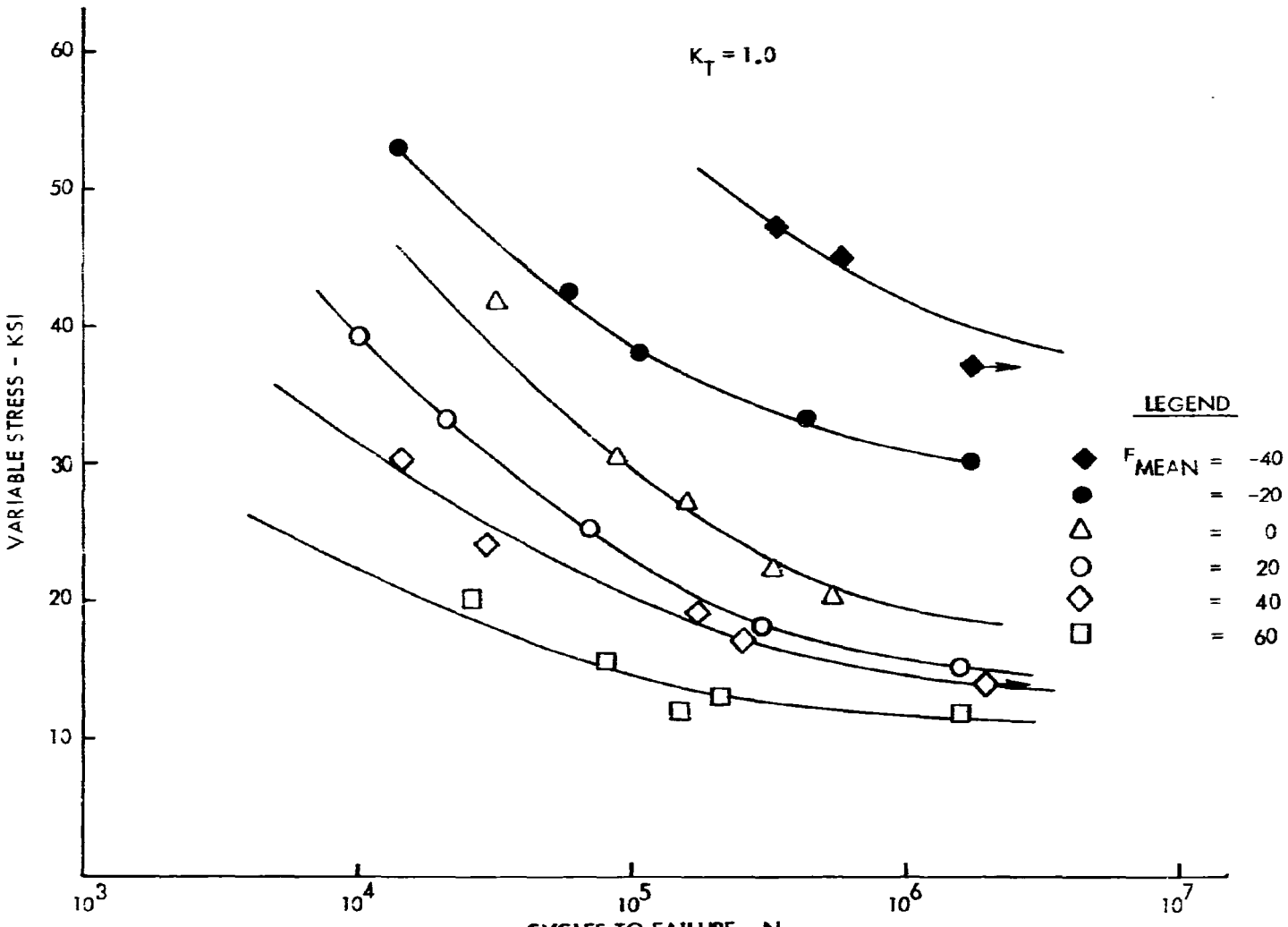

Figure 11. Unnotched Fatigue Data for 7075-T651 Plate

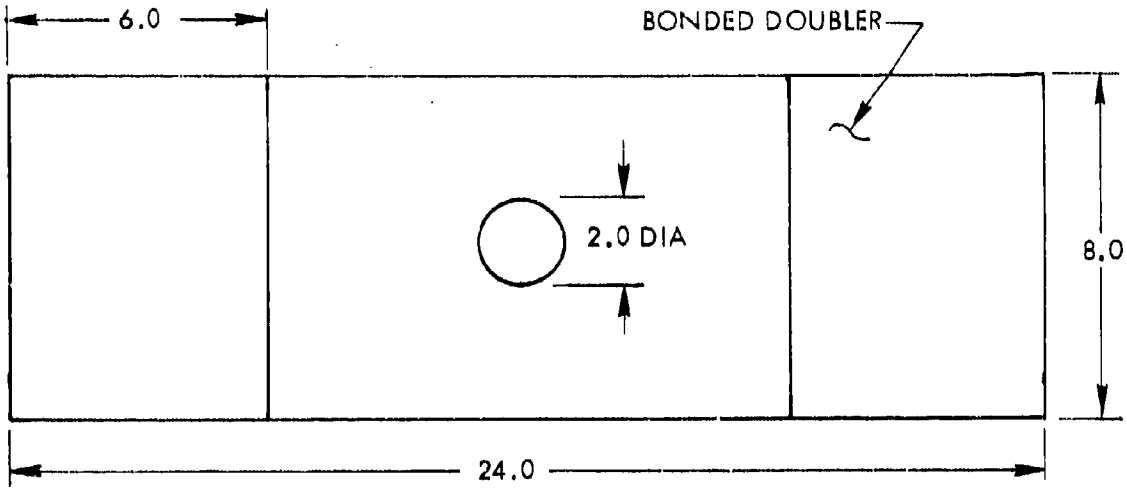

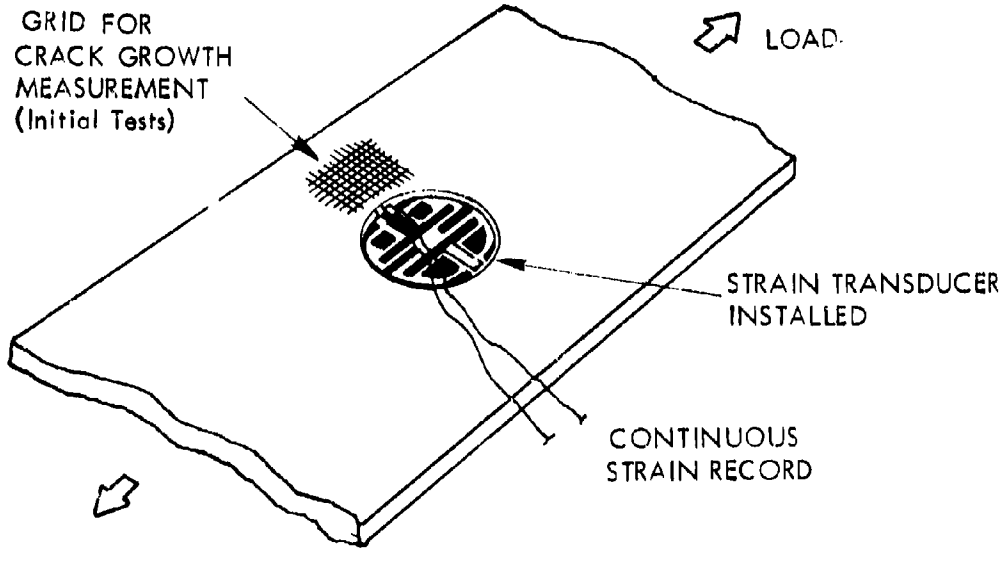

Figure 12. Super Scale Test Specimen - $K_T = 2.43$

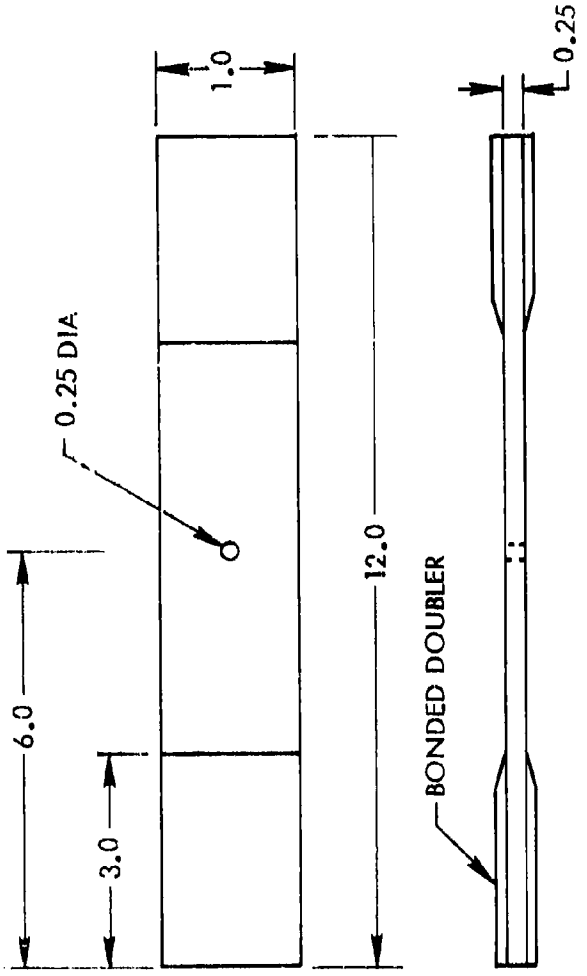

Figure 13. Notched Coupon Test Specimen - $K_T = 2.43$

All specimens were cut from three standard 4' x 12' plates, 0.25-inch thick. Specimen location within the plate is illustrated in Figure 14. The specimens for materials properties evaluation were randomly selected from each plate as shown. Super-scale specimens were taken from Zones A through F and were further identified as to plate number and location within a zone. For example, Specimen No. 1A-1 was cut from Plate 1, Zone A, and is the first specimen at the "top" edge of the plate.

Doublers were adhesively bonded to all the specimen ends to preclude fatigue failures at the end grips and each specimen was laterally supported to prevent buckling during application of compression loads. Figure 15 shows a super-scale specimen installed for testing with the lateral supports and strain transducer in place.

3.3.2 Initial Residual Stresses

The nature of this experimental program dictated that residual stresses at the stress risers due to manufacturing must be near zero. Two investigative studies were conducted to evaluate the manufacturing residual stresses around the holes in both the super-scale and notched coupon specimens. All holes were cut under size using a trepanning tool and then successive boring operations were made to obtain final hole size. This approach was taken to minimize residual stresses at the holes and was confirmed by the test discussed below.

The initial study involved the measurement of strains around the hole in both a super-scale and a notched coupon specimen. Data were recorded from axial and rosette strain gages located at the center of and immediately adjacent to the hole in each specimen during the cutting and boring operation. Four 3/8" diameter holes were drilled remote to the strain gaged area and the specimen was mounted on four adjustable studs on the machine fixture. The specimen installation is shown in Figure 16. Strain gage locations are shown in Figure 17. With the test specimen free-standing in an unloaded condition, all 12 strain gages were zeroed on the strain indicator. These initial readings were checked after approximately 15 minutes to determine if any zero drift had occurred. None was apparent. The specimen was then mounted on the adjustable studs on the milling machine and by monitoring the strain gage readings to assure no induced stresses, the necessary adjustments were made to securely attach the specimen for machining.

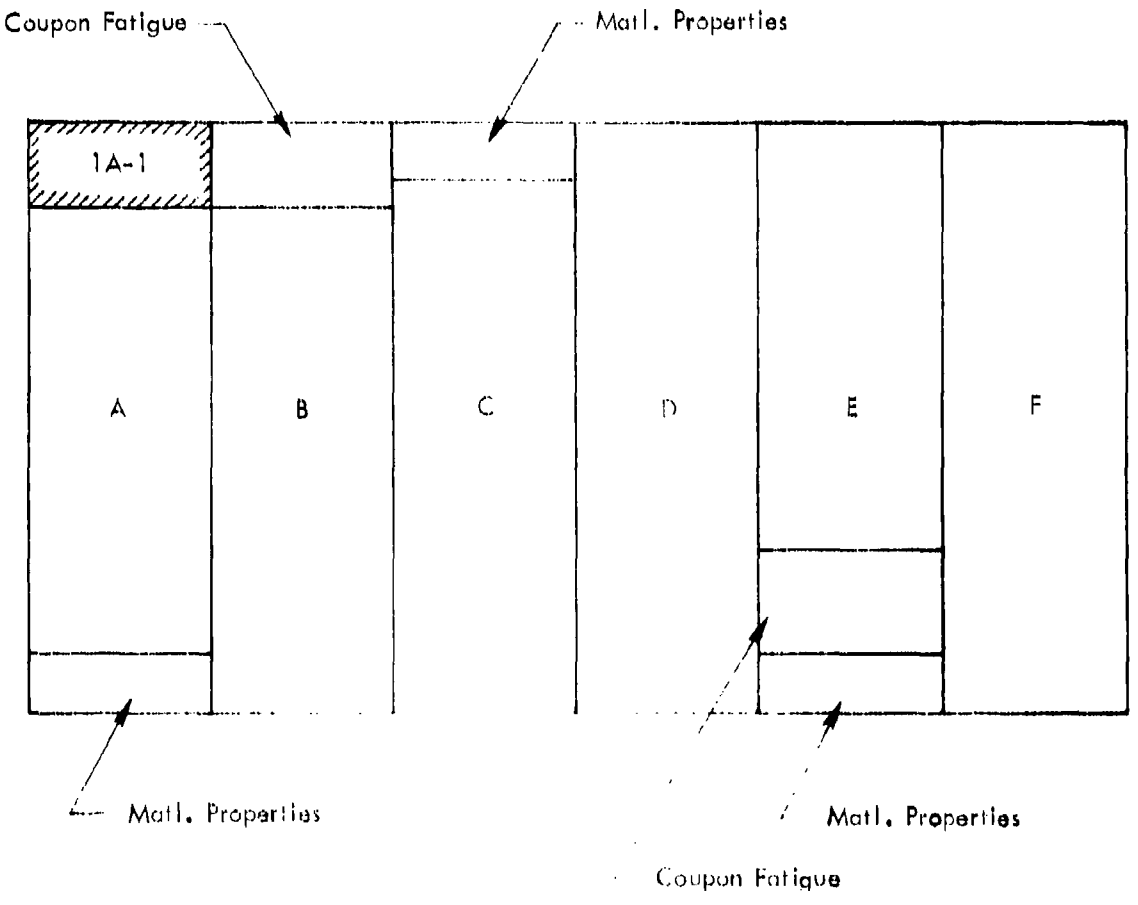

Figure 14 Specimen Locations

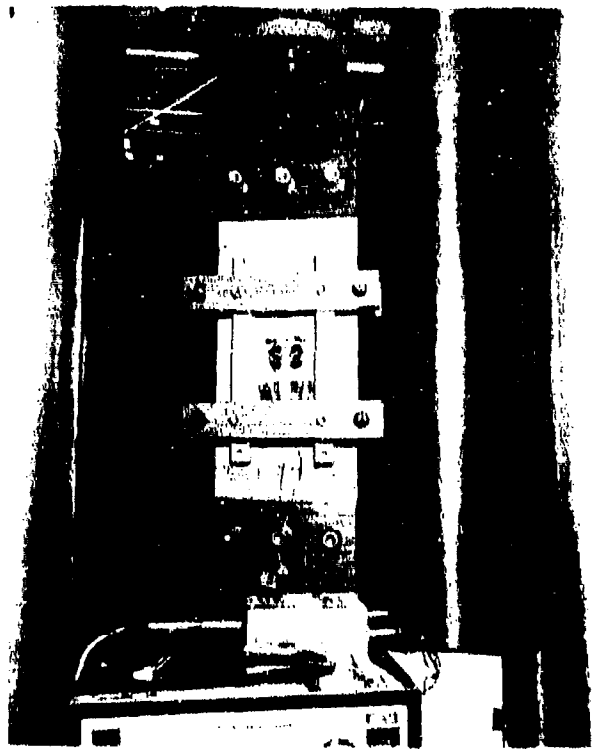

(a) Super-Scale Specimen with Lateral Supports

(b) Strain Transducer Installation

Figure 15. Super Scale Test Specimen Installation

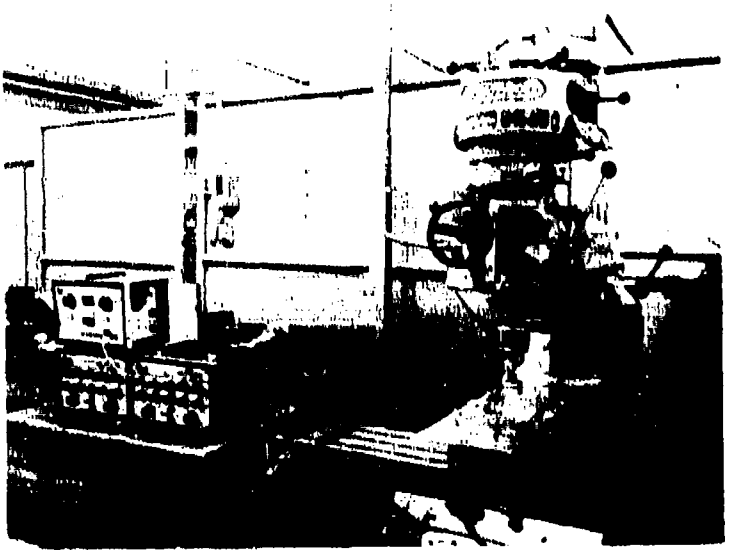

(a) Specimen Installed in Milling Machine

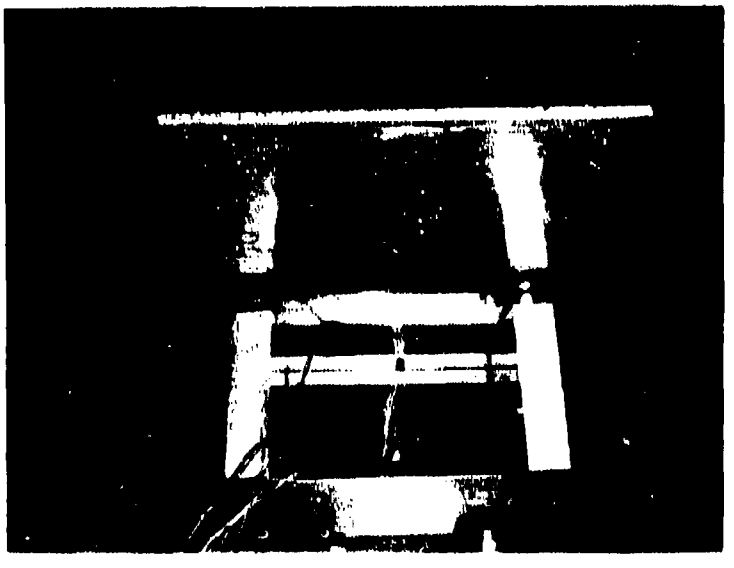

(b) Specimen Supports and Strain Gages on Underside

Figure 16 Initial Residual Stress Investigation

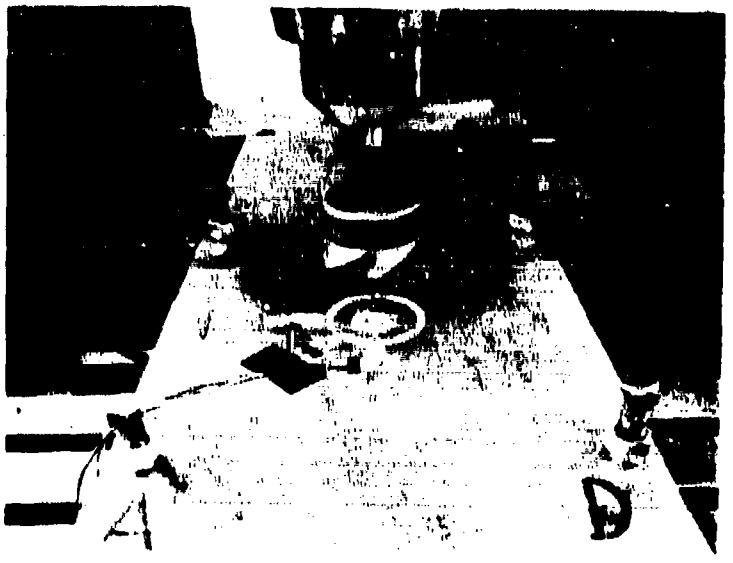

(c) Initial Saw Cut - .23" Depth

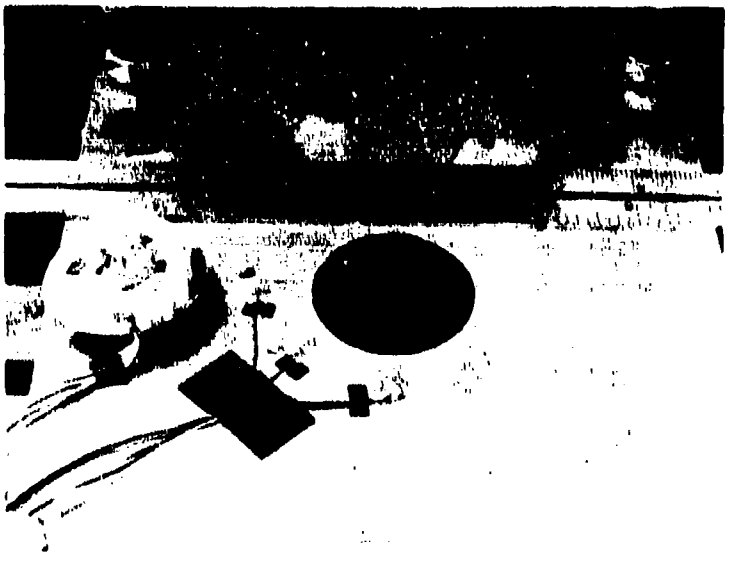

(d) Center Disk Removed - 1.884" Hole Dia.

Figure 16 Initial Residual Stress Investigation (Concluded)

The first cut consisted of sawing out the center disc (Figure 16) to a diameter approximately 1.88" and a depth of 0.23" (just prior to breaking through the thickness). Strain data were recorded from all gages and are listed in Table III. The center disc was then removed and successive boring operations were made until the final hole size was achieved. As noted in Table III significant compressive residuals were introduced around the hole on the initial saw cut; however, they were successfully reduced to insignificant levels with the boring operation for final sizing.

Four rosette gages were bonded on the small specimen as shown in Figure 17. Prior to installation in the vice jaws on the machine, all gages were again zeroed and checked for zero drift. Strain data are listed in Table IV. An initial 1/8" diameter hole was drilled and strain data recorded from all gages. This was followed by a 3/16" diameter drilling operation and the successive boring operations until final hole size was reached. Again, the final residual stresses are insignificant. This investigation has demonstrated that the residual stresses after machining the holes in each specimen type were in fact a minimum and would not affect the experimental results.

A static tensile test was conducted to verify the results discussed above. This included instrumenting a super-scale specimen with strain gages and recording elastic-plastic strains from the gages as well as the transducer during loading. After loading, tensile coupons were cut from the specimen and stress-strain data recorded. A Neuber analysis of the resulting data is shown in Figure 18 which indicated a residual stress of approximately 15.0 ksi.

Subsequent to this test and analysis a second super-scale specimen was instrumented and tested. This repeat was run for several reasons; i.e., (1) transducer was not properly seated in the first test, (2) additional gages were installed on the hole side wall to check the transducer, and (3) the Neuber analysis was questionable. A sketch of the specimen and instrumentation locations is shown in Figure 19. Recorded data are tabulated in Tables V and VI.

It is significant to note in Table V that strain gages 3 and 4 located on the hole wall track very closely the transducer up to the point where the gages were lost. The X-Y plot of load versus deflection (inches) is shown in Figure 20. The specimen was loaded incrementally

TABLE III. RESIDUAL STRESS INVESTIGATION - SUPER-SCALE SPECIMEN

SPECIMEN CONDITION	STRAIN MEASUREMENT AT GAGE NUMBERS (μ in/in)											
	1	2	3	7	8	9	4	5	6	10	11	12
Free Standing (Unloaded)	0	0	0	0	0	0	0	0	0	0	0	0
Clamped Down Before Machining	-5	0	+10	+6	+3	-19	-2	-2	+15	+3	+3	-8
Saw Cut to .23" Depth	+53	+40	+37	+42	+45	+36	-285	-240	-215	-325	-285	-223
Center Disc. Removed (10 Mins. Later) Hole = 1.884" Dia.	+55	+53	+45	+45	+40	+32	-276	-237	-210	-323	-300	-226
After 1st Bore Hole Dia. = 1.9225							-74	-70	-67	-28	-53	-57
After 2nd Bore ① Hole Dia. = 1.9525							-95	-92	-80	-43	-64	-68
After 3rd Bore Hole Dia. = 1.9825							-137	-128	-114	-70	-90	-96
After 4th Bore Hole Dia. = 1.9920							-63	-67	-67	+2	-27	-47
After 5th Bore Hole Dia. = 1.9970							-6	-14	-22	+56	+23	-7
After 6th Bore Hole Dia. = 2.000							+30	+17	0	+34	+46	+20
Specimen Released (Free Standing)	+57	+57	+47	+47	+44	+35	+33	+20	-7	+32	+43	+24

NOTE ① Lapsed Time Between Boring Operations Was About 5 Minutes.

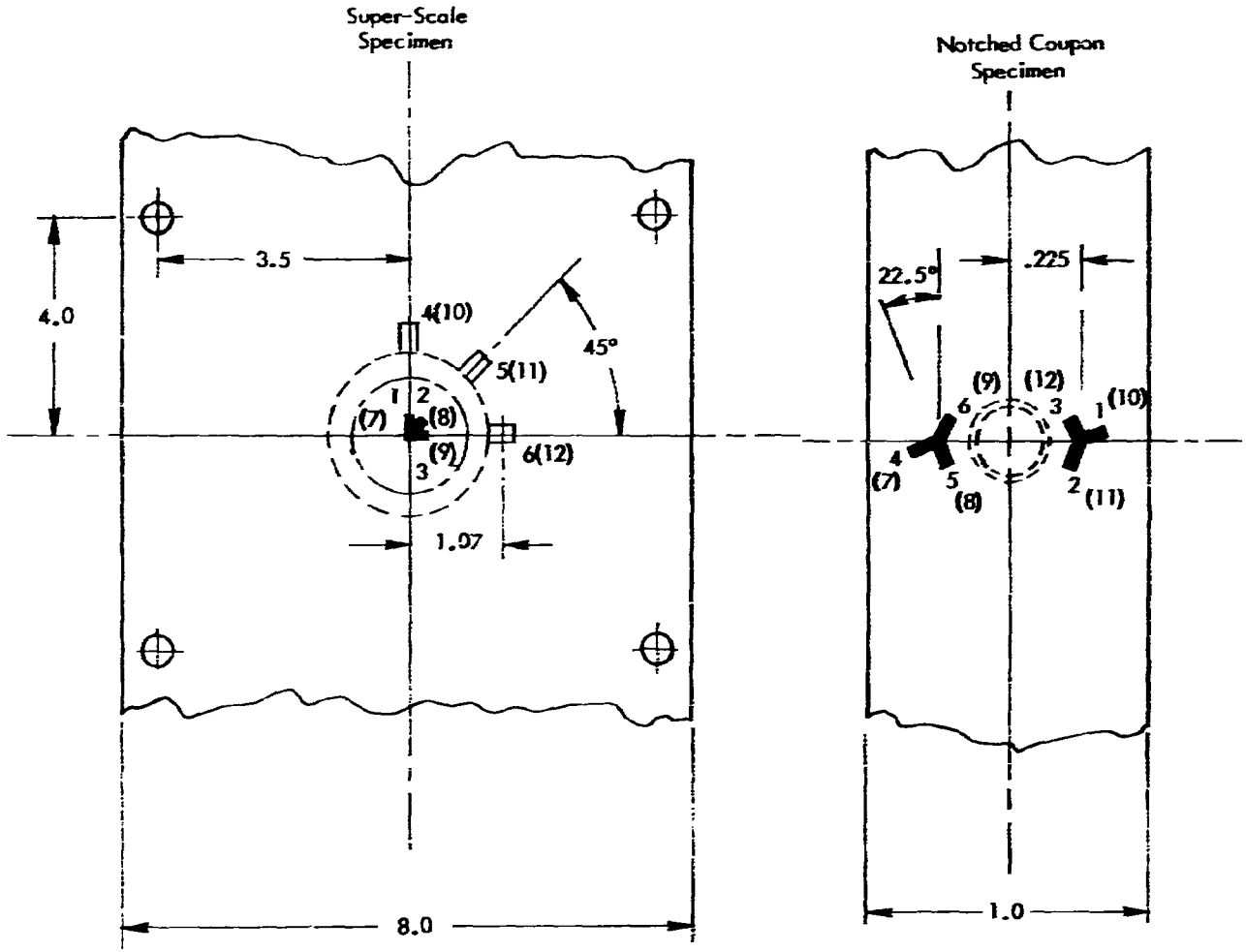

NOTE: Numbers in ( ) indicate gages on back side.

Figure 17 Strain Gage Locations – Residual Stress Investigation

TABLE IV. INITIAL RESIDUAL STRESS INVESTIGATION - SMALL SCALE SPECIMEN

SPECIMEN CONDITION	STRAIN (μ in/in) AT GAGE NOS. 1	2	3	4	5	6	7	8	9	10	11	12
Free (Unclamped)	0	0	0	0	0	0	0	0	0	0	0	0
Zero-Clamped In Machine	0	+5	+5	+3	+8	+10	+6	-4	-7	+2	-7	-8
Drilled Hole 1/8" Dia.	-20	+20	+20	-35	+30	+25	-15	-15	-13	-22	-22	-20
Drilled Hole 3/16" Dia.	-96	+39	+18	-160	+43	+25	-87	-10	+8	-150	-8	+12
1st Boring Dia. = 0.191	-50	+45	+20	-150	+50	+30	-74	-7	+3	-93	-17	-5
2nd Boring Dia. = 0.211	-20	+25	+22	-37	+27	+24	-17	-23	-17	-20	-20	-17
3rd Boring Dia. = 0.232	-25	+28	+25	-50	+30	+30	-22	-20	-15	-35	-23	-18
4th Boring Dia. = 0.241	-22	+25	+23	-45	+25	+26	-23	-23	-17	-30	-24	-20
5th Boring Dia. = 0.2475	-15	+28	+24	-40	+25	+24	-15	-22	-22	-26	-26	-26
6th Boring Dia. = 0.2505	-17	+27	+23	-40	+26	+25	-15	-22	-18	-25	-25	-25
Free (Unclamped)	-12	+8	+4	-32	+4	+8	-6	+5	+10	-20	+4	+5

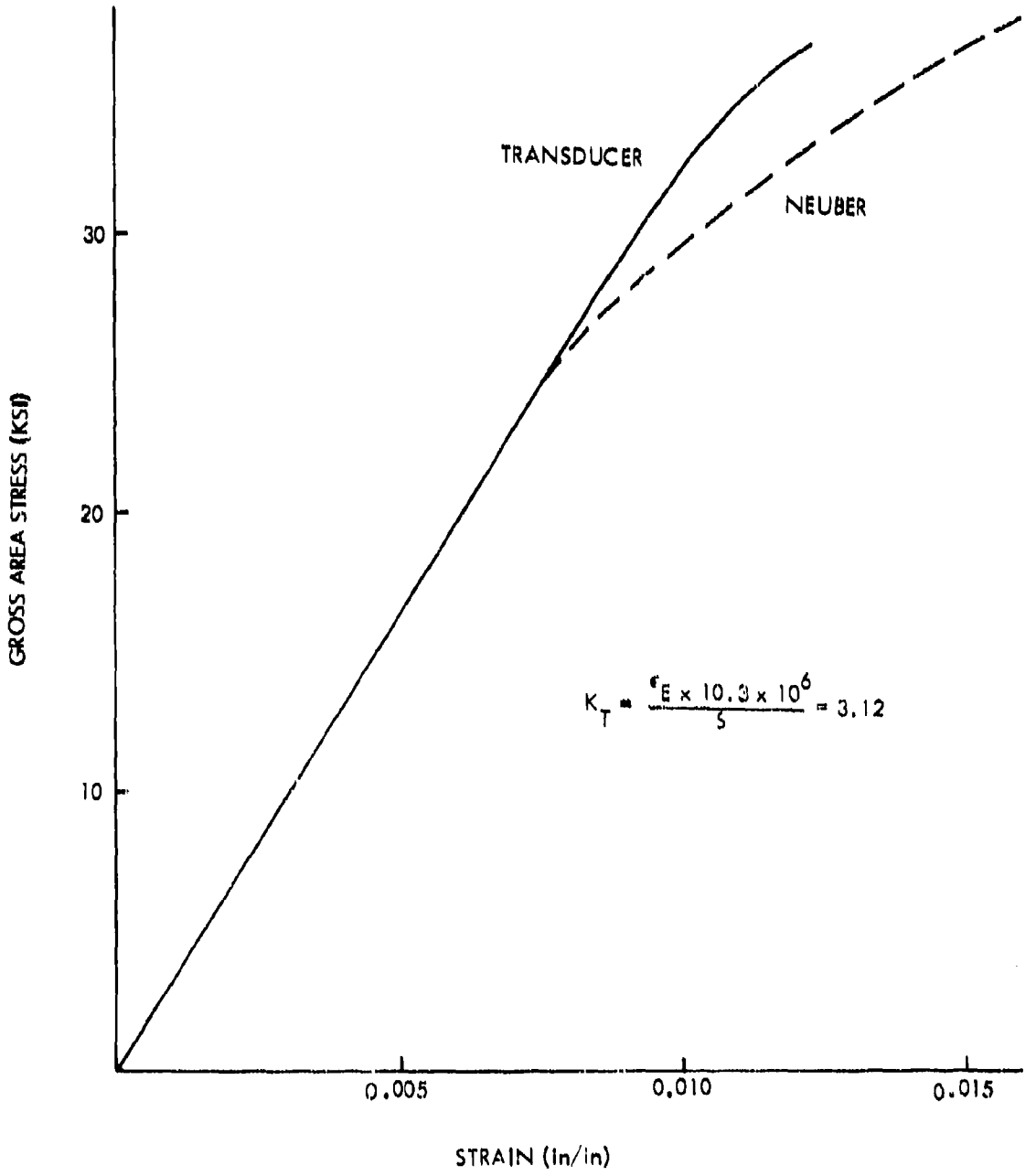

Figure 18. Transducer Strain vs. Neuber Analysis
1st Super-Scale Specimen

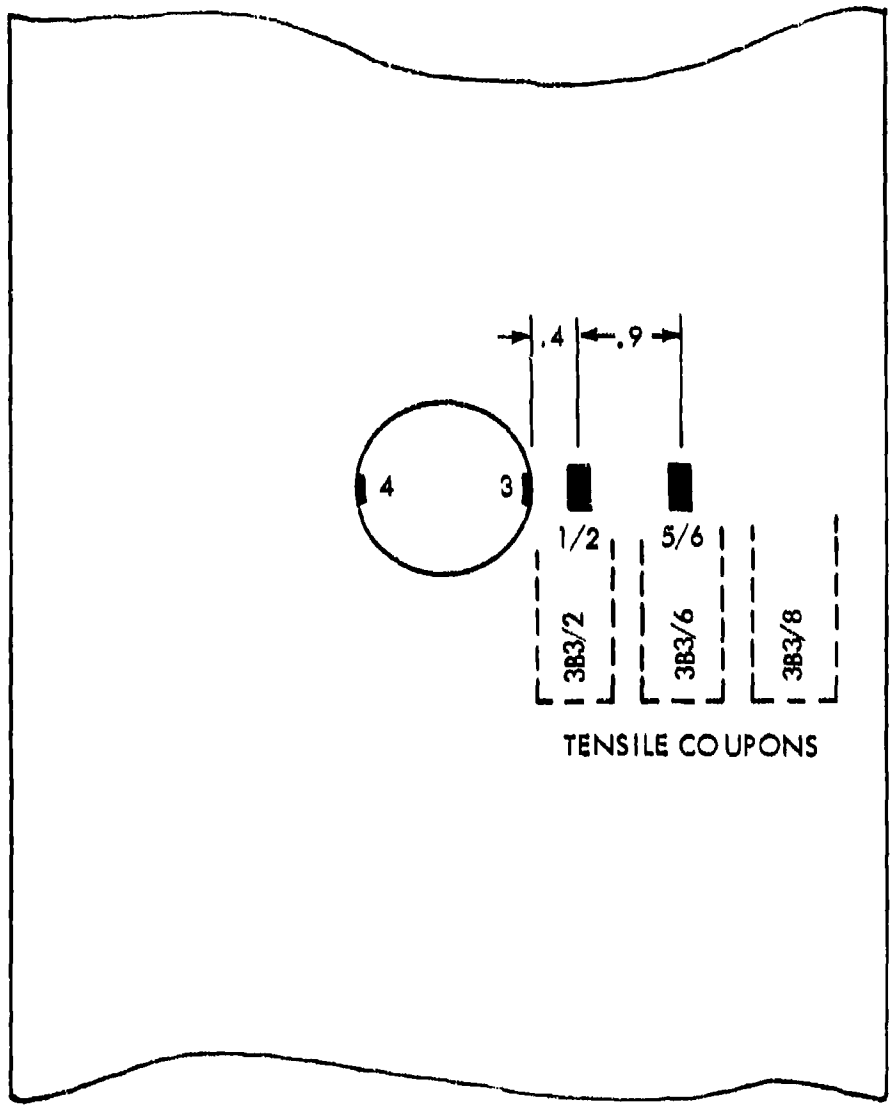

Figure 19 Strain Gage and Tensile Coupon Location
Second Super-Scale Specimen

TABLE V

RECORDED STRAIN VS LOAD DATA
SECOND SUPER-SCALE SPECIMEN

Load ($lb. \times 10^{-3}$)	Measured Strain * (in./in.)			
	Transducer	Gages 3/4	Gages 1/2	Gages 5/6
10	0.00148	0.00155	0.00078	0.00055
20	0.00321	0.00311	0.00156	0.00111
30	0.00494	0.00469	0.00235	0.00165
40	0.00667	0.00629	0.00315	0.00222
50	0.00840	0.00795	0.00394	0.00278
60	0.01086	0.0105	0.00479	0.00335
65	0.0126	Gages Out	0.00534	0.00364
69	0.0140		-	-
70	-		0.00593	0.00394
73	0.0157		-	-
75	-		0.00673	0.00426
77	0.0180		-	-
77.5	-		0.00711	0.0044
80	-		0.0077	0.00457
Zero	0.0074		0.00135	0.000088

* Average of two strain gages.

TABLE VI

TENSILE TEST DATA - SECOND SUPER SCALE SPECIMEN

	Spec. 3B3/8		Spec. 3B3/6		Spec. 3B3/2	
Load	Stress	Strain	Stress	Strain	Stress	Strain
1500	11720	0.00116	11720	0.00116	11810	0.00116
3000	23440	0.00232	23440	0.00236	23620	0.00234
4500	35160	0.00354	35160	0.00360	35430	0.00356
6000	46880	0.00478	46880	0.00476	47240	0.00476
7500	58590	0.00596	58590	0.00596	59060	0.00596
9000	70310	0.00726	70310	0.00732	70870	0.00728
9300	72660	0.00760	72660	0.00766	73230	0.00768
9600	75000	0.00828	75000	0.00836	75590	0.00826
9750	76170	0.00946	76170	0.00956	76770	0.00974
9900	77340	0.01486	77340	0.01466	77950	0.01614
10000	78120	0.0228				

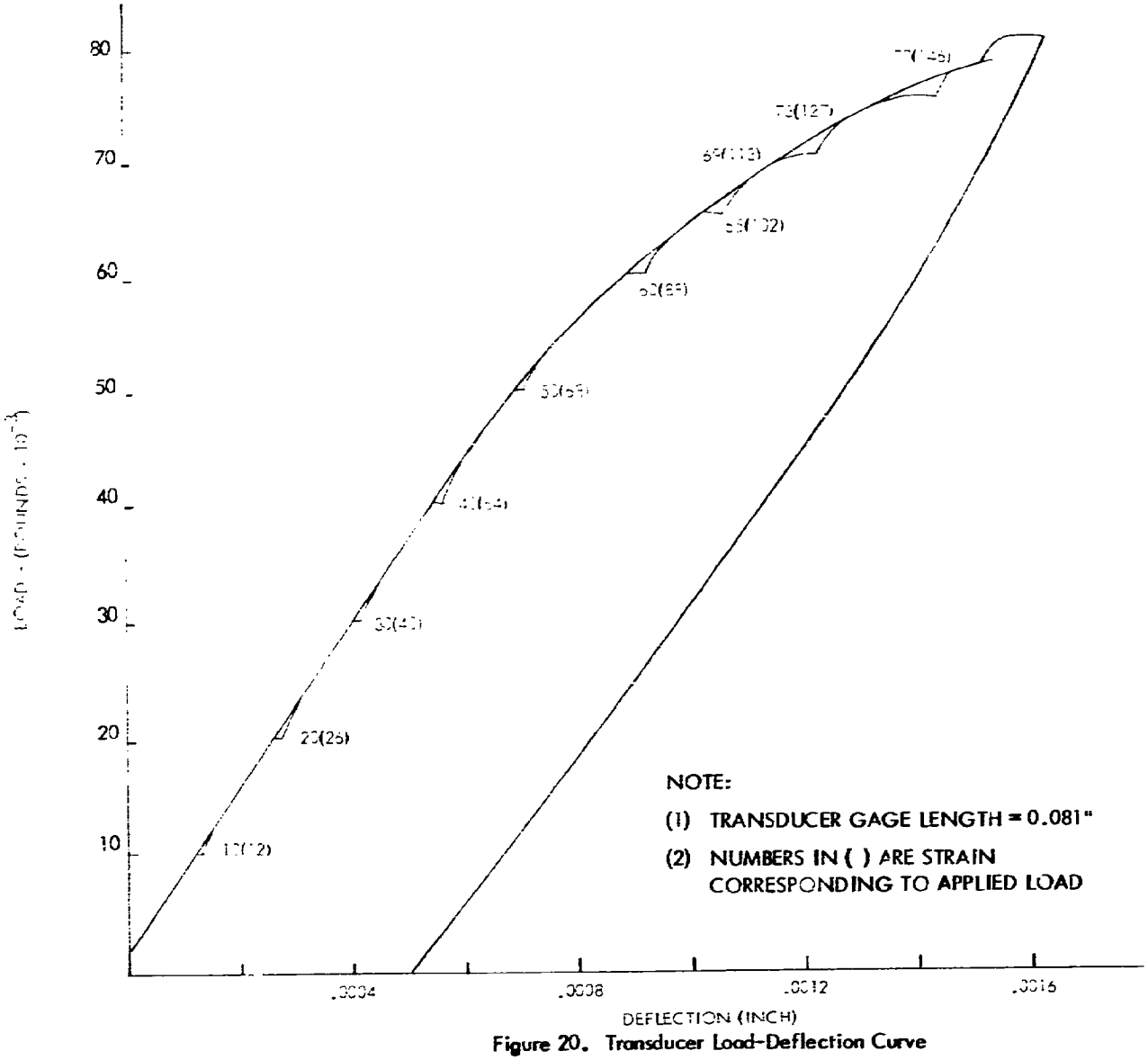

Figure 20. Transducer Load-Deflection Curve

in order to read data from the strain gages and at each incremental load the transducer recorded specimen creep, as illustrated in the figure. This creep occurred within the first few seconds after reaching the desired load level and no further creep was evident while the data was being recorded. The data tracked the elastic-plastic surface when the next load level was applied. At the conclusion of this static test, three one-half inch wide tensile coupons were machined from the super-scale specimen and tested to obtain stress-strain data. In this instance, sufficient load-deflection data were recorded to reproduce a stress-strain curve to 0.022 in/in strain. These data track the stress-strain data shown in Figure 3.

A Neuber analysis of the data was run using this stress-strain curve and the data compared with that from the transducer. As was seen earlier, this analysis indicated significant residual stresses around the hole. The Neuber analysis was then modified to include residuals and the data compared with the transducer measurements. The assumptions for this modification are illustrated in Figure 21. Results of this analysis indicate a 20 ksi residual at the hole as shown in Figure 22. The Neuber analysis was run for residuals of 0, -10, and -20 ksi and, as shown, the -20 ksi analysis correlates with the transducer strains.

Initially, it was assumed that there were residual stresses around the hole as evidenced by the analyses shown in Figures 18 and 22. However, a previous analysis at Lockheed, for an infinite plate with a central hole, using finite element methods of analysis and the Neuber analysis had shown similar trends for zero residual stress. This analysis is shown pictorially in Figure 23. The Neuber analysis deviates from the finite element analysis in much the same manner as the data analysis from the super-scale specimens. Further, the finite element analysis, of a similar geometry, closely approximates the transducer response.

It was concluded that there are in fact minimum residual stresses at the hole and that the Neuber analysis must be modified to accurately predict the stress-strain history at the stress riser in a centrally notched hole. A finite element analysis of the super-scale specimen was then run to determine correlation with the transducer response. This analysis is reported in detail in Section IV.

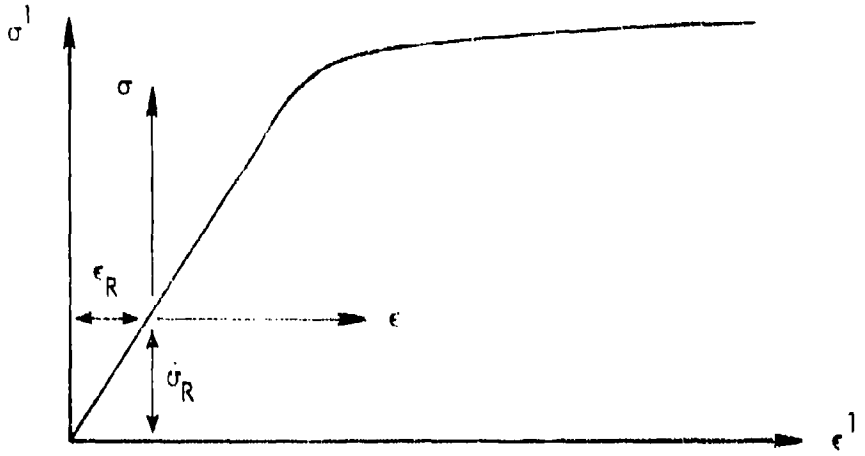

σ^1, ϵ^1 TRUE NOTCH STRESS & STRAIN

σ_R, ϵ_R RESIDUAL NOTCH STRESS & STRAIN

σ, ϵ NOTCH STRESS & STRAIN RESULTING FROM A FAR FIELD STRESS 'S'

NEUBER'S RULE STATES

$$K_t^2 = K_\sigma K_\epsilon = \frac{\sigma}{S}\,\frac{\epsilon}{S}\,E = \frac{(\sigma^1 - \sigma_R)}{S}\,\frac{(\epsilon^1 - \epsilon_R)}{S}\,E$$

IF THE RESIDUALS ARE ELASTIC

$$\epsilon_R = \frac{\sigma_R}{E}$$

$$(K_t S)^2 = (\sigma^1 - \sigma_R)\,(E\,\epsilon^1 - \sigma_R)$$

Figure 21. Residual Stress Calculations Using Neuber's Rule

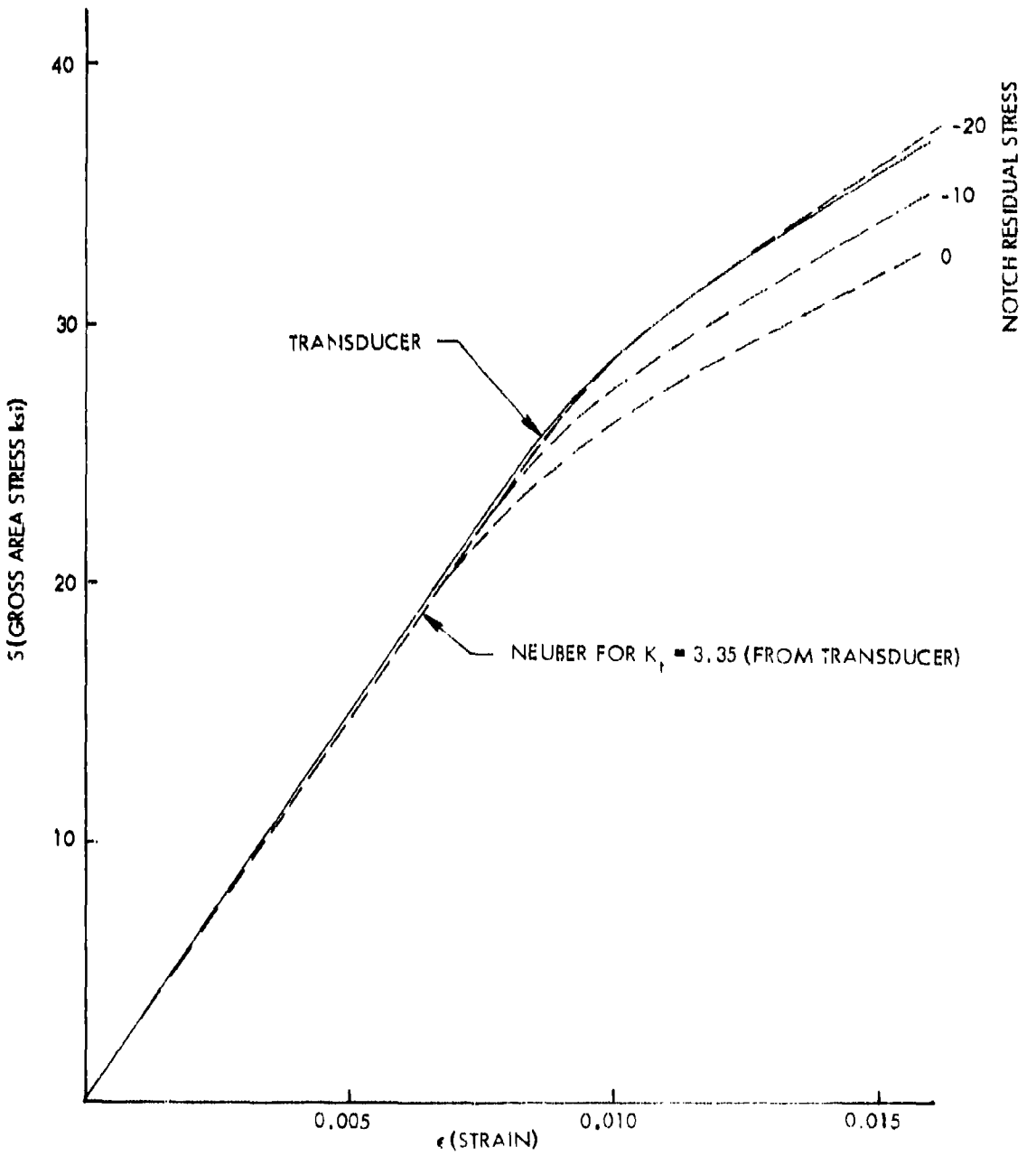

Figure 22 Neuber Analysis 2nd Super-Scale Specimen

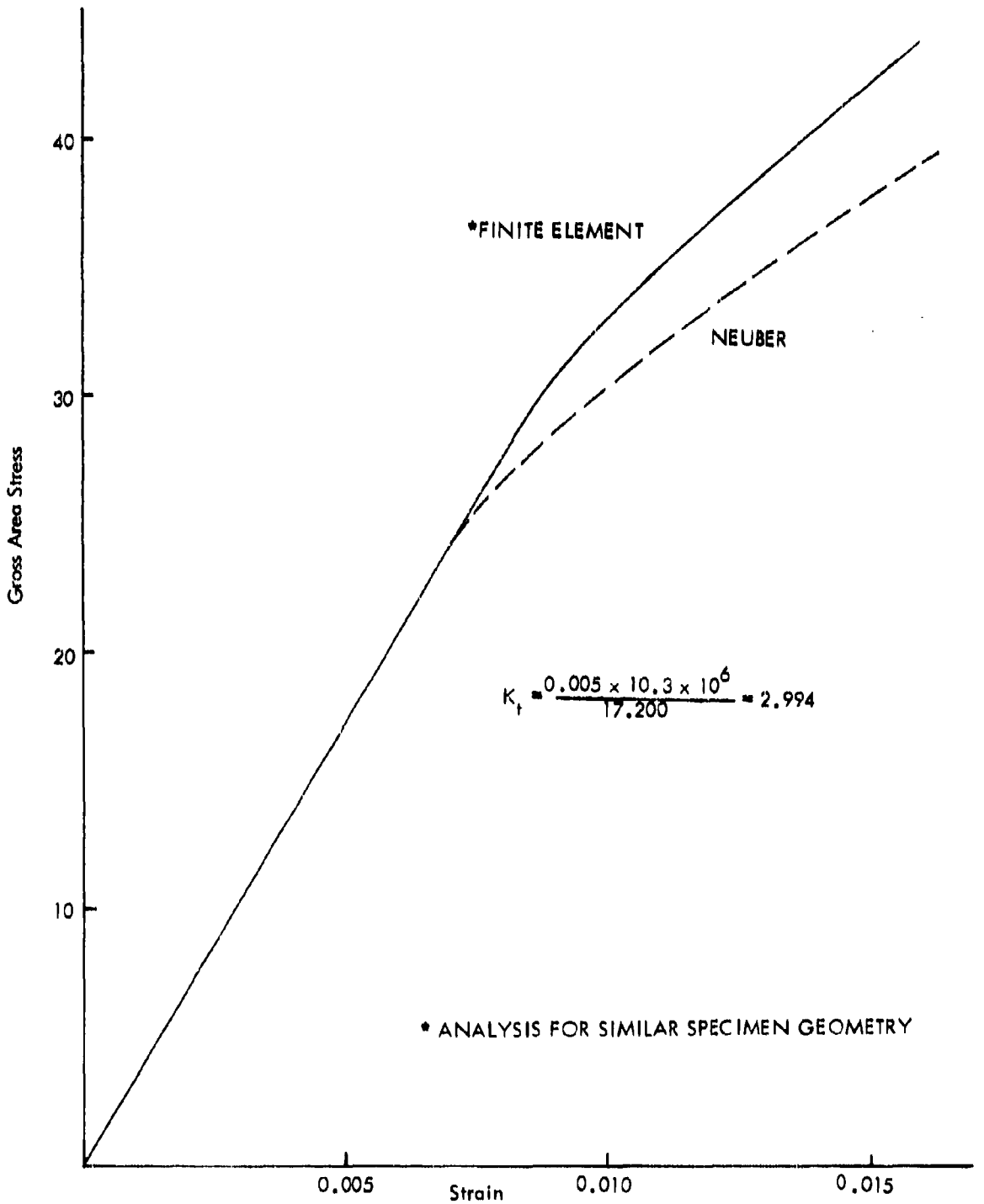

Figure 23. Comparison Of Neuber And Finite Element Analysis

3.4 EXPERIMENTAL TECHNIQUES

The following paragraphs discuss the test techniques used, details of the strain transducer, and the strain data recording system.

3.4.1 Small Scale Notched Coupon Tests

A quantity of small coupon specimens were cut from the test material and machined to the configuration shown in Figure 13. These specimens were tested at room temperature in an electro-hydraulically controlled closed-loop servo system, interfaced to a computerized two channel load programmer. In order to maintain consistency throughout the test program all specimens were laterally supported during fatigue loading. All small scale notched coupon fatigue test data are reported in paragraph 3.5.1.

3.4.2 Super Scale Tests

The super scale test specimens were cut from the test material and identified in relation to the sheet of material used and the precise location within the sheet. The specimen configuration is shown in Figure 12. All tests were done in an electro-hydraulically controlled closed-loop servo system, interfaced to the same computerized two-channel load programmer that was used for the small scale notched coupon tests. An aluminum alloy frame fixture was attached to each specimen to provide lateral support during compression loading. A typical test arrangement is shown in Figure 24. The strain transducer description, calibration procedures, strain measurement and recording details are discussed in sections 3.4.3 and 3.4.4.

Two super scale specimens were tested at +160°F. The test setup was similar to that used for the room temperature tests and heating was provided by "Briskheat" heating tape, wrapped around the support fixture as shown in Figure 25. The specimen and end fittings were then wrapped with many layers of glass-cloth in order to confine the low level of heating to the specimen. A low heating level was necessary to prevent damage to the strain gages on the transducer. Copper-constantan thermocouples were attached to the specimen with aluminum-foil tape. Two thermocouples were used, both were located 0.40-inch from the hole wall with one on the centerline of the specimen length and the other 90° apart on the centerline of the specimen width. Power input to the

Set-up for Room Temperature Test

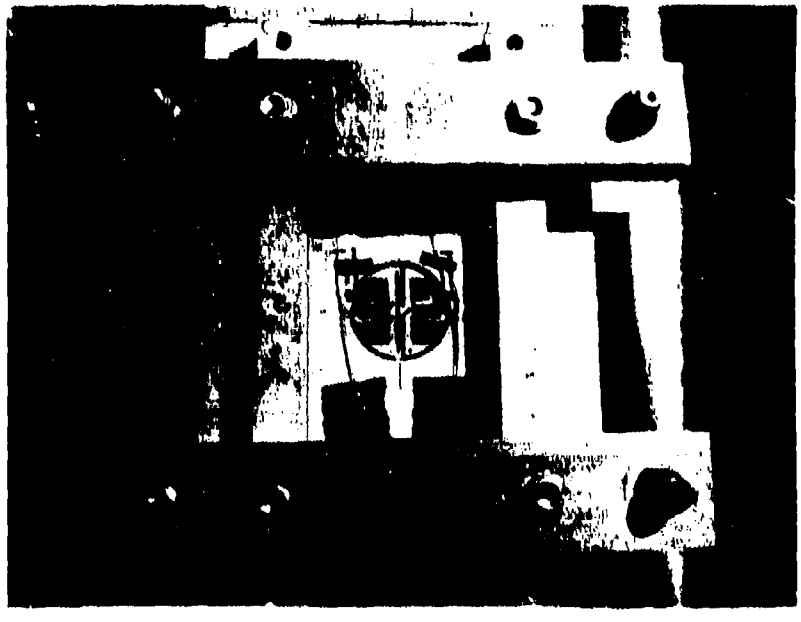

Specimen with Support Fixture In Place

Figure 24 Typical Room Temperature Test Arrangement for Super-Scale Specimens

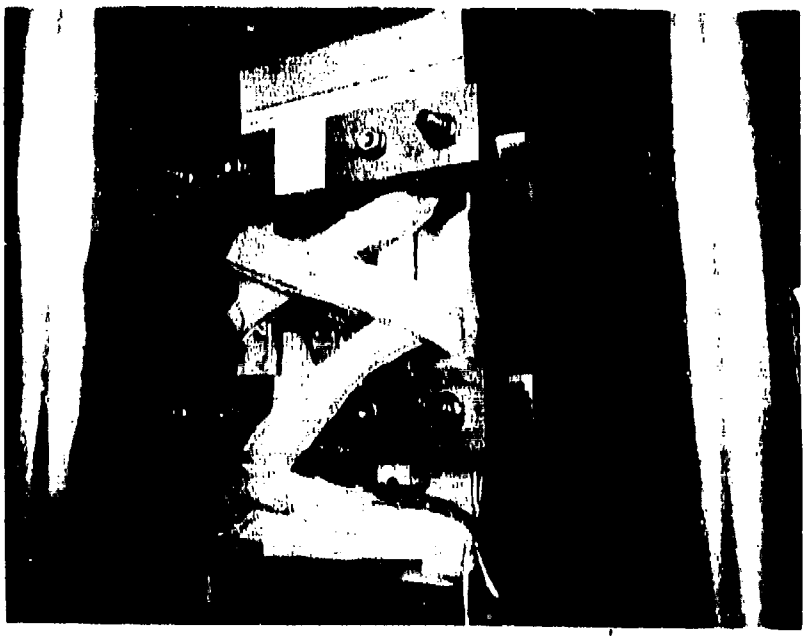

Super-Scale Test Specimen
Wrapped with Heater Tape

Glass Cloth Wrap

Figure 25. Elevated Temperature Test Set-Up

heating tape was controlled by a manually operated autotransformer and specimen temperature was monitored on a multichannel strip chart recorder. The elevated temperature test setup is shown in Figure 25.

3.4.3 Strain Measurement

Strain measurements were made on all super scale specimens with a specially developed strain transducer that was located in the specimen 2.0-inch diameter hole. The transducer is shown in Figure 26, and was fabricated from 0.125-inch thick 7075-T6 aluminum sheet material. The design is based on a NASA self-supporting strain transducer, Reference 4, and allows measurement of large strain changes under repeated loading. A pair of surface contact pins (1 & 2) are held in intimate contact with an area of high stress concentration (3) by spring pressure acting diametrically in the hole. Pin (1) is held rigidly while pin (2) is held by a flat cantilever spring beam (4), instrumented with electrical resistance strain gages. As load is applied to the test specimen a change in strain causes the gage length (distance between pins 1 and 2) to change. The movement of pin (2) relative to pin (1) then causes the spring beam (4) to deflect which in turn produces an electrical output from the strain gages. Applied load also causes dimensional changes to the hole diameter which then changes the stress level in the spring beam (4). It can be seen from Figure 26 that a vertical displacement of pin (2) will create a loading moment to the spring beam (4) and produce additional changes in output from the strain gages. This unwanted output is cancelled out (or nearly so) with a suitably attenuated and opposing strain output from a secondary spring beam (5). The transducer has two sets of contact pins and also two strain gaged cantilever spring beams. The gage length of the transducer contact pins is approximately 0.080 inches and the output from the spring beams are combined to produce an average strain measurement over the measured average gage length of the contact pins. The strain transducer output is then amplified and conditioned before passing through a special data logger system, described in Section 3.4.4.

Sudden specimen failure was likely to disturb the calibration of the highly sensitive transducer, therefore calibrations were performed prior to each test. Each calibration was performed in a certified Tinius Olsen calibrator equipped with a specially designed mounting attachment for the transducer as shown in Figure 27. The attachment consisted of two plates with each plate having a semi-circle cut into it on one side. Each plate was attached to the calibratory column (one on the movable part and one on the fixed

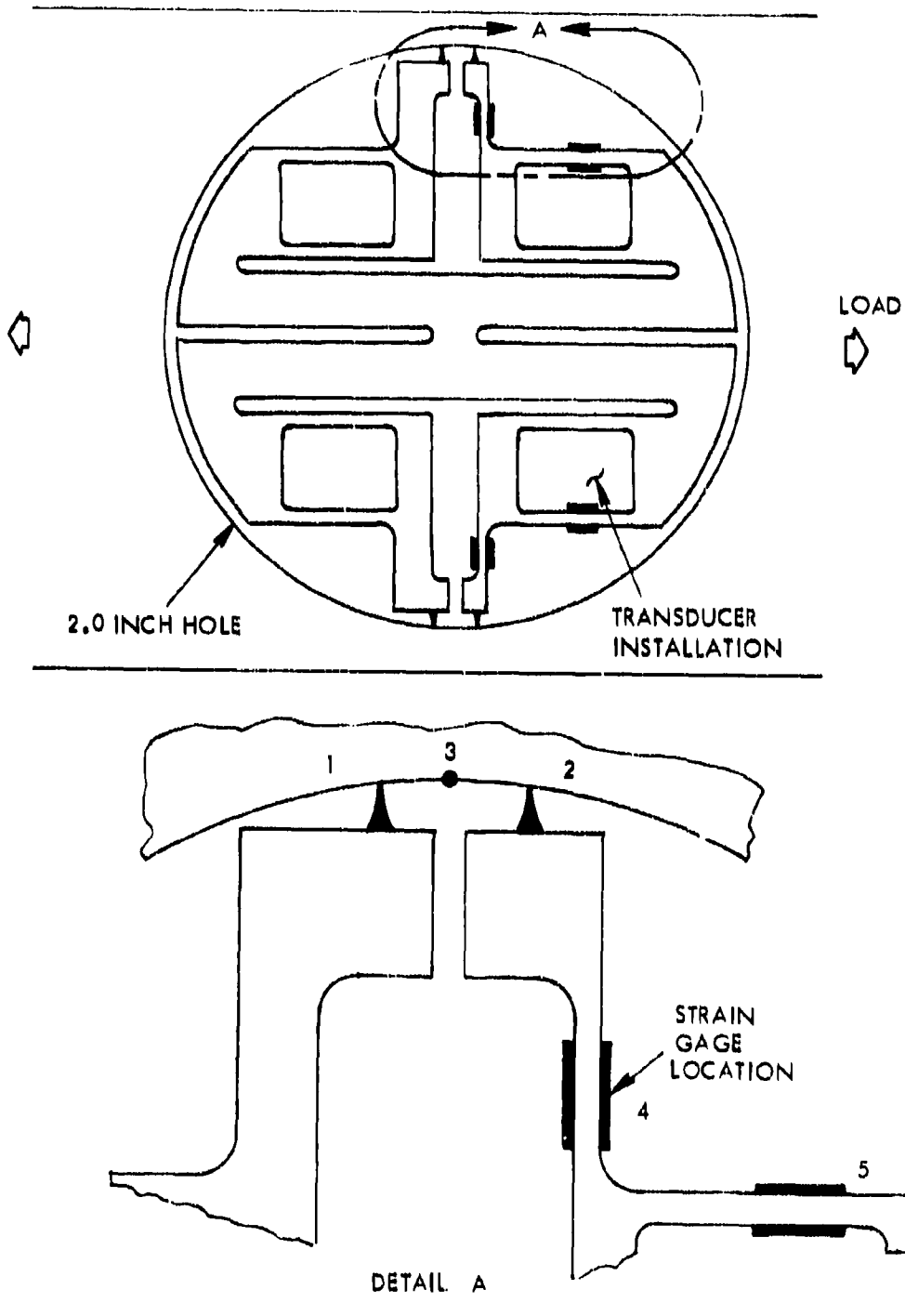

Figure 26. Strain Transducer

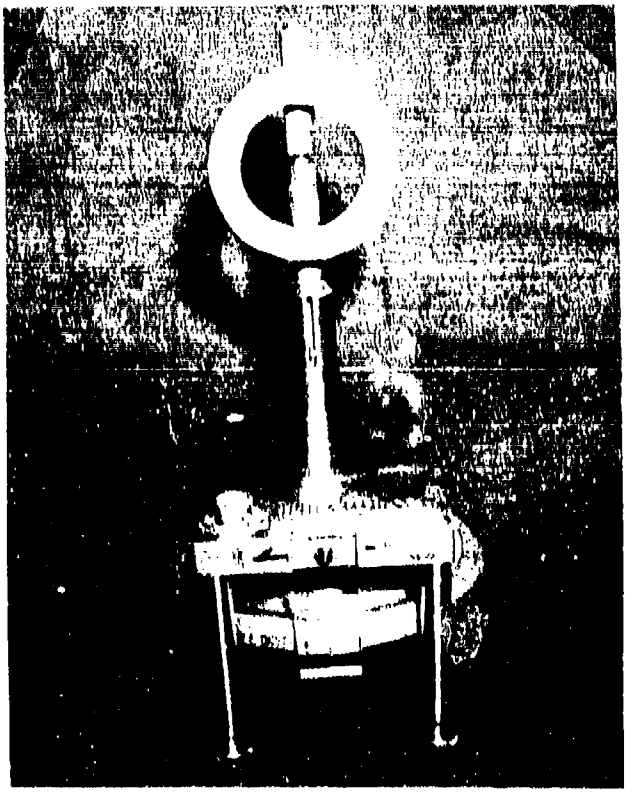

Figure 27. Tinuis Olsen Calibrator With Mounting Attachment

part) such that the two semi-circular cutouts formed a complete circle of 2.0-inch diameter. Movement of the micrometer screw on the calibrator would displace the movable column and change the diameter of the circle. The transducer was mounted in the circle and calibrated to establish strain gage output for known contact pin displacement as shown in Figure 28 and also for known diametric changes by repositioning the transducer as shown in Figure 29. In addition to the pretest calibration, provision was made for performing periodic calibrations as required during test. This was achieved by switching in a fixed shunt resistor having a value that was related to a known transducer displacement. This relationship was also established during the pretest calibration of the transducer.

After calibration the transducer was carefully positioned in the specimen hole and the four contact pins were "bedded-down" by applying light pressure to the free end of each pin. A binocular microscope, equipped with a calibrated filar eyepiece was then used to accurately measure the contact pin gage lengths from which an average value was determined.

3.4.4 Continuous Strain Recording

Continuous strain monitoring was achieved with a peak data logger system. A block schematic diagram of the system is shown in Figure 30, it consisted of a two-channel multiplexer, 12 bit analog to digital converter, 8 bit microprocessor, and 7 track digital incremental tape recorder.

High level load and strain inputs were fed into the system but only the positive and negative peaks were detected. The strain peaks were compared with previous data and if the current strain peak data had deviated by more than a pre-selected percentage from the last recorded peak data, the new strain and corresponding load peak values were logged on the recorder along with an event number. The event number was computed by counting total cycles applied. During programmed hold periods the system recorded load and strain data whenever the latest strain data deviated from the last recorded data by more than the pre-selected percentage. In this case the event number was determined by counting the elapsed time in seconds from the beginning of the hold period. The pre-selected percentage for data collection or rejection in the system was intended to allow collection of only those

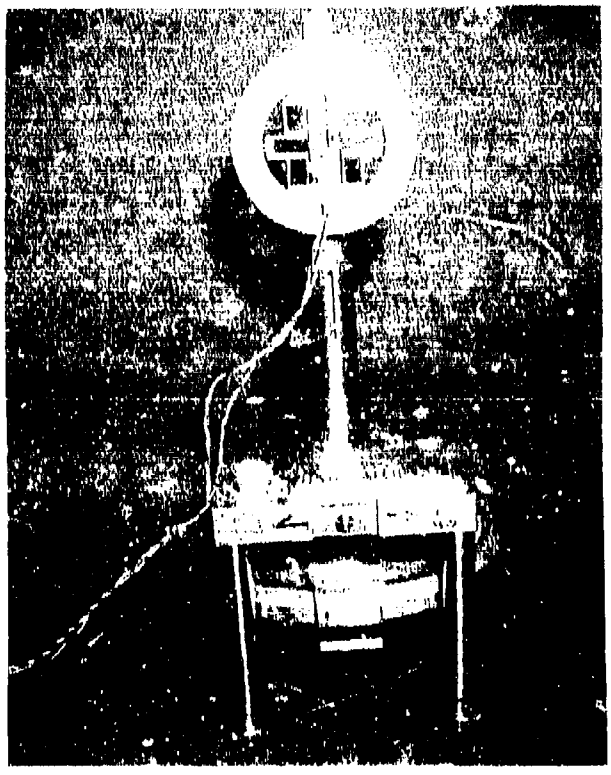

Figure 28 Calibrator with Transducer Mounted to Measure Normal Displacement

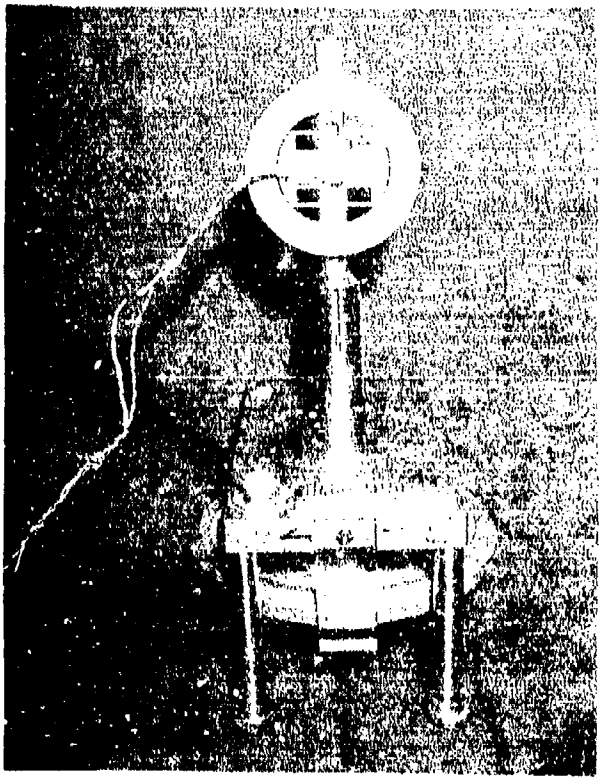

Figure 29 [illegible]

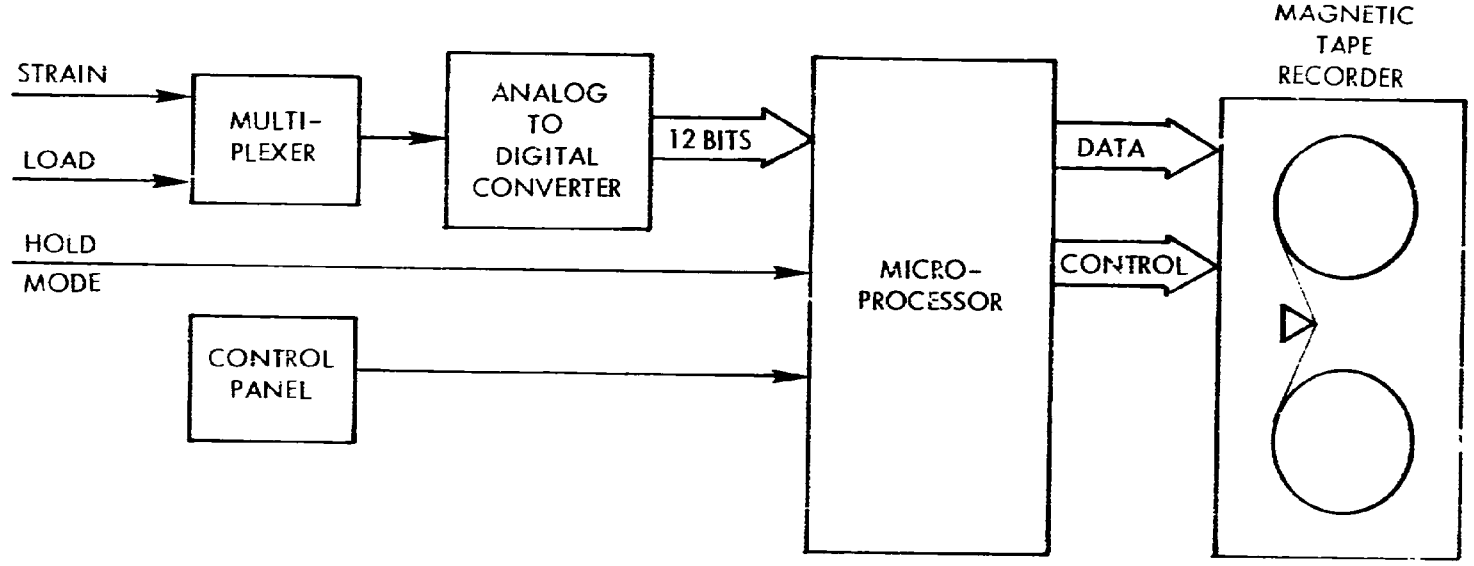

Figure 30 . Block Schematic Diagram of Data Collection System

data having significance. Testing was accomplished under load control which in general is accurate to ± one percent. Data recording, however, was under strain control, and a ± one percent change in load for some cases would produce a greater percentage change in strain. Generally, the pre-selected percentage was set to allow changes in strain of ± 110 microinches or greater to be recorded on the magnetic tape.

3.5 COMPLEX SEQUENCE TESTS

The load-time-temperature test sequences discussed in Section 3.1 and illustrated in Figure 1 were applied to thirty super-scale and 18-notched coupon specimens. Twenty-seven of the super-scale specimens and all of the coupons were tested to failure. Three super-scale tests were to evaluate cyclic and time dependent creep only and were not tested to failure. Failure data, strain histories, crack growth data, and fractographic analyses are presented in the following paragraphs. Data analysis and correlation studies are included in Section V.

3.5.1 Data Presentation

(a) Failure Summary

A summary of the fatigue data for the super-scale and notched coupon tests is included in Tables VII and VIII. The super-scale summary includes sequence, specimen identification, cycles to failure, cycles to crack initiation, and for convenience in comparing data sets, the test conditions for each sequence are included. Refer to Figure 1 for a complete description of each sequence. The residual strength data in Table VIII is from static tension tests after cyclic loading when fatigue runout was encountered. Cycles to crack initiation for the super-scale tests is an accurate indication of the onset of macroscopic cracking and was measured from a change in the magnitude of strain recorded with the transducer. In all cases, these strain changes were apparent before a crack was visually observed. In these tests, failure is defined as complete fracture of the specimen or fracture from the hole to one edge.

This series of tests was started with Sequence 1 to simply define the stress-strain state at the stress riser and time to failure for constant amplitude cycling. Then in successive steps the test complexity was increased by adding overloads, underloads, and periods of sustained loadings. The intent was to determine relative effects of sequence variation and to measure and quantify strain relaxation and/or creep.

TABLE VII - SUPER-SCALE TEST SUMMARY

Sequence Number	Test Conditions	Specimen Ident. Number	Cycles to Failure	Crack Initiation
1	Constant Amplitude, S_{mean} = 15.8, S_V = 10.6	2F-1	47,647	
2	1 Hr. @ 47.3 Ksi, CA	2B-1	668,277	
3	24 Hr. @ -7.9 Ksi, CA	2E-1	27,280	
4	24 Hr. @ -15.8, CA	3C-4	41,776	
5	1 Hr. @ -7.9 Ksi, CA	3E-4	30,137	
6	+47.3, N_{OL} = 15000 CA	3E-2	1,977,450	No Failure(1)
7	+47.3, N_{OL} = 1,000 CA	1F-1	1,028,090	
8	+47.3, -7.9, N_{OL} = 15,000 CA	2C-2	715,180	712,000
9	+47.3, -15.8, N_{OL} = 15,000 CA	1B-3	166,932	159,000
10	+47.3, -7.9, N_{OL} = 1,000 CA	2E-4	308,616	
11	+47.3, -15.8, N_{OL} = 1,000 CA	2E-2	129,259	
12	+47.3, -25, N_{OL} = 15,000 CA	2F-2	64,249	60,000
13	+47.3, 24 Hr. @ -7.9, N_{OL} = 15,000 CA	1E-1	141,329	140,500
14	+47.3, 1.0 Hr. @ -7.9, N_{OL} = 15,000 CA	3B-1	336,755	
15	+47.3, 24 Hr. @ -15.8, N_{OL} = 15,000 CA	1A-1	113,591	111,700
16	+47.3, 24 Hr. @ -7.9, N_{OL} = 1,000 CA	1C-3	101,316	
17	+47.3, 1.0 Hr. @ -7.9, N_{OL} = 1,000 CA	3B-4	153,756	
18	+47.3, 24 Hr. @ -15.8, N_{OL} = 1,000 CA	1F-2	129,750	
19	+47.3, 1.0 Hr. @ -15.8, N_{OL} = 1,000 CA	2B-2	63,090	
20	+47.3, 24 Hr. @ -7.9, N_{OL} = 15,000 CA, + 160°F	1E-3	114,196	

TABLE VII - SUPER-SCALE TEST SUMMARY (Concluded)

Sequence Number	Test Conditions	Specimen Ident. Number	Cycles to Failure	Crack Initiation
21	+47.3, 1.0 Hr. @ -7.9, N_{OL} = 15,000 CA, + 160°F	3C-2	148,518	
22	+47.3, -32.5, N_{OL} = 15,000 CA	1B-1	45,006	41,500
23	+47.3, -32.5, N_{OL} = 1,000 CA	2B-4	31,062	
24	+47.3, -32.5, 1.0 Hr. @ +15.8, N_{OL} = 15,000 CA	1B-4	40,547	39,000
25	+47.3, -32.5, 1.0 Hr. @ 15.8, N_{OL} = 1,000 CA	2F-4	28,056	
26	-50, N_{OL} = 15,000 CA	1F-3	32,382	
27	-50, 1.0 Hr. @ +15.8, N_{OL} = 15,000, CA	1F-4	27,880	

(1) Specimen did not fail. Tensile residual test run and specimen failed at 79.4 ksi.

TABLE VIII - NOTCHED COUPON TEST SUMMARY

Sequence Number	Specimen Ident. Number	Cycles To Failure		Residual Strength (1)
1	2E-2	103,620		
	2E-3	270,910		
	3B-1	96,290		
		156,940	Ave.	
6	1E-1	1,606,590	NF	85.9 Ksi
	3B-2	2,387,950	NF	84.6 Ksi
	3E-2	1,763,820	NF	83.5 Ksi
8	1E-2	368,523		
	1E-3	1,435,400	NF	83.3 Ksi
	2E-4	997,333		
		933,752	Ave.	
14	1E-4	398,280		
	3B-4	745,326		
	1B-3	506,061		
		549,889	Ave.	
22	3A-1	45,006		
	3A-2	48,611		
	3A-3	37,232		
		43,616	Ave.	
24	3E-4	49,698		
	1F-1	40,864		
	3A-4	43,714		
		44,759	Ave.	

(1) Residual strength tests run on specimens which did not fail in fatigue.

Several pertinent data trends are evident from the data in Tables VII and VIII.

(1) Application of initial tension overloads and/or periodic tension overloads significantly increases the specimen fatigue life as compared to the baseline constant amplitude testing. The single one-hour sustained overload in Sequence 2 does not produce the same magnitude of increase in life as the periodic overloads in Sequences 6 and 7, however. Both the notched coupons and super-scale specimen for Sequence 6 were cycled in excess of 1.5-million cycles with no failure and showed no reduction in tensile residual strength when tested statically.

(2) Initial compression underloads, either sustained and/or repeated periodically, result in reducing the baseline constant amplitude life. This is illustrated in Sequences 3-5 and 26 and 27.

(3) A compressive underload immediately following a tensile overload tends to negate the beneficial residual stresses resulting from the applied overload alone. By including the -7.9 Ksi underload immediately following the 47.3 Ksi overload the life was reduced approximately seventy percent from the case with an overload only (Sequences 7 and 10). In general, the fatigue life decreases as the magnitude of the underload increases. This trend is shown in the comparison of data from Sequences 8, 9, 12 and 22 for cyclic periods between overloads (N_{OL}) of 15,000 cycles. The same trend for N_{OL} = 1000 cycles is shown in Sequences 10, 11, and 23.

The trends discussed in (1) through (3) have been reported by other investigators; however, qualitative stress-strain data has not been available to model these trends and this program was run to attempt to obtain this necessary experimental data. This will be discussed in more detail in subsequent paragraphs.

(4) Including a sustained load hold period immediately following the compressive loading results in a further life reduction. For example, comparing Sequences 8 and 13 shows a life reduction by a factor of 5 with the hold period included. The reduction

is not as pronounced with hold periods at -15.8 Ksi, however. There is some life reduction for the 24-hour hold period when N_{OL} = 15,000 cycles (Sequences 9 and 15) but no change for N_{OL} = 1000 cycles (Sequences 11 and 18). A sustained 24-hour hold at -7.9 Ksi, which is typical for a transport wing on-ground, has substantially negated the beneficial effects which were introduced by the tensile overload. This time dependent relaxation/creep is a crucial part of understanding and modeling notched specimen fatigue life. A further study of this phenomena was done in test Sequences 28 and 29 which are discussed in subsequent paragraphs.

Hold times at the flight mean (15.8 Ksi) did not show an effect in either increasing or reducing specimen life. This can be seen in comparing Sequences 22,24 and 23,25.

(5) In general, sequences with N_{OL} = 1,000 cycles resulted in shorter test lives than identical sequences with 15,000 cycles between overloads. This is illustrated in a comparison of Sequences (6, 7), (8, 10), (9, 11), (14, 17), etc. Only one sequence pair (15 and 18) violates this trend. The reduced life may be attributed to the magnitude of each major cycle (-7.9 to 47.3 Ksi) repeated more frequently with the shorter N_{OL} period, but conclusive data to this effect has not been developed. On the other hand, Potter, in Reference 3, has shown that the trend with decreasing periods between overloads is an increased life. The data here appears to contradict Potter's data; however, there is insufficient data here to show this is the case. Additional overload periods should be evaluated to better establish a data base for analytical modeling. There may be cyclic relaxation around the stress riser which also contributed to the increased life with the longer overload period.

(6) For Sequences (13, 14), (16, 17), and (20, 21) the 24-hour hold period resulted in a shorter life than the sequence with the one hour hold period. It was noted in (4) that each sequence with sustained loading at -7.9 Ksi resulted in significant life reductions compared to sequences without the sustained load period. This data is an indication of creep following the plastic deformation at the stress riser due to the tensile overloads. At -15.8 Ksi the trend is reversed; i.e., the shorter hold period results in a shorter life as in Sequences 18 and 19. At -7.9, there is much less variation in life with and without the -15.8 sustained load than there is with the -7.9 load as pointed out in (4).

No conclusions have been drawn about the -15.8 Ksi data and additional tests should be run to evaluate the trends here.

An additional study of the creep at -7.9 Ksi was run and these data are reported in paragraph 3.5.2.

(b) Load - Strain Histories

The strain response for the transducer was continuously recorded during each test sequence. These data have been plotted as time histories for typical sequences in Figures 31 through 43. Maximum and minimum notch strains are illustrated for the major overload/underload cycles along with the upper and lower strain limits for the constant amplitude cycling. Each major cycle is identified by number. Mean strain was only recorded before and after each block of constant amplitude cycles and a dashed line is shown connecting these two data points. The constant amplitude limits are shown as a dash mark at the beginning, mid-point, and end of each block of cycles. All of the data shown were recorded over an 0.080 gage length inside the central hole in the super scale specimens and are considered typical of the data recorded.

Several trends are obvious from these time histories. For example, in each sequence there is a change in the recorded mean strain during the blocks of constant amplitude cycling. Also, the major load cycles, overloads and underloads, affect a change in the mean strain. There is a minimum change in the peak strain during any sequence and little change in the constant amplitude peak strain until underloads of -25 ksi or larger are applied. The more significant time dependent changes which appear are the changes in the mean strain, minimum constant amplitude strains, and the minimum strain associated with the underloads. These are more pronounced with increasing underload also.

It was pointed out earlier, that the sequences with 1000-block cyclic periods resulted in shorter test lives than the sequences with 15,000 cycle blocks. Sequences 9 and 11 (Figures 32 and 33) are typical of the data recorded for fifteen-and one-thousand cycle block tests. There is a greater rate of change in the mean and minimum strains for Sequence 11 (1000 cycles) which may offer some insight into explaining this phenomena.

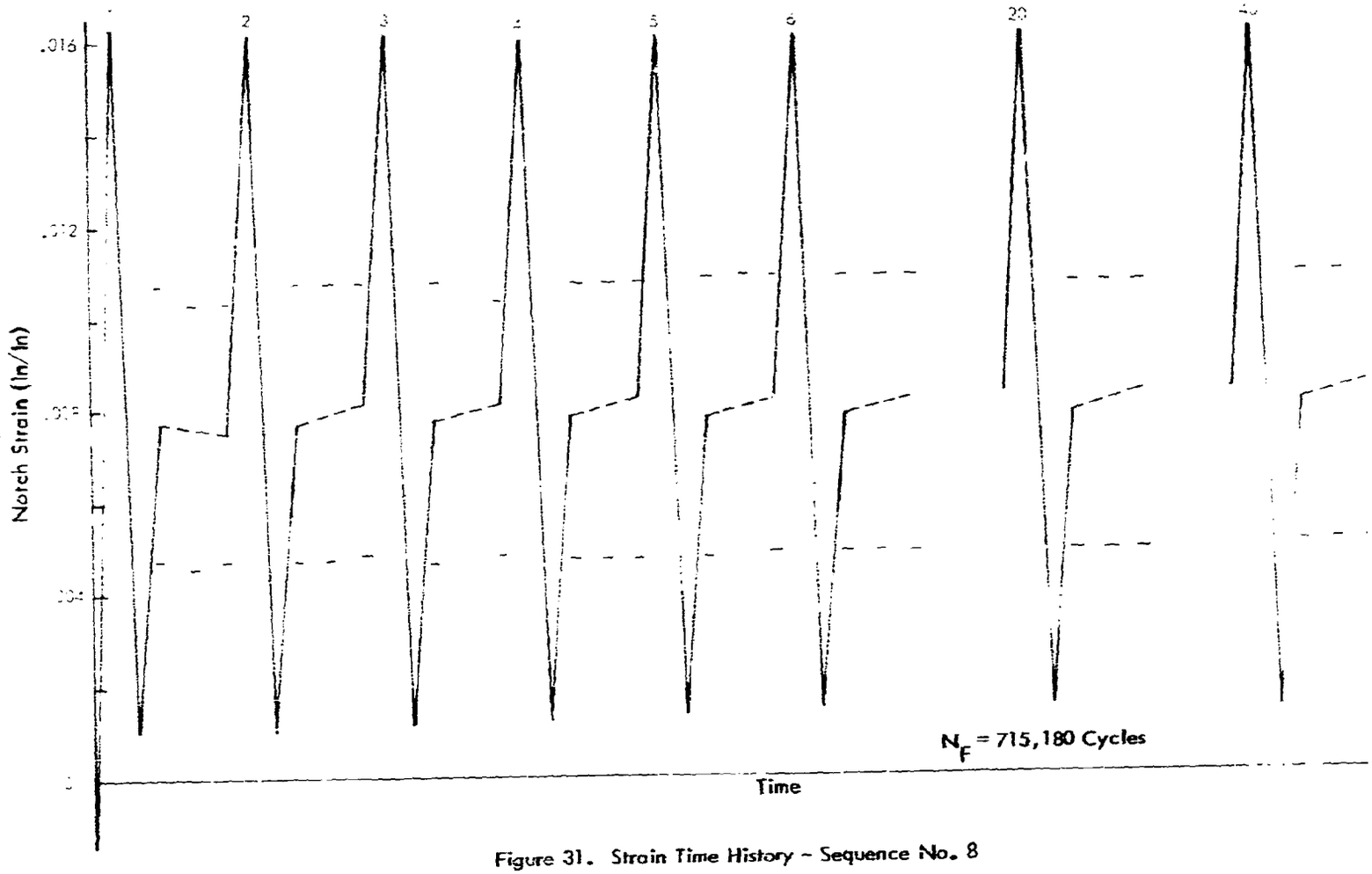

Figure 31. Strain Time History - Sequence No. 8

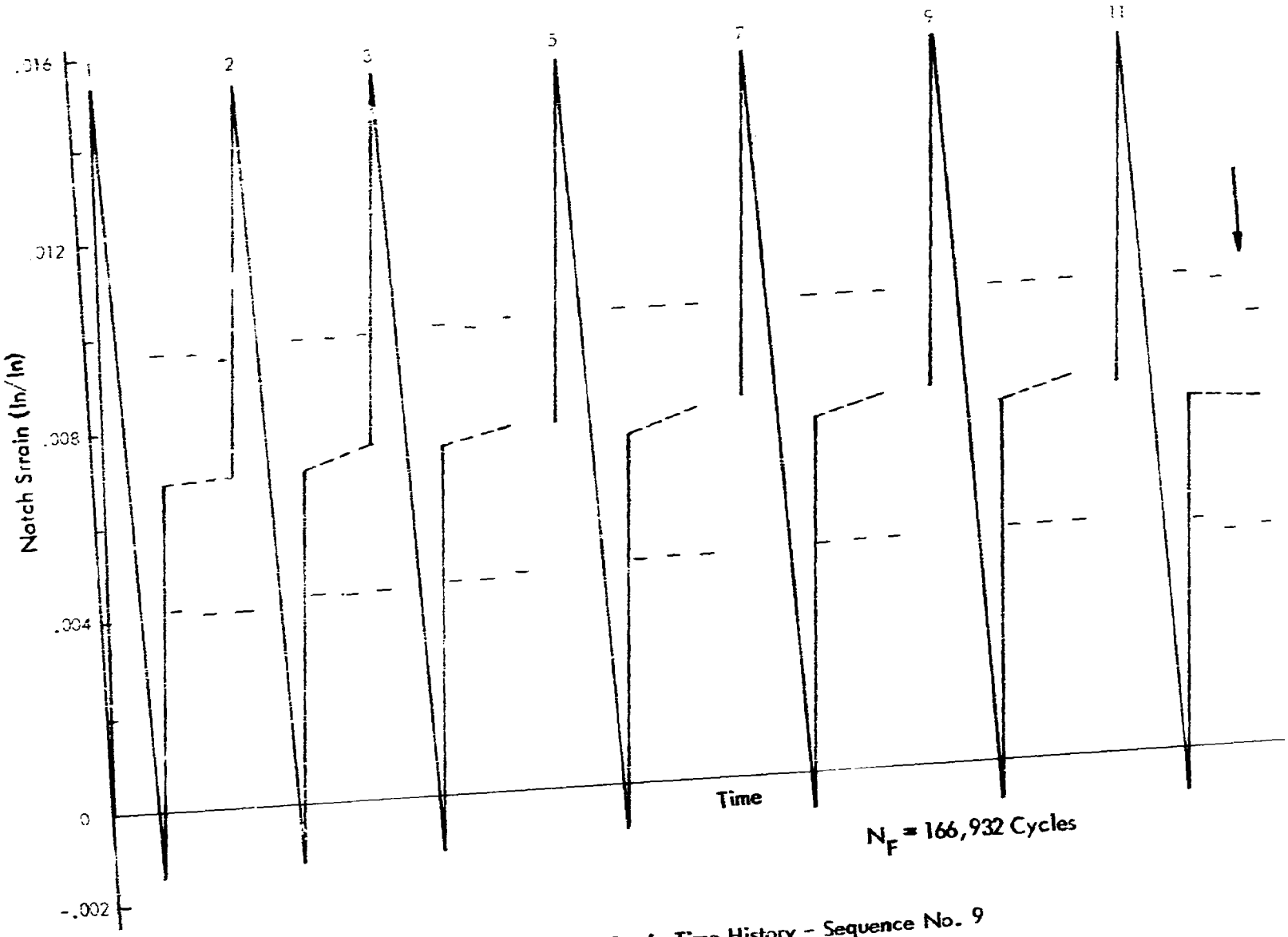

Figure 32. Strain Time History - Sequence No. 9

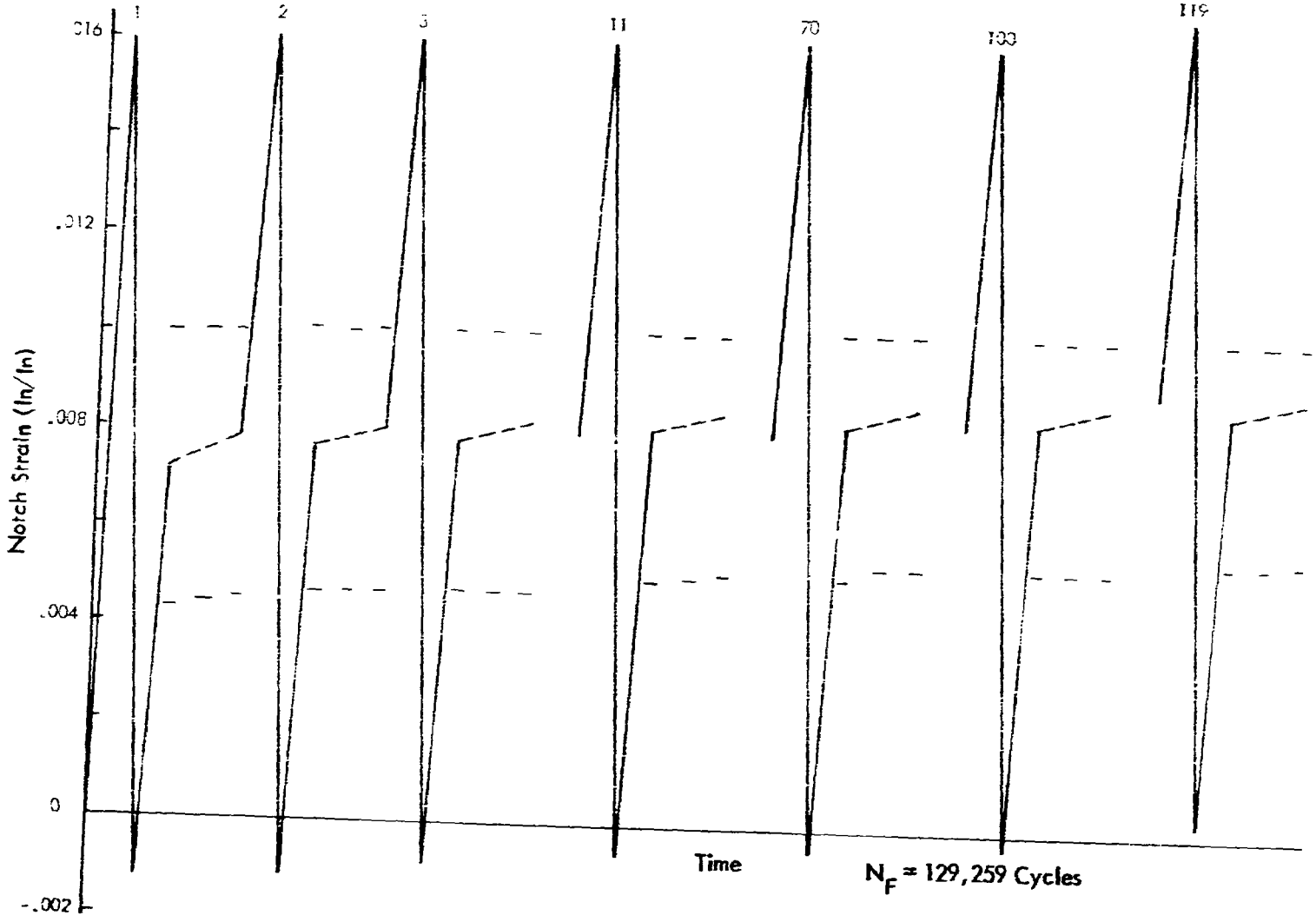

Figure 33. Strain Time History – Sequence No. 11

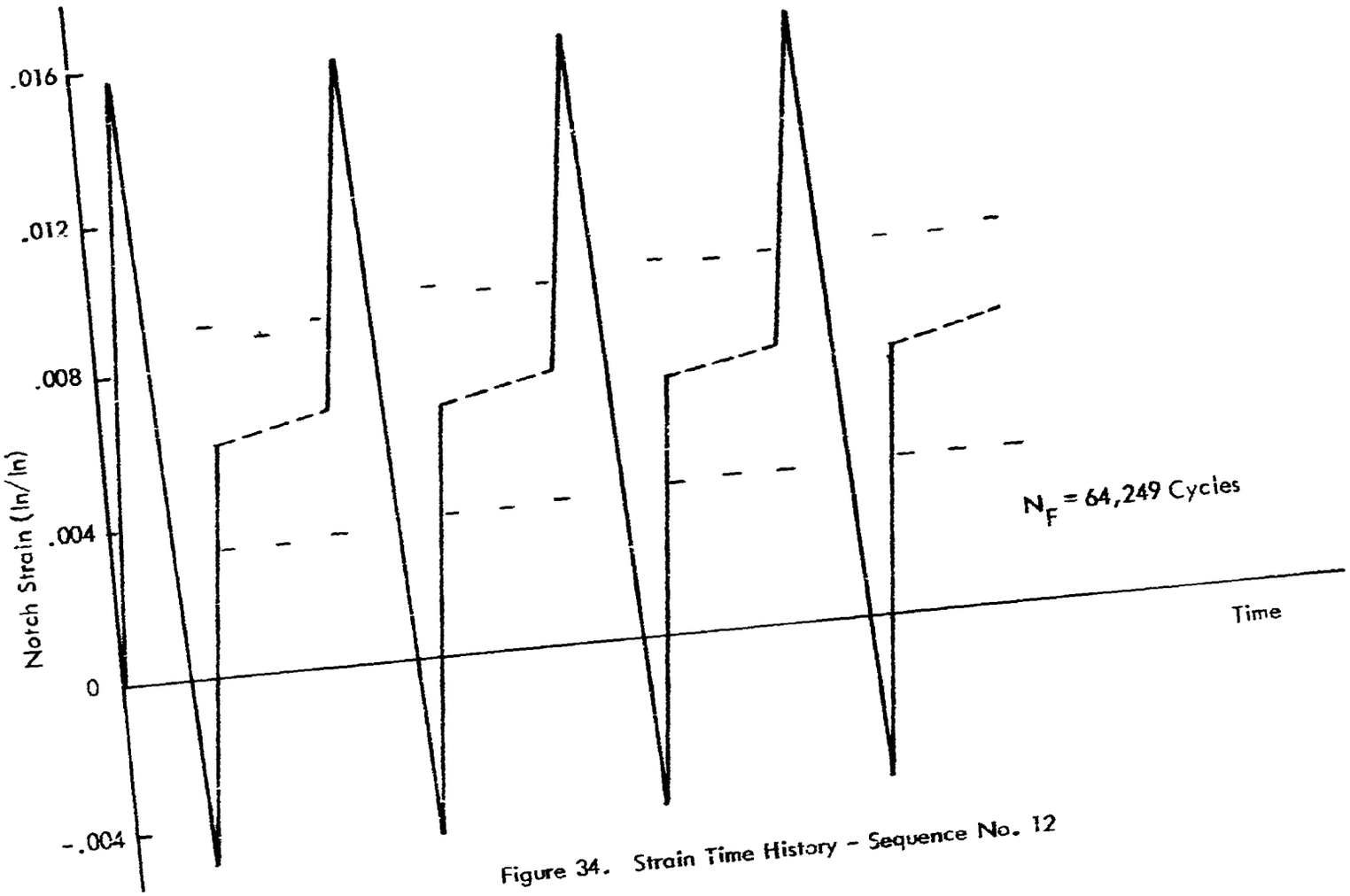

Figure 34. Strain Time History - Sequence No. 12

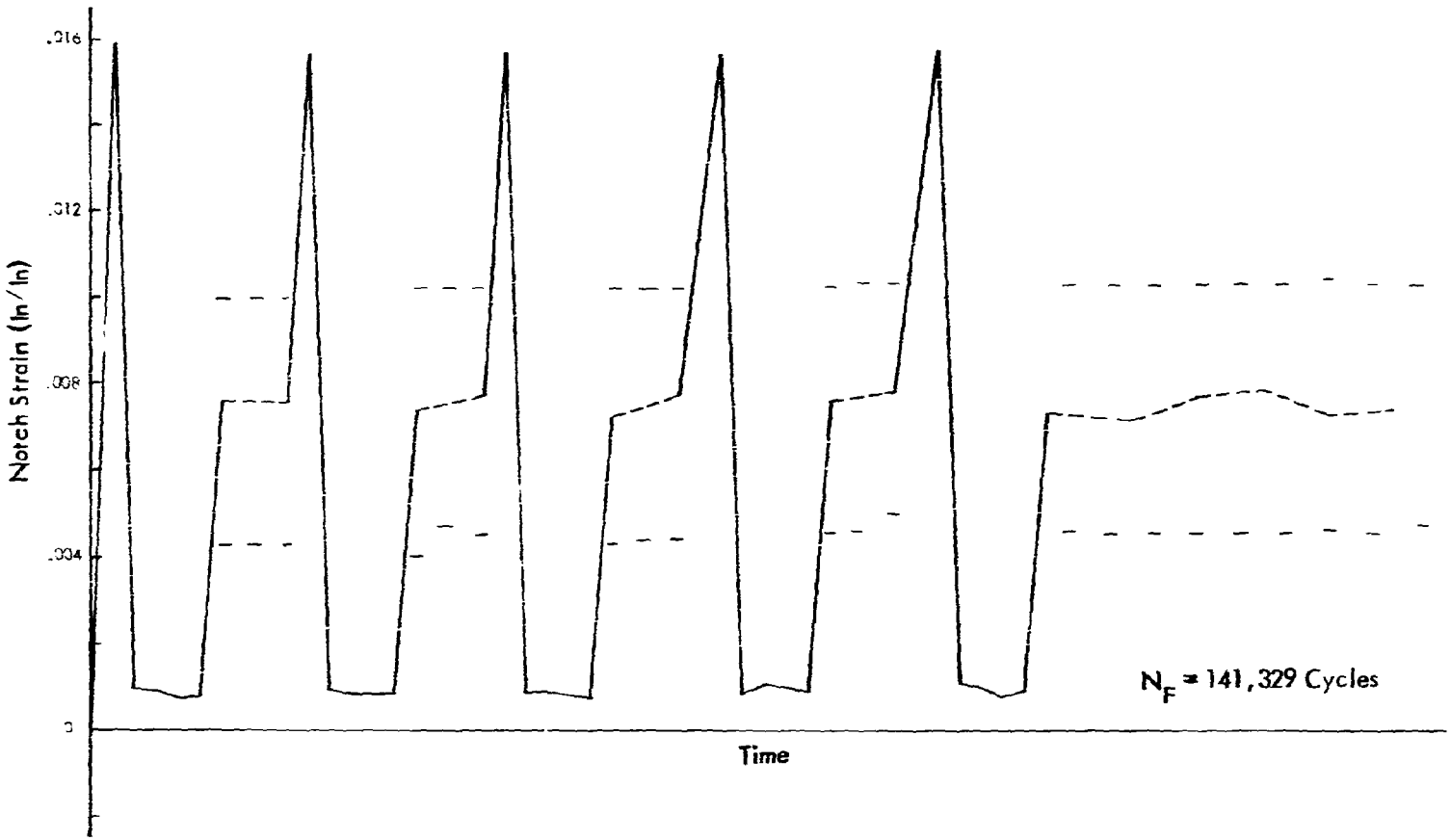

Figure 35. Strain Time History - Sequence No. 13

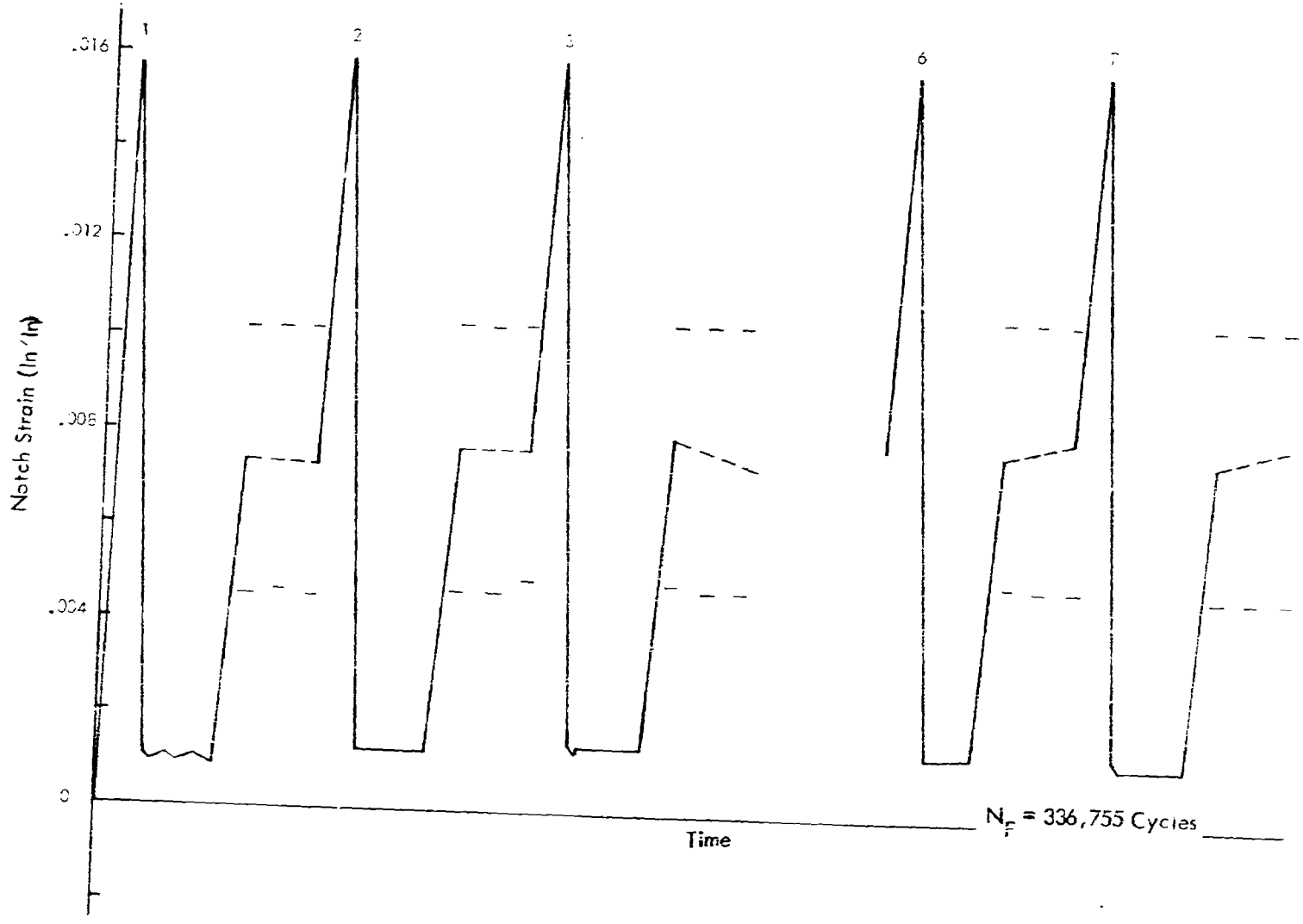

Figure 36. Strain Time History - Sequence No. 14

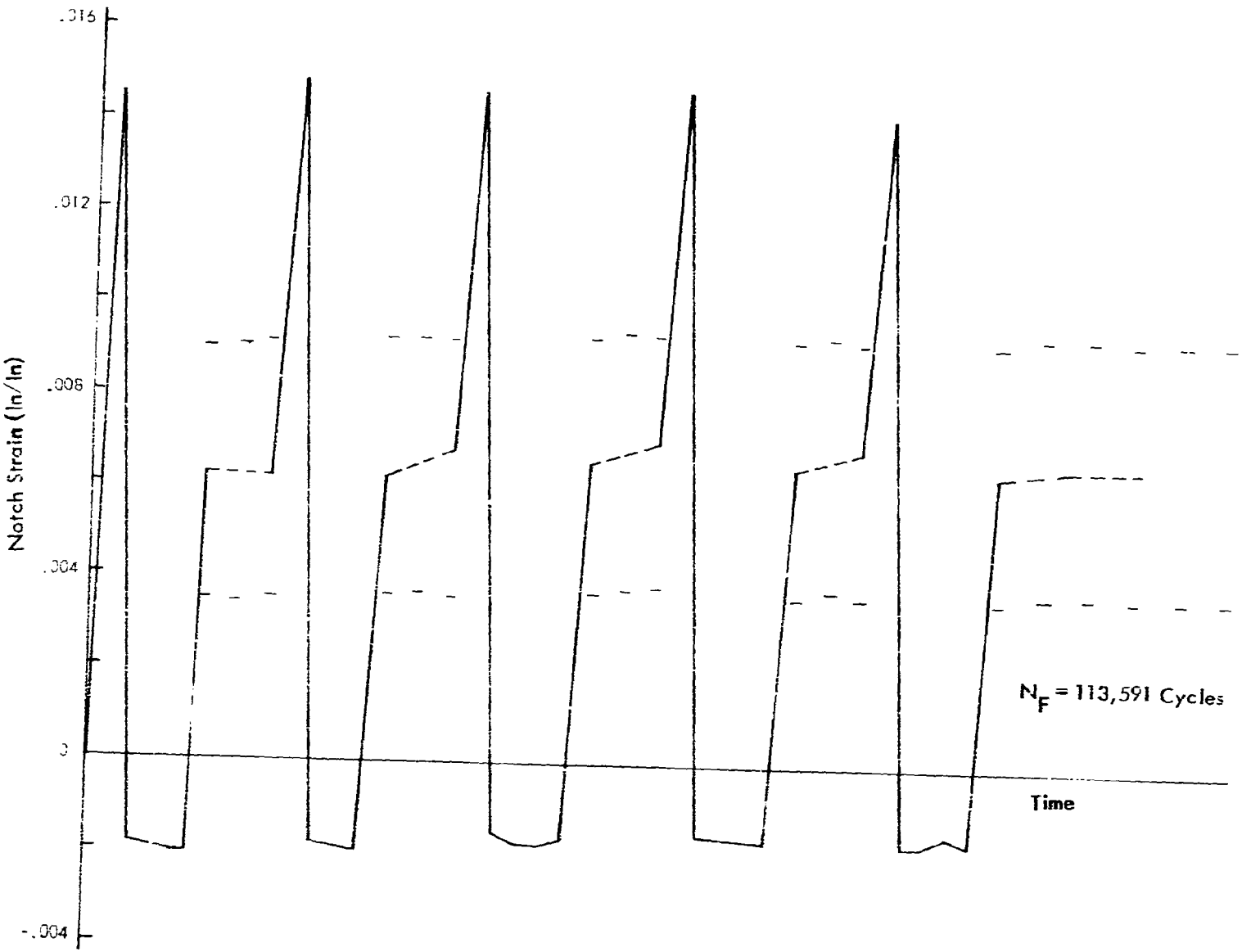

Figure 37. Strain Time History - Sequence No. 15

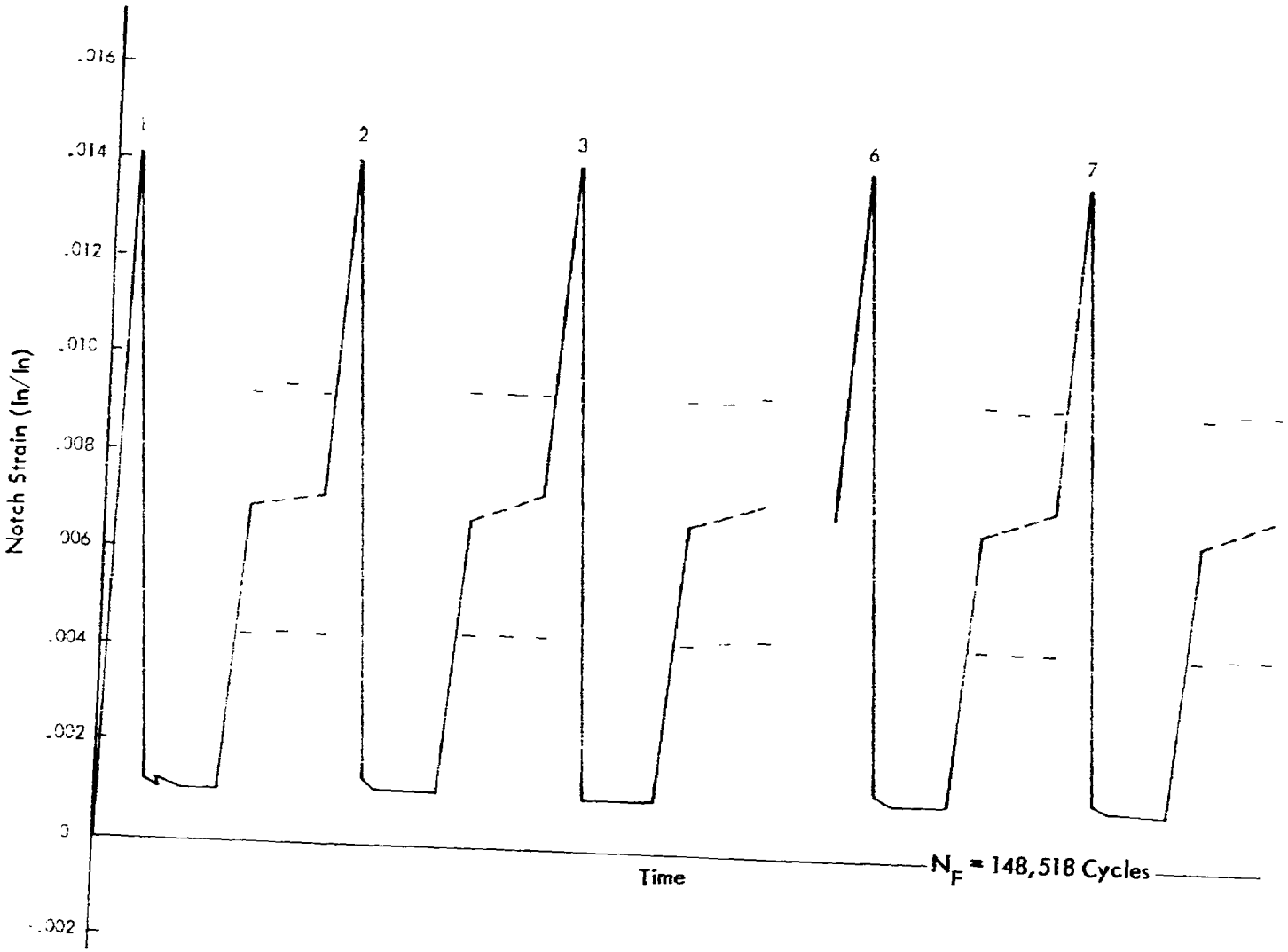

Figure 38. Strain Time History - Sequence No. 21

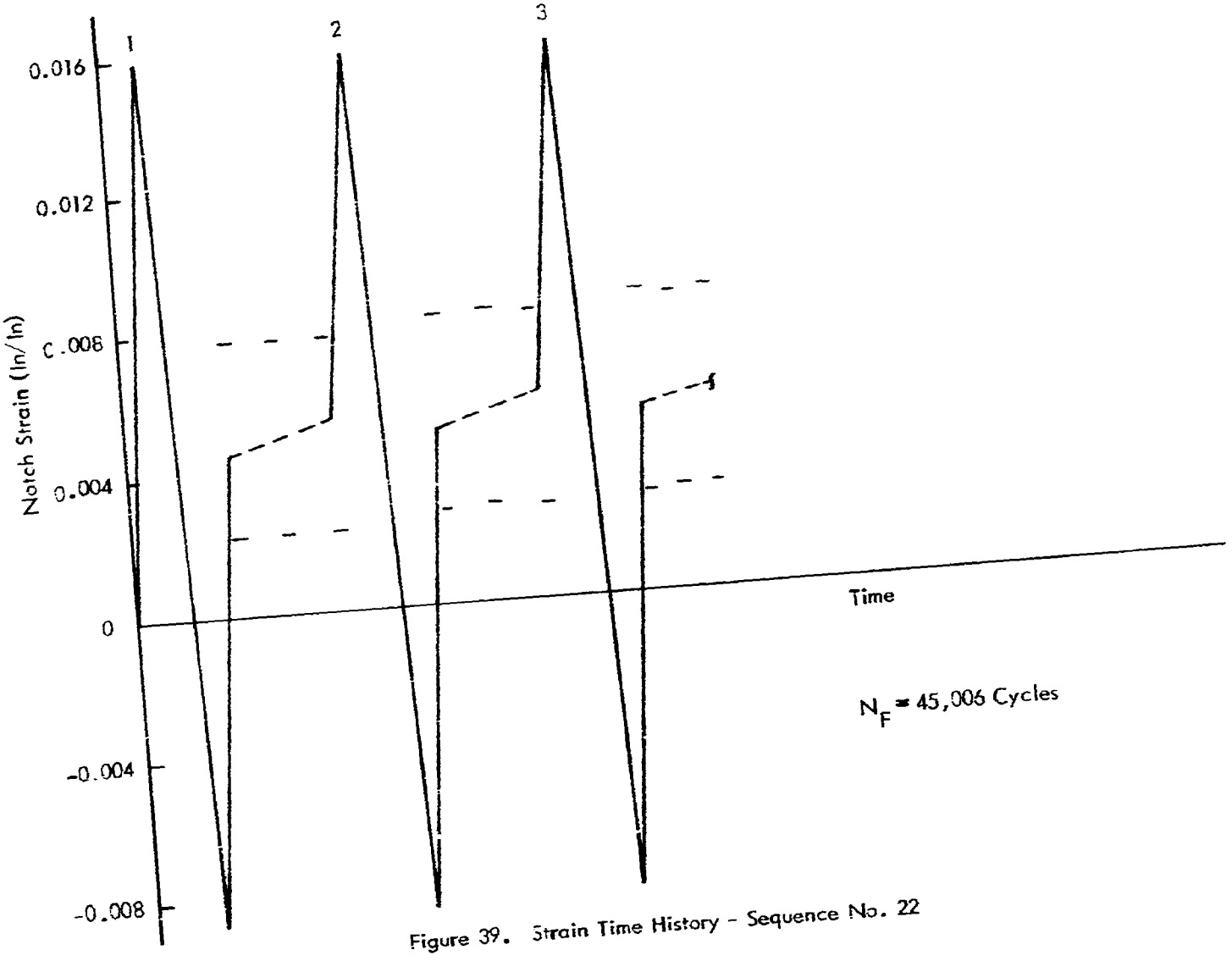

Figure 39. Strain Time History - Sequence No. 22

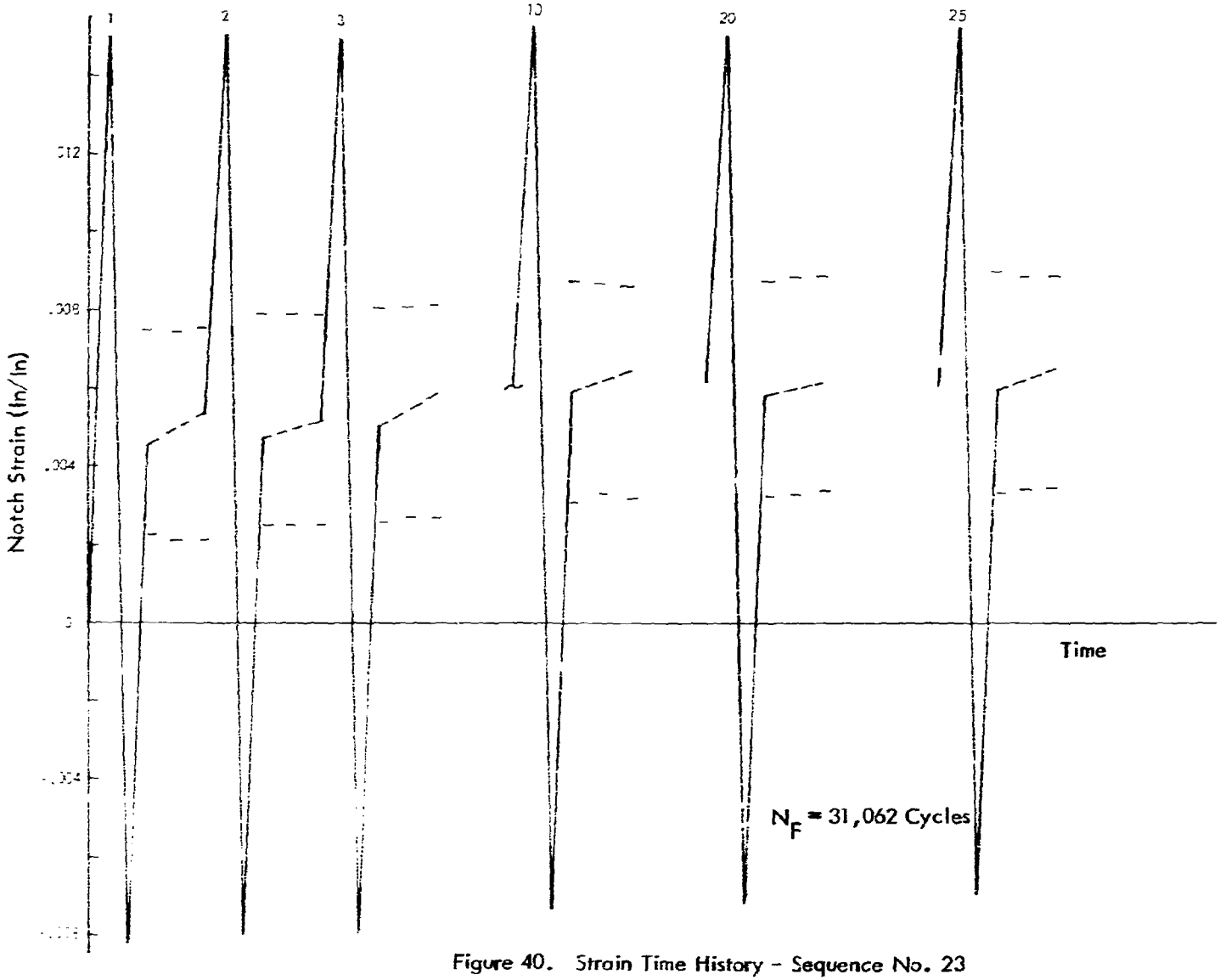

Figure 40. Strain Time History - Sequence No. 23

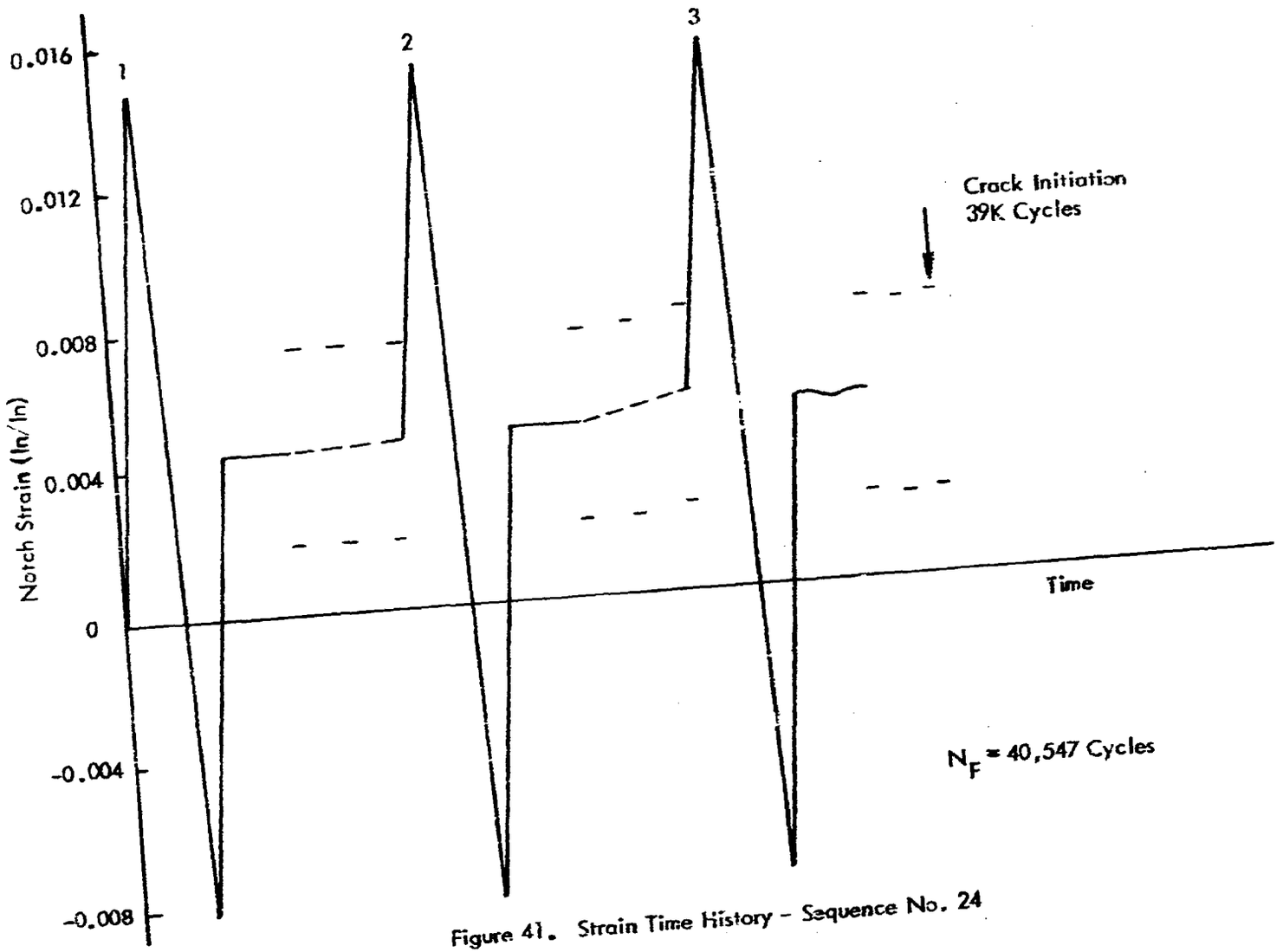

Figure 41. Strain Time History - Sequence No. 24

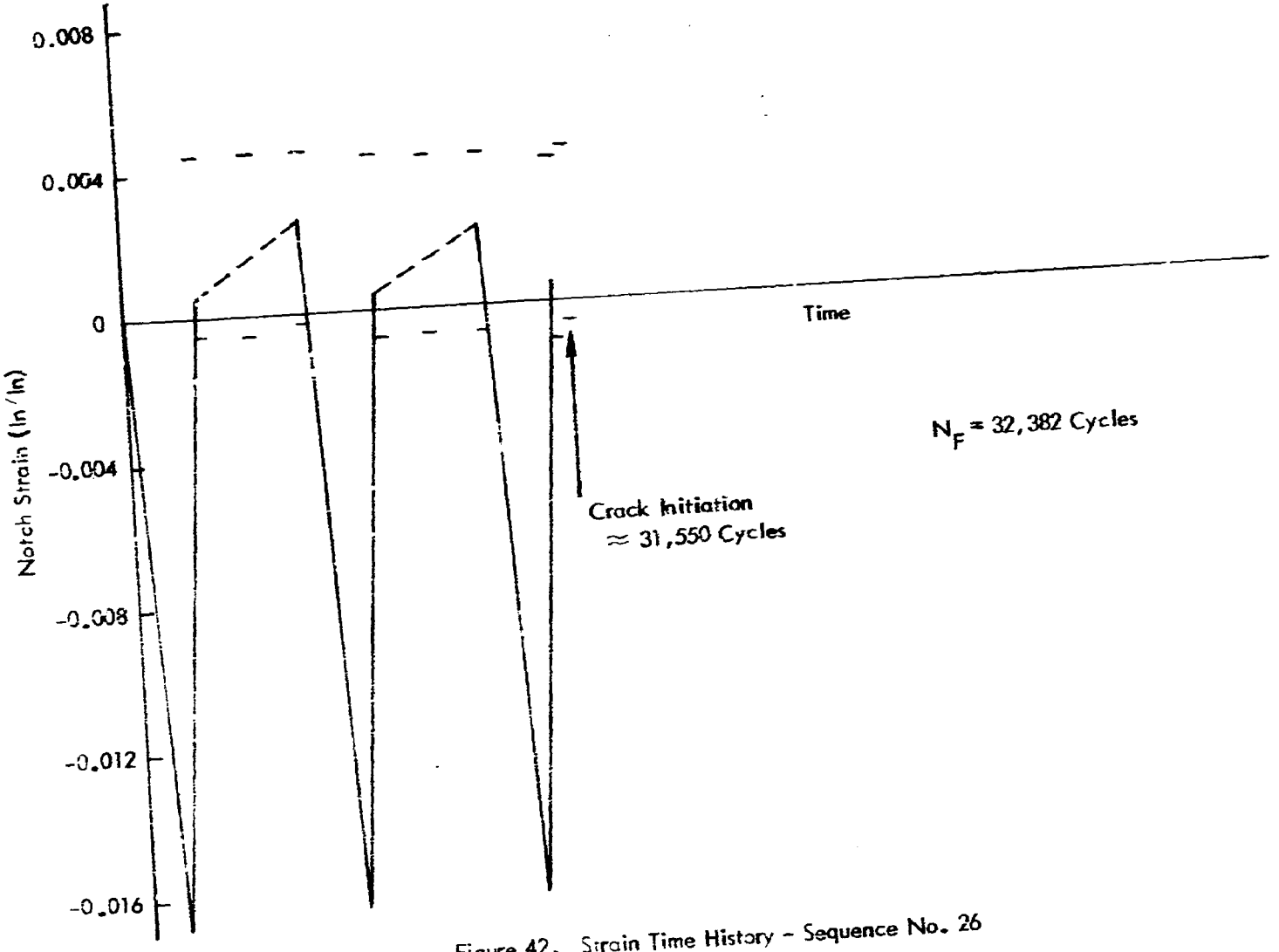

Figure 42. Strain Time History – Sequence No. 26

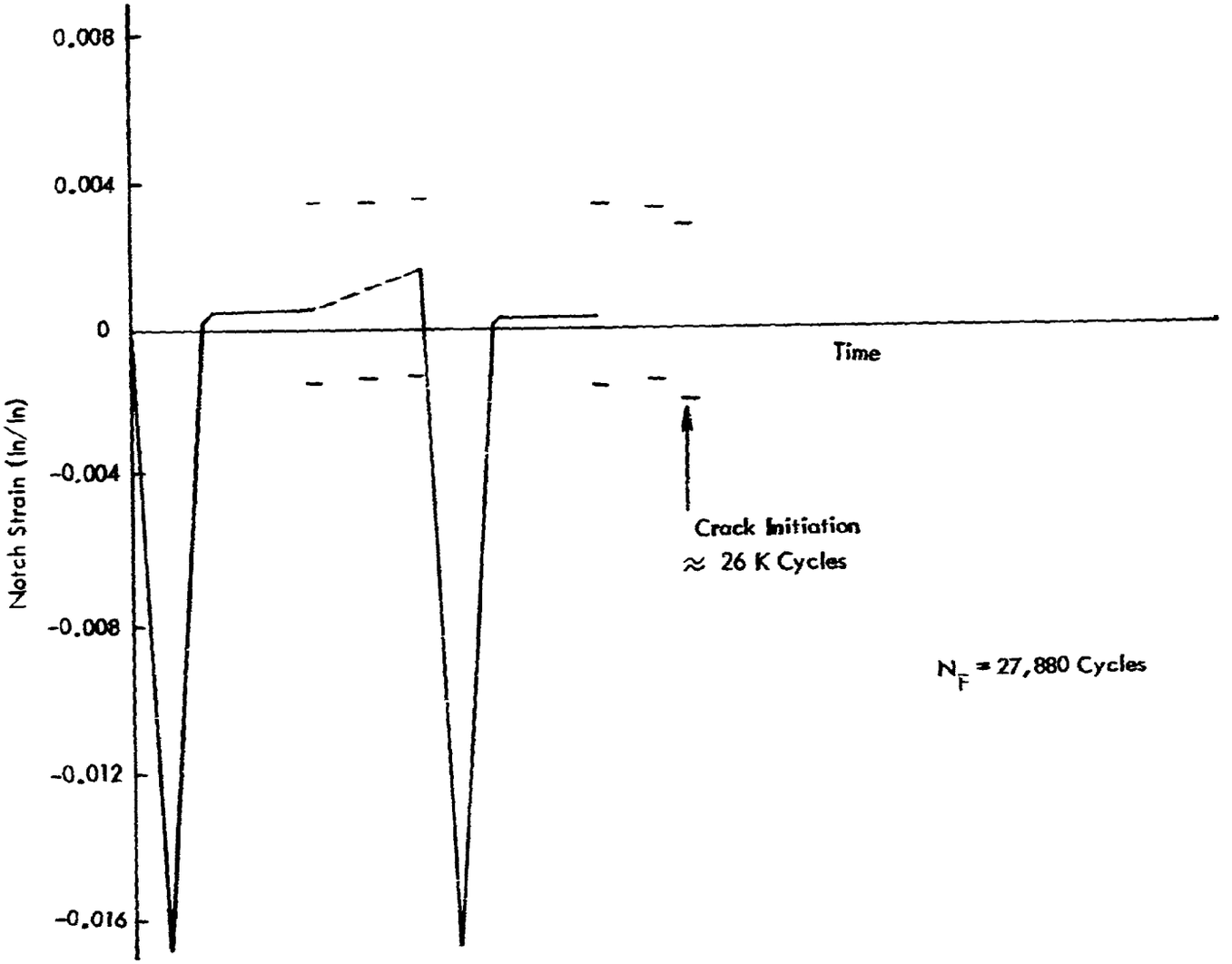

Figure 43. Strain Time History - Sequence No. 24

The sequences with hold times at the compressive loads have shown evidence of time dependent creep during periods of sustained load. This creep is more pronounced in the 24-hour hold periods than during the one-hour hold periods as illustrated in Figures 35 through 37. In each case there is creep indicated for all five of the 24-hour hold periods but only during the first of the one hour hold periods. Again, earlier discussion had pointed out that the 24-hour hold period resulted in a shorter life than a one-hour hold, except for the -15.8 ksi sustained stress, and this data tends to substantiate that trend. Another observation is the time dependent changes in the constant amplitude strain limits in Sequences 8, 13, and 14 with and without the sustained underload of -7.9 ksi. Without a sustained underload (Sequence 8) there is little change in the constant amplitude strains; but, following the hold period in Sequences 13 and 14 there is a definite trend toward more positive strain limits. This again substantiates the shorter life obtained when the hold periods are included in sequences with -7.9 ksi underloads. In Sequences 9 and 15 with a -15.8 ksi underload, the trend is different, however. As shown in Figures 32 and 37, there is a change in strain with or without the hold period. Sequences with the -15.8 ksi underload did not follow the same trends of significant reductions in life with hold times that is quite apparent with the -7.9 ksi underload and this apparent strain change may be a partial explanation of the phenomena.

There was evidence of creep during the hold periods at negative loads; however, no creep was apparent during the sustained loads at the flight mean loading conditions. This is illustrated in Figures 41 and 43 and reflected in the times to failure for Sequences (22, 24), (23, 25), and (26, 27).

In addition to the strain time histories discussed above, the recorded load-strain histories for selected sequences are illustrated in Figures 44 through 52. The first and third major load cycle is plotted for each sequence shown. These curves do not include strain data from the constant amplitude cycles or the sustained loading periods. This data does illustrate the time dependent changes in mean and peak strains discussed earlier. In each case, the new origin for initial loading for the third cycle is indicated as point A.

3.5.2 Creep Studies

As the experimental program evolved it became apparent that there are significant effects of the creep during the sustained load periods and this does effect fatigue life.

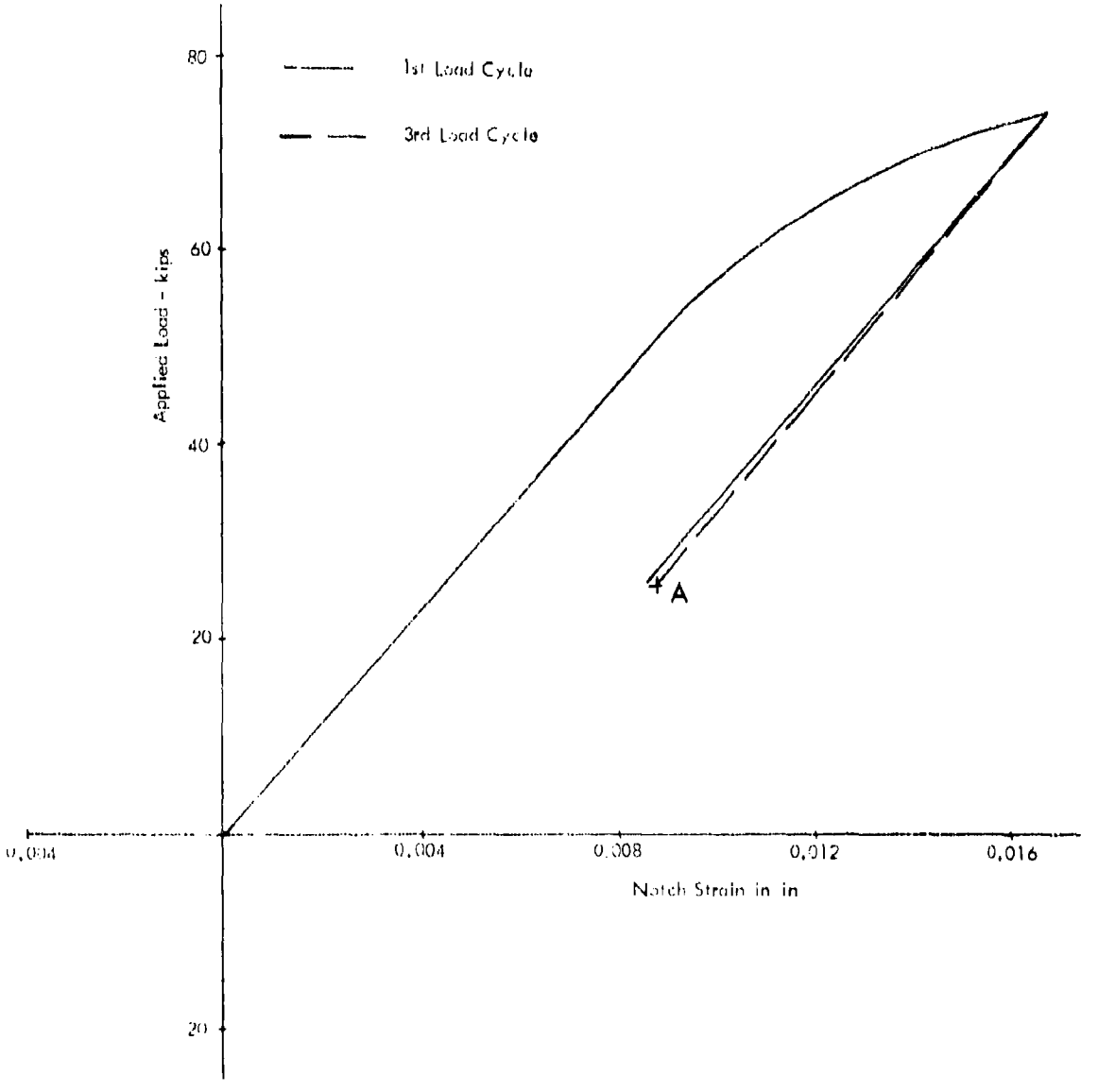

Figure 44. Recorded Load - Strain Data Sequence 6

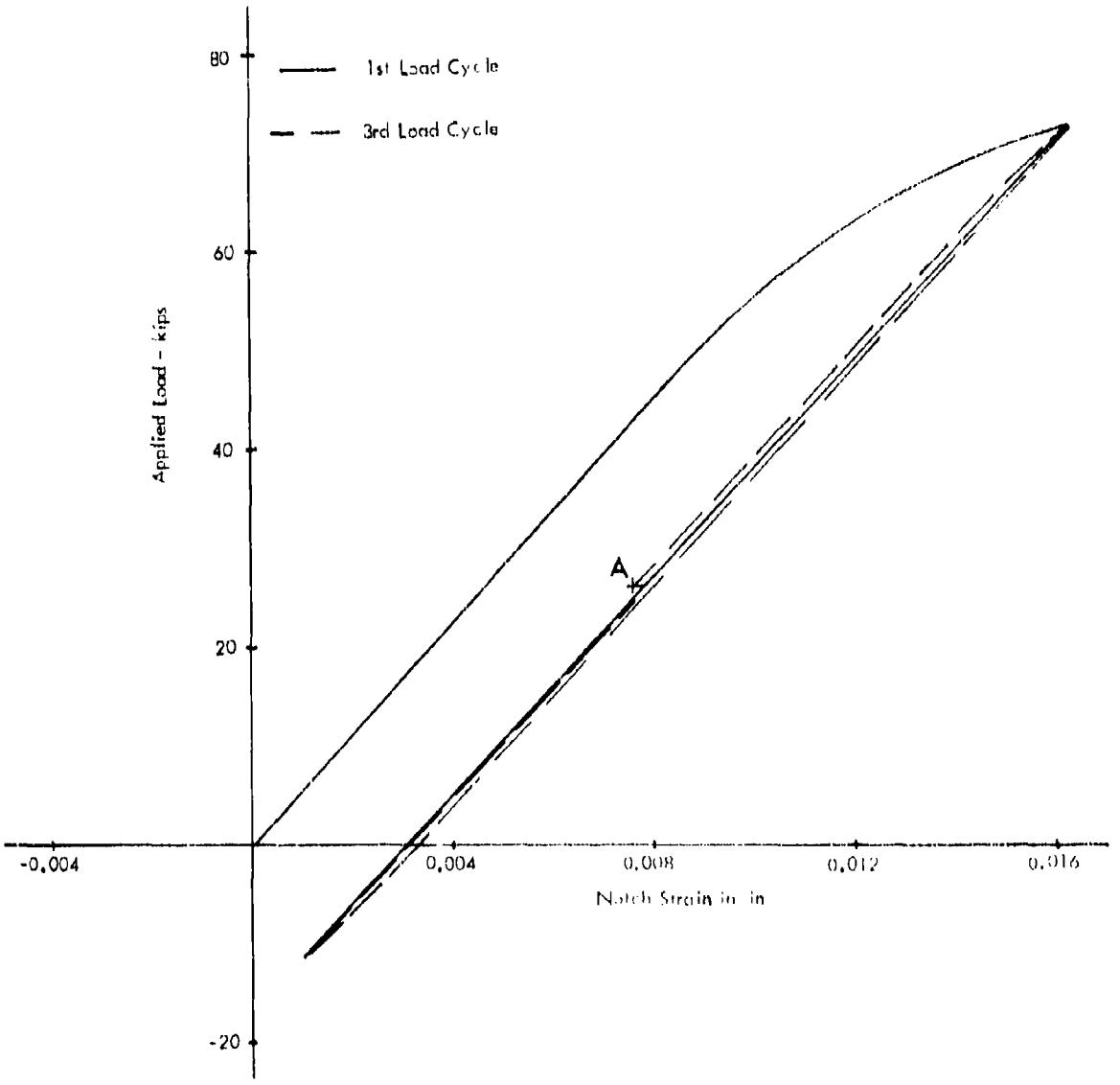

Figure 45. Recorded Load - Strain Data Sequence 8

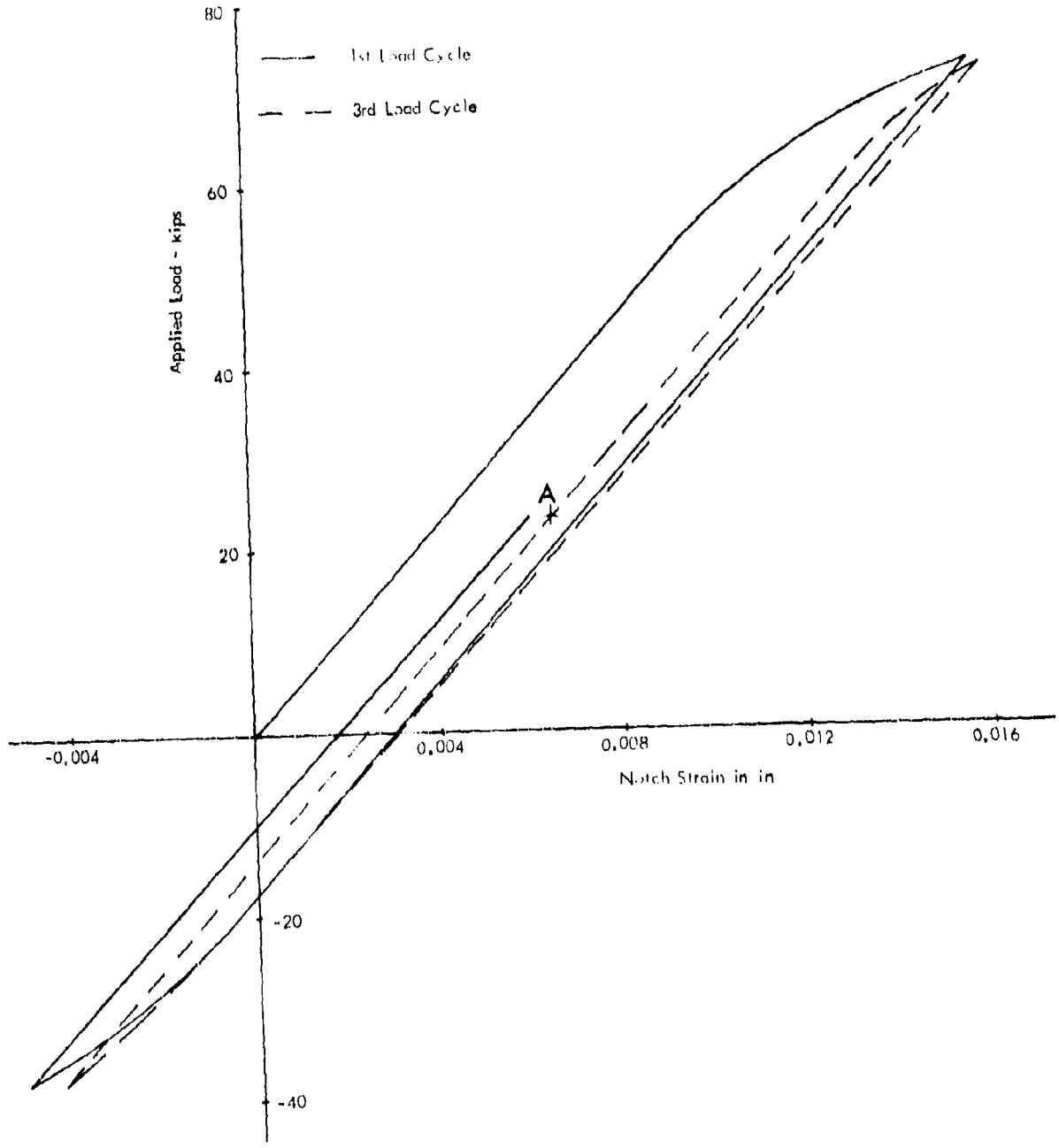

Figure 46. Recorded Load - Strain Data Sequence 12

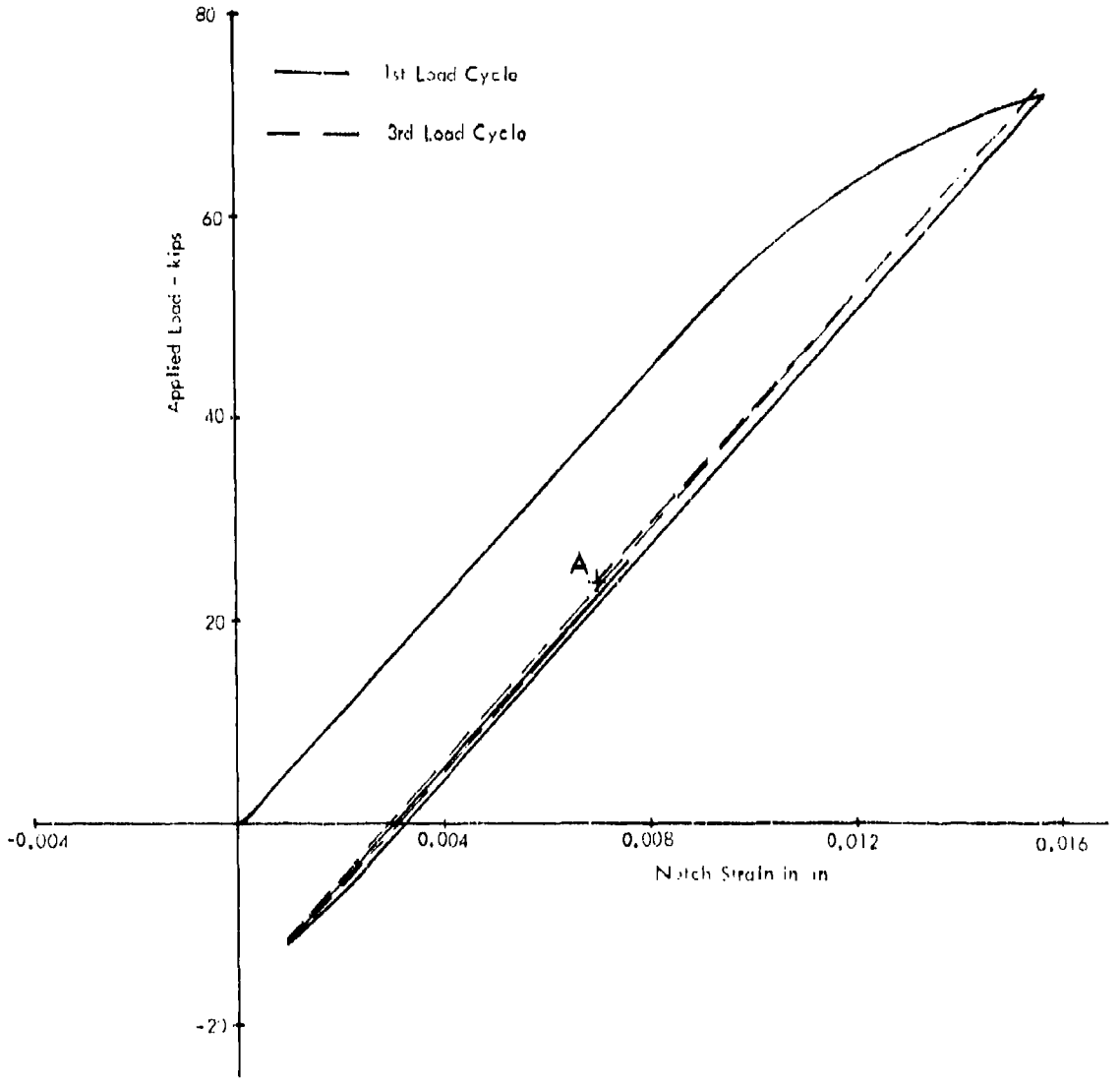

Figure 47. Recorded Load - Strain Data Sequence 13

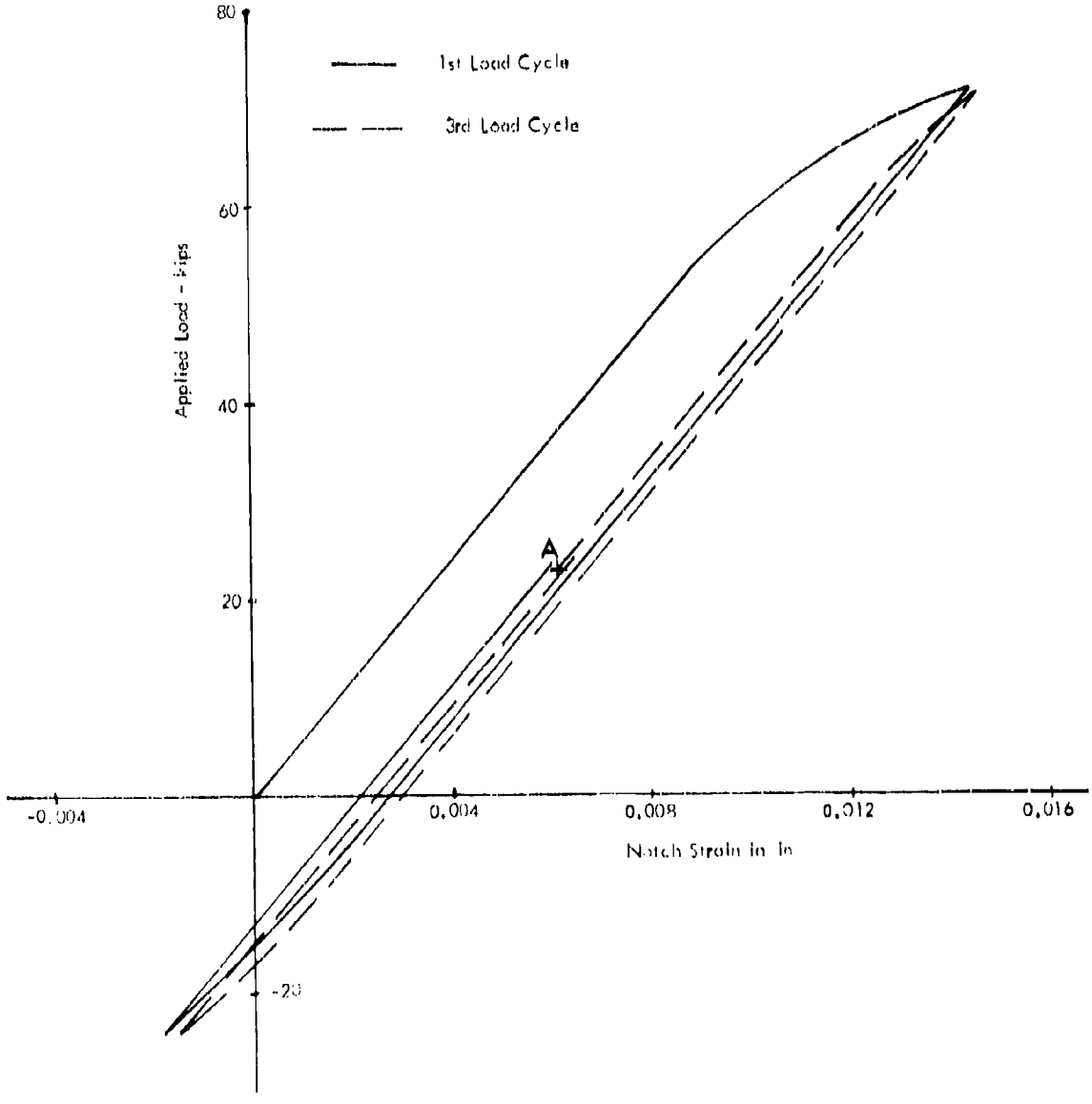

Figure 48. Recorded Load - Strain Data Sequence 15

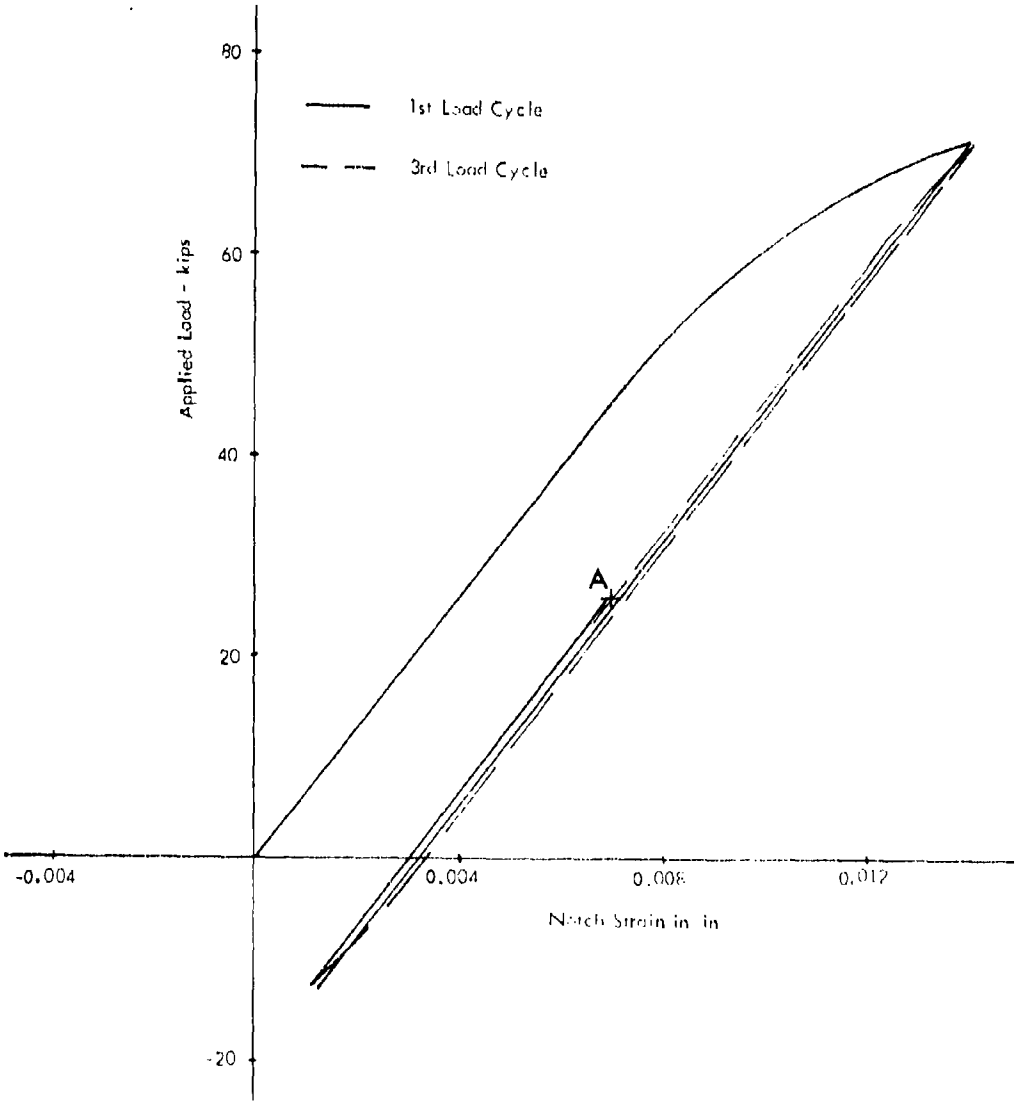

Figure 49. Recorded Load - Strain Data Sequence 21

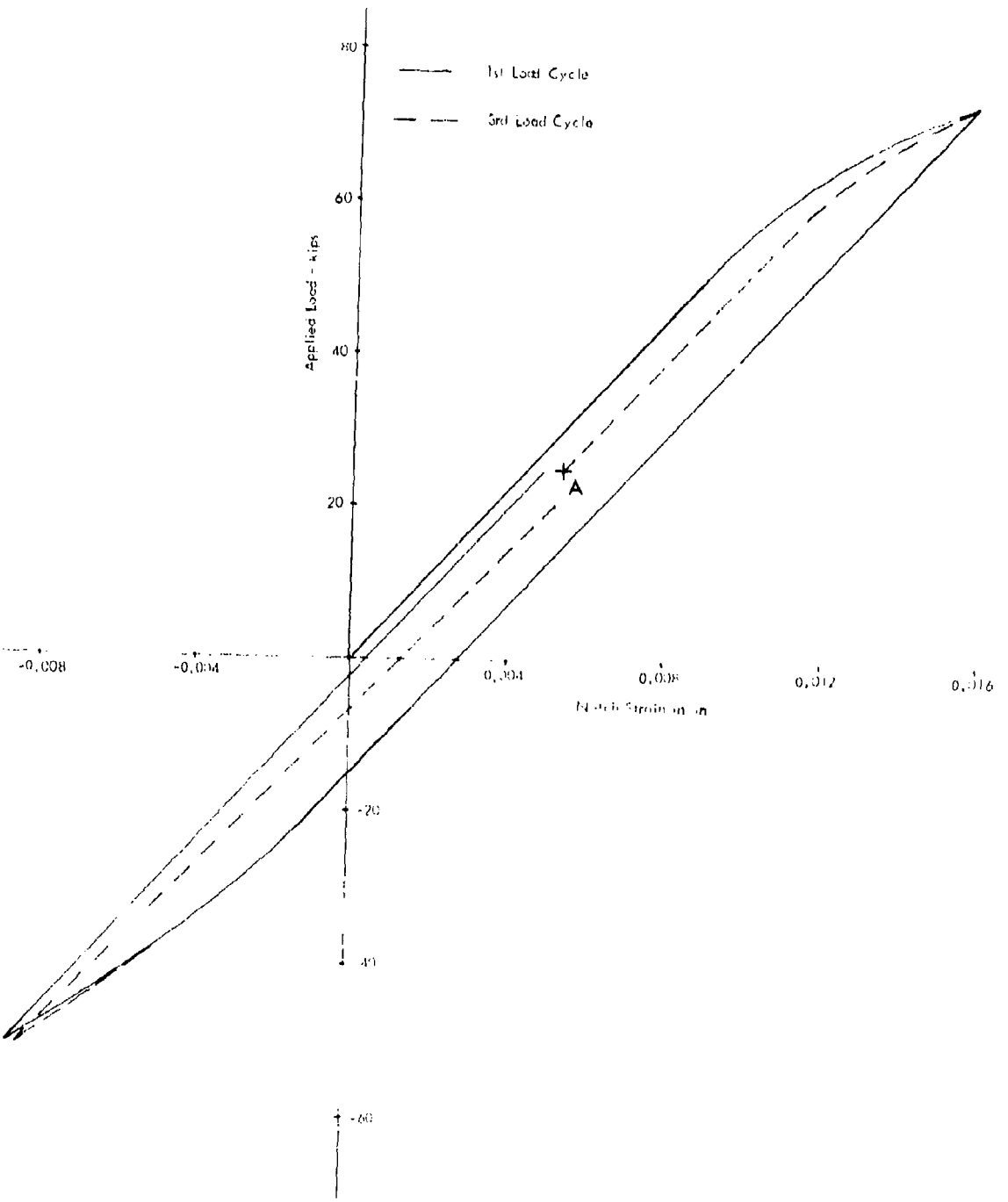

Figure 50. Recorded Load - Strain Data Sequence 22

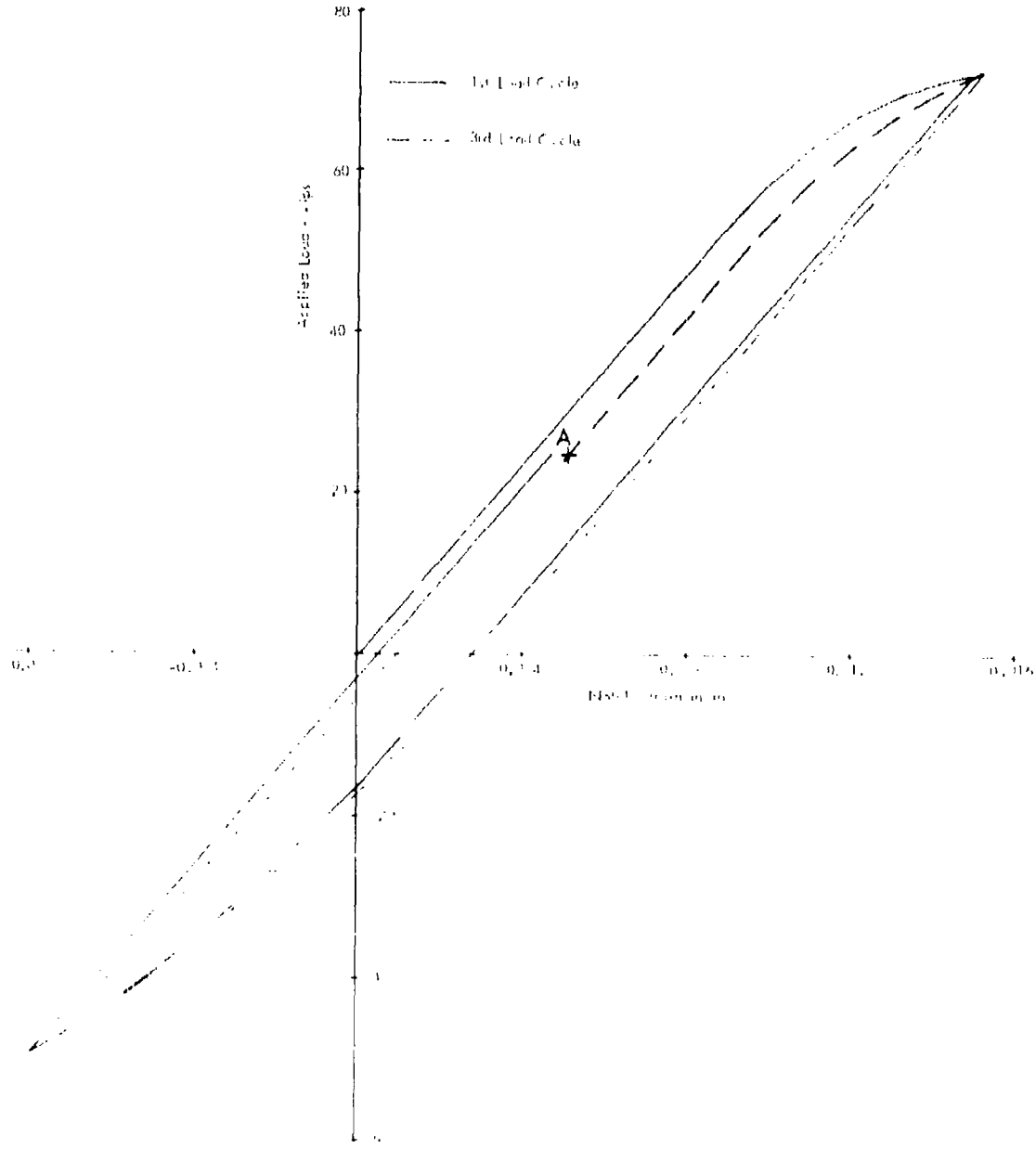

Figure 51. Recorded Load - Strain Data Sequence 24

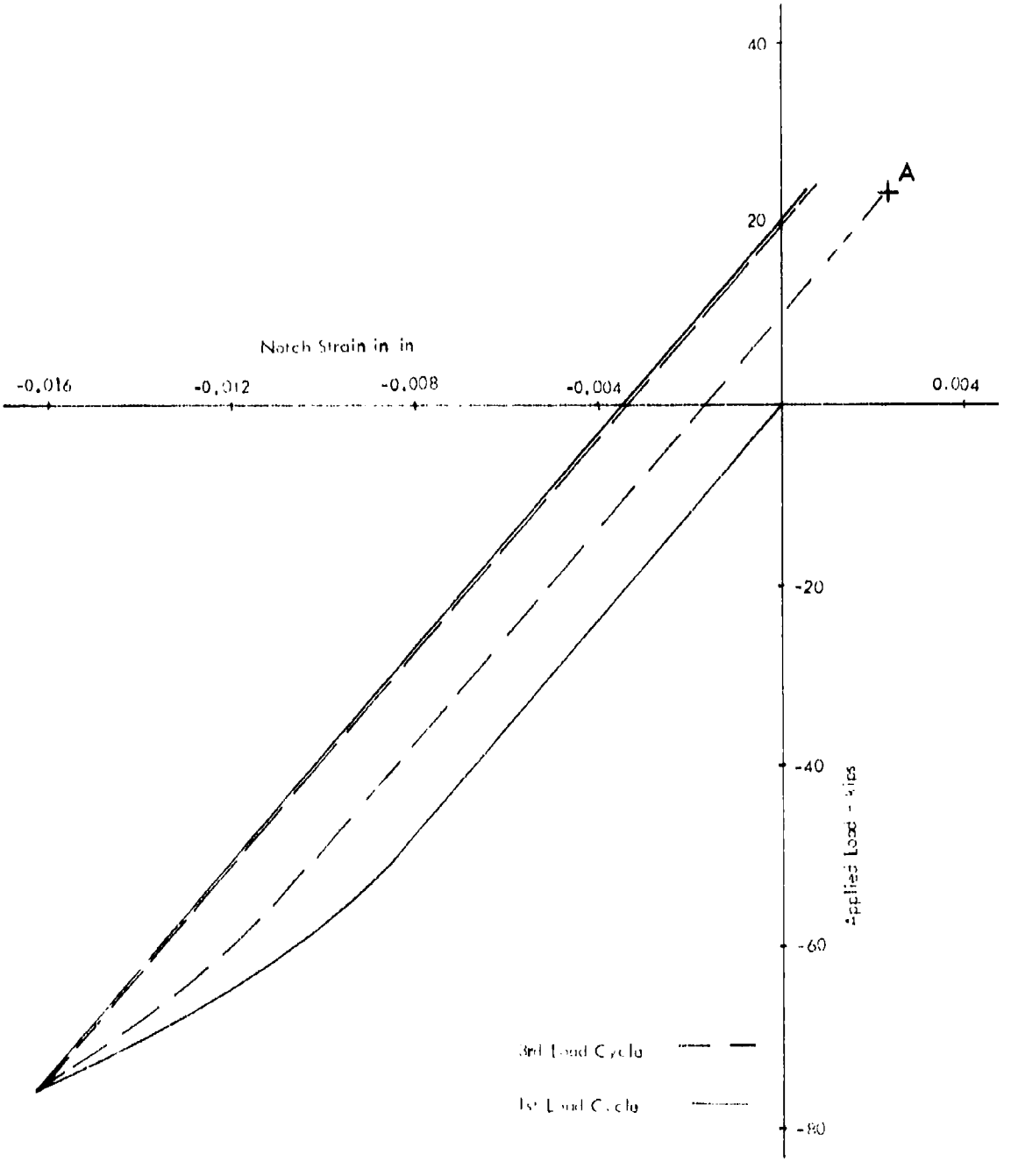

Figure 52. Recorded Load - Strain Data Sequence 26

Two sequences were run to obtain additional strain data at the stress concentration and to define a distribution of strain across the net section of the specimen. These tests are identified as Sequences 28 and 29 in Figure 1. For Sequence 28, the tensile overload was applied, then the specimen was held at the -7.9 Ksi stress for 24-hours. In Sequence 29 the tensile overload was applied followed by a -32.5 Ksi underload and then held at +15.8 Ksi for one hour. In each case the transducer was installed in the hole and eight strain gages were located on the specimen surface as illustrated in Figure 53. Data was continuously recorded from all nine data channels and is listed in Tables IX and X.

The strain distribution across the specimen is plotted in Figure 54. This includes the transducer and strain gage measurements at the start of the hold period and then at one-minute, one-hour, and 16-hours. These data definitely confirm that creep is taking place immediately adjacent to the stress riser. Strains inside the hole, as measured by the transducer, are decreasing from 1130 μ inches initially to 980 μ inches after 16-hours. However, data for strain gages 1, 2, and 3 (Figure 53) show a significant increase in strain adjacent to the hole. There is a 1000 μ inch change in strain recorded on Gage 2, located 0.15-inches from the edge of the hole. Figure 55 illustrates the time dependent creep data from the transducer and Gages 1 and 2. Also included in this figure are the recorded strains after unloading the specimen. Apparently, the strain and associated stress changes shown here are of sufficient magnitude to result in differences in specimen fatigue life with and without the hold periods in the test sequence. Test life is significantly reduced when the hold periods at -7.9 Ksi are included as discussed earlier.

Since only strain can be measured directly in a test such as Sequence 28, changes in stress and subsequent effect on life have been hypothesized as illustrated in Figure 56. In evaluating Sequences 8, 9, and 12, for example, it is evident that the reduced life associated with increasing compressive load magnitude is dependent on the notch stress limits during constant amplitude cycling and not on the strain limits. Therefore, it is hypothesized that during the sustained load periods when there is strain creep there must also be a stress relaxation such that subsequent constant amplitude cycling will give a shorter life than expected without the hold time included. In Figure 56, a specimen loaded from O-A-B with no hold at B would cycle between the limits C-D. With a hold time at B and the known reduction in notch strain (Table IX), it is assumed that there is a stress

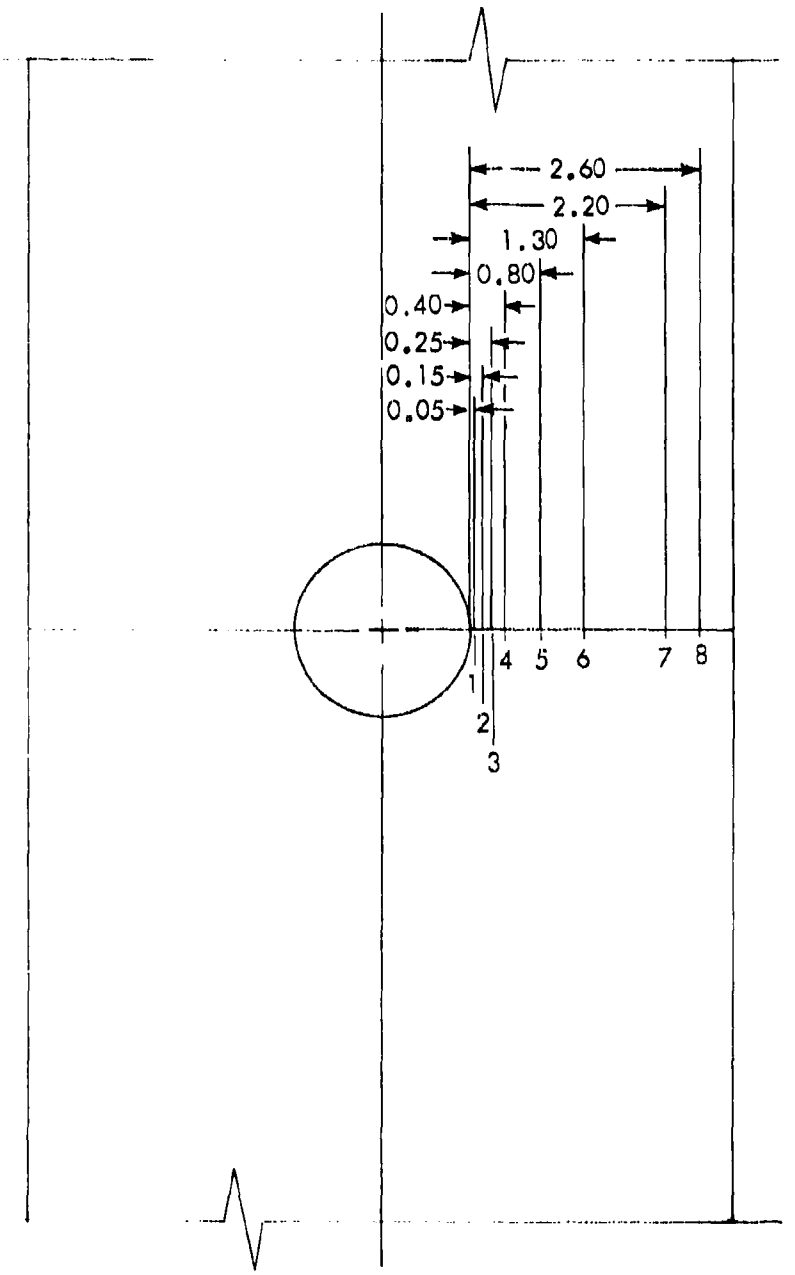

Figure 53. Strain Gage Locations
Sequences 28 and 29

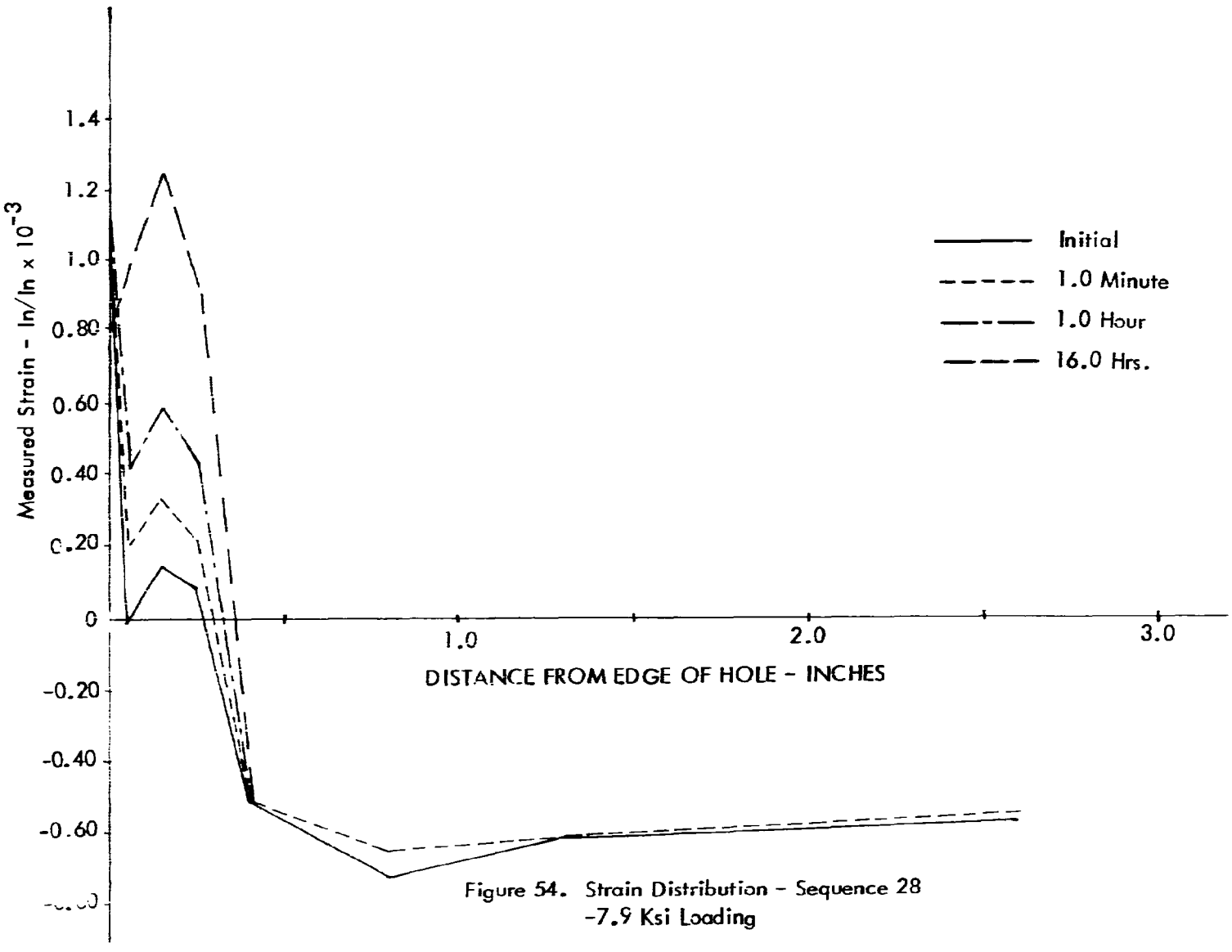

Figure 54. Strain Distribution - Sequence 28
-7.9 Ksi Loading

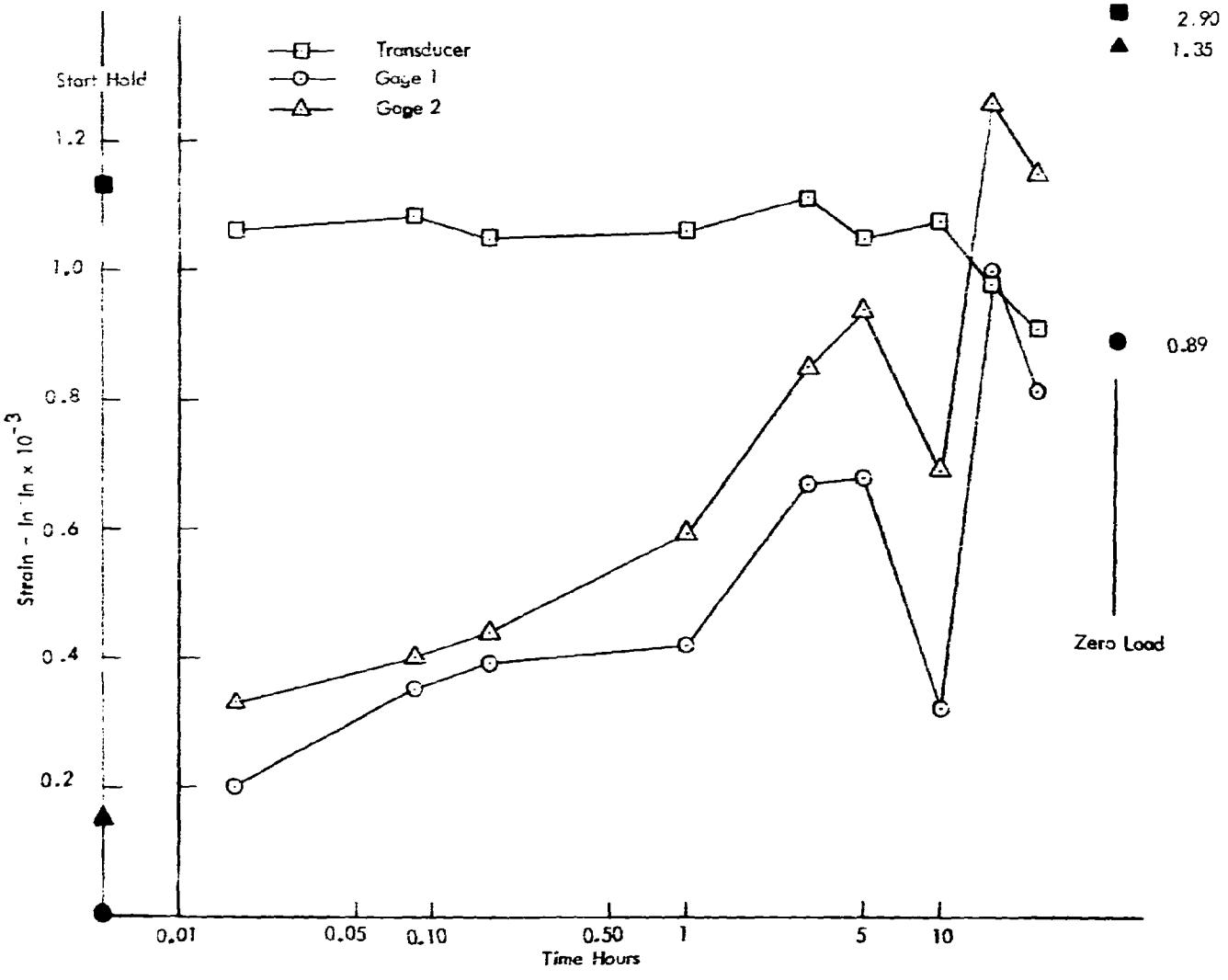

Figure 55. Creep Data – Sequence 28
-7.9 Ksi Loading

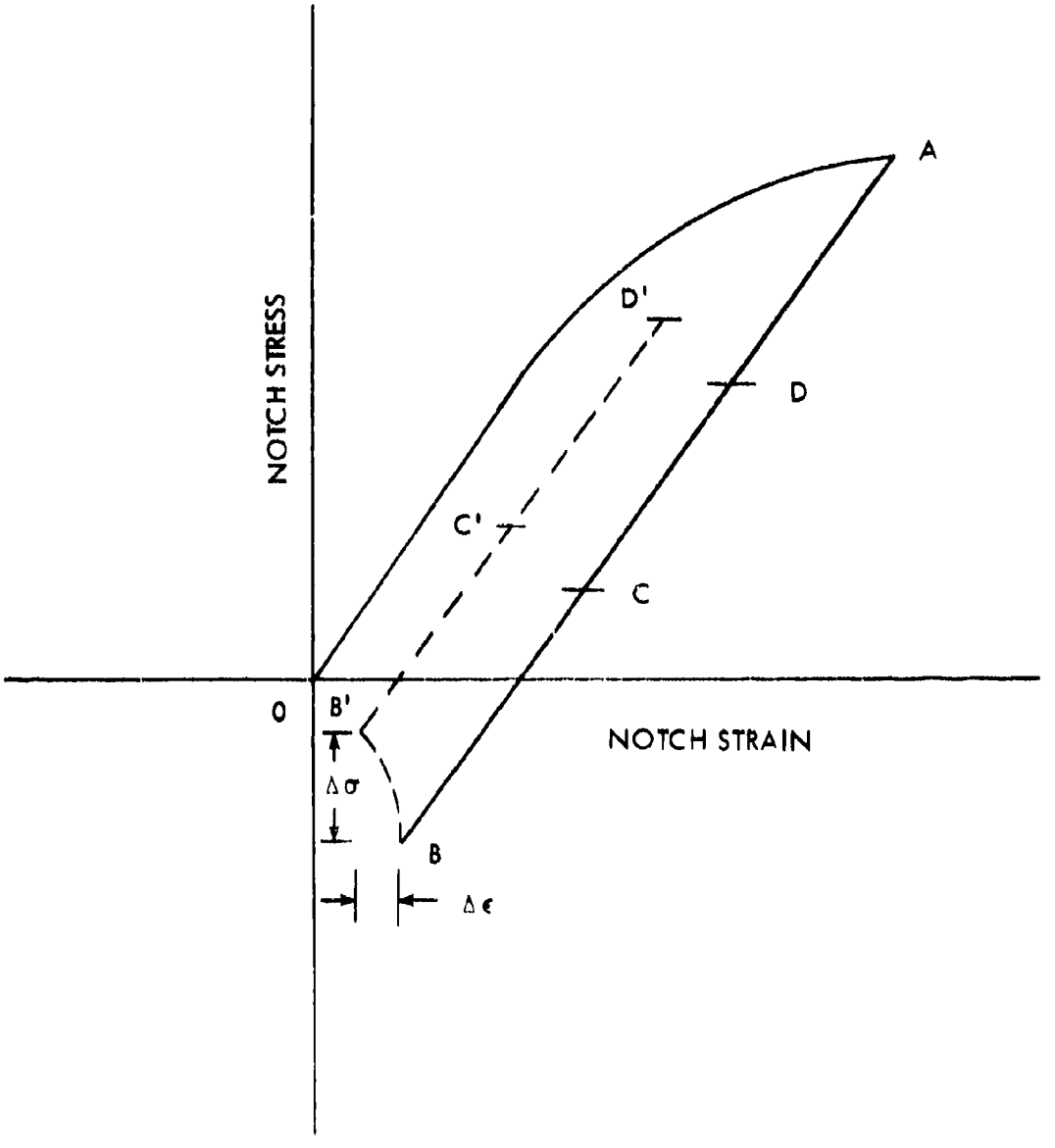

Figure 56. Hypothesis of Time Dependent Stress-Strain Change

TABLE IX - RECORDED STRAIN - SEQUENCE 28
SUSTAINED LOAD AT -7.9 KSI

Time	Measured Strain - μ in/in								
	Strain Gage								
	Trans	1	2	3	4	5	6	7	8
Start	1130	30	150	90	-510	-660	-610	-590	-560
10 Sec	1100	150	260	180	-510	-670	-610	-590	-560
30 Sec	1090	180	300	200	-510	-660	-610	-580	-550
1 Min	1070	200	330	220	-510	-650	-610	-580	-550
5 Min	1080	250	400	270	-500	-660	-600	-580	-550
10 Min	1050	290	440	300	-510	-660	-600	-580	-550
1 Hour	1065	420	590	430	-500	-650	-610	-570	-550
5 Hours	1060	680	940	680	-490	-630	-570	-520	-510
10 Hours	1075	320	690	450	-500	-640	-580	-550	-530
16 Hours	980	1000	1260	930	-510	-670	-600	-580	-560
24 Hours	910	810	1150	850	-490	-650	-590	-560	-550
Zero Load	2900	890	1350	1150	420	90	70	50	30

TABLE X - RECORDED STRAIN - SEQUENCE 29
SUSTAINED LOAD AT 15.8 KSI

Time	Measured Strain - μ in/in								
	Strain Gage								
	Trans	1	2	3	4	5	6	7	8
Start	4460	4090	3270	2680	2070	1610	1380	1280	1220
10 Sec	4470	4120	3290	2690	2070	1610	1380	1280	1220
30 Sec	4500	4130	3290	2690	2070	1600	1380	1270	1220
1 Min	4510	4130	3290	2690	2060	1600	1370	1270	1220
30 Min	4540	4130	3290	2690	2060	1600	1410	1270	1220
1 Hour	4530	4130	3290	2690	2060	1600	1450	1270	1220

relaxation from B to B'. Subsequent cycling will then be between C' and D'. This will then result in the decrease in life shown when hold times are included in the sequences.

Additional experimental studies and finite element simulations are planned to further evaluate this phenomena.

3.5.3 Crack Growth Data

Initially it was planned to record crack growth data for all test sequences, but this was deleted as the program evolved. Accurate measurements were difficult to obtain as crack growth was very rapid at the high alternating stresses for this program. Crack growth was a small percentage of the total life to fracture. The limited data which was recorded is listed in Table XI.

3.5.4 Fractographic Studies

The strain transducer when installed in the hole, has four contact pins which are inbedded into the hole sidewall for support. These pin marks were not thought to influence specimen cracking; however, several failed specimens were evaluated to determine if cracks did originate from these marks. Fractographic study results for two specimens are shown in Figures 57 and 58. In Figure 57 the crack goes between the pin marks and initiated at the corner of the hole. Figure 58 shows a crack outside the transducer pin marks which started from imbedded flaws in the hole sidewall. These are typical of all failures and no failure originated from the pin marks caused by transducer installation.

TABLE XI- CRACK GROWTH DATA

Specimen 1E-2 Super-Scale (Sequence 1)

Cycles	44000	44350	44450	44600	44700	44800	44900	44960
Crack Length	0.094	0.13	0.15	0.23	0.26	0.32	1.0	Failure

Specimen 1E-4 Super-Scale (Sequence 1)

Cycles	20940	31740	32330	32700	32850	32900	33020
Crack Length	0.08	0.17	0.24	Thru Thickness	0.39	0.61	Failure

Specimen 1B-1 Super-Scale (Sequence 22)

Cycles	44250	44500	[illegible]	44822	44910	45006
Crack Length	0.09	0.15		0.30	0.55	Failure

Specimen 2E-2 Coupon (Sequence 1)

Cycles	96600	97900	99200	100400	101500	101900	103620
Crack Length	0.06	0.09	0.13	0.15	Thru Thickness	0.19	Failure

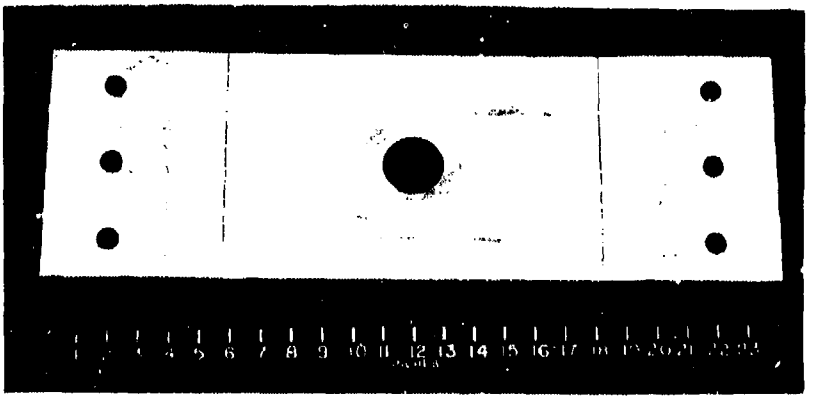

.17X

Broken Specimen 1E-4

13X

Transducer Contact Pin Marks
On The Hole Wall

Figure 57. Fractographic Analysis of Specimen 1E-4 Failure

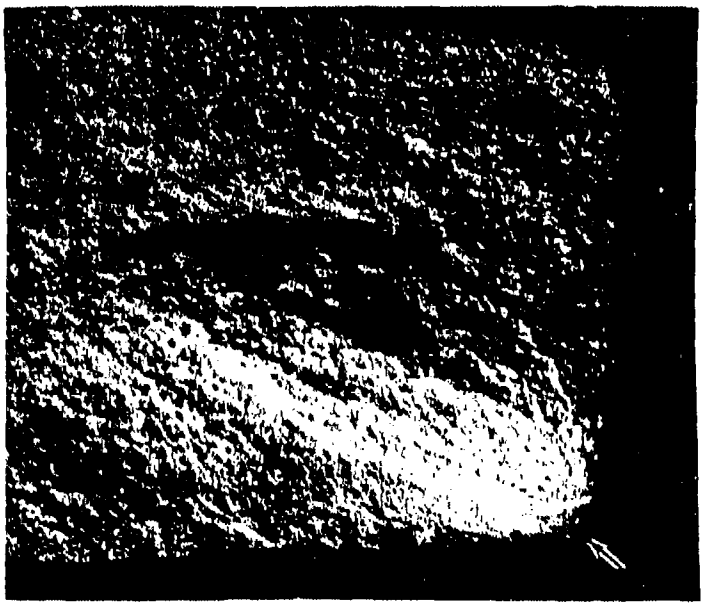

10X

Fracture Surface With The Crack Origin
Location Noted By The Arrow

Figure 57. (Concluded)

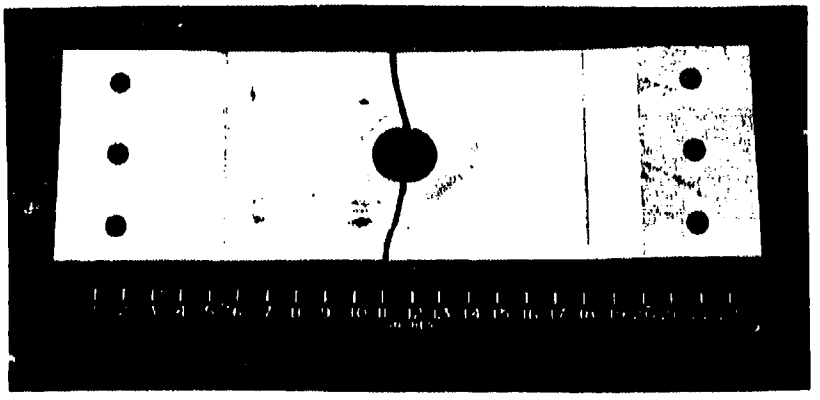

.17X

Broken Specimen 2F-1

13X

Transducer Contact Pin Marks
On The Hole Wall

Figure 58. Fractographic Analysis of Specimen 2F-1 Failure

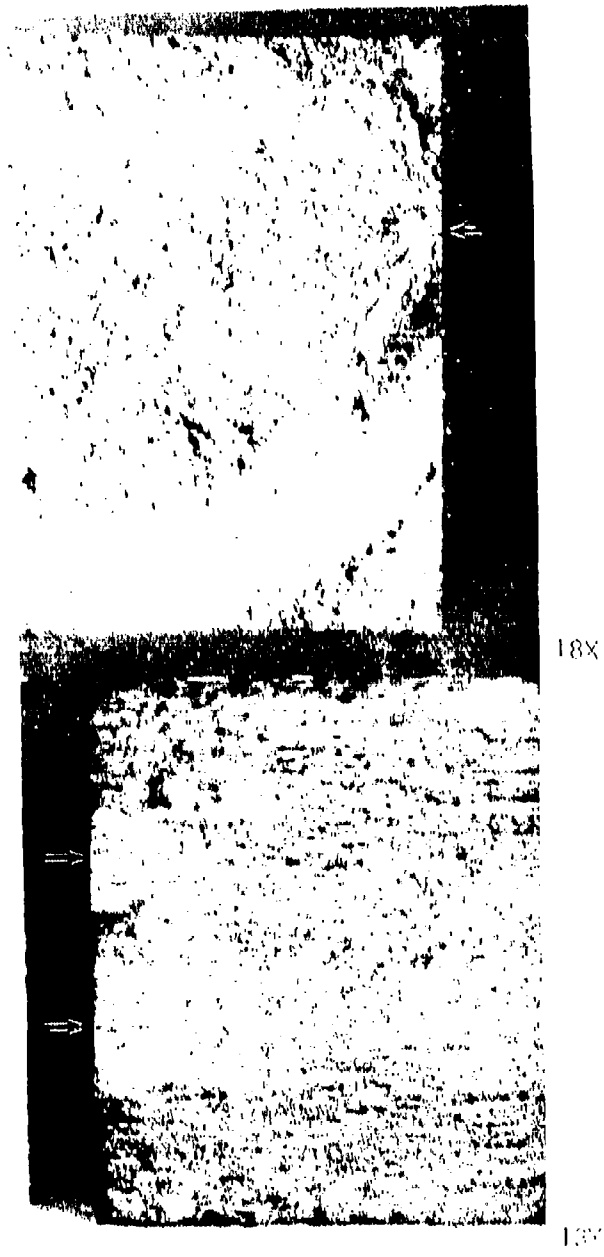

Crack Origins — Imbedded Fibers In Hole Sidewall

Figure 58. (Concluded)

SECTION IV
ANALYTICAL

4.1 ANALYTICAL PROGRAM

A conventional fatigue analysis which uses notched S-N data and computes an accumulative damage based on the Palmgren-Miner rule neglects many parameters which can have an effect on fatigue life. The parameters and their effect are generally understood but have to be discarded for the sake of economy. One such parameter is the sequencing of applied loads. H. Neuber in his paper, Reference 5, presents a theory which makes it economically feasible to include the effects of load sequencing in a fatigue analysis.

Fatigue cracks originate from structural discontinuities such as fastener holes. The discontinuities cause stress concentrations which are usually large enough that the material becomes plastic when the structure is subjected to normal aircraft operating loads. Upon removal of a load which has caused plasticity, residual stresses become locked into the material. These residuals are additive to the stresses resulting from subsequent load applications and in the case of fatigue they alter the mean stress and hence the damage caused by subsequent cycles. An analysis procedure based on Neuber's theory calculates the peak elastic-plastic stresses in a discontinuity (notch) which includes the residuals from previous cycles.

This report presents an analysis procedure which uses the stresses resulting from Neuber's theory together with unnotched S-N data to calculate a damage based on the Palmgren-Miner rule. The analysis, which is in the form of a Fortran V computer program, is based on algorithms which simulate the following three phenomena:

- Material response
- Notch response
- Damage predictions

The algorithms, and the development work leading to them, are presented in the following sections.

4.1.1 Material Response Characterization of 7075-T651 Aluminum

A study of the cyclic stress-strain response resulting from the strain controlled tests GJ1 through GJ37 is presented in this section. The purpose of this study is to characterize the cyclic response for 7075-T651 aluminum both during hardening and in the stable condition.

When a material is cycled between fixed strain limits, the increment of stress required for each successive cycle will initially either increase or decrease depending on whether the material is hardening or softening. After a number of cycles, which depends on the strain increment, this hardening or softening stops at which time the material is said to be in a stable condition. The strain controlled tests GJ1 through GJ37 show that 7075-T651 aluminum both hardens and softens. The response for four of these tests is plotted in Figures 59 through 62. Shown is the initial loading curve called the monotonic locus curve and the initial and stable cyclic curves consisting of an upper and lower branch. The stable cyclic curves for these tests have been superimposed in Figure 63 and a line plotted through the peaks. This line defines the cyclic locus curve.

4.1.1.1 Stable Response - The algorithm for simulating the stable response of 7075-T651 will be based on the assumption that when a material is hardened at a particular strain increment it is in the hardened condition for all higher increments. From this it can be said that

(1) The stress and strain will always expand along the cyclic locus curve.

(2) Excursions from the cyclic locus curve, for intermediate loadings, will follow a branch curve.

In reality there are an infinite number of branch curves, the particular one that is followed being dependent on the previous loading history. To efficiently represent the response, it is necessary to characterize these curves into a conveniently usable form. For example, the cyclic locus curve can be characterized by the Rumberg-Osgood expression

$$\varepsilon = \frac{\sigma}{E} + \left(\frac{\sigma}{F}\right)^{n}$$

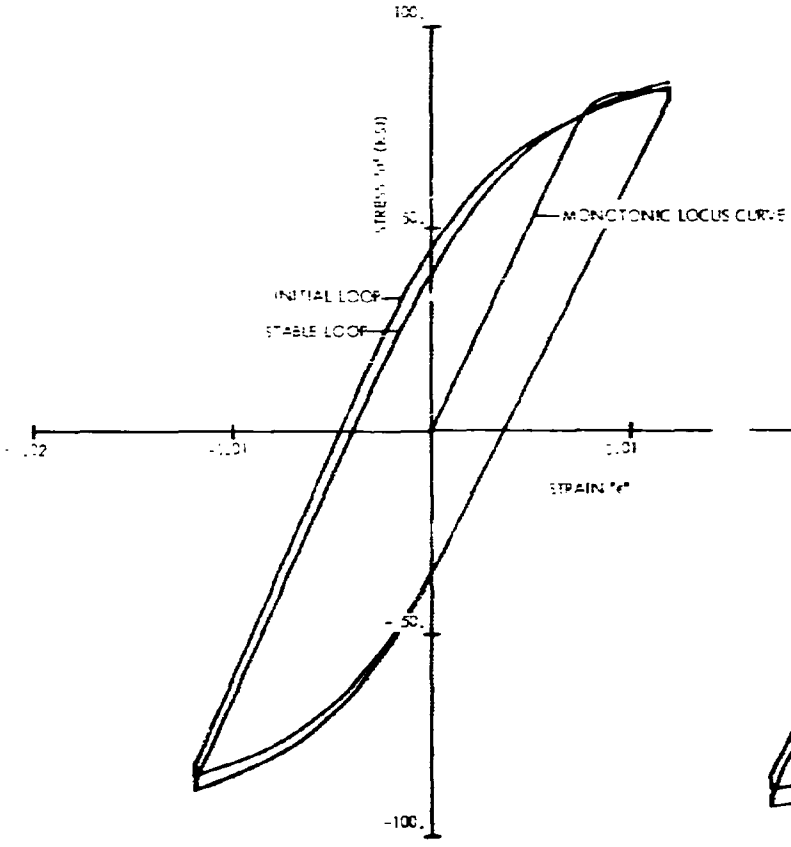

Figure 59. Hysteresis Loops for Test GJ3 ($\Delta\epsilon/2 = 0.0119$)

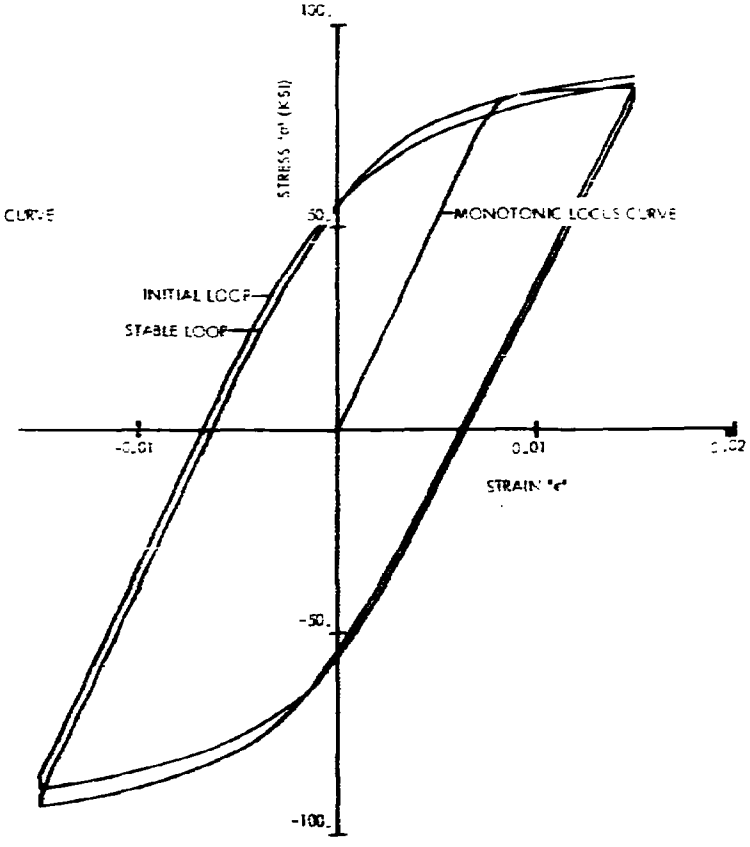

Figure 60. Hysteresis Loops for Test GJ6 ($\Delta\epsilon/2 = 0.0149$)

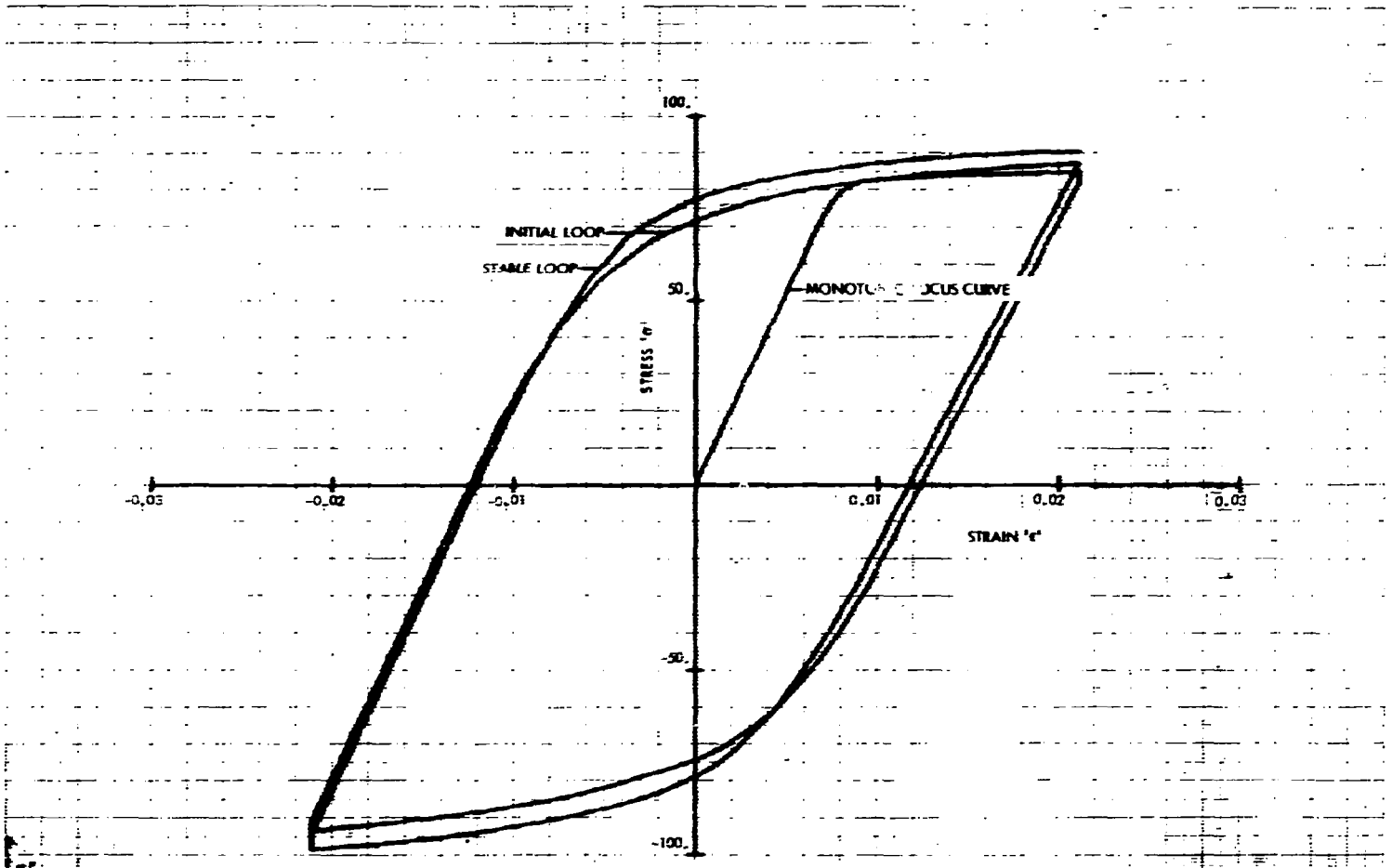

Figure 61. Hysteresis Loops for Test GJ9 ($\Delta\epsilon/2 = 0.0211$)

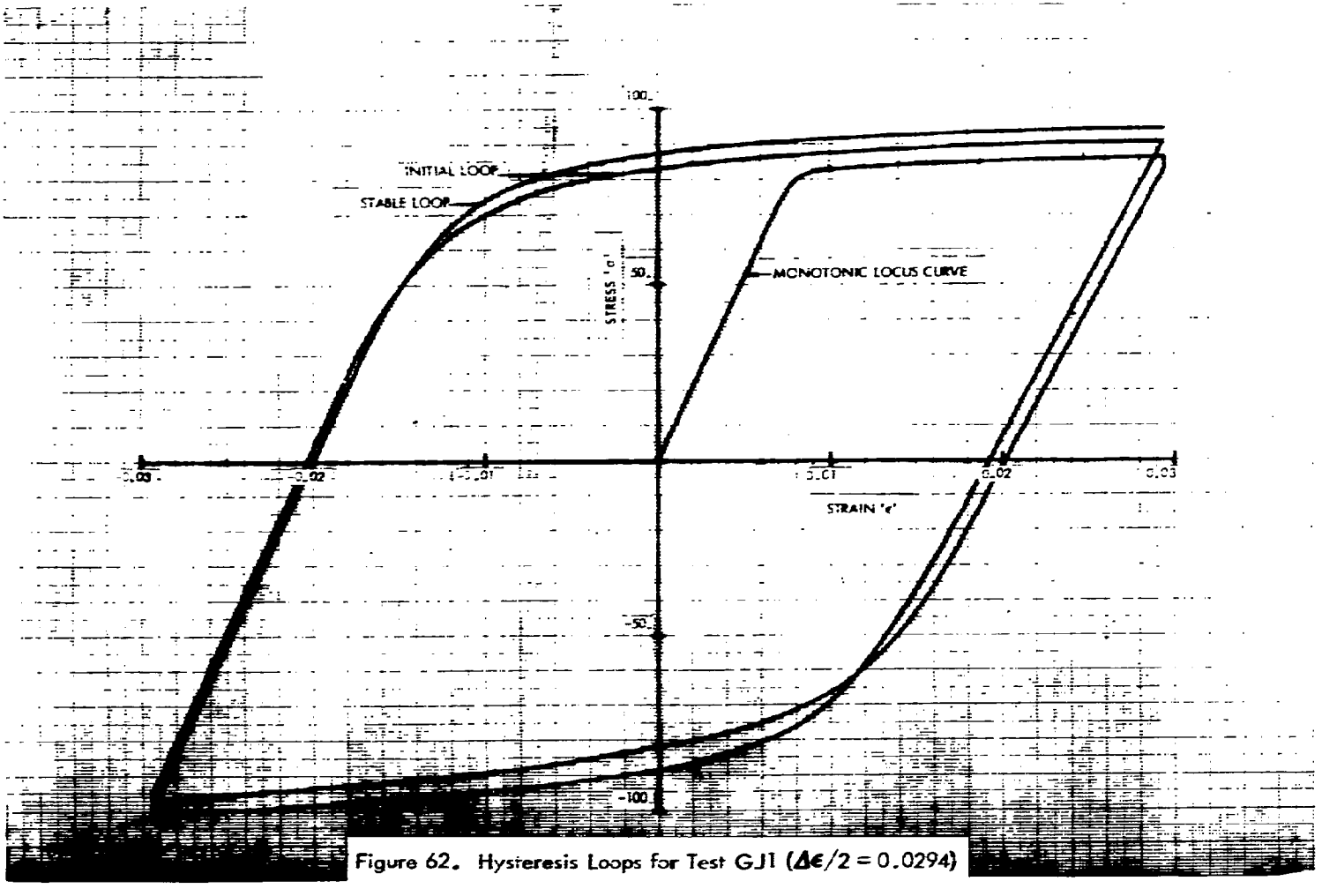

Figure 62. Hysteresis Loops for Test GJ1 ($\Delta\epsilon/2 = 0.0294$)

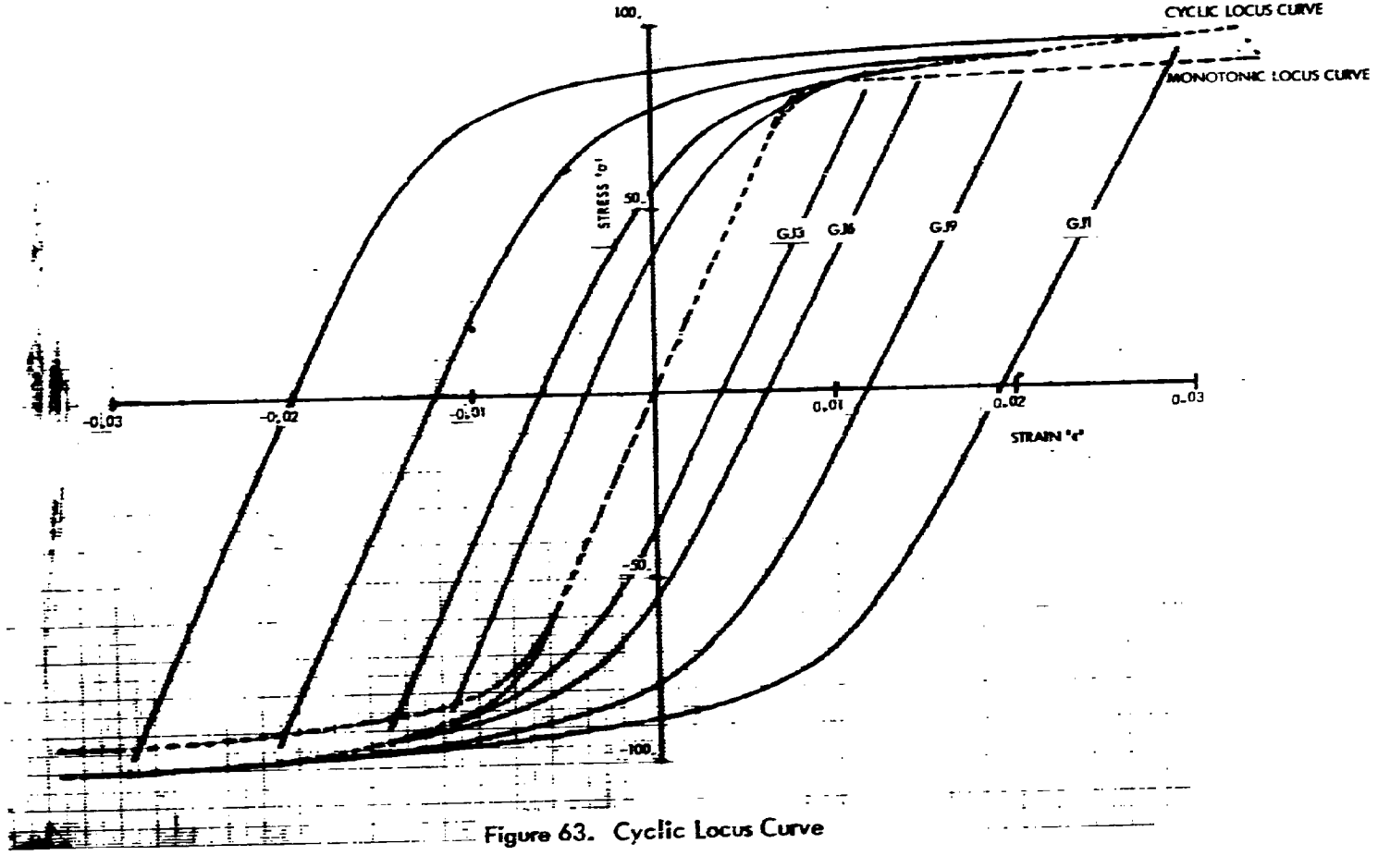

Figure 63. Cyclic Locus Curve

and assumes that all the branch curves are geometrically similar to this but magnified by a factor of 2, i.e.

$$\sigma^{B} = \sigma^{B}_{0} + 2\left(\frac{\sigma^{B}_{0}}{E}\right)^{n}$$

where superscript 'B' refers to branch curve.

Consider the stable cyclic curves plotted in Figure 64 with their lower tips matching. Obviously none of the upper branches, as they leave the cyclic locus curve, are similar nor are any of them similar to the cyclic locus curve magnified by a factor of 2.0. Jhansale, in Reference 6, characterizes a material that exhibits this phenomenon as a "Non Massing" material. Jhansale does, however, suggest that these branch curves are similar if an appropriate translation is made along the linear slope. This has been done in Figure 65, which shows that the upper branches, as they leave the cyclic locus curve for 7075-T651 aluminum, can be characterized by a single curve.

A similar study of the lower branches is not so successful, as is shown in Figure 66, in which the upper tips are matched. Obviously, since the elastic modulii are not the same no amount of translation along the linear slope will make the curves match. Therefore, consider a basic lower branch curve

$$\sigma^{B} = \sigma^{B}_{0} + 2\left(\frac{\sigma^{B}_{0}}{E_{B}}\right)^{n} \qquad (1)$$

defined in a basic branch curve system 'B' and which has the same elastic modulus 'E' as the locus curve. Now, consider a typical lower branch curve,

$$\sigma^{LB} = \sigma^{LB}_{0} + 2\left(\frac{\sigma^{LB}_{0}}{E_{LB}}\right)^{n} \qquad (2)$$

defined in a lower branch curve system 'LB' and which has an elastic modulus of 'E_B'. If the origin of the lower branch curve is located on the linear portion of the basic branch curve at point 'O', see Figure 67, the transformation between the two systems is:

$$\begin{aligned} \sigma &= \sigma^{LB}_{0} + \sigma^{B}_{0} \quad \text{or} \quad \sigma^{LB} = \sigma - \sigma_{0} \\ \sigma^{B}_{0} &= \sigma^{LB}_{0} + \sigma^{B}_{0} \quad \text{or} \quad \sigma^{LB}_{0} = \sigma^{B}_{0} - \sigma^{B}_{0} \end{aligned} \qquad (3)$$

The elastic modulii are defined

$$\frac{d\sigma^{LB}}{d\sigma^{LB}_{0}} = \frac{1}{E_{B}} \qquad (4)$$

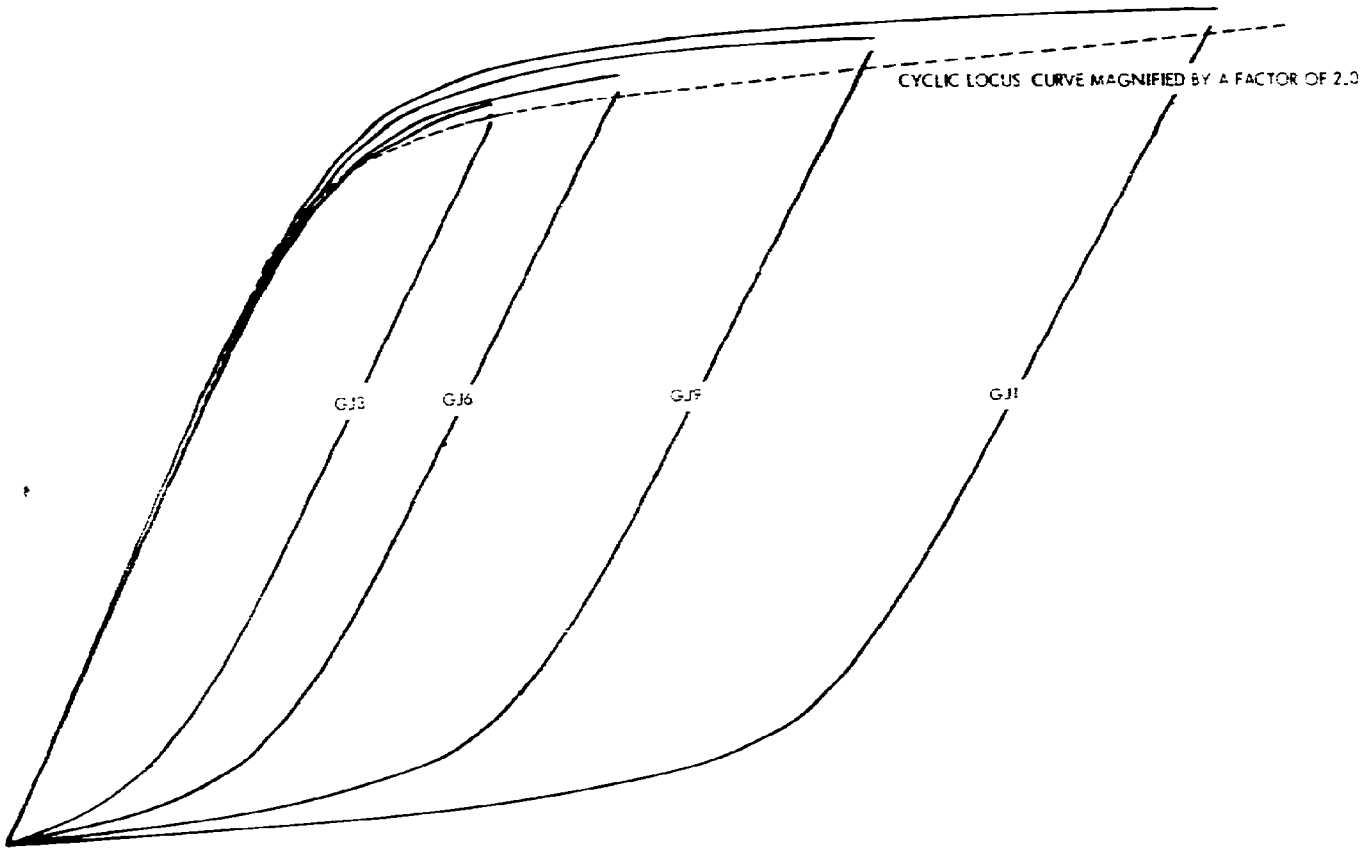

Figure 64. Stable Hysteresis Loops with Matching Lower Tips

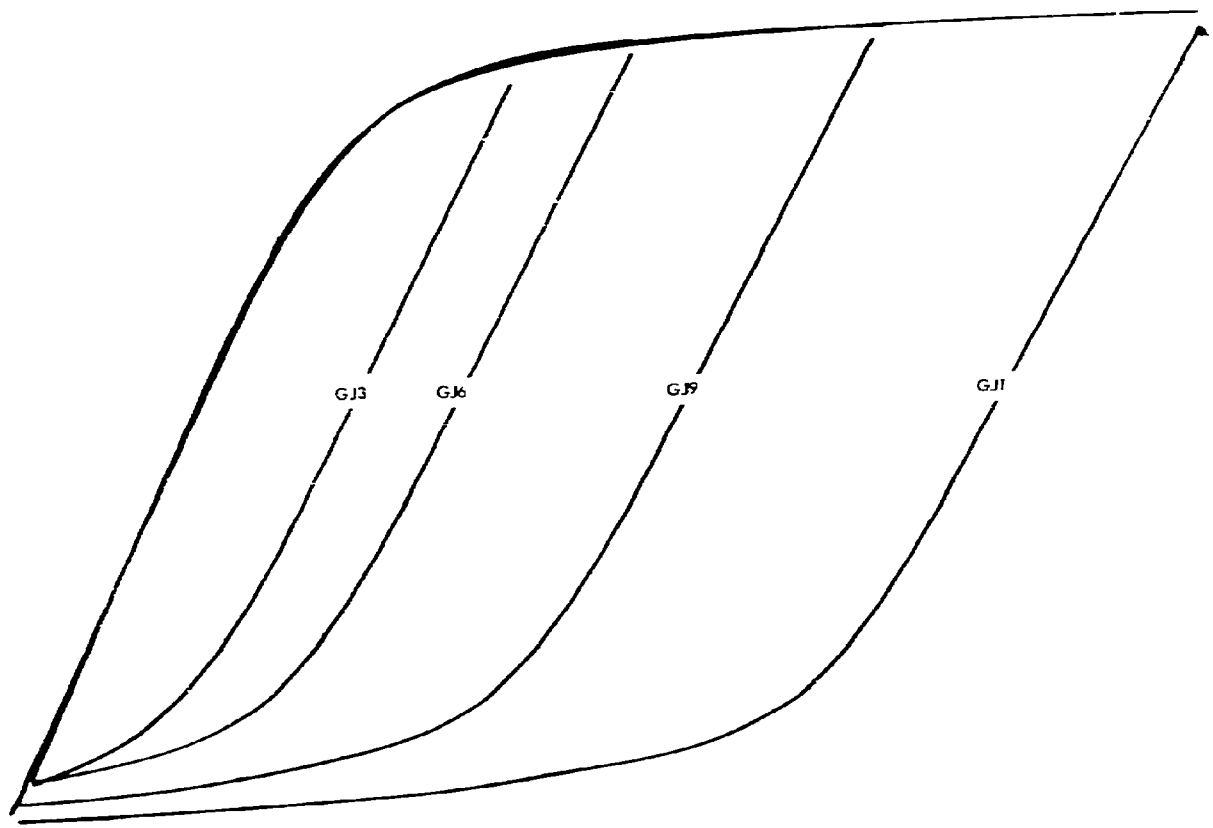

Figure 65. Stable Hysteresis Loops with Matching Upper Branches

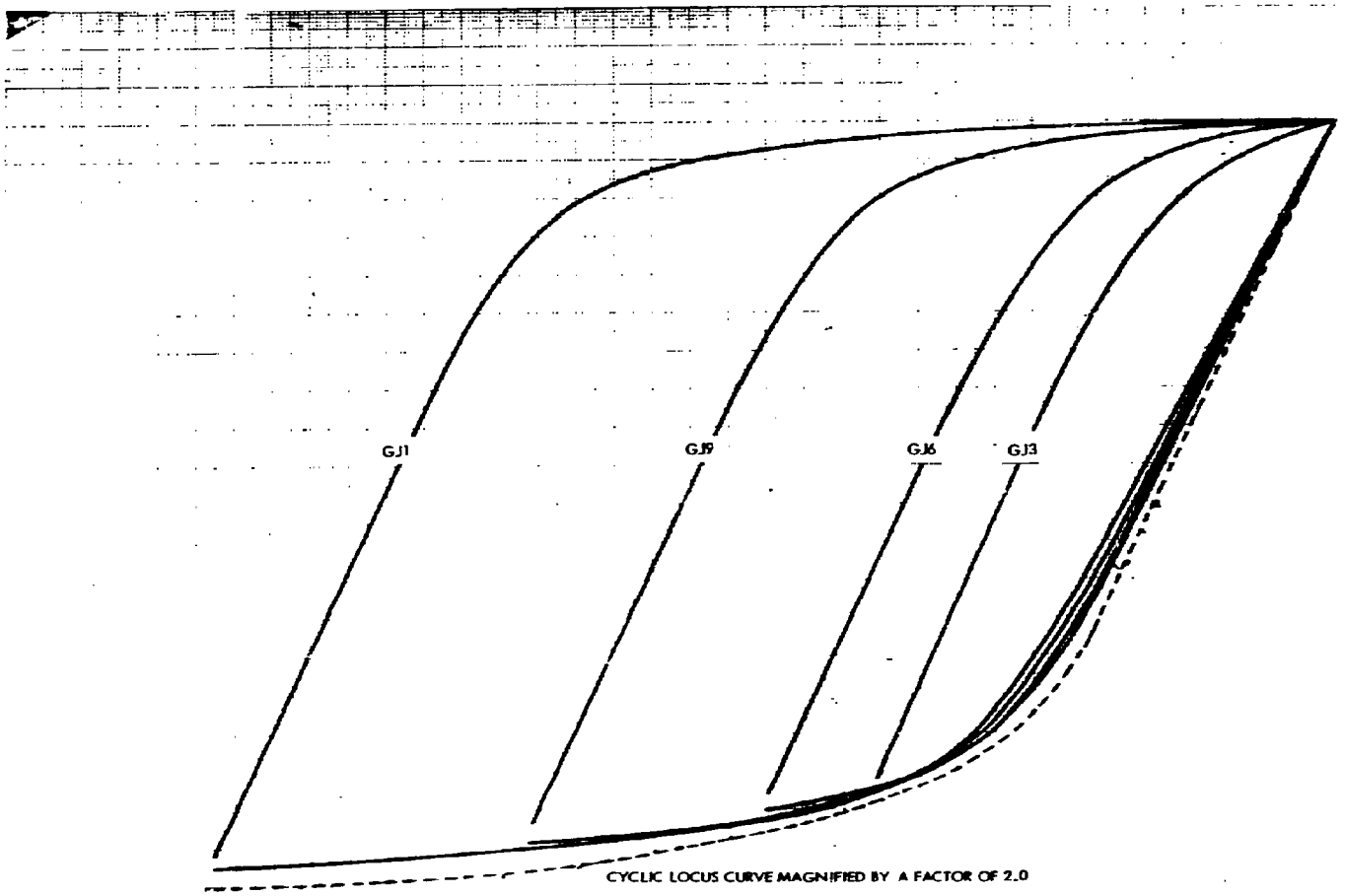

Figure 66. Stable Hysteresis Loops with Matching Upper Tips

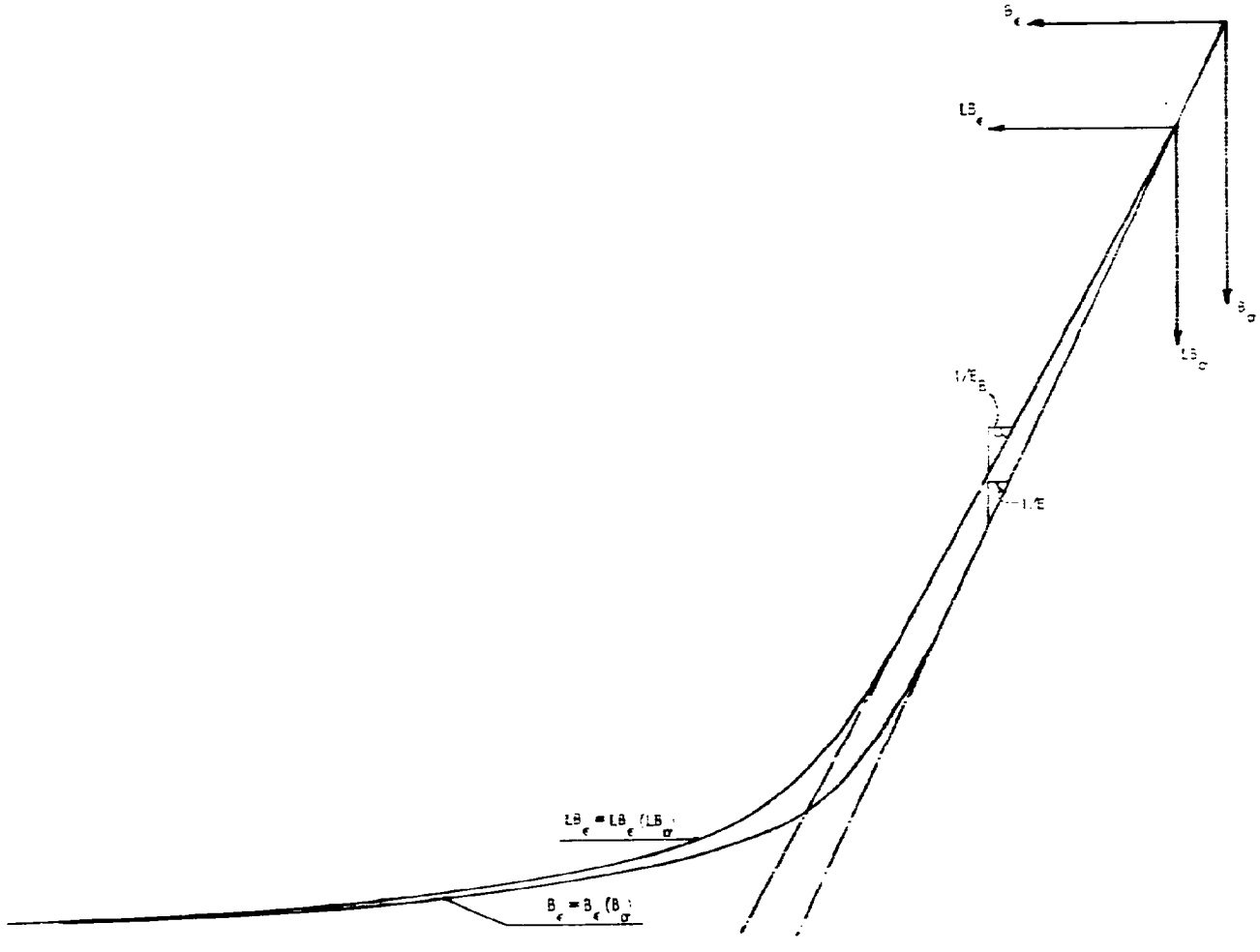

Figure 67 A Basic Stable Lower Branch Curve

and

$$\frac{d^{B}\epsilon_{B}}{d^{B}\sigma} = \frac{1}{E} \tag{5}$$

From (3) equation (4) can be written

$$\frac{d^{B}\epsilon_{LB}}{d^{B}\sigma} = \frac{1}{E_{B}} \tag{6}$$

Then as long as $^{B}\epsilon_{B}$ and $^{B}\epsilon_{LB}$ remain elastic equations (5) and (6) give

$$d^{B}\epsilon_{LB} - d^{B}\epsilon_{B} = \left(\frac{1}{E_{B}} - \frac{1}{E}\right) d^{B}\sigma$$

Integrating

$$^{B}\epsilon_{LB} - {}^{B}\epsilon_{B} = \left(\frac{1}{E_{B}} - \frac{1}{E}\right) {}^{B}\sigma + C$$

Now $^{B}\epsilon_{LB} = {}^{B}\epsilon_{B}$ when $^{B}\sigma = E \cdot {}^{B}\epsilon_{o}$

then

$$C = -\left(\frac{1}{E_{B}} - \frac{1}{E}\right) E \cdot {}^{B}\epsilon_{o}$$

and

$$^{B}\epsilon_{LB} - {}^{B}\epsilon_{B} = \left(\frac{1}{E_{B}} - \frac{1}{E}\right)\left({}^{B}\sigma - E \cdot {}^{B}\epsilon_{o}\right) \tag{7}$$

It will now be assumed that equation (7) defines the relationship between a basic branch curve and the lower branch curve for the full elastic/plastic range. Then the term

$$\left(\frac{1}{E_{B}} - \frac{1}{E}\right) \cdot {}^{B}\sigma$$

lines up the elastic slopes of the curves and the term

$$\left(\frac{1}{E_{B}} - \frac{1}{E}\right) E \cdot {}^{B}\epsilon_{o}$$

is a translation along the elastic axis of the basic branch curve such that the nonlinear portions match. To verify this the curve $^{B}\epsilon_{B}\left({}^{B}\sigma\right)$ has been created from equation 7 for each of the five tests shown in Figures 59 through 62 with the translations along the elastic axis chosen to give the best match over the nonlinear portions of the curve. These are superimposed in Figure 68 showing that a single basic curve together with equation (7) can adequately be

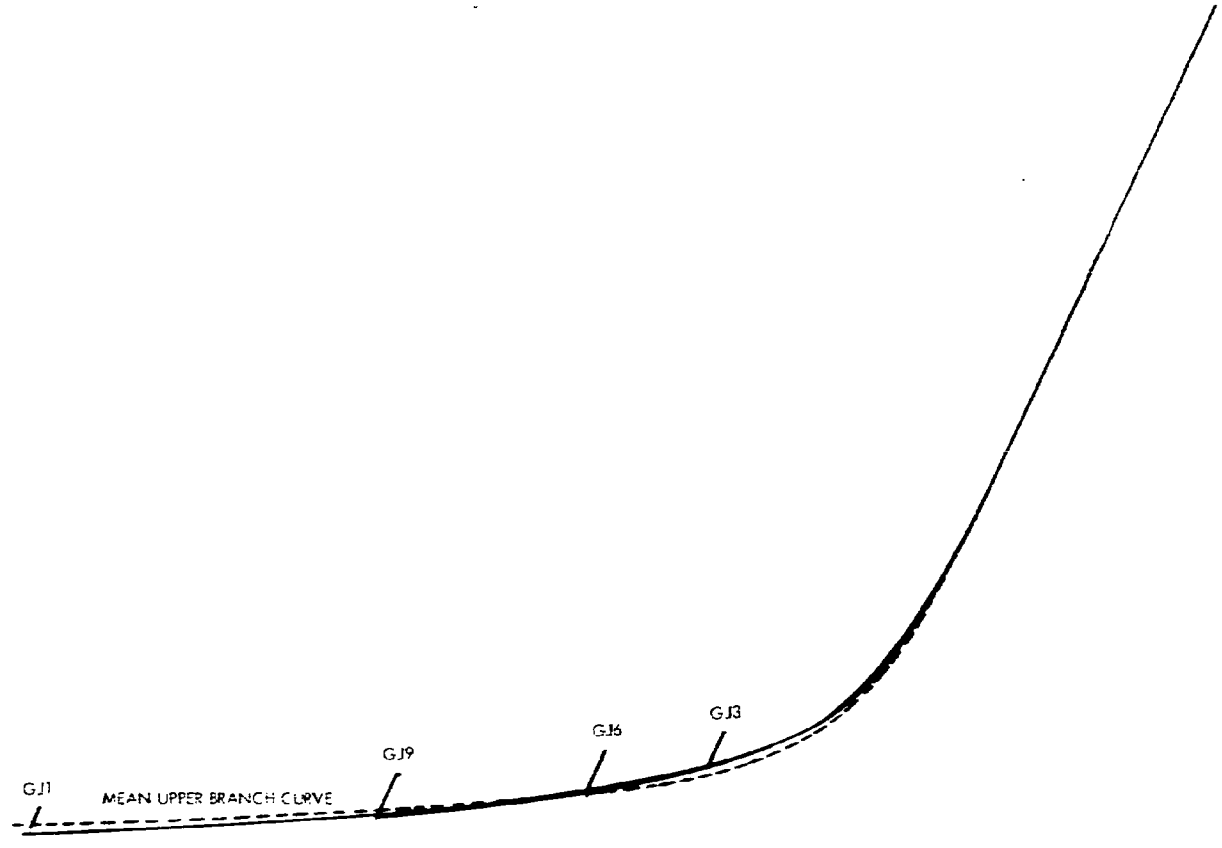

Figure 68. Stable Hysteresis Loops with Matching Modified Lower Branches

be used to represent all the lower branch curves. Figure 68 also shows that the upper branch curve is very similar to the basic lower branch curve. Therefore, the single basic branch curve shown in Figure 69 will be used for both the upper and lower branches. To use equation (7), it is necessary to relate the branch curve modulus E_B to the strain increment $\Delta\epsilon/2$. This has been done in Figure 70, using the lower branch elastic moduli from the five basic tests. Finally, the branch curves are located in the basic stress-strain space by requiring that they reintersect the cyclic locus curve at a magnitude of strain equal and opposite to that for the point on the cyclic locus curve from which they started.

From the above procedure the trace of the upper branch curves leaving the compression segment of the cyclic locus curve and the trace of the lower branch curves leaving the tension segment of the cyclic locus curve are defined. What is still not known is the trace of a branch curve when it leaves another branch curve. Although the tests thus far run are not loaded to this condition it is expected that when a branch curve leaves the elastic portion of another branch curve they will have the same elastic moduli. This means that the upper branch curves will also have to change their shape. It will therefore be assumed that the shape of both the upper and lower branch curves vary linearly between the basic curve and the lower branch curve corresponding to the maximum $\Delta\epsilon/2$ thus far experienced, see Figure 71. If the material has been loaded along the cyclic locus curve to a strain whose absolute magnitude is $|\Delta\epsilon/2|$ then the lower branch curve would leave the point P on the tension segment of the locus curve with an elastic modulus of $\bar{E}_B$ defined in Figure 70. The upper branch curve would leave the point P' on the compression segment of the locus curve with an elastic modulus of E. Now, consider a loading from point P along the lower branch curve to S. Then a loading from S will follow an upper branch curve which has an elastic modulus defined as follows.

$$\epsilon_{MAX} = \epsilon_P - \sigma_P / \bar{E}_B \tag{8}$$

$$\epsilon_{MIN} = \epsilon_{P'} - \sigma_{P'} / E \tag{9}$$

$$\Delta\epsilon_1 = \epsilon_S - \sigma_S / E_B - \epsilon_{MIN} \tag{10}$$

$$\Delta\epsilon_2 = \epsilon_{MAX} - \epsilon_{MIN} \tag{11}$$

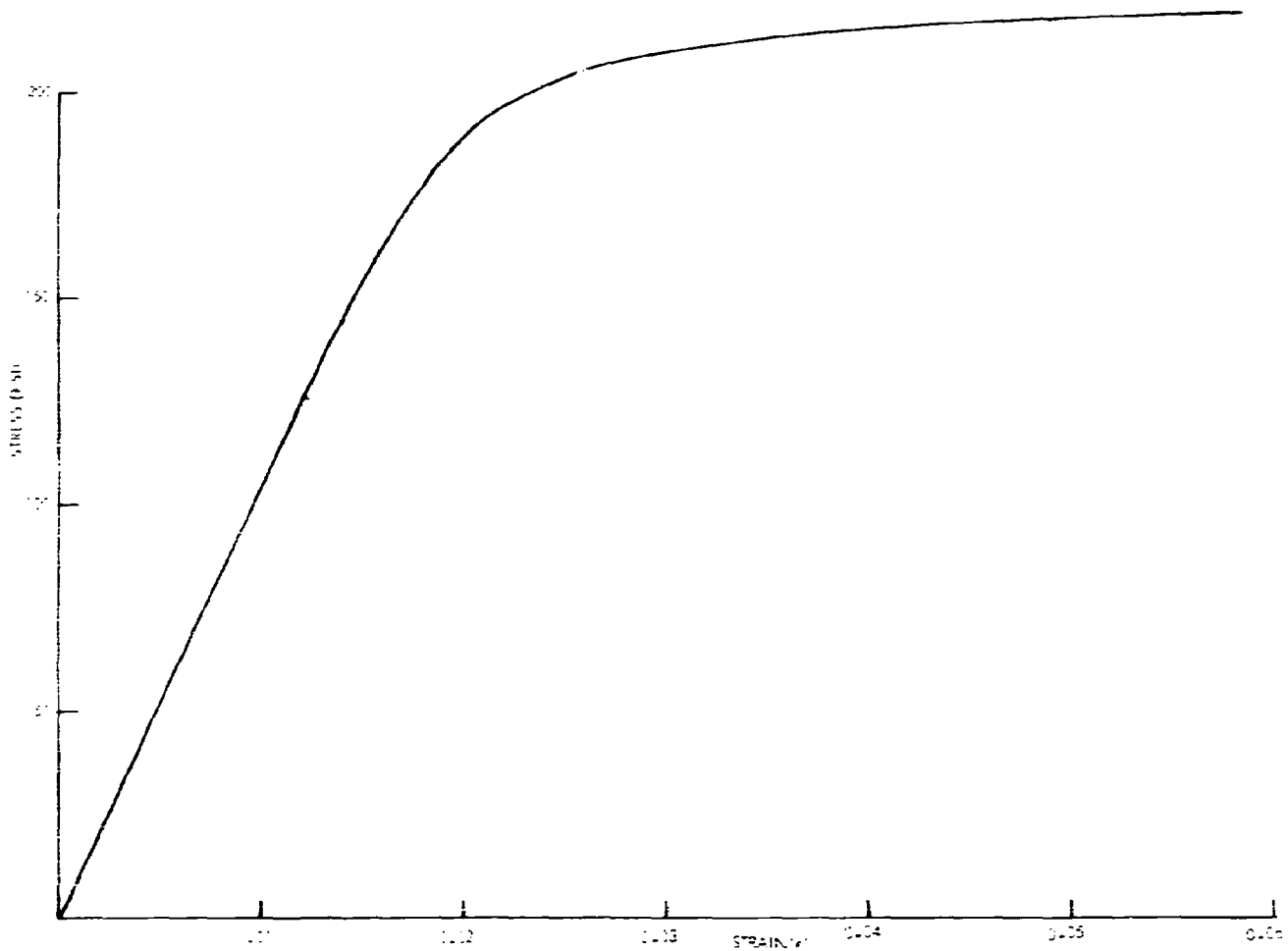

Figure 69. Basic Branch Curve

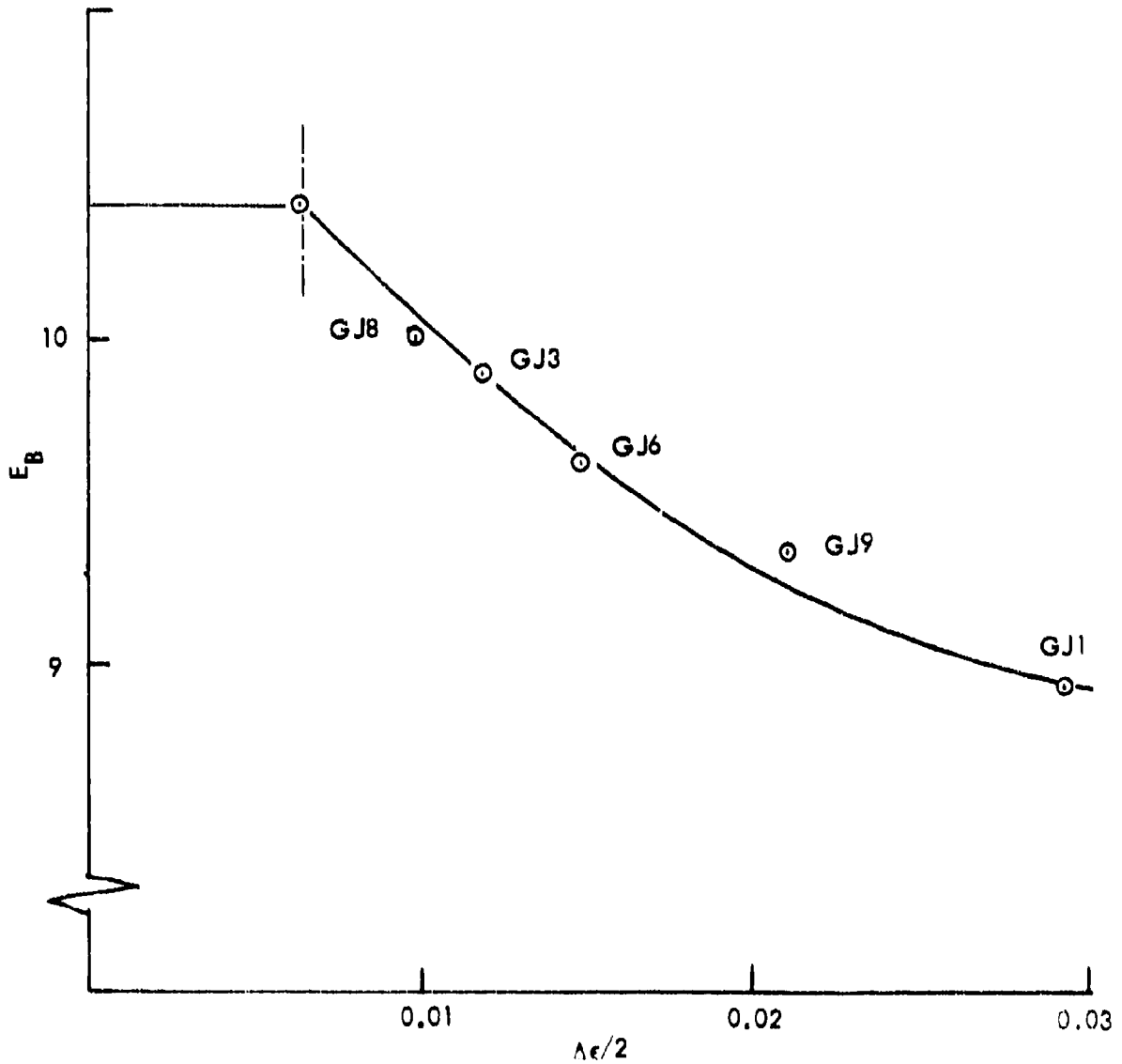

Figure 70. Lower Branch Curve Elastic Modulus

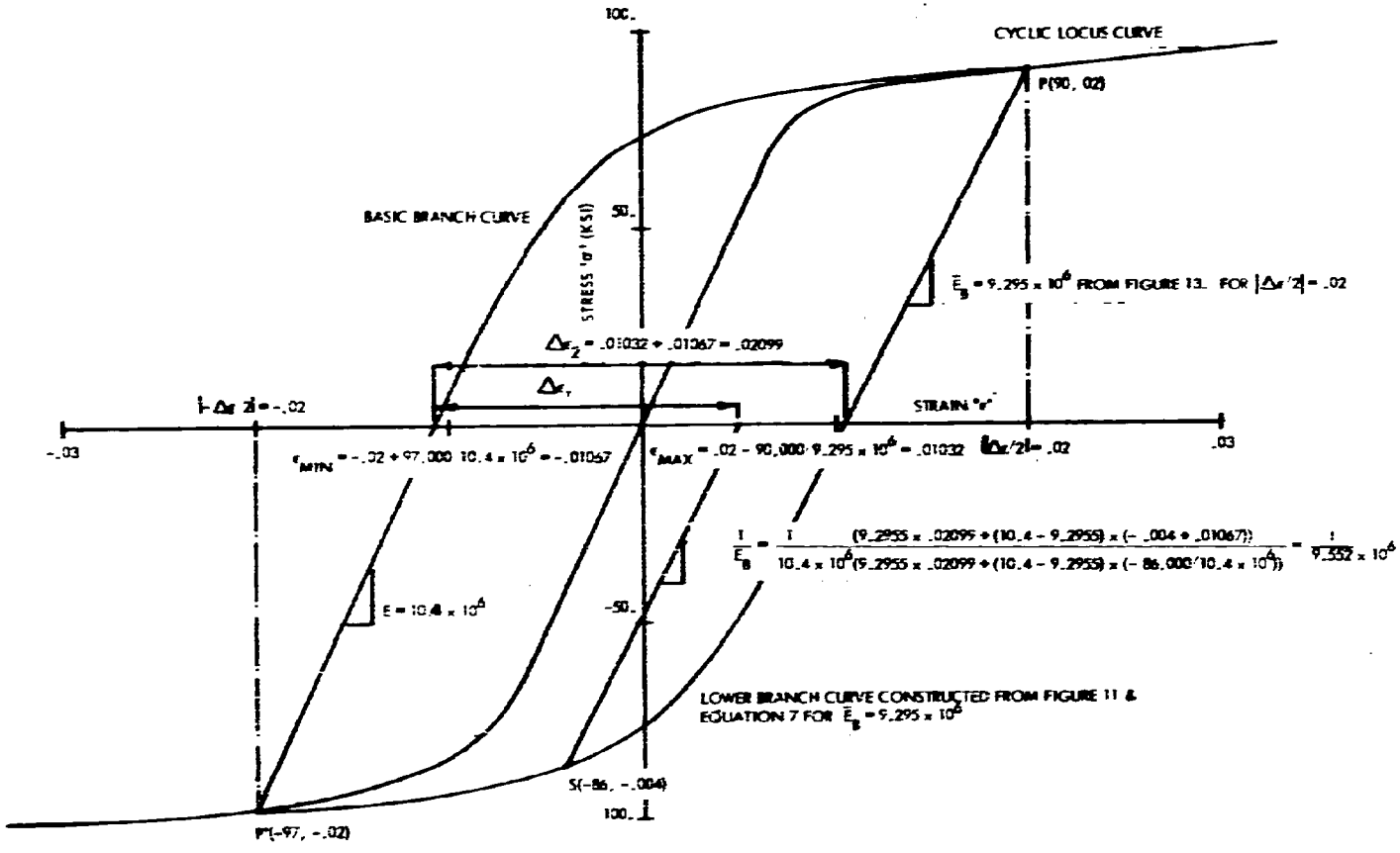

Figure 71. Variation Of The Branch Curve Modulii

Then

$$\frac{1}{E_B} = \left(\frac{1}{\bar{E}_B} - \frac{1}{E}\right)\frac{\Delta\epsilon_1}{\Delta\epsilon_2} + \frac{1}{E} \tag{12}$$

Substituting for $\Delta\epsilon_1$

$$\frac{1}{E_B} = \left(\frac{1}{\bar{E}_B} - \frac{1}{E}\right)\frac{\left(\epsilon_S - \sigma_S / E_B - \epsilon_{MIN}\right)}{\Delta\epsilon_2} + \frac{1}{E}$$

or

$$E_B = E\left[\frac{1 + (\sigma_S/E)(E/\bar{E}_B - 1) / \Delta\epsilon_2}{1 + (\epsilon_S - \epsilon_{MIN})(E/\bar{E}_B - 1) / \Delta\epsilon_2}\right] \tag{13}$$

Finally, the branch curves, when they leave another branch curve, are located in the stress-strain space by requiring that they always form closed loops. More specifically, this can be stated by the condition that the branch curve must intersect the origin of the branch curve that it leaves.

The complete algorithm for simulating the stable response of 7075-T651 aluminum is illustrated in Figure 72. This example proceeds through the following steps.

- Assume that the material has been cyclic hardened to point A(90,0.02) on the cyclic locus curve

  $\Delta\epsilon_2 = 0.02$

  $\bar{E}_B = 9.295\times10^6$ from Figure 70

  $\bar{P}_1 = (90, 0.02)$, $\bar{P}_1' = (-97, -0.02)$

  $\epsilon_{MAX} = 0.02 - 90{,}000 / 9.295\times10^6 = 0.01032$

  $\epsilon_{MIN} = -0.02 + 97{,}000 / 10.4\times10^6 = -0.01067$

  $\Delta\epsilon_2 = 0.01032 + 0.01067 = 0.02099$

- Loading from A to B(-90,-0.007) along the branch curve which has an elastic modulus of 9.295×10^6. The branch curve is located so that it passes through points A and P'. Then S' (-90,-0.007) and the elastic modulus for the next loading increment is

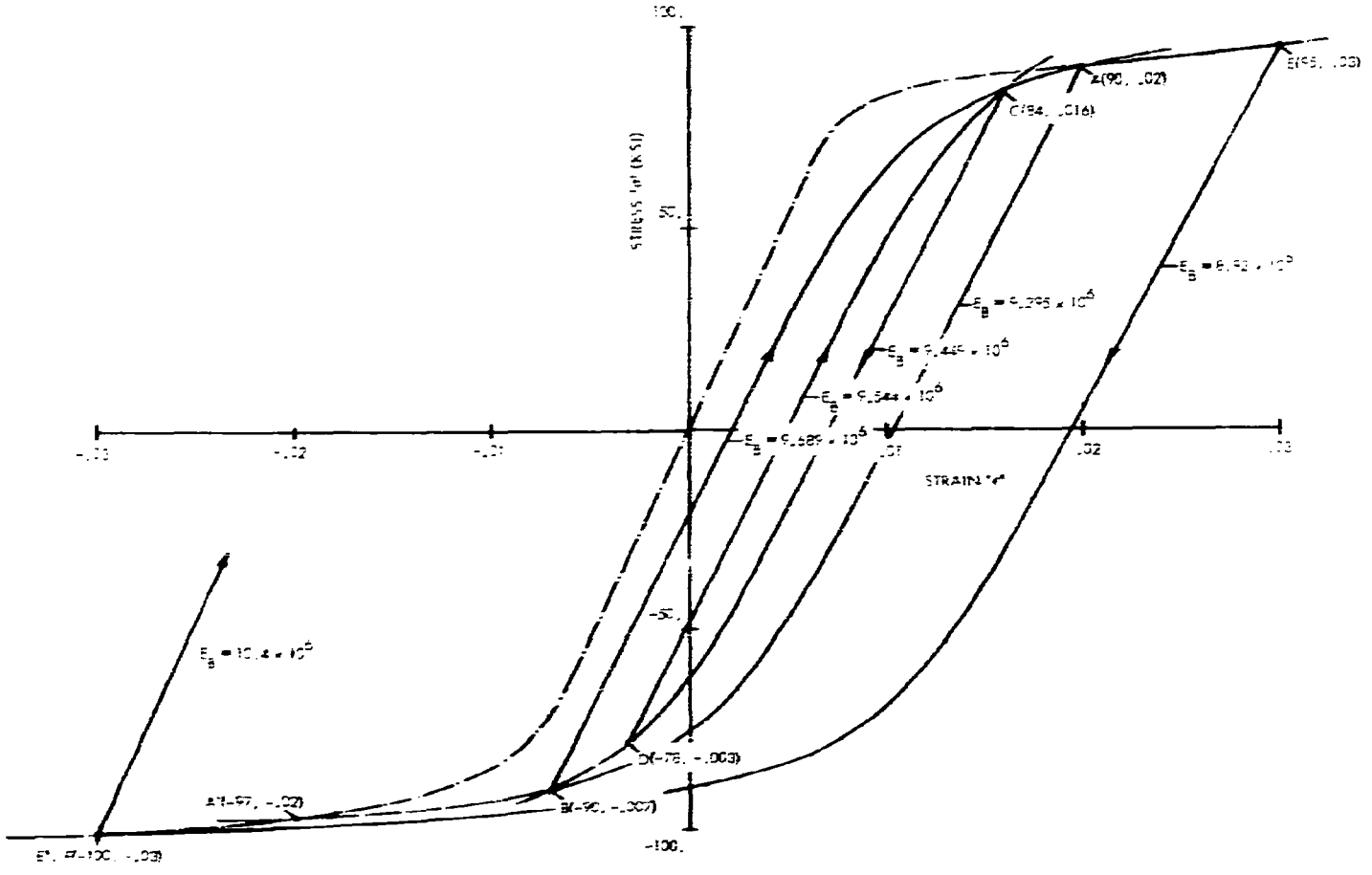

Figure 72. Example of Stable Response Algorithm

$$E_B = 10.4\times10^6 \left[\frac{1 + (-90{,}000/10.4\times10^6)(10.4/9.295 - 1)0.02099}{1 + (-0.007 + 0.01067)(10.4/9.295 - 1)/0.02099}\right] = 9.689\times10^6$$

- Loading from B to C(84, 0.016) along the branch curve which has an elastic modulus of 9.689×10^6. The branch curve is located so that it passes through points B and A. Then $\vec{S} = (84, 0.016)$ and the elastic modulus for the next loading increment is

$$E_B = 10.4\times10^6 \left[\frac{1 + (84{,}000/10.4\times10^6)(10.4/9.295 - 1)/0.02099}{1 + (0.016 + 0.01067)(10.4/9.295 - 1)/0.02099}\right] = 9.449\times10^6$$

- Loading from C to D(-78, -0.003) along the branch curve which has an elastic modulus of 9.449×10^6. The branch curve is located so that it passes through points C and B. Then, $\vec{S} = (-78, -0.003)$ and the elastic modulus for the next loading increment is

$$E_B = 10.4\times10^6 \left[\frac{1 + (-78{,}000/10.4\times10^6)(10.4/9.295-1)/0.02099}{1 + (-0.003 + 0.01067)(10.4/9.295-1)/0.02099}\right] = 9.544\times10^6$$

- Loading from D to E(95, 0.03). The material is first loaded to C along the branch curve which has an elastic modulus of 9.544×10^6. It then follows the branch curve which has a modulus of 9.689×10^6 and passes through points B and A. At Point A follows the cyclic locus curve to E.

  $\Delta\epsilon/2 = 0.03$

  $\bar{E}_B = 8.92\times10^6$ from Figure 70

  $\vec{P}_2 = (95, 0.03)$, $\vec{P}_2' = (-100, -0.03)$

  $\epsilon_{MAX} = 0.03 - 95{,}000/8.92\times10^6 = 0.02087$

  $\epsilon_{MIN} = -0.03 + 100{,}000/10.4\times10^6 = -0.02038$

  $\Delta\epsilon_2 = 0.02087 + 0.02038 = 0.04125$

- Loading from E to F(-100, -0.03) along the branch curve which has an elastic modulus of 8.92×10^6. Then, $\vec{S} = (-100, -0.03)$ and the elastic modulus for the next loading increment is

$$E_B = 10.4\times10^6 \left[\frac{1 + (-100{,}000/10.4\times10^6)(10.4/8.92-1)0.04125}{1 + (-0.03 + 0.02038)(10.4/8.92-1)0.04125}\right] = 10.4\times10^6$$

- Loading from point F will follow the basic branch curve which has an elastic modulus of 10.4×10^6.

4.1.1.2 Cyclic Hardening and Softening - It is first necessary to represent the transient loops in a similar fashion to the stable loops. The loops generated during the first cycle for four of the tests are superimposed on the basic stable branch curve in Figure 73 with the upper branches matching. Also, a basic branch curve has been generated for the initial lower branch curve of each of the four tests using equation 7 and are superimposed on the basic branch curve in Figure 74. Figures 73 and 74 show that the basic branch curve can be used to represent the transient loops in the same way it is used to represent the stable loops.

In order to include cyclic hardening or softening in a hysteresis loop fatigue analysis it is necessary to define the rate at which the material hardens for each cycle. Based on observations of the fully reversed cyclic tests GJ1 through GJ37 it is shown that the hardening of 7075-T651 aluminum can be adequately defined by two simple curves. Figure 75 shows the plots of the peak tension stress versus the number of fully reversed cycles for four of the tests. From these plots the number of fully reversed cycles required to completely harden the material 'n_H' has been defined and is plotted in Figure 76 versus the strain increment $\Delta\epsilon/2$. Also, from Figure 75 the increment '$\Delta\sigma_H$' between the completely hardened peak tension stress (points on the cyclic locus curve) and the peak monotonic tension stress (points on the monotonic locus curve) have been defined. The data points in Figure 76 have been normalized by 'n_H' and '$\Delta\sigma_H$' and replotted in Figure 77. This shows that a single curve adequately defines the hardening rate of 7075-T651. Therefore, this curve, together with the curve in Figure 76, can be used to calculate the amount of hardening '$\Delta\sigma/\Delta\sigma_H$' due to fully reversed cycles at any strain increment '$\Delta\epsilon/2$'. Consider an example in which a specimen of 7075-T651 is cycled between strains of ± 0.02. Then

$\Delta\epsilon/2 = 0.02$

$n_H = 7.4$ from Figure 76

$n = n_H \cdot 7.4 = 0.135$ for the first cycle

$\Delta\sigma/\Delta\sigma_H = 0.415$ from Figure 77

i.e. the amount of hardening for the first cycle is 41.5%

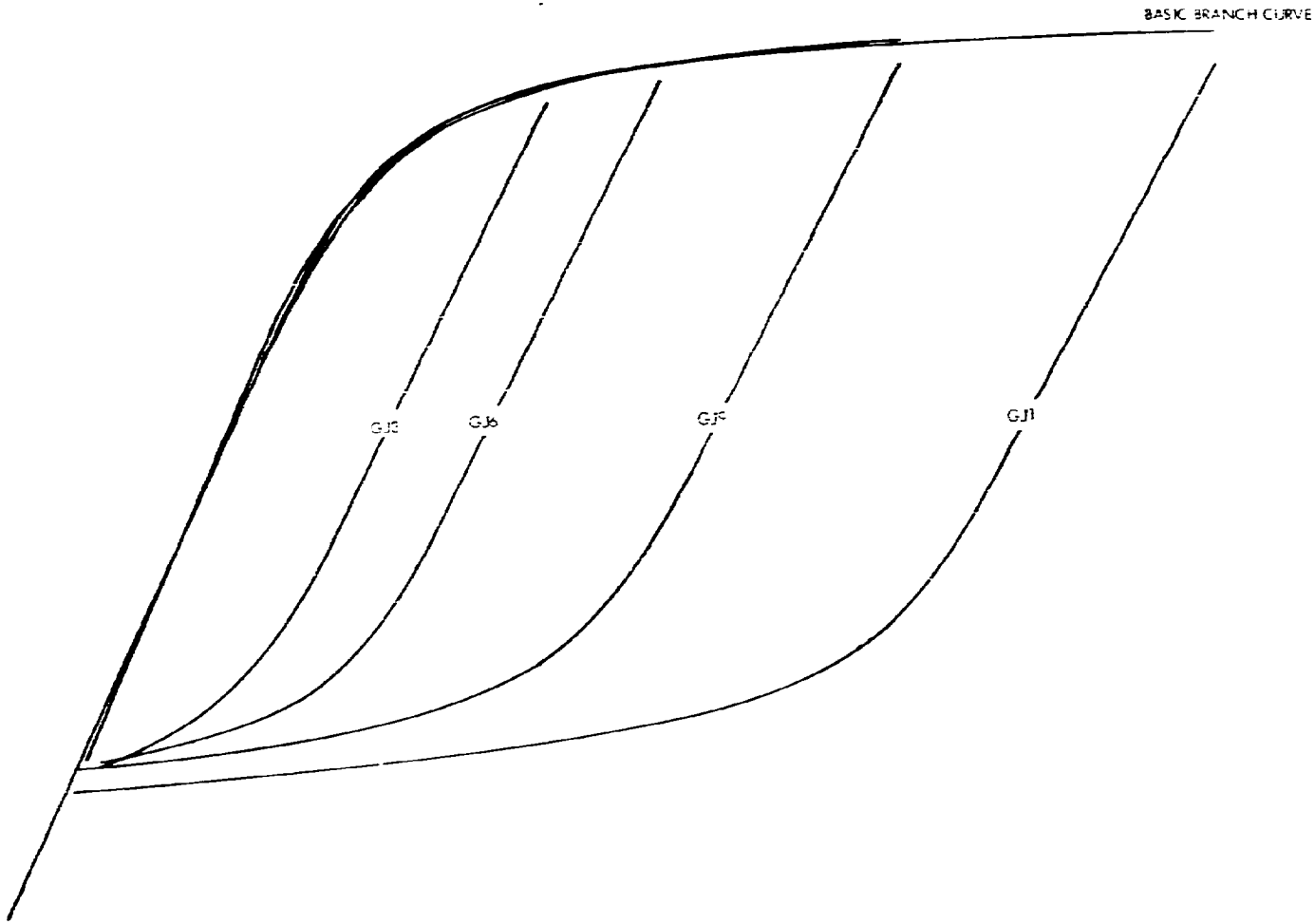

Figure 73. Initial Hysteresis Loops with Matching Upper Branches

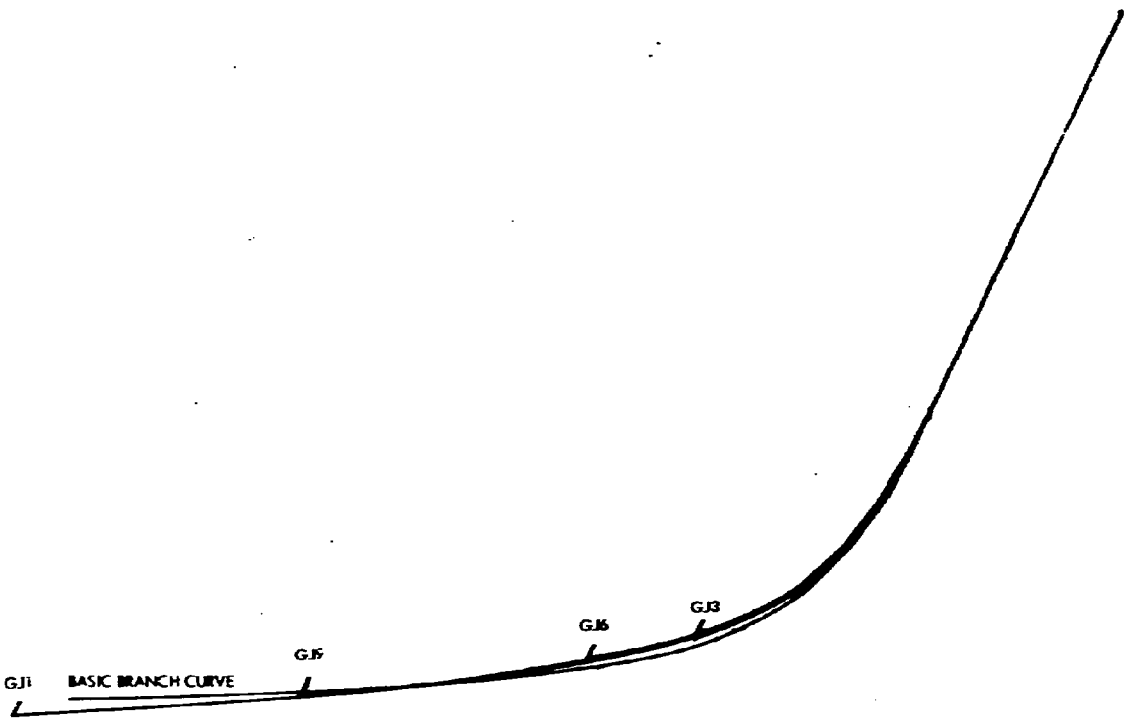

Figure 74. Initial Hysteresis Loops with Modified Lower Branches Matching

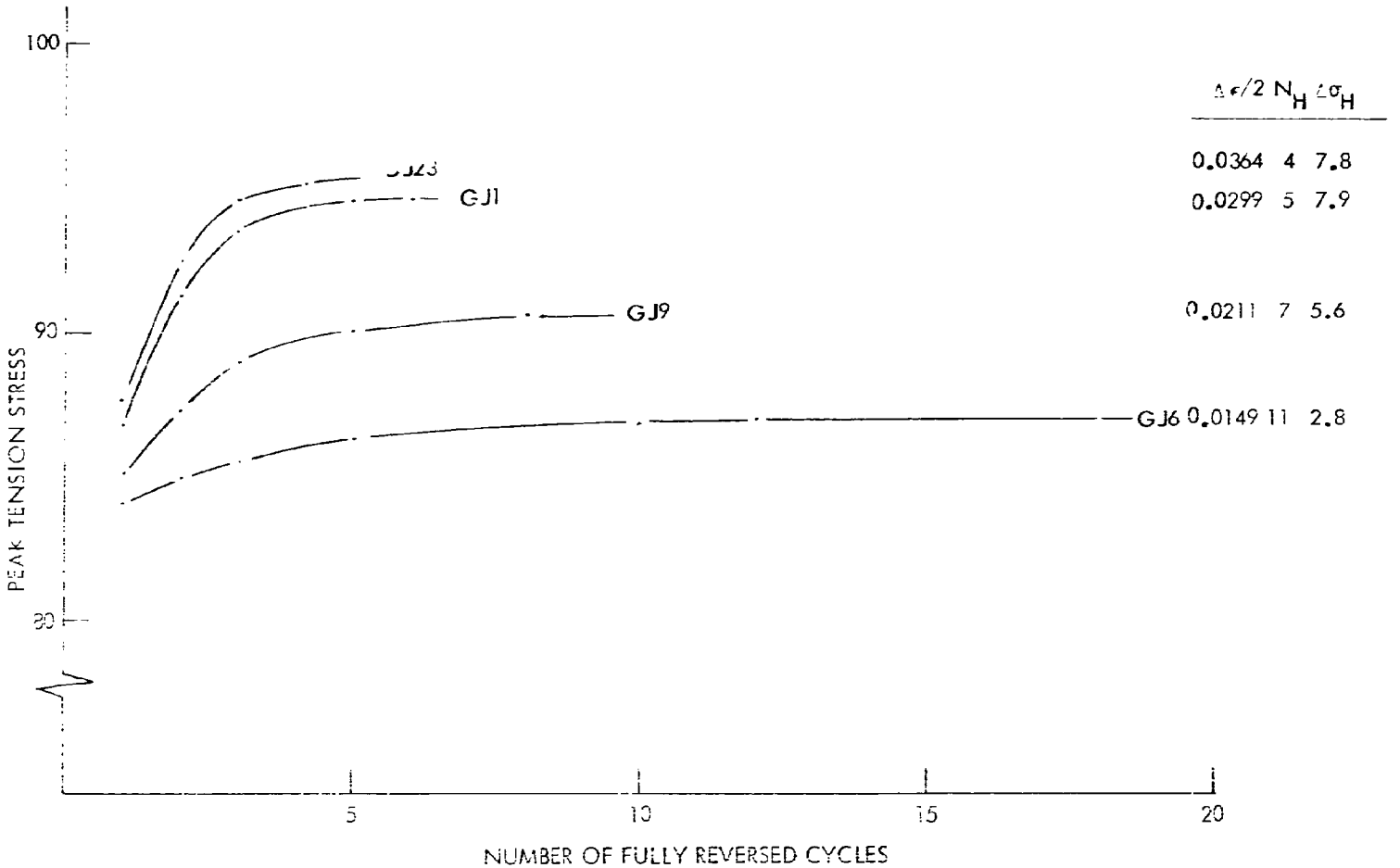

	$\Delta\epsilon/2$	N_H	$\Delta\sigma_H$
GJ1	0.0364	4	7.8
GJ3	0.0299	5	7.9
GJ9	0.0211	7	5.6
GJ6	0.0149	11	2.8

Figure 75. Tension Hardening Curves

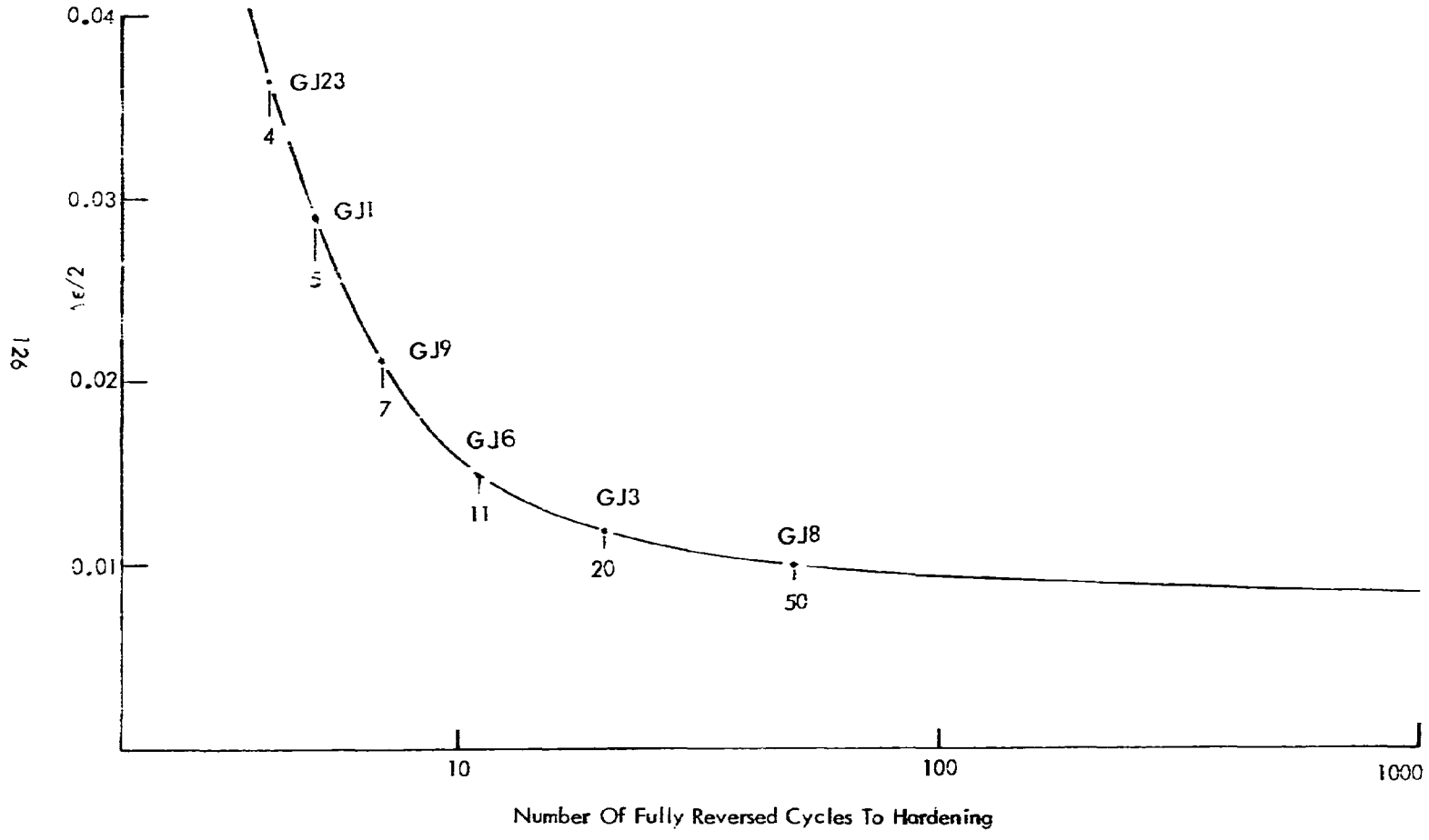

Figure 76. Number of Reversals to Harden

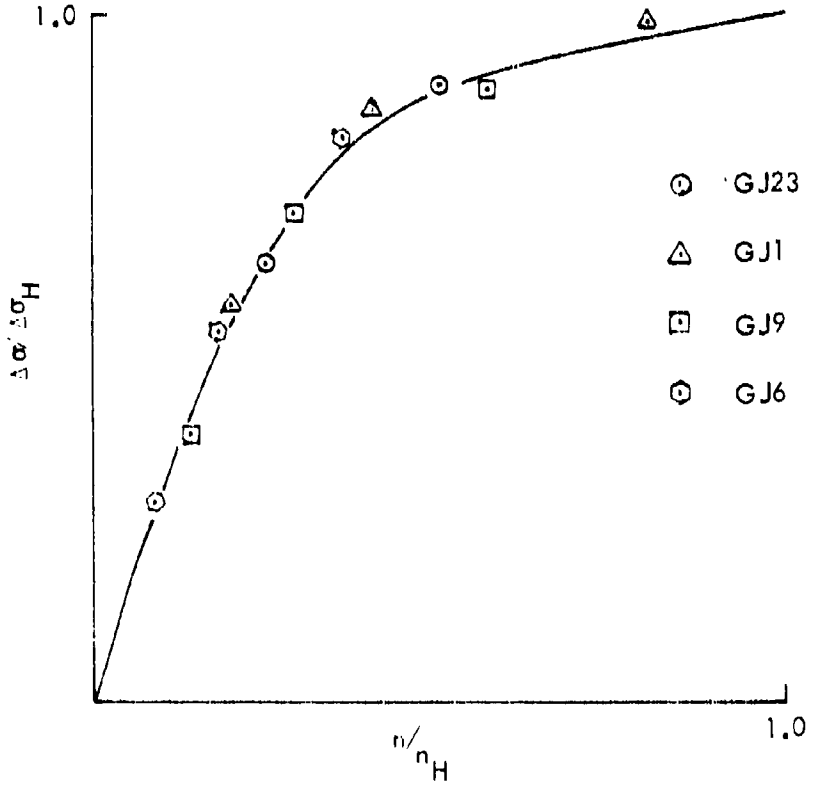

Figure 77. Normalized Hardening Curve

$n/n_H = 2/7.4 = 0.270$ for the second cycle

$\Delta\sigma/\Delta\sigma_H = 0.685$ from Figure 77

i.e. the amount of hardening after the second cycle is 68.5%

This procedure is based on tests for fully reversed cycles between strains of equal and opposite magnitude. In reality, this very rarely occurs, the hysteresis loops being generally offset along the strain axis. Also, full hardening usually results from loops of various sizes and not from loops of fixed size. In order that the analysis procedure may be applied to these general conditions the following assumptions will be made.

(1) The strain increment $\Delta\epsilon$ used in Figure 76 is independent of where it is located on the strain axis (i.e. mean strain).

(2) The hardening rate term 'n/n_H' is accumulative for cycles, i.e.

$$\frac{n}{n_H} = \sum_{i=1}^{T} \frac{n^i}{n_H^i}$$

(3) The percent of hardening '$\Delta\sigma/\Delta\sigma_H$' effects the full range of the monotonic locus curve.

When the material is loaded along the tension segment of the monotonic curve to a strain of ϵ and then unloaded an amount 2ϵ a specific amount of hardening will have occured to the compressive segment of the monotonic curve. A similar affect will be seen to have occurred to the tension monotonic curve if the material were first loaded in compression. When the material is loaded along the tension monotonic curve an amount ϵ and then unloaded and reloaded back to ϵ elastically no hardening will have occurred to the tension segment of the monotonic curve. The same effect would be seen for the compression segment of the monotonic curve. Based on these two observations it will be assumed that the hardening of the tension and compression segments of the monotonic curves are uncoupled. The hardening of the compression monotonic curve will be based on the amount of incremental strain associated with either the tension monotonic curve or the upper branch curve. Similarly, the hardening of the tension monotonic curve will be based on the amount of incremental strain associated with either the compressive monotonic curve or the lower branch curves. Finally, to simulate closed loops during the transient condition, it will be assumed that

the points in the stress strain space will expand along the elastic slope of the branch curve that initiates from that point.

Consider now this procedure included in the following example which is shown graphically in Figure 78. Initial loading to $A_1(86, 0.025)$ along the tension segment of the monotonic locus curve. Then $A_1'(-92,-0.025)$ is the point on the compressive segment of the monotonic locus curve which a branch curve leaving A_1 must pass.

$\Delta\epsilon/2=0.025$

$\bar{E}_B = 9.06\times10^6$ from Figure 70

$\epsilon_{MAX}=0.025 - 86{,}000/9.06\times10^6=0.01551$

$\epsilon_{MIN}=-0.025 + 92{,}000/10.4\times10^6 = 0.01615$

$\Delta\epsilon_2=0.03166$

$n_H = 5.7$ from Figure 76

$(n/n_H)_{TEN} = 1/5.7=0.1754$

$\Sigma(n/n_H)_{TEN} =0.1754$

$(\Delta\sigma/\Delta\sigma_H)_{COMP} =0.51$ or 51% hardening, from Figure 77.

Loading from A_1 (86,0.025) to B_1 (-89.5,-0.008) along the branch curve which has an elastic modulus of 9.06×10^6 and intersects the point A_2' (-95.5,-0.0253). A_2' lies on the 51% hardened compression locus curves at the intersection with the extension of a basic branch curve originating from A_1'.

$\Delta\epsilon/2=0.0165$

$$E_B = 10.4\times10^6 \left[\frac{1 + (-89{,}500/10.4\times10^6)(10.4/9.06-1)/0.03166}{1 + (-0.008+0.01615)(10.4/9.06-1)/0.03166} \right] = 9.616\times10^6$$

$n_H = 9.5$ from Figure 76

$(n/n_H)_{COMP} = 1/9.5=0.1053$

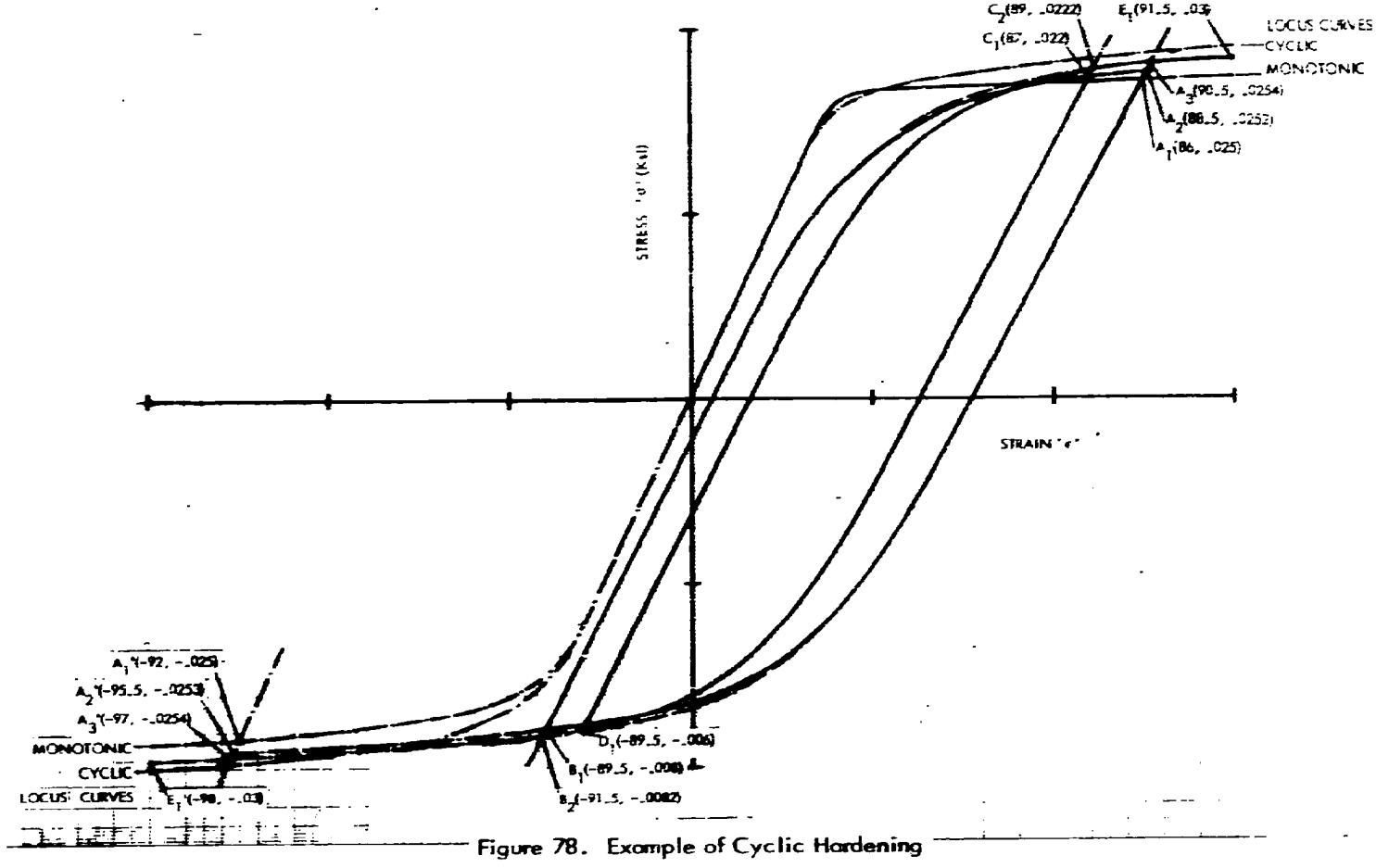

Figure 78. Example of Cyclic Hardening

$$\Sigma(n/n_H)_{COMP} = 0.1053$$

$$(\Delta\sigma/\Delta\sigma_H)_{TEN} = 0.335 \text{ or } 33.5\% \text{ hardening from Figure 77.}$$

Loading from $B_1(-89.5,-0.008)$ to $C_1(87,0.022)$ along the branch curve which has an elastic modulus of 9.616×10^6 and intersects the point $A_2(89.5,0.0252)$. A_2 lies on the 33.5% hardened tension locus curve at the intersection with the extension of the branch curve originating from point A_1 and having an elastic modulus of 9.06×10^6

$$\Delta\epsilon/2 = 0.015$$

$$E_B = 10.4\times10^6 \left[\frac{1 + (87{,}000/10.4\times10^6)(10.4/9.06-1)/0.03166}{1+(0.022+0.01615)(10.4/9.06-1)/0.03166}\right] = 9.172\times10^6$$

$$n_H = 11 \text{ from Figure 76}$$

$$(n/n_H)_{TEN} = 1/11 = 0.0909$$

$$\Sigma(n/n_H)_{TEN} = 0.1754 + 0.0909 = 0.2663$$

$$(\Delta\sigma/\Delta\sigma_H)_{COMP} = 0.68 \text{ or } 68\% \text{ hardening, from Figure 77.}$$

Loading from $C_1(87,0.022)$ to $D_1(-89.5,-0.006)$ along the branch curve which has an elastic modulus 9.172×10^6 and intersects the point $B_2(-91.5,-0.0082)$. B_2 lies on the branch curve which originates from A_2, has an elastic modulus of 9.06×10^6 and passes through $A_3'(-97,0.0254)$ at the intersection with the extension of the branch curve which originates from point B and has a modulus of 9.616×10^6. A_3' lies on the 68% hardened compression locus curve at the intersection with the extension of a basic branch curve originating from point A_1'.

$$\Delta\epsilon/2 = .014$$

$$E_B = 10.4\times10^6 \left[\frac{1 + (-89.5/10.4\times10^6)(10.4/9.06-1)/0.03166}{1+(-0.006+0.01615)(10.4/9.06-1)/0.03166}\right] = 9.53\times10^6$$

$$n_H = 12.8 \text{ from Figure 76}$$

$$(n/n_H)_{COMP} = 1/12.8 = 0.078$$

$$\Sigma(n/n_H)_{COMP} = 0.1053 + 0.078 = 0.1833$$

$(\Delta\sigma/\Delta\sigma_H)_{TEN}$ = 0.55 or 55% hardening, from Figure 77.

Loading from D_1(-89.5,-0.006) to E_1(91.5,0.03) initially along the branch curve which has an elastic modulus of 9.53×10^6 and intersects the point C_2(89,0.0222). C_2 lies on the branch curve which has an elastic modulus of 9.616×10^6 and passes through points B_2 and A_3(90.5,0.0254) at the intersection with the extension of the branch curve which originates from C_1 and has an elastic modulus of 9.172×10^6. A_3 lies on the 55% hardened tension locus curve at the intersection with the branch curve which originates from point A_2 and has an elastic modulus of 9.06×10^6. Loading continues from C_2 to A_3 then from A_3 to D_1 along the 55% hardened tension locus curve. E_1' (-98,-0.003) is then the point on the 68% hardened compression locus curve through which a branch curve leaving E_1 must pass.

$\Delta\epsilon/2 = 0.03$

$\bar{E}_B = 8.92 \times 10^6$ from Figure 70

$\epsilon_{MAX} = 0.03 - 91{,}500/8.92 \times 10^6 = 0.01974$

$\epsilon_{MIN} = -0.03 + 98{,}000/10.4 \times 10^6 = 0.02058$

$\Delta\epsilon_2 = 0.04032$

n_H = 4.8 from Figure 76

$(n/n_H)_{TEN} = 1/4.8 = 0.2083$

$\Sigma(n/n_H)_{TEN} = 0.2663 + 0.2083 = 0.4746$

$(\Delta\sigma/\Delta\sigma_H)_{COMP}$ = 0.88 or 88% hardening, from Figure 77.

4.1.2 Notch Response

Neuber's equation states that the product of the true notch stress and strain is equal to the product of the stress and strain if the material remains elastic, i.e.

$$\sigma \times \epsilon \times E = (S \times K_t)^2$$

Hence in order to predict the stress and strain at a notch with a concentration of K_t under the action of a far-field stress S. This equation has to be solved simultaneously with the material stress strain response.

This relationship was developed for a very specific type of notch under the action of a very specific loading condition. Upon applying it to the super scale specimens tested in this program poor correlation was obtained in the high plastic regions. Based on a study of this correlation the following modified Neuber's equation was developed.

$$\frac{\sigma \times \epsilon \times E}{\left[1 - \left(\frac{\epsilon}{0.0745}\right)^{1.507}\right]^2} = (S \times K_t)^2$$

This equation gives a much better correlation with the test data as can be seen in Figure 79.

4.1.3 Cyclic Creep

In an effort to understand the notch response to cyclic creep and or relaxation, a special sequence (Sequence 30 in Figure 1) of load was applied to the super scale specimen 2E3. The sequence of loads applied to the specimen is shown in Figure 80. The specimen was first loaded to 29,800 psi, A to B, which was high enough to cause the edge of the hole to go plastic. The load was then removed, resulting in a residual stress of 15,000 compression. It was then cycled 10,000 times between stresses of $\pm$5000 psi, C to D, and reloaded to 33,200 psi, E. If any cyclic relaxation accured during the cycling between C and D then the trace in the gross area stress-strain space would break away before it achieved the previous reached value at B. The specimen was then unloaded and again cycled 10,000 times between 5,000 psi and 25,000 psi. Again, reloading and relaxation would show up as an early break away in the gross area stress-strain space. The results of the test is shown in Figure 81.

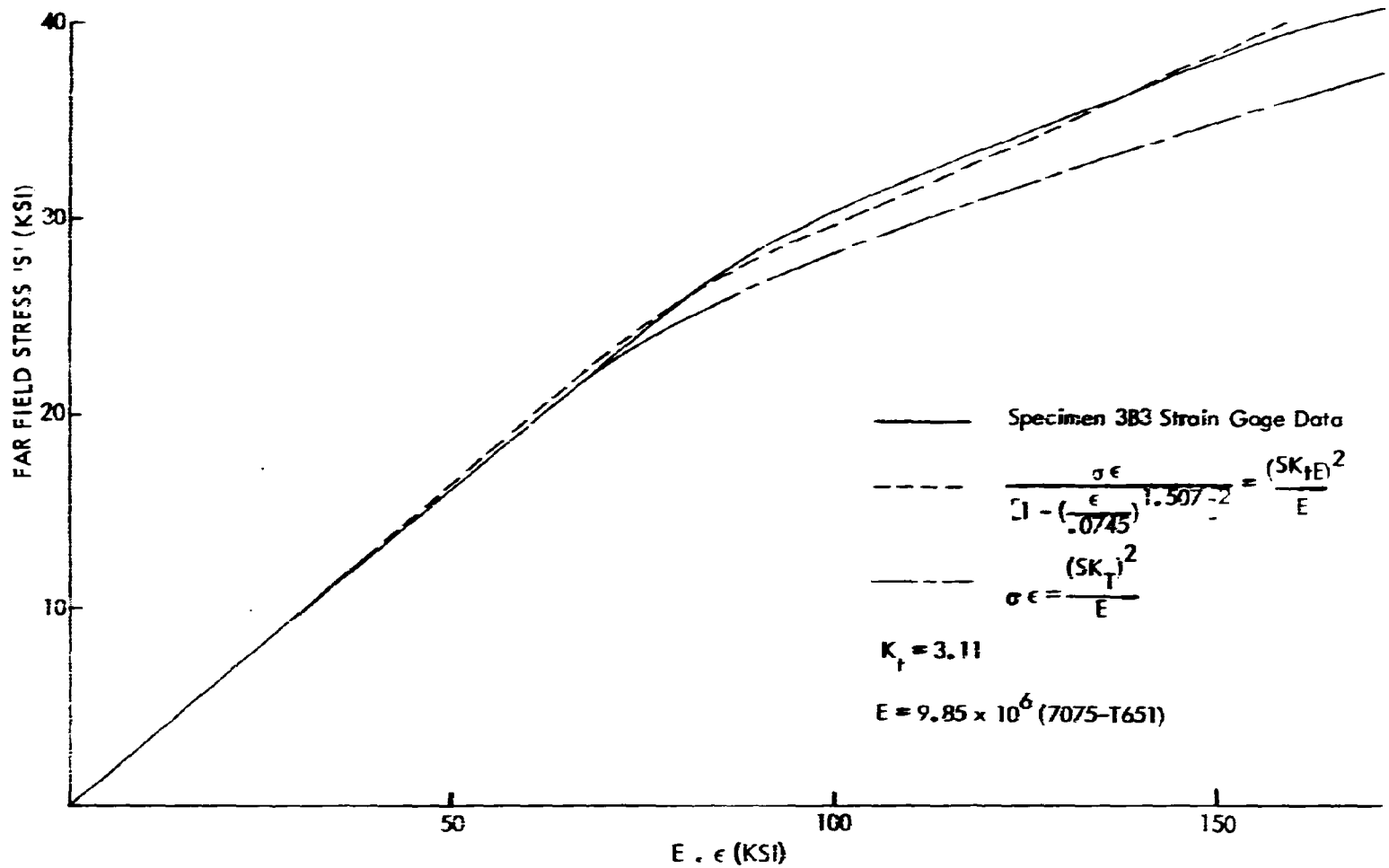

Figure 79 – Modified Neuber's Equation for the Second Super Scale Specimen

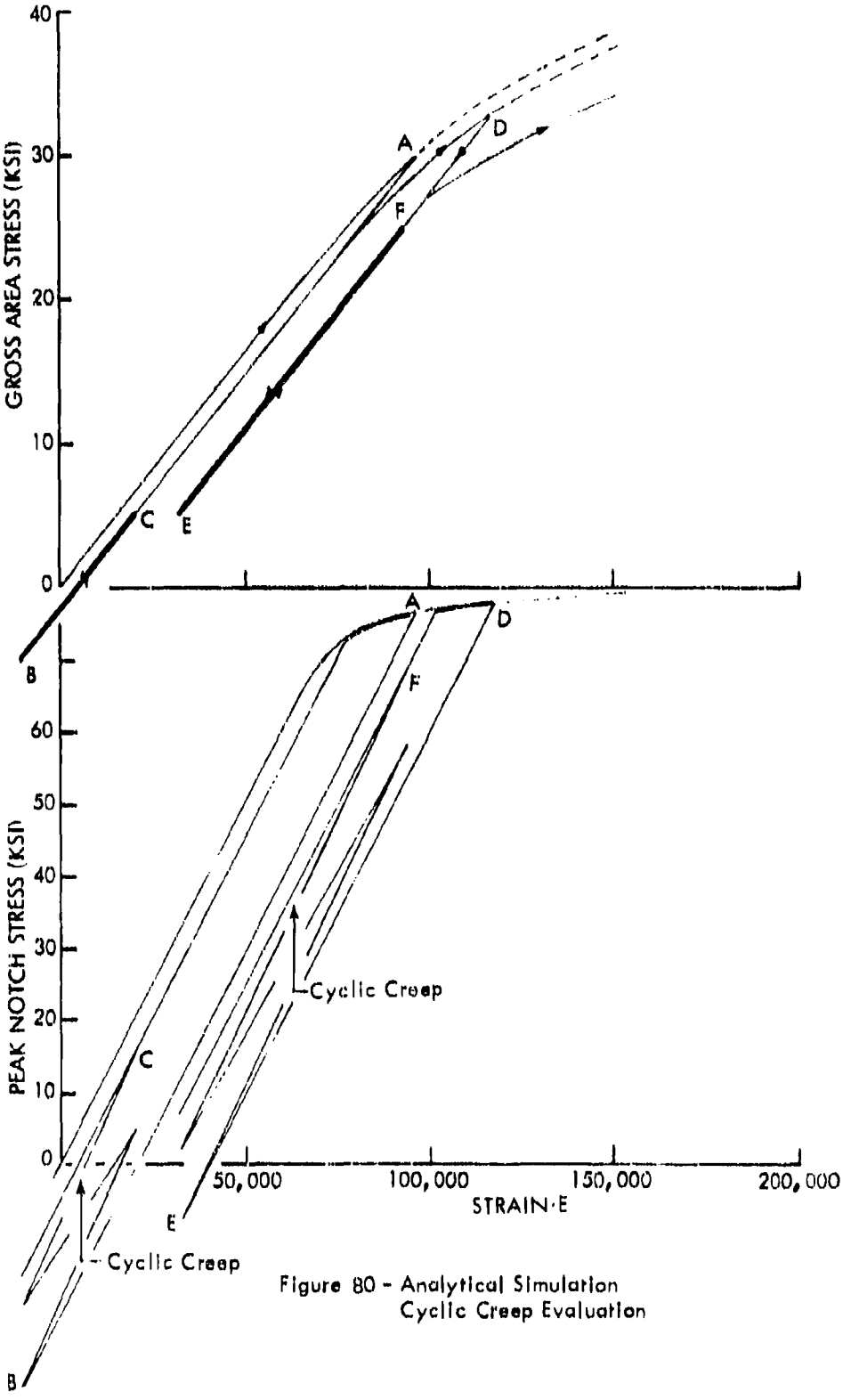

Figure 80 - Analytical Simulation
Cyclic Creep Evaluation

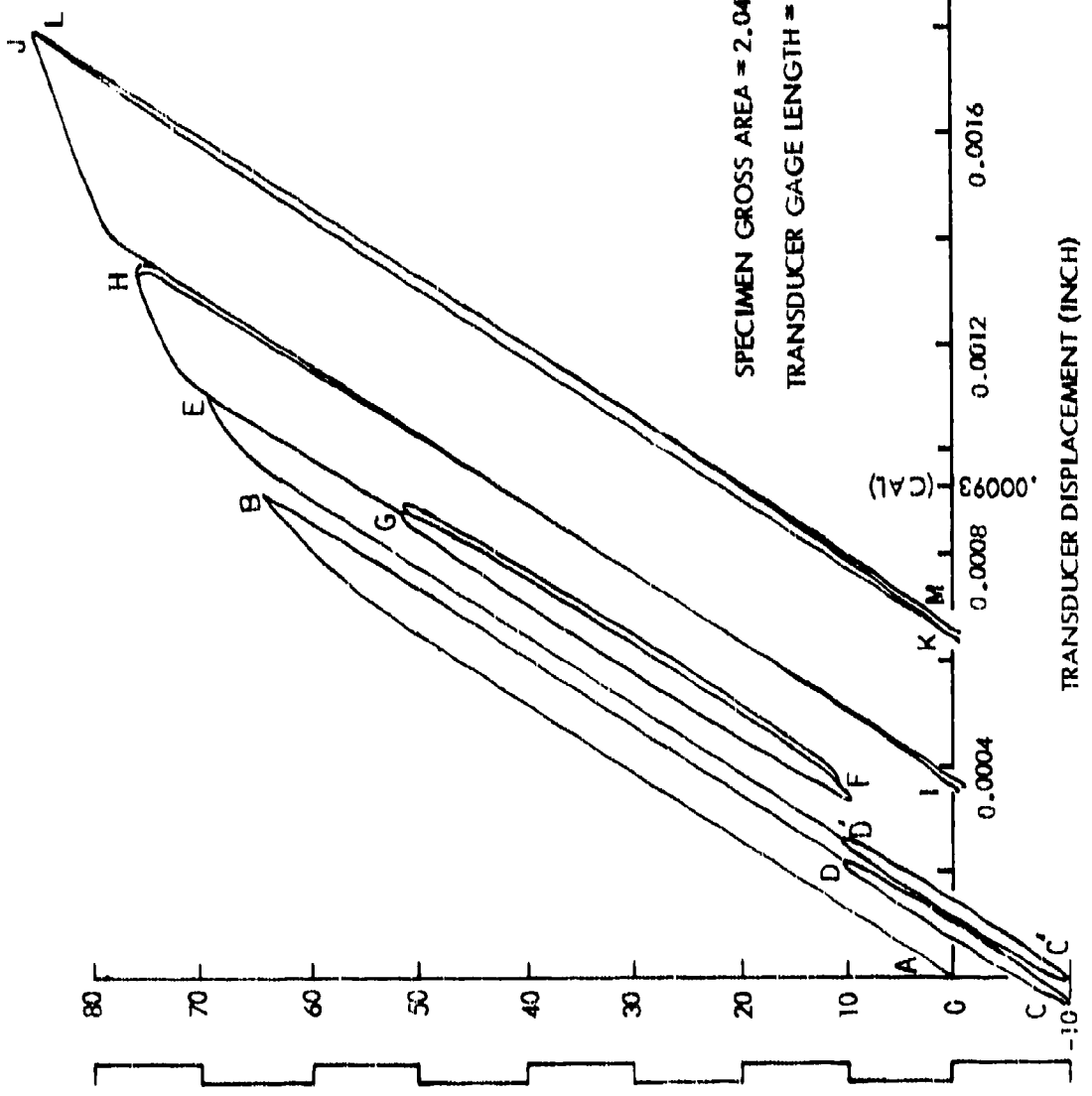

Figure 81. Cyclic Creep Evaluation, Sequence No. 39, Specimen No. 2E-3

4.1.4 Damage Predictions

The damage for each block of cyclic loads can be calculated once the true notch stresses are known. The damage due to the transition from one block to another has to be handled in a special manner. This analysis uses the rain flow technique to determine, from the strain history, the equivalent cyclic stresses and the number of cycles which represent the transition between blocks of data.

The rain flow method uses the peak strains from each block of data to determine the equivalent cyclic stresses and the number of cycles. The name Rain Flow comes from the analogy that is made to rain flowing off a roof. The roofs are considered as the lines joining the peak strains in a strain-time plot where the time is the vertical axis. Rain is allowed to flow from roof to roof until it encounters rain that has flowed over a larger horizontal distance. The horizontal length of each rain flow is then counted as half a cycle and the mean and alternate stresses are determined from the stresses at the beginning and end of the half cycle. Figure 82 taken from Reference 7 shows an example of this method.

In applying this procedure to repeated cycles it is assumed that the results from individual half cycles can be superimposed. This is illustrated in Figure 83, where, for the initial loading increment the material follows the locus curve. Upon unloading the material, follows the branch curve until it meets the modified Neuber curve defined relative to the start of the unloading branch.

The analysis calculates an accumulative damage based on the Palmgren-Miner theory. The accumulative damage is the sum of the damages from each individual block of cyclic stresses and from each half cycle representing the transition between blocks of data. The individual damages are defined as the number of cycles (n) applied at the specific stress levels divided by the number of cycles (N) it takes for a crack to nucleate at the specific stress level. The accumulated damage is then:

$$\text{DAMAGE} = \Sigma\, n/N$$

The number of cycles (N) to crack nucleation is obtained from the test data of unnotched coupon specimens. This data can be interpreted for either the stresses or strains results from the Neuber analysis. Predicted versus actual time to failures are discussed in Section V.

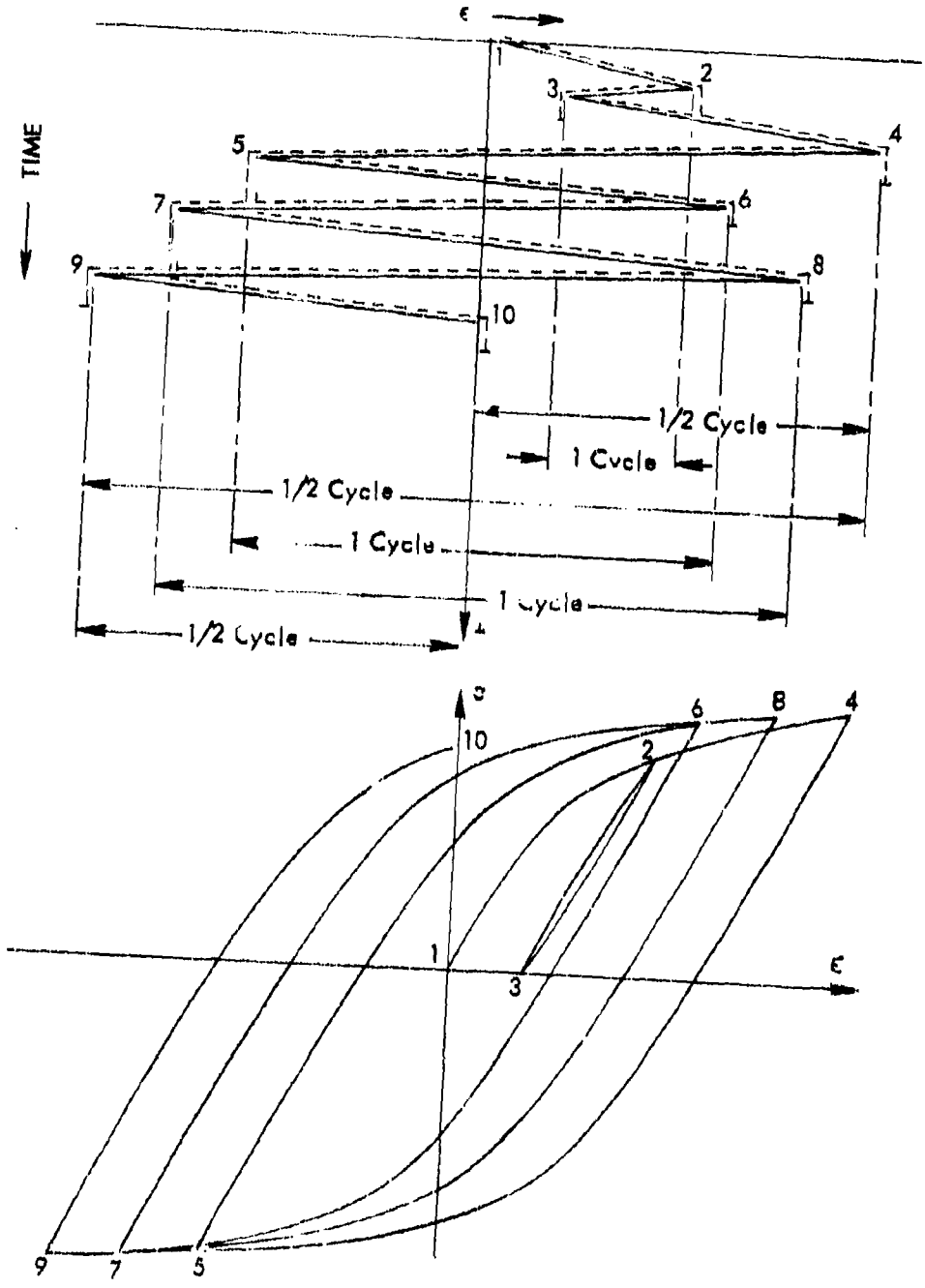

Figure 82 - Rain Flow Counting

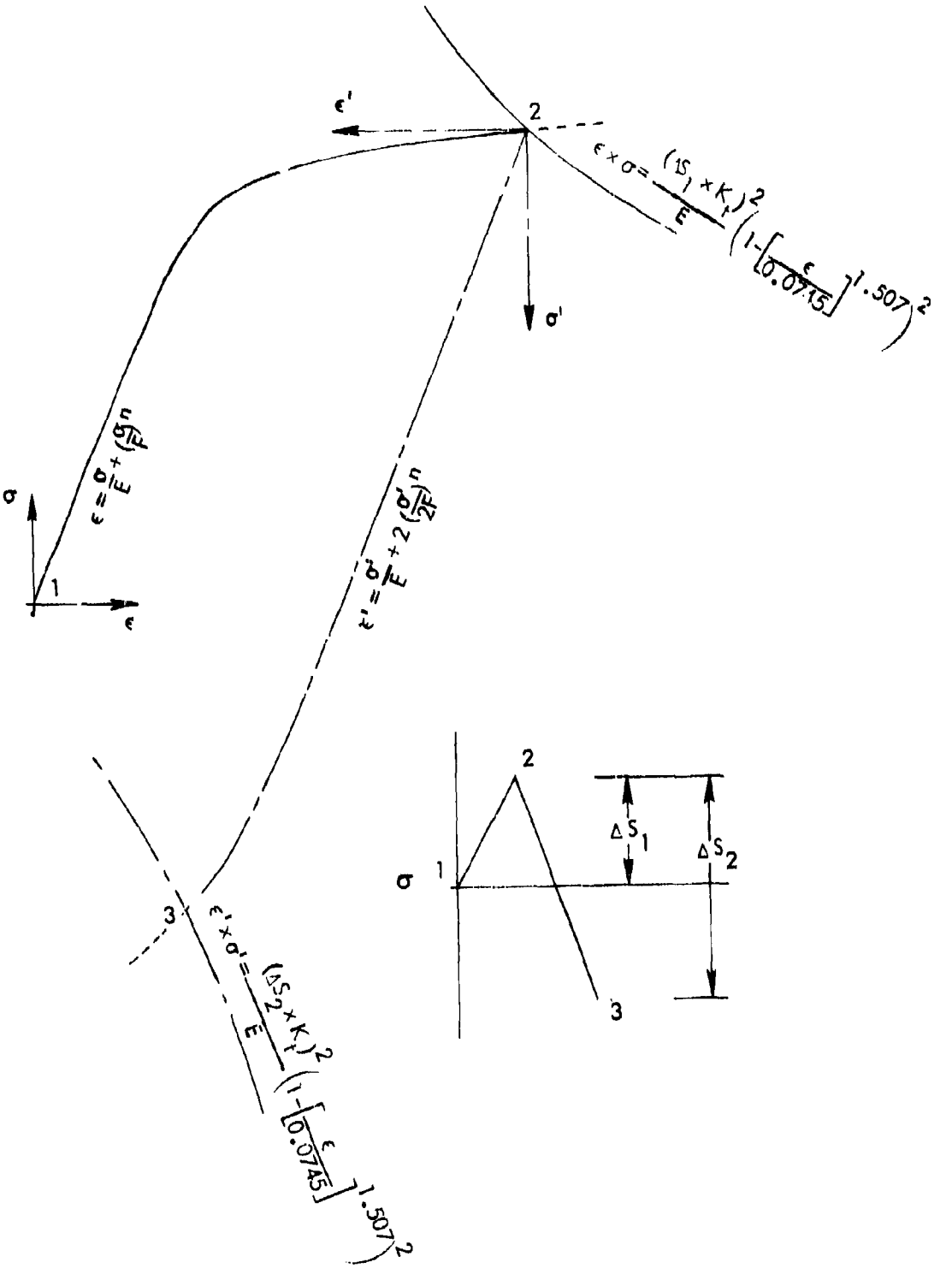

Figure 83 - Simultaneous Solution of Neuber's Equation and the Stress-Strain Curve

SECTION V
DATA ANALYSIS AND CORRELATION

A vast amount of experimental data has been collected during Phase I in an attempt to quantify and model the stress and strain state at a stress riser. These tests include a materials characterization study as well as a matrix of fatigue tests to measure the notch strain history during complex loading sequences. The materials data has been used to analytically model the cyclic response during hardening and in the stable condition, Section IV. Notch response and damage predictions using this analysis model are compared with experimental results in the following sections.

5.1 NOTCH RESPONSE

The analysis discussed in 4.1.1.1 has been used for predicting the notch strain response for each super-scale test sequence. A plot routine was developed from this algorithm for plotting either applied load versus notch strain or notch stress versus notch strain. This uses the cyclic locus curve and branch curve whose development was outlined in 4.1.1.1. The locus curve is used to locate in space the initial loading, either overload or underload. Then the branch curve, from Figure 69, is used to fit through the input data (test loadings) to define excursions from the cyclic locus curve in the stress strain space. Either the whole or parts of the branch curve are used to describe the load-strain history as a best fit through the data points. Figures 84 through 91 illustrate typical load versus notch strain plots using this analysis and plot routine. These curves are the first cycle loading only for the sequences shown. The solid curves are from the analysis. The asterisk symbols represent the applied load conditions (maximum, minimum, and mean loads). Test data for each sequence is represented by the open symbols. The test data shown is from the transducer measurements illustrated previously in Figures 44 through 52.

In general, the test data correlates very well with the analytical predictions. This then tends to substantiate the analysis development in Section IV, specifically the cyclic locus curve and branch curve development. With this analysis, it is now possible to efficiently represent material response in a conviently usable form.

In addition to the load versus notch strain data, plots were generated of notch stress versus notch strain. These data are illustrated in Figures 92 through 99. The modified

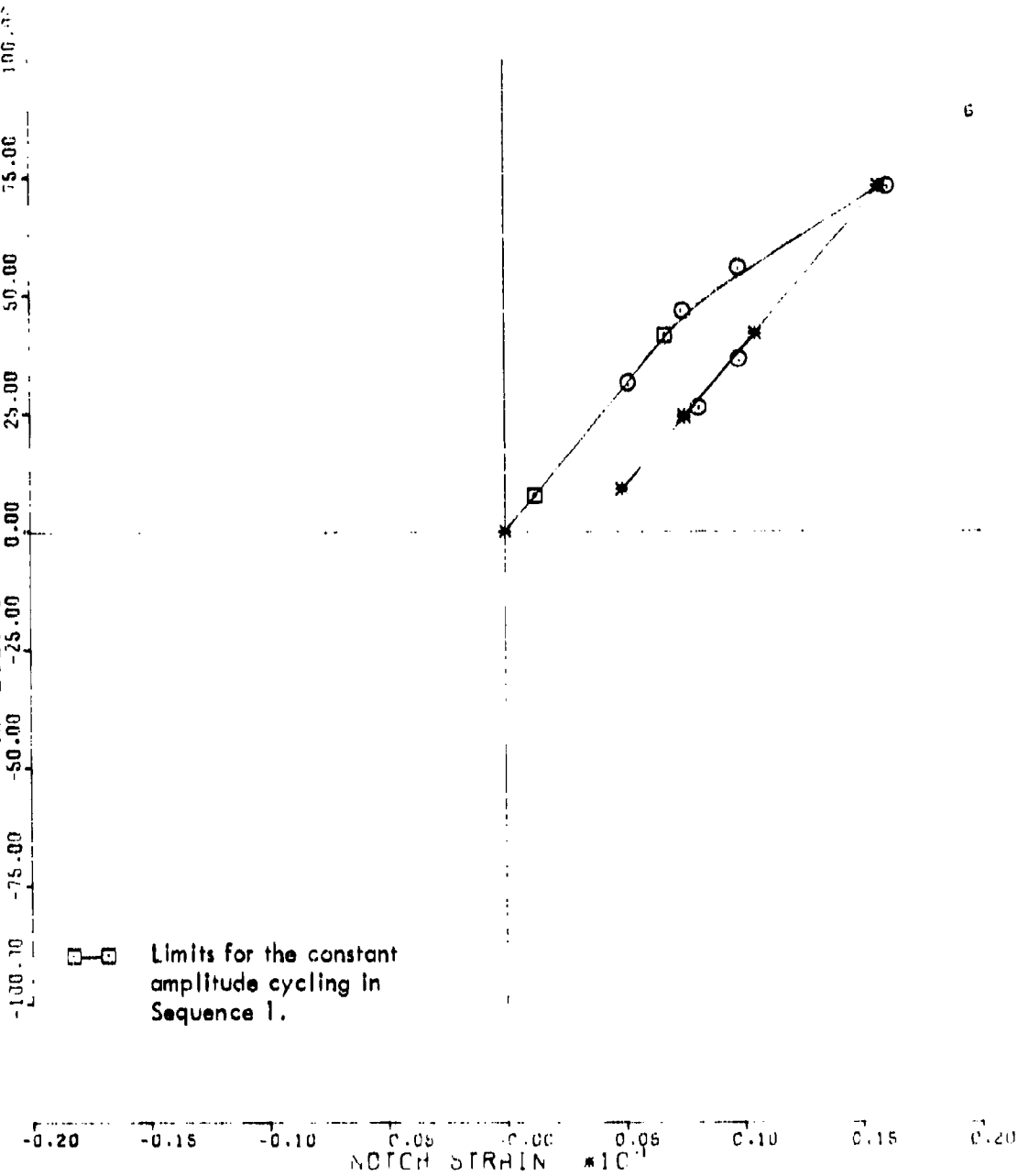

Figure 84 Predicted vs. Measured Load Strain Data Sequence 6

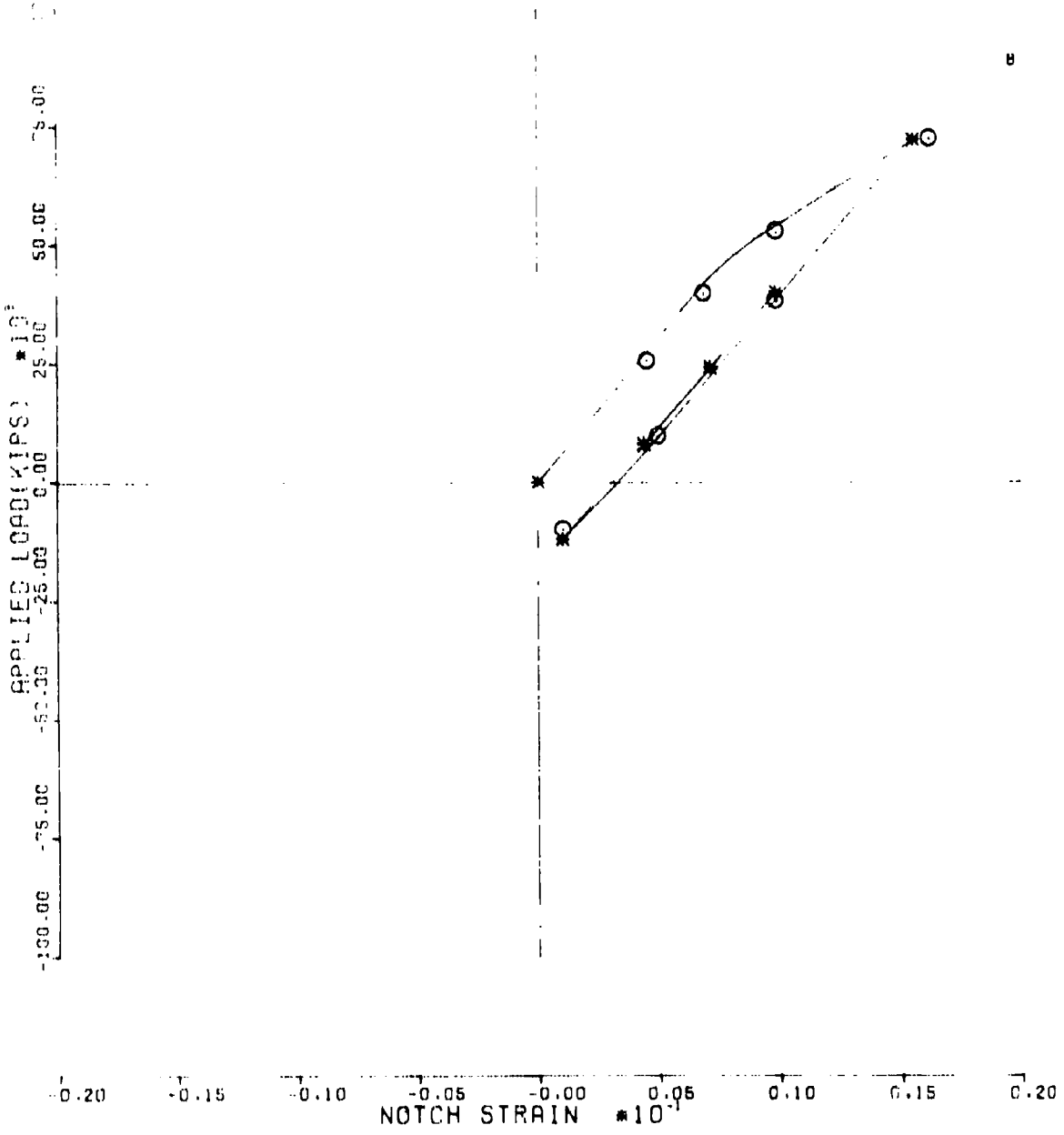

Figure 85. Predicted vs. Measured
Load Strain Data Sequence 8

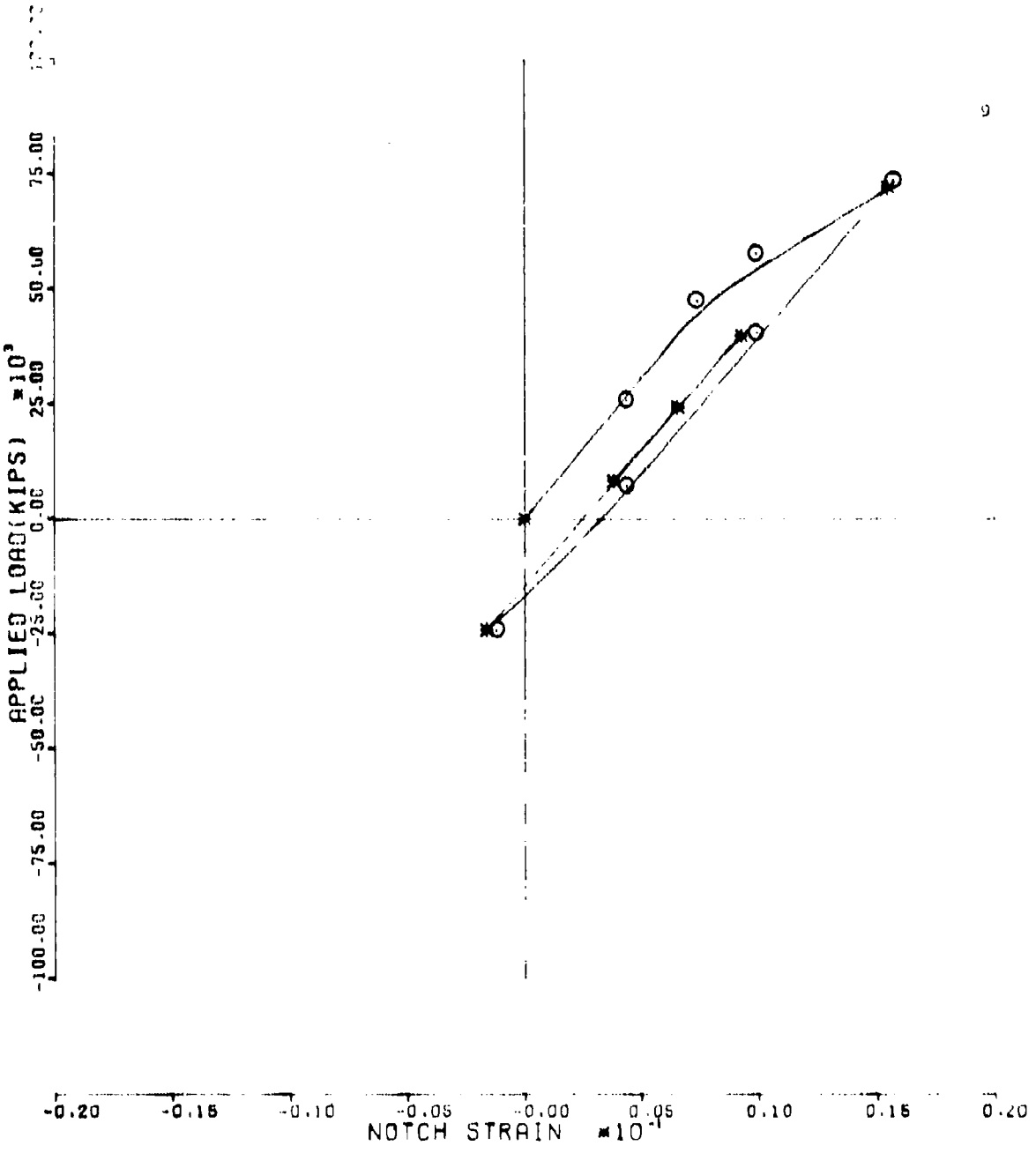

Figure 86. Predicted vs. Measured Load Strain Data Sequence 9

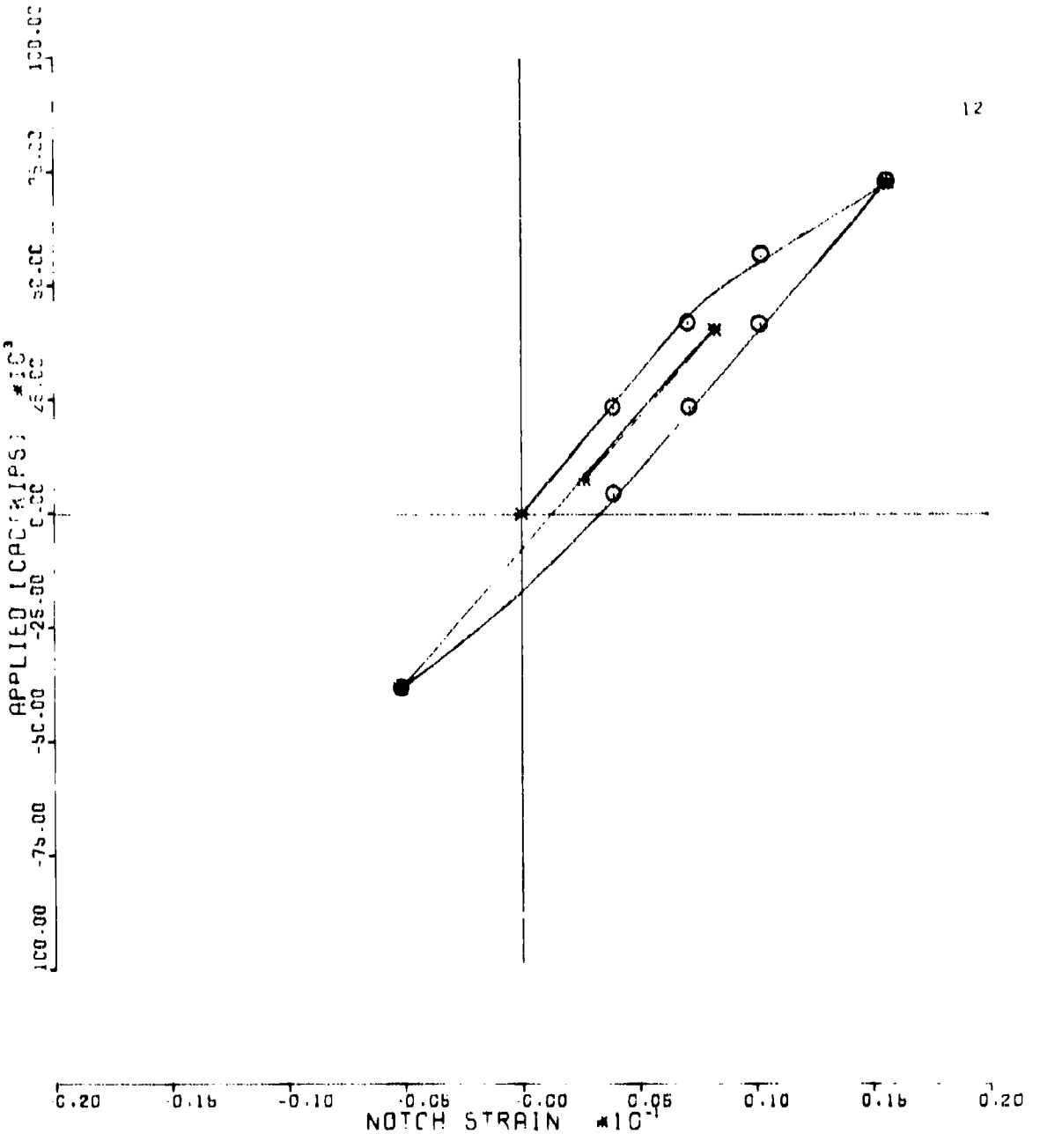

Figure 87. Predicted vs. Measured
Load Strain Data Sequence 12

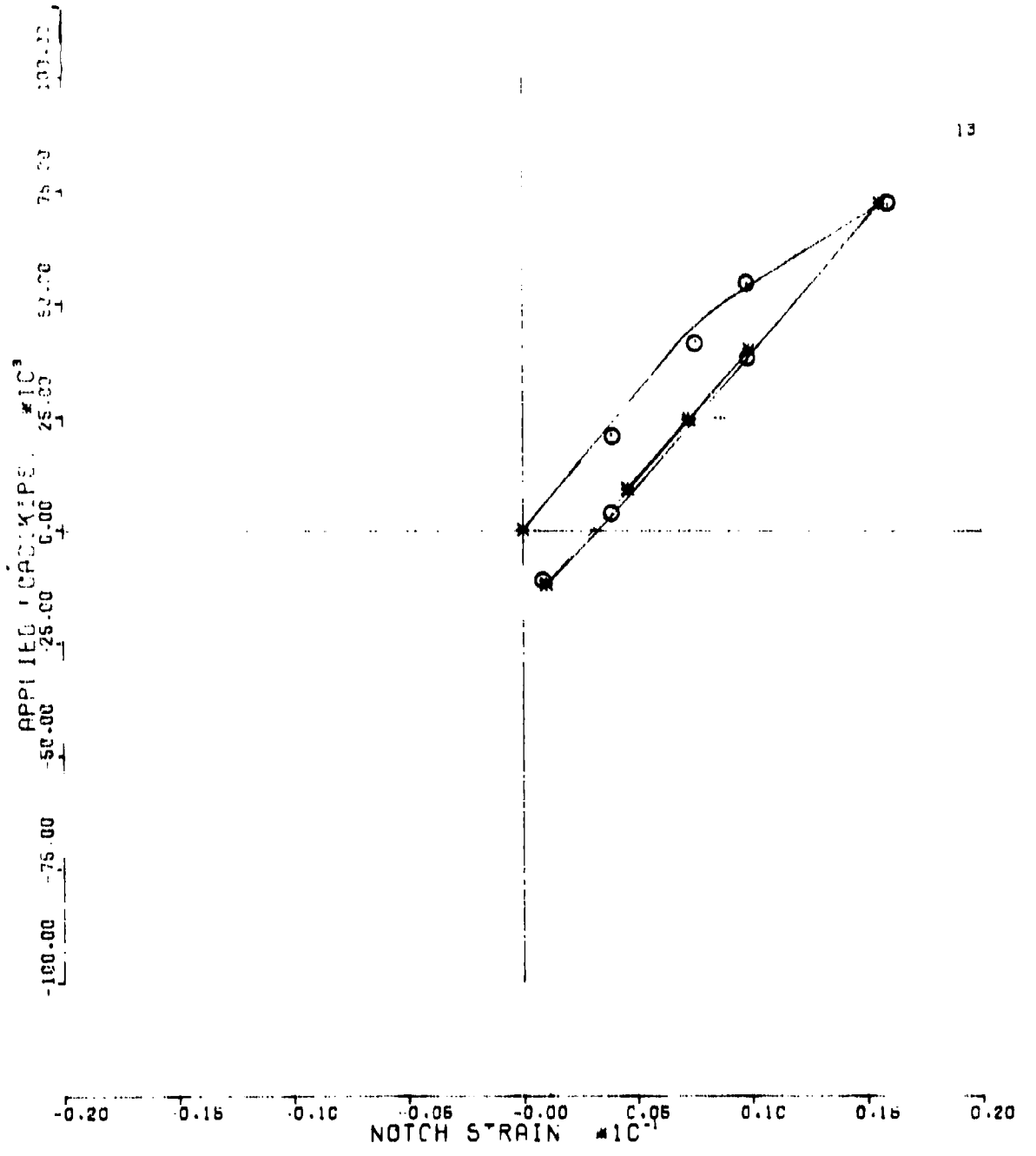

Figure 88. Predicted vs. Measured
Load Strain Data Sequence 13

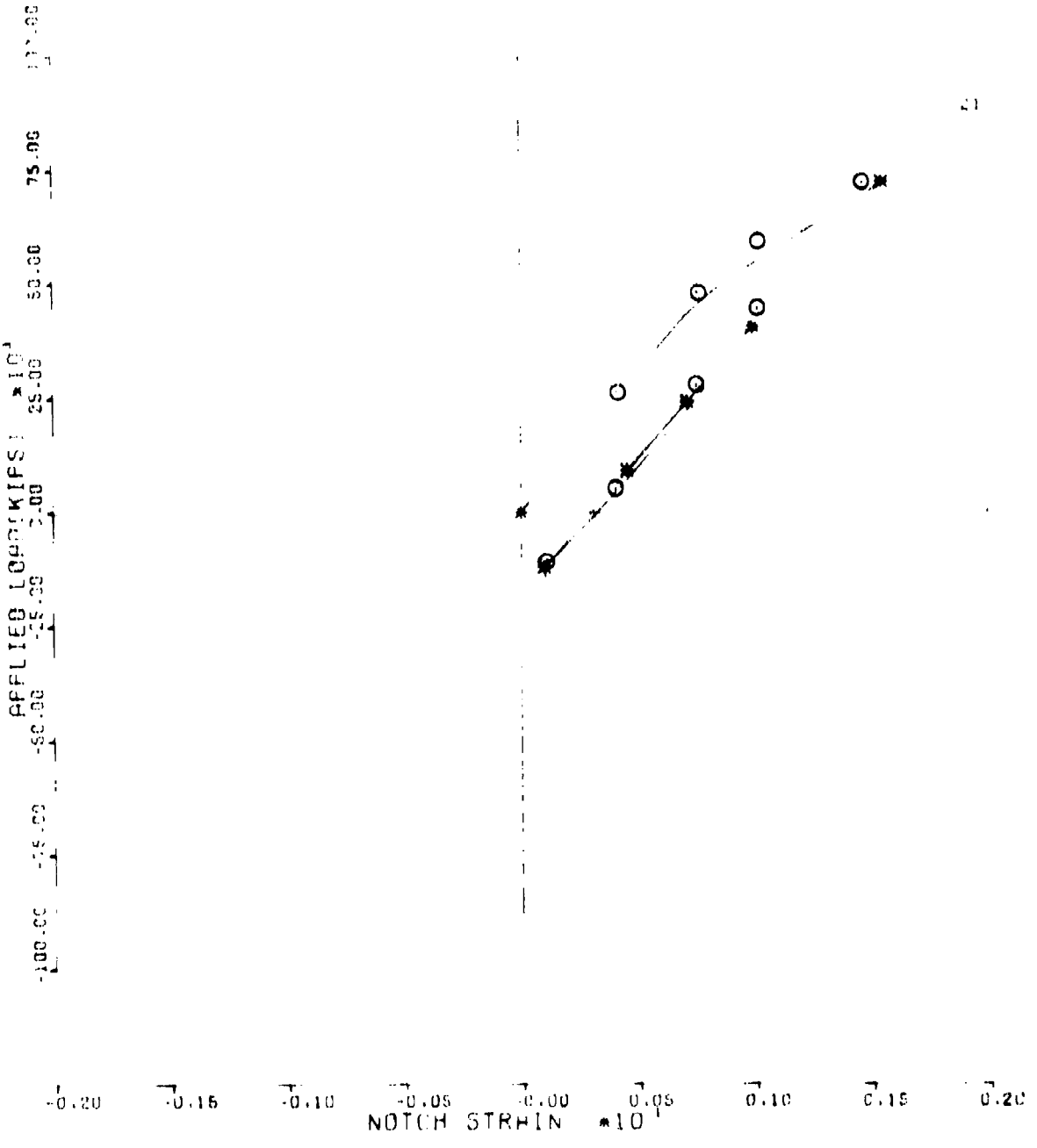

Figure 89. Predicted vs. Measured
Load Strain Data Sequence 21

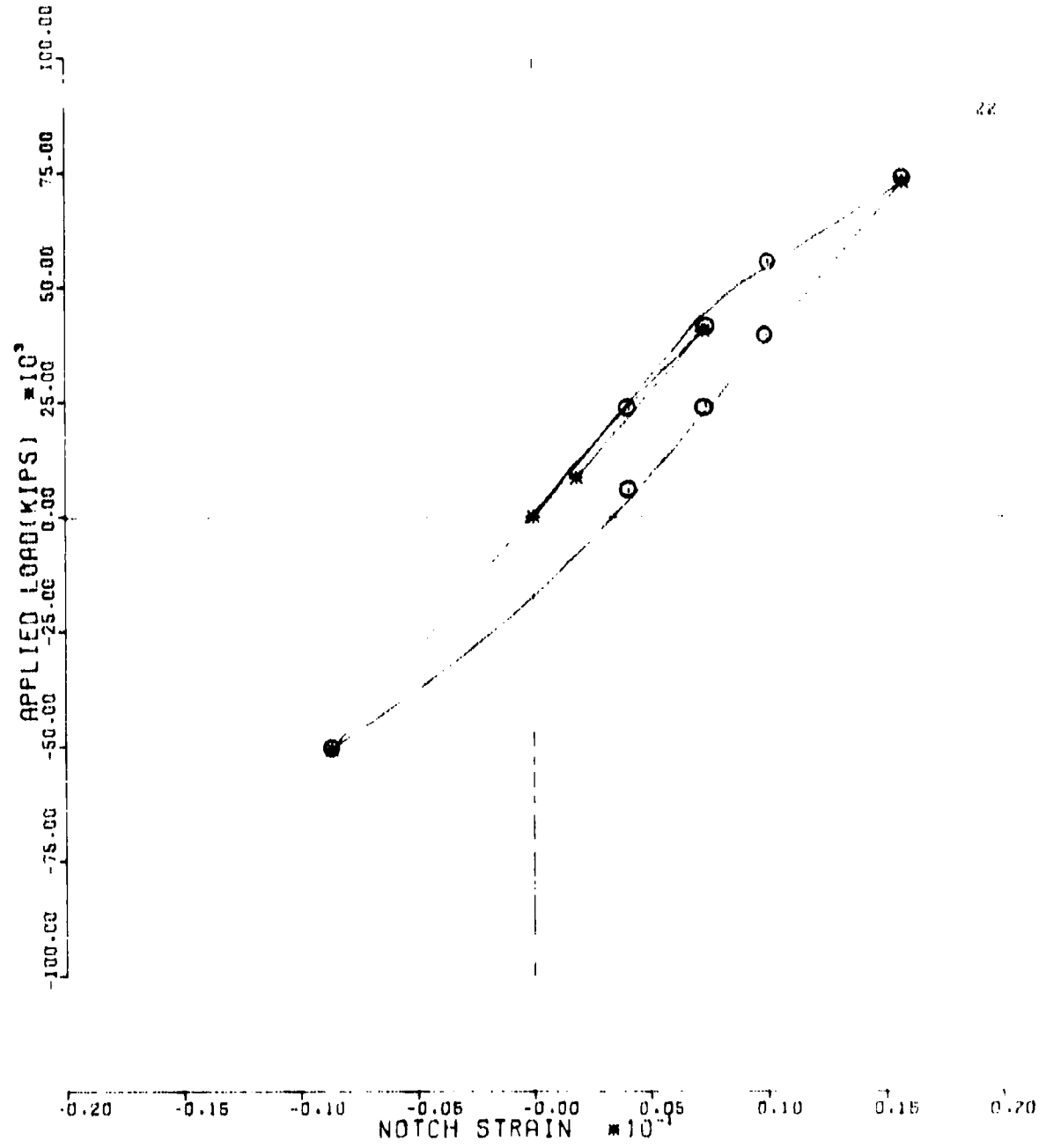

Figure 90. Predicted vs. Measured
Load Strain Data Sequence 22

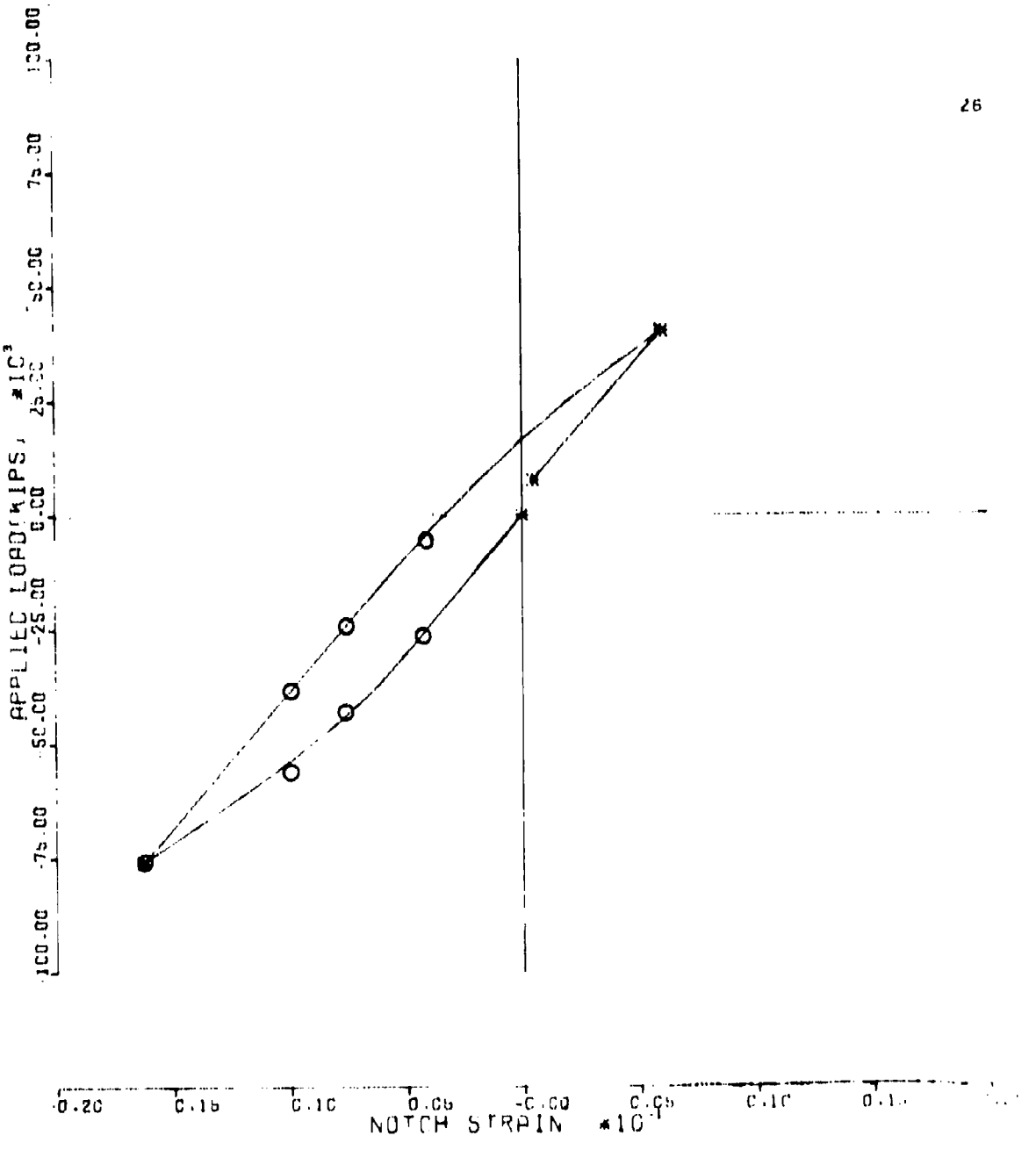

Figure 91. Predicted vs. Measured
Load Strain Data Sequence 26

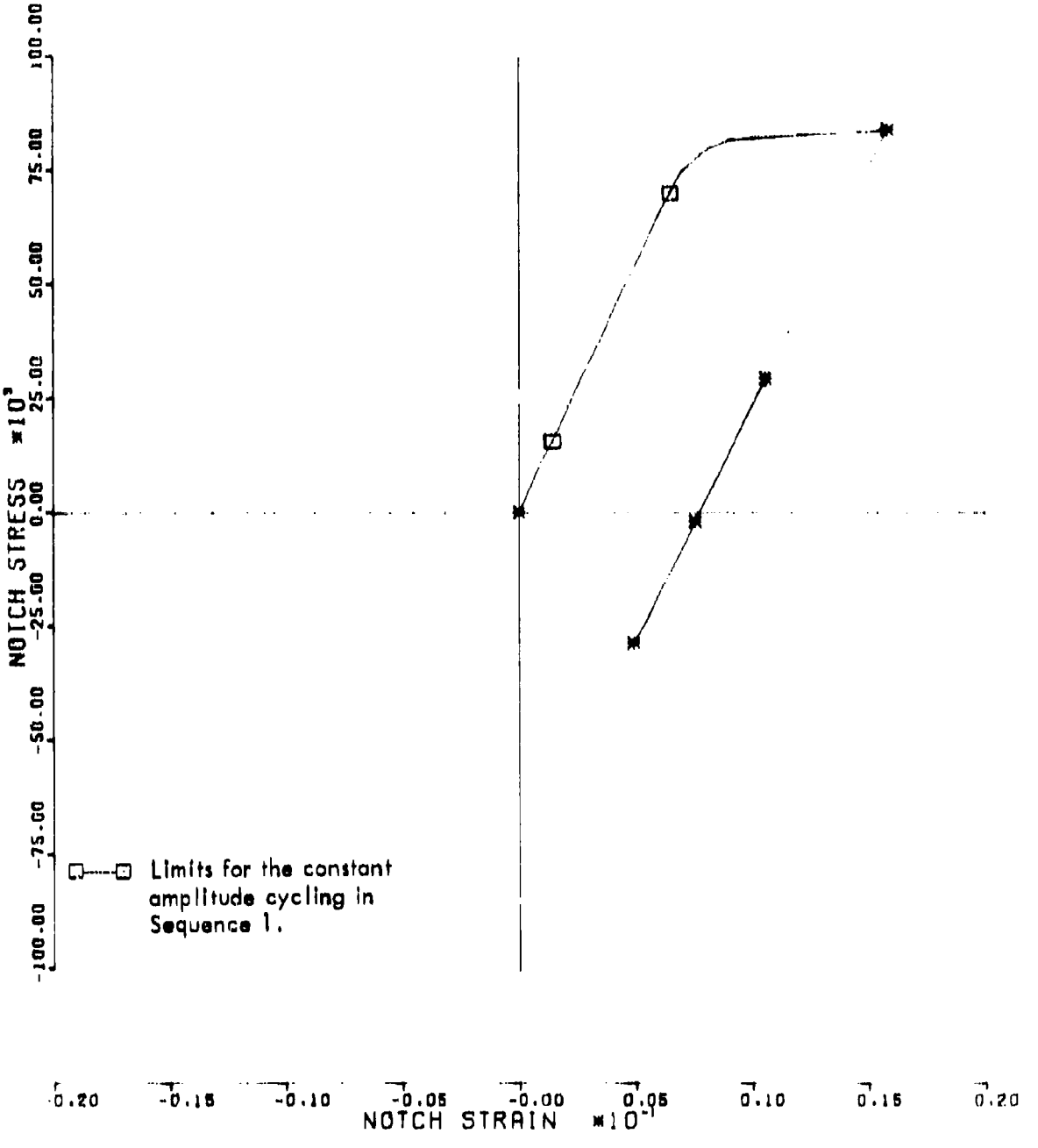

Figure 92. Notch Stress vs. Notch Strain
Sequence 6

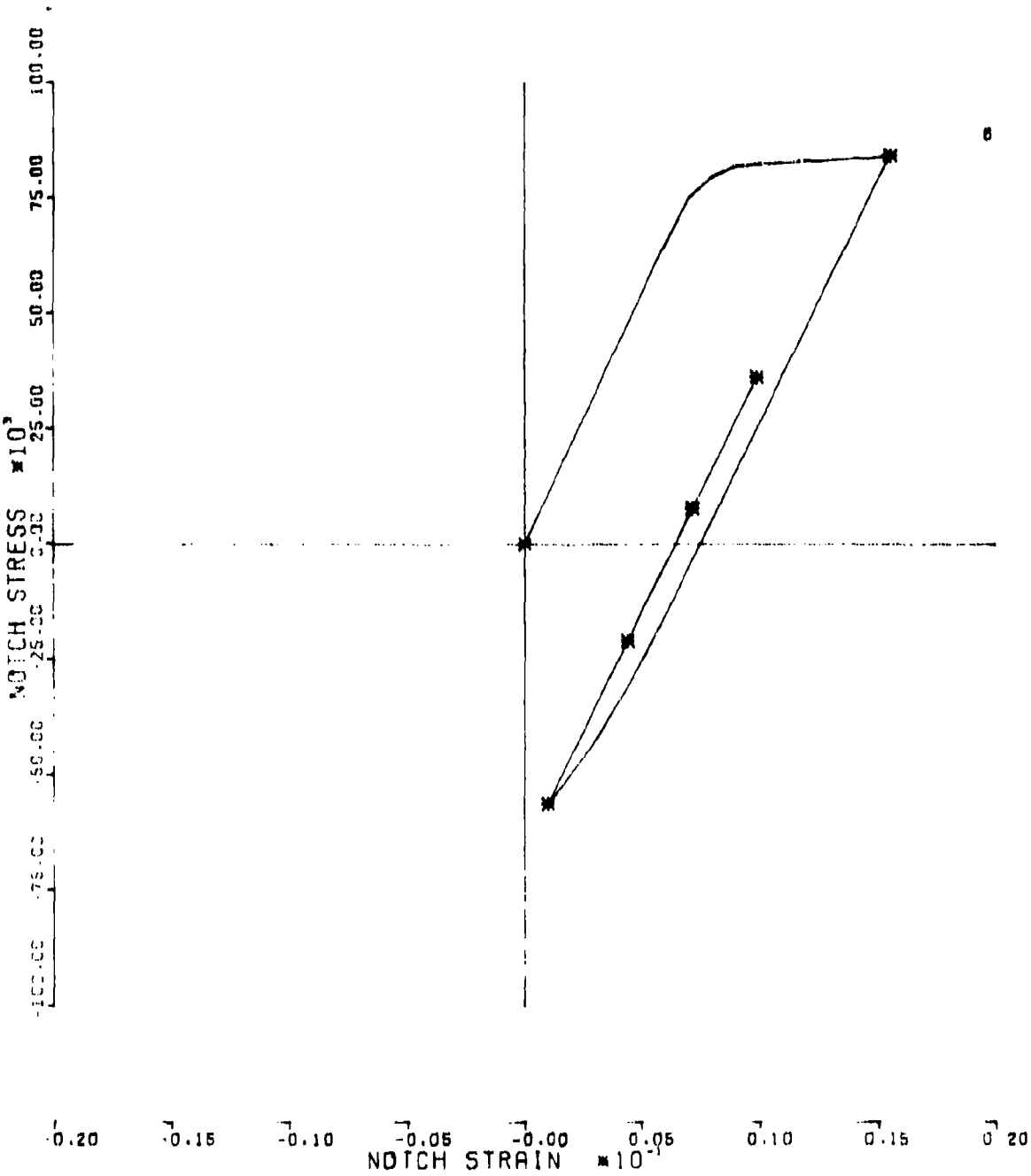

Figure 93. Notch Stress vs. Notch Strain
Sequence 8

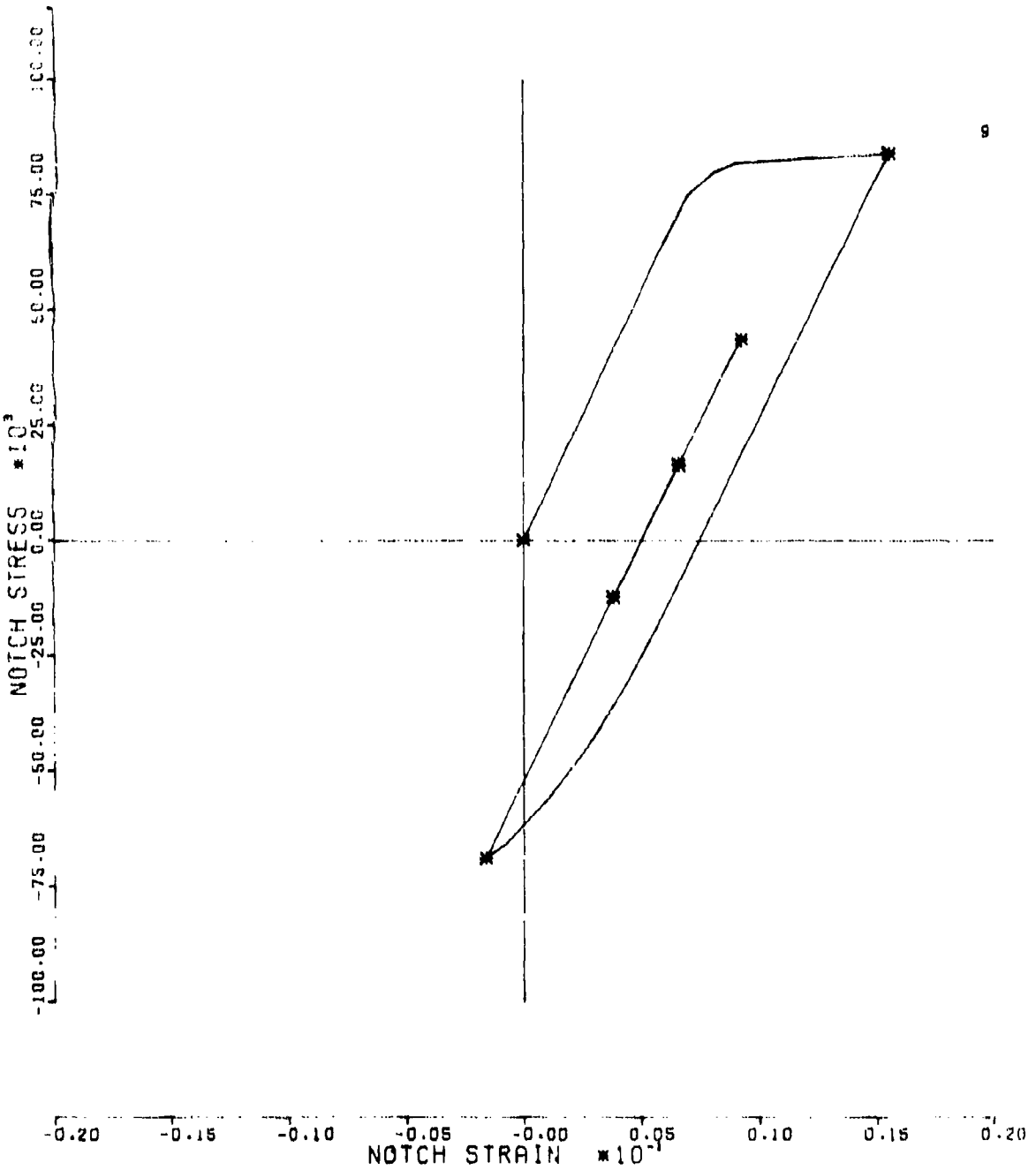

Figure 94. Notch Stress vs. Notch Strain
Sequence 9

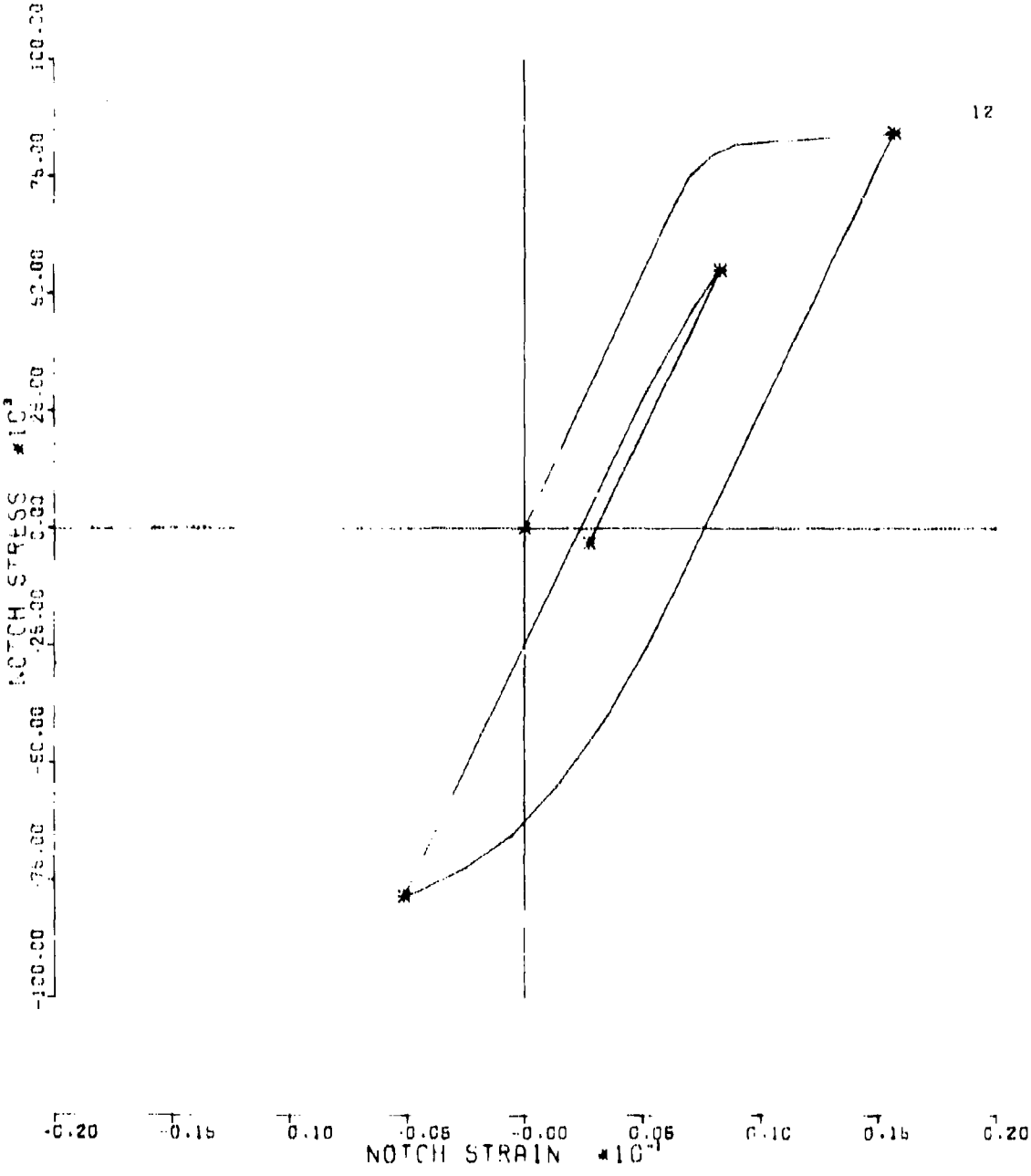

Figure 95. Notch Stress vs. Notch Strain
Sequence 12

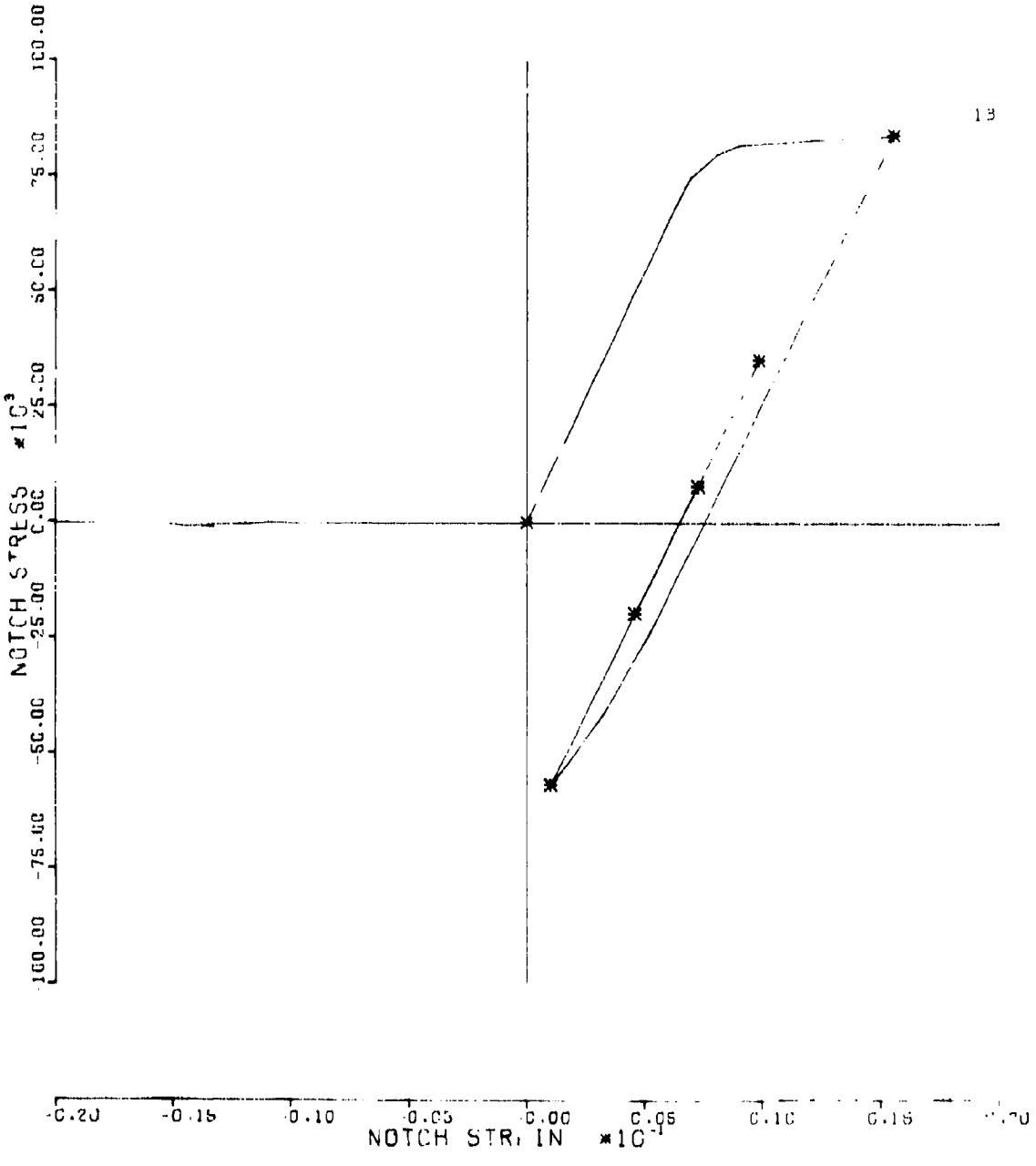

Figure 96. Notch Stress vs. Notch Strain
Sequence 13

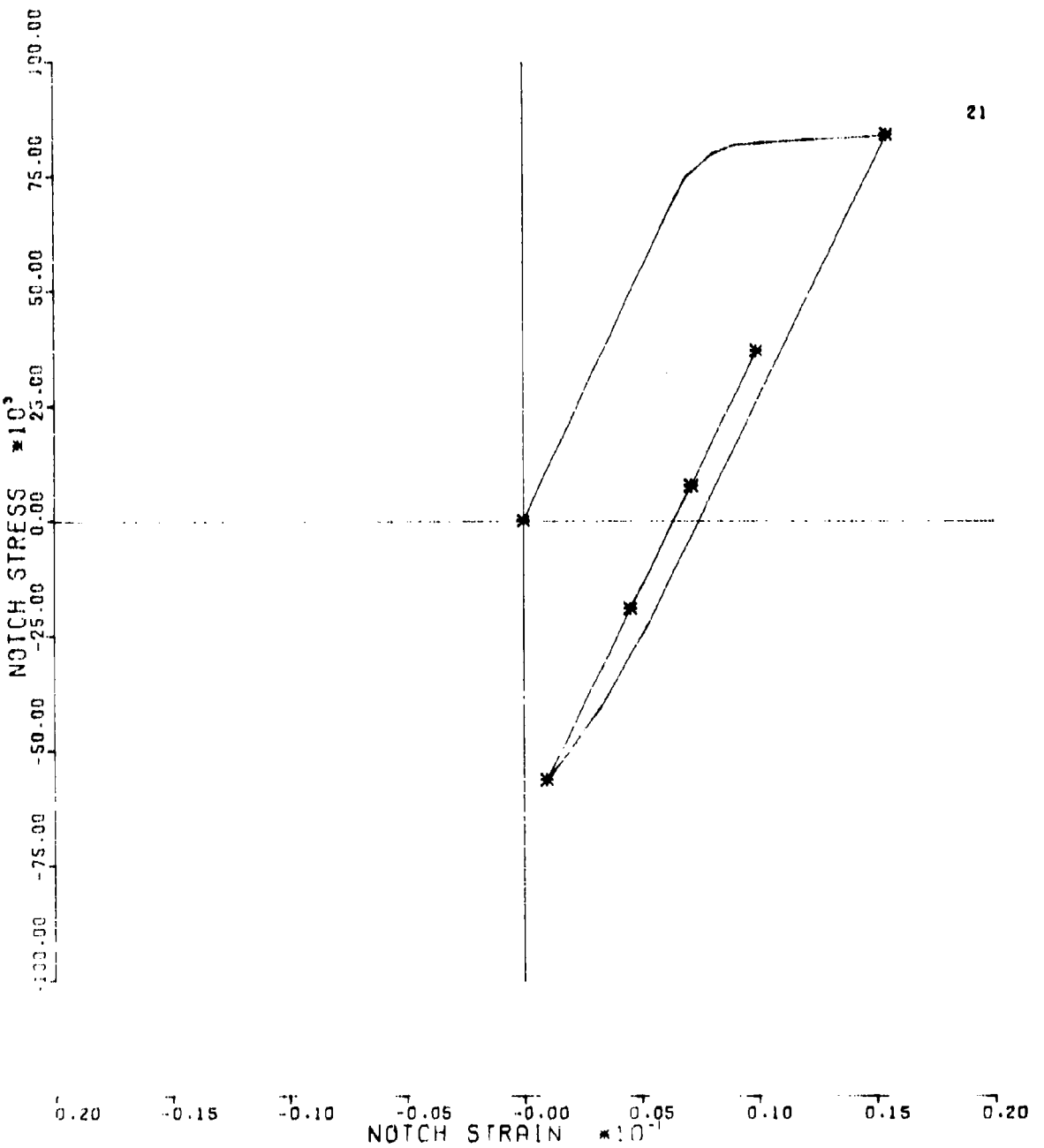

Figure 97. Notch Stress vs. Notch Strain
Sequence 21

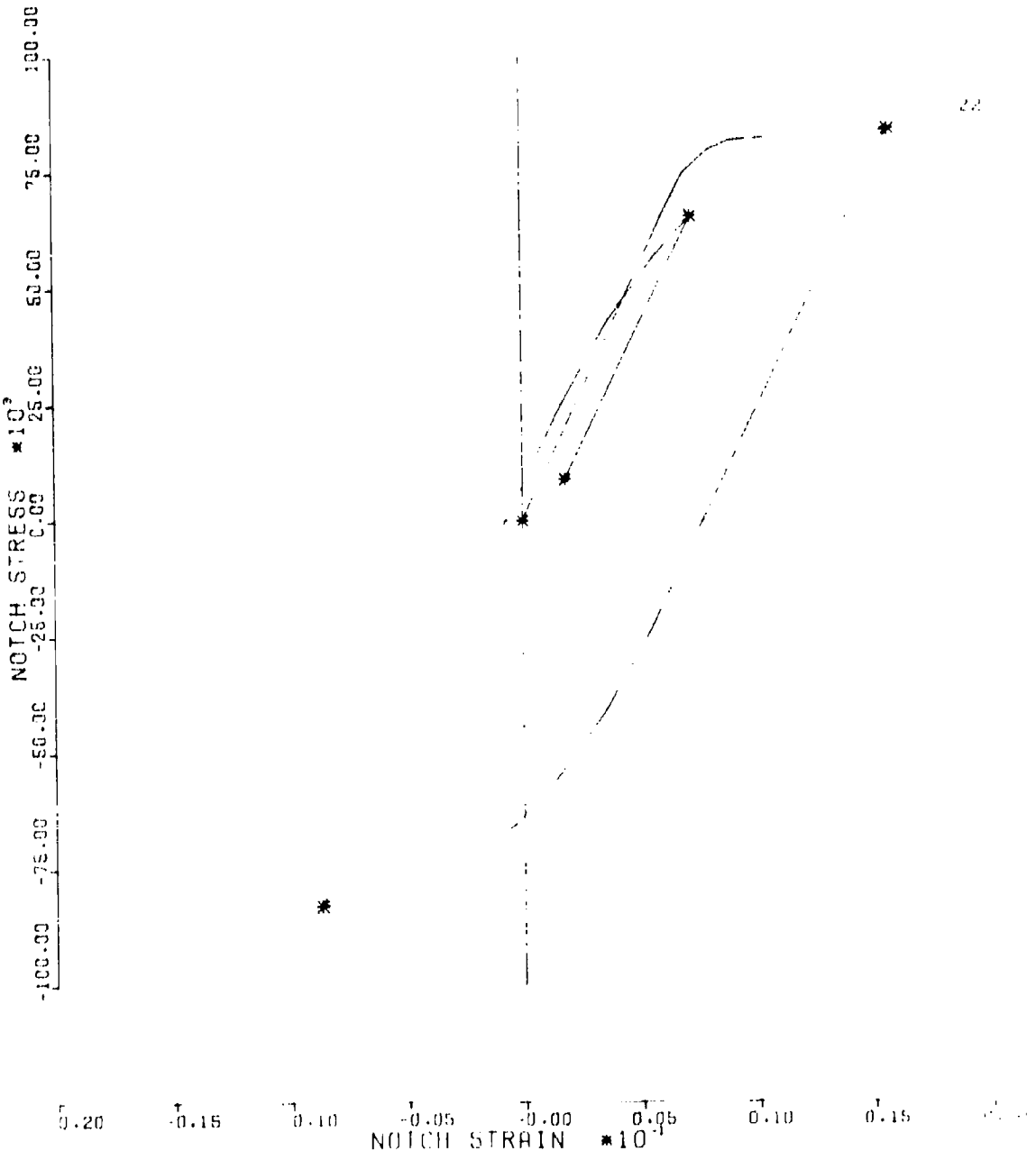

Figure 98. Notch Stress vs. Notch Strain
Sequence 22

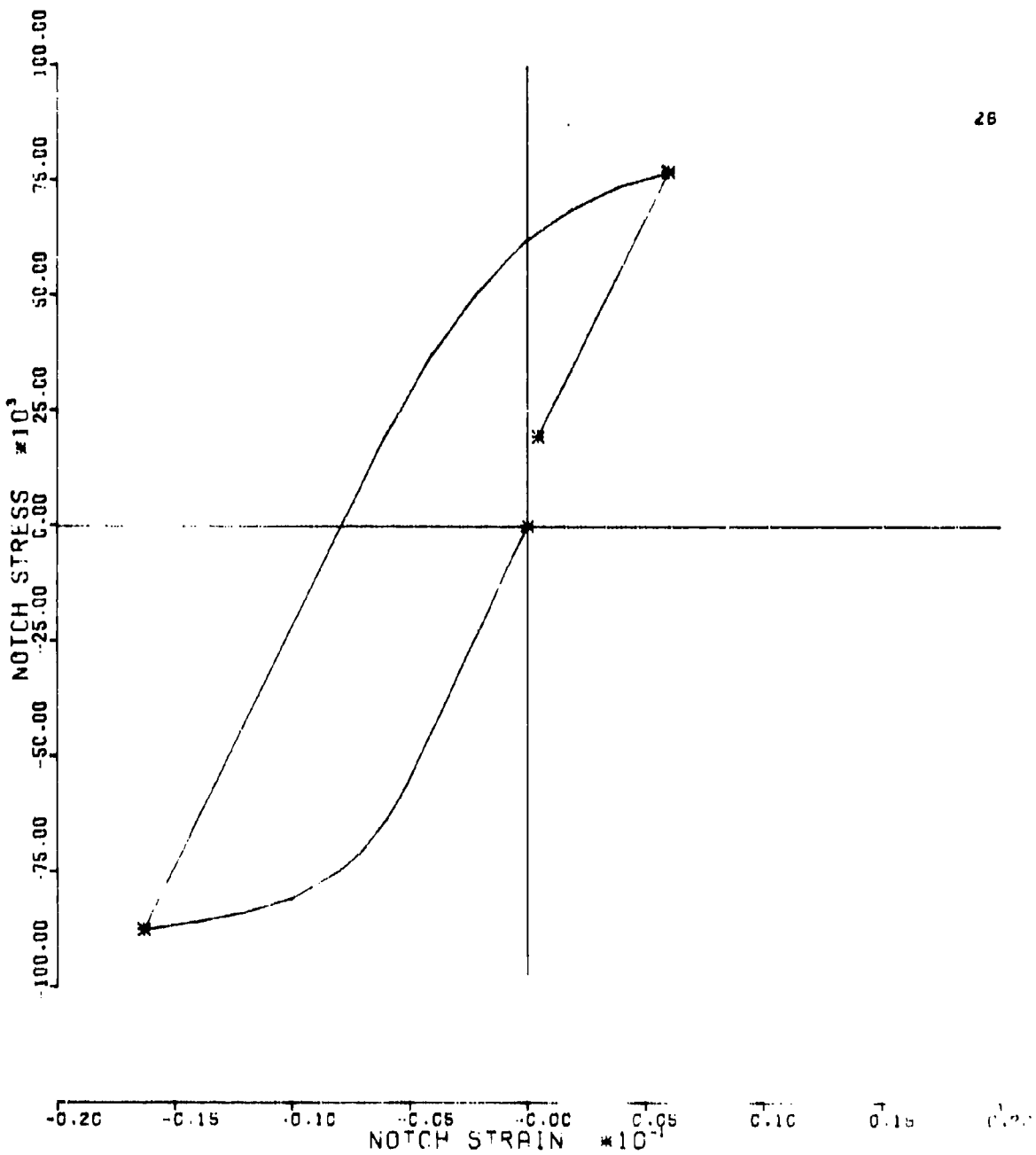

Figure 9. Notch Stress vs. Notch Strain
Sequence 26

Neuber equation discussed in 4.1.2 is used in the analysis for developing these data. Damage or life predictions are made using these calculated notch strains along with the cyclic counting technique discussed in 4.1.4.

At this point, there is good correlation between the predicted and measured load-notch strain data using the analysis model as it currently exists. The analysis does not currently include a cyclic or time dependent creep module. This will be the subject of the Phase II study and will be included in the analysis after completion of that study.

5.2 DAMAGE PREDICTIONS

Two analysis methods have been used to compare predicted versus actual fatigue life for the super-scale tests. Both a simple Miner's linear analysis and the hysteresis analysis in 4.1.4 were used for life predictions. Typical results are shown in Table XII.

For the Miner analysis, damage for the constant amplitude portion of each sequence was based on the data from Sequence No. 1. Cycles to failure for this sequence is 47,647 cycles as listed in Table VII. Then for each sequence

$$D = \Sigma \frac{\text{constant amplitude cycles}}{47,647}$$

and $D = 1.0$ at failure.

Damage from the overload and underload cycles was derived from the data presented in Figure 100. Based on these assumptions and the linear damage analysis, the maximum life for any sequence would be 47,647 cycles - Sequence No. 1. This is a prime example of the short comings of any analysis which does not account for residual stresses or plasticity.

The hysteresis predictions do not correlate as well as expected with the test data; however, the same trends in the test data are evident from the analysis. Better correlation is achieved in the test sequences with underloads greater than 7.9 Ksi. Perhaps the delta stress between the tensile and compression yield was greater for the super scale

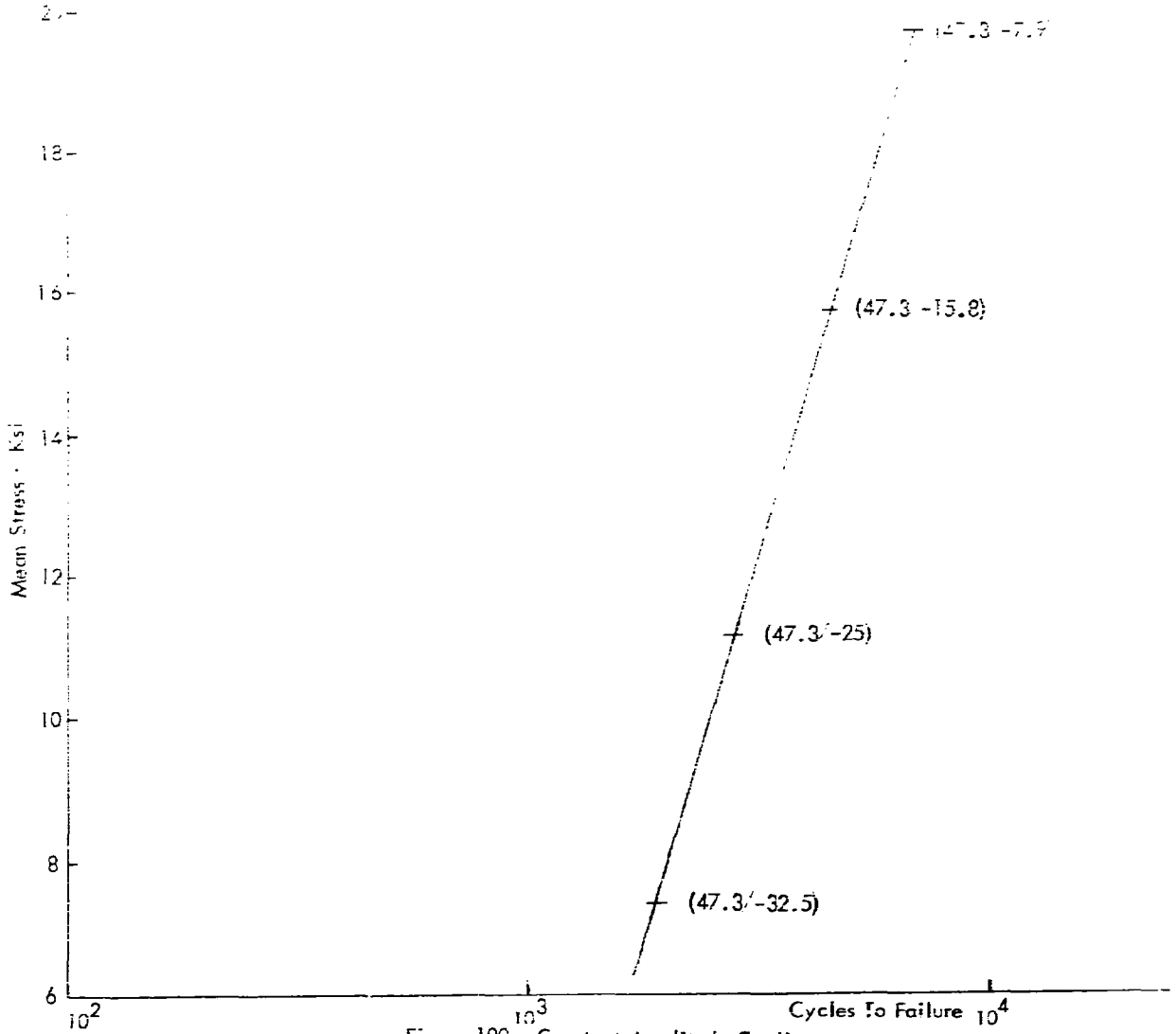

Figure 100. Constant Amplitude Cycling at Max Overload and Max Underload Only

TABLE XII - ACTUAL VERSUS PREDICTED LIFE
SUPER-SCALE TEST SPECIMENS

SEQUENCE	TEST LIFE	ANALYTICAL LIFE MINER'S $\epsilon \frac{n}{N}$	ANALYTICAL LIFE HYSTERESIS
6	2×10^6	47,539	655,000
7	1.03×10^6	46,451	343,000
8	715,000	47,597	430,738
9	166,932	47,586	210,900
10	308,616	47,296	157,400
11	129,259	47,125	142,300
12	64,249	47,565	138,900
22	45,006	47,539	62,900
23	31,062	46,451	55,800
26	32,382	47,640	18,300

plate material than for the 1.0" plate stock used to generate unnotched cyclic data. Still missing in the predictions, however, is the creep module to account for periods of sustained loadings. For example, 430,000 cycles is the predicted life for Sequence 8. The same life is calculated for Sequences 13 and 14. These two sequences are identical to Sequence 8, except for the 24- and 1.0-hour hold periods (see Table VII) but the test life is significantly different for the three sequences. The same is true for Sequences 10, 16, and 17 and Sequences 9, 14, and 15, for example.

Creep studies to be conducted in Phase II of this program are expected to provide data to formulate an analysis module to account for these periods of sustained loading.

SECTION VI
CONCLUSIONS

The following conclusions are based on the Phase I results.

1. The experimental approach used here has produced quantative results; however, improvements in the data recording methods and system sensitivity are necessary for the Phase II study. Expected variations in the strain field were observed and were measurable.

2. The Neuber Hypothesis is not sufficiently accurate for a notch stress-notch strain study of a finite width plate with a central circular notch.

3. Overloads and underloads do effect specimen life. Cyclic block size has a significant effect on life and rate of change of strain. Strain variation during blocks of constant amplitude cycling is dependent on the previous load history.

4. Specimen life is effected by sustained compression loadings and there is evidence that creep exists during the loading periods. This creep/relaxation at a notch is very complex and is a function of both notch stress and notch strain. Elastic-plastic stress and strain field definition is important to both crack initiation and crack growth in the damage process.

5. Events included in test sequences do occur in service and will effect structural life. Both component and full scale tests are effected specifically as regards test spectra development and interpretation of data.

REFERENCES

1. Simpkins, D., Neulieb, R. L., Golden, D. J., "Load-Time Dependent Relaxation of Residual Stresses," Journal of Aircraft, Vol. 9, No. 12, December 1972.

2. Potter, J. M., "The Effect of Load Interaction and Sequencing on the Fatigue Behavior of Notched Coupons," Cyclic Stress-Strain Behavior Analysis, Experimentation and Failure Predictions, ASTM STP No. 519, March 1973.

3. Carroll, J. R., "Time Dependent Residual Stress Relaxation in Low Load Transfer Joints," Lockheed Report SMN 388, to be published.

4. Awards Abstract, "Self-Supporting Strain Transducer," NASA Case LAR 11263-1, Filing date May 23, 1974.

5. Neuber, H. "Theory of Stress Concentration for Shear-Strained Prismatic Bodies with Arbitrary Nonlinear Stress-Strain Law," ASME Journal, Vol. 28, Dec. 1961.

6. Jhansole, H. R. "A New Parameter for the Hysteretic Stress-Strain Behavior of Metals," Journal of Engineering Materials and Technology, Jan 75, pp 33-38.

7. Dowling, N. E., "Fatigue Failure Predictions for Complicated Stress-Strain Histories." Journal of Materials, Vol 7 #1. ASTM, March 1972, pp. 71-87.